



HAL
open science

Peptide mimics of the thrombospondin C-terminal binding domain : analysis of their therapeutic potential to trigger immunogenic death of cancer cells targeting the TSP1–CD47 axis

Luis Gómez-Morales

► **To cite this version:**

Luis Gómez-Morales. Peptide mimics of the thrombospondin C-terminal binding domain : analysis of their therapeutic potential to trigger immunogenic death of cancer cells targeting the TSP1–CD47 axis. Medicinal Chemistry. Sorbonne Université; Universidad autónoma de Nuevo León, 2021. English. NNT : 2021SORUS150 . tel-03482025

HAL Id: tel-03482025

<https://theses.hal.science/tel-03482025v1>

Submitted on 15 Dec 2021

HAL is a multi-disciplinary open access archive for the deposit and dissemination of scientific research documents, whether they are published or not. The documents may come from teaching and research institutions in France or abroad, or from public or private research centers.

L'archive ouverte pluridisciplinaire **HAL**, est destinée au dépôt et à la diffusion de documents scientifiques de niveau recherche, publiés ou non, émanant des établissements d'enseignement et de recherche français ou étrangers, des laboratoires publics ou privés.

Sorbonne Université
Universidad Autónoma de Nuevo León

École doctorale de Chimie Moléculaire Paris-Centre

Laboratoire des Biomolécules UMR 7203

Laboratorio de Inmunología y Virología FCB UANL

**Peptide mimics of the thrombospondin C-terminal binding domain:
Analysis of their therapeutic potential to trigger immunogenic death
of cancer cells targeting the TSP1–CD47 axis**

by Luis GÓMEZ-MORALES

PhD thesis of Medicinal Chemistry and Immunobiology

Directed by

Pr. Philippe KAROYAN and Pr. Ana Carolina MARTÍNEZ-TORRES

Presented and defended publicly in July the 27th, 2021

In front of a jury composed by:

Pr. Vincent MARECHAL (Professor, Sorbonne Université)

Pr. Lorenzo GALLUZZI (Professor, Weill Cornell Medicine)

M.D. Gerardo PALACIOS SAUCEDO (Director of research, IMSS)

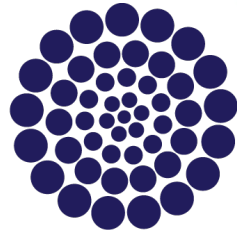
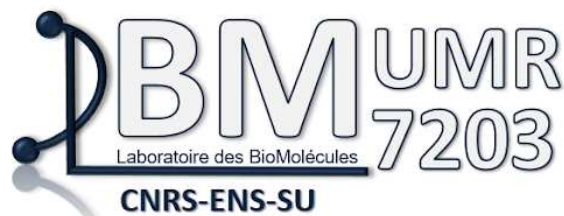
Pr. Cristina RODRÍGUEZ PADILLA (Professor, UANL)

Pr. Ana Carolina MARTINEZ TORRES (Professor, UANL)

Pr. Philippe KAROYAN (Professor, Sorbonne Université)



SPECIAL ACKNOWLEDGEMENTS



CONACYT

Consejo Nacional de Ciencia y Tecnología



The present work would not have been possible without the economic support and the infrastructure provided by Kaybiotix/SATT Lutech, the Laboratory of Biomolécules UMR 7203, the Laboratory of Immunology and Virology at the FCB-UANL, the Mexican Council of Science of Technology (CONACYT) and ECOS-Nord.

ACKNOWLEDGEMENTS

I would like to thank the members of the jury; it is an honor for me to count with your recognized expertise in the field. Thanks to Dr. **Vincent Marechal**, and to Dr. **Cristina Rodríguez-Padilla**, for accepting to examine my work. Thanks to the reporters, who evaluated in depth the present manuscript: Dr. **Gerardo Palacios-Saucedo** for his opportune revisions and supporting commentaries, and to Dr. **Lorenzo Galluzzi**, for providing such a valuable, expeditious, deep, and constructive criticism to this work.

Of course, thanks to my thesis advisors Dr. **Philippe Karoyan** and Dr. **Ana Carolina Martínez-Torres**, for letting me be part of their teams as their student and to trust me to work in this project. Thank you, Philippe, for your full trust in me, and for letting me develop myself freely but always being there to guide me. Thank you, Caro, for challenging me so, push me outside my limits, and believing that I could do it. Thank you both, Philippe, Caro, for all your personal efforts (impossible to mention here but be sure that I treasure them in my heart), done to let me develop and live my passion; thank you for sharing me yours, and for guiding me towards the best version of myself as a professional and as a person. You are the best mentors that I could ever wish and make an amazing team; I am so proud of having been part of it. Thank you.

Next, I want to thank to the laboratories that hosted the present work: the Laboratoire des Biomolécules UMR 7203 (Paris, France), chaired by Dr. **Sandrine Sagan** and Dr. **Olivier Lequin**, at the beginning and the last part of my thesis, respectively, and the Laboratorio de Inmunología y Virología (LIV) of the FCB-UANL (Monterrey, Mexico), presided by Dr. **Cristina Rodríguez-Padilla**. Thank you, Dr. Sandrine, and Dr. Olivier, for accepting me in your lab and for your support to the project. Thank you, Dr. Cristina, for the enriching discussions and your flawless support to the project, and to me, personally, both during my stay in your lab and when I left abroad. Additionally, I thank Dr. **Fabrice Viviani** and Dr. **Alexis Denis** as well, for welcoming me at the Oncodesign facilities.

Thanks to the organisms that financed this work. I deeply thank the **Kaybiotix GmbH** and Mexican National Council of Science and Technology (**CONACYT**) for providing me economic support during my PhD thesis; to the **SEP-CONACYT-ANUIES-Ecos Nord agreement**, which supported the international mobility of the teams; and to the **Kaybiotix**, the **SATT-Lutech**, and the **Laboratory of Immunology and Virology** of the FCB-UANL, which provided the economic support for this project.

Thanks to the great scientists and friends, part of the CD47 team from the labs of Dr. Martínez-Torres and Dr. Karoyan. Especially, to Dr. **Kenny Misael Calvillo-Rodríguez**, and to Dr. **Ashanti Uscanga-Palomeque**, for being such great team partners inside and outside the lab and becoming like family to me; to Dr. **Eva Lardé**, and Dr. **Thomas Denèfle**, who offered me their friendship from the moment I arrived in France and technically formed me and assisted me as a chemist during my first year here; and to **Estelle Odile** and **Rodolfo Mendoza-Reveles**, fresh fellow students with whom scientific and non-scientific discussion is always enriching.

I also want to thank the people who helped our team to develop this international collaboration, the first between both universities. Thanks to the Doctoral School of Molecular Chemistry of Sorbonne Université, its director Dr. **Cyril Ollivier**, and to the Bureau of International Relationships of Sciences-Sorbonne Université, in charge of Mme. **Patricia Zizzo**, for their understanding, flexibility and willingness to help. In a similar way, thanks to the team of the Doctoral School of the FCB-UANL and its former and current directors, Dr. **Diana Reséndez-Pérez**, and Dr. **Katiushka Arévalo Niño**, respectively, to the academic secretariat, managed by Dr. **Pablo Zapata Benavides**, and to the rest of the team, who worked hard to establish an administrative protocol suitable for this collaboration.

My acknowledgments to the many other people (professors, researchers, and students) who contributed with my thesis work technically, conceptually, or assisted my formation as student, most of you know how much I value your opinion and amity:

From **Sorbonne Université**: The former students at the DRUG-Lab, Dr. **Lucrezia Chappuit**, Dr. **Mikail Levasseur**, and **Clara Newton**; my fellow chemist students and researchers at the LBM, MSc. **Taleen Peker**, and MSc. **Agathe Brudo**, and Dr. **Rodrigue Marquant**; and the follow-up committee of this thesis, Dr. **Michèle Salmain** and Dr. **Nicolas Pietrancosta**.

From **Oncodesign**: Dr. **Pascal Grondin**, Dr. **Akanksha Gangar**, Dr. **Nicolás Ancellin**, MSc. **Kenny Herry**, Dr. **Anne Lazzari**, **Valerie Linhart**, **Sandrine Martin**, and **Raphaëlle Guillard-Huet**; and Dr. **Nicolas Grandchamp**, from **GEG-Tech**.

From the **UANL**: The follow-up committee of this thesis, Dr. **Diana Caballero-Hernández**, Dr. **Moisés Franco-Molina**, and Dr. **Diana Reséndez-Pérez**; the members (or former members) of the LIV: Dr. **Diana Zárate Triviño**, MSc. **Alejandra Arreola Triana**, Dr. **Ericka Coronado Cerda**, Dr. **Yarellys Ramos Zayas**, and Dr. **Santiago Saavedra-Alonso**; and the members of the PhD program of Pharmacy of the FCQ-UANL (who offered me freedom to take chemistry courses before prior to my arrival at the LBM), Dr. **Aracely Hernández Ramírez**, Dr. **Lucía Cantú-Cárdenas**, Dr. **María del Rosario González-González**, and Dr. **Francisco Ávalos Alanís**.

Also, thanks to our collaborators from the **Centre de Recherche de Cordeliers**: Dr. **Hélène Merle-Béral**, Dr. **Santos Susin** and his team, including Dr. **Elodie Pramill**, and MSc. **Linda Herbi**.

Thanks to the scientists that indirectly helped me to achieve this thesis by offering me their friendship (as many of the above mentioned): my fellow students at the LIV, **Helen**, **Karla**, **Alan**, **Martín**, **María**, **Ale**, **Rafa**, **Zack**, **Alejo**; and the chemists and biologists at Oncodesign **Maxime**, **Jérôme**, **Christopher**, **Aurélien**, **Stéphane**, **Corine**, **Erick**, **Pascal**.

Thanks to my family who stood by my side during this part of my life and fueled me with love and support. To my dad, **Luis Gómez Valencia**, *gracias por apoyarme incesablemente y hacerme el hombre que soy, que al igual que tú, decidió ayudar a otros como científico; te amo y admiro con toda el alma, papi*. Thanks to my mom, **Anastasia Morales Hernández**, *solo tú sabes cuánto te agradezco, cuánto te extraño, y cuánto quisiera que me vieras aquí...* Thanks to my sister, **Meztli Gómez Morales**, and

to my brother-in-law **Salvador Gutiérrez Martínez**, for giving me the most amazing gifts that I could have ever imagine, **Eliel** and **Jared** drew smiles in my face that I thought impossible when I needed them the most in the last steps of this journey. Thanks to my aunts and uncles, **Rochy**, **Carmita**, **Martín**, **Toña**, to my cousins **Vane**, **Adri**, y **Oscar**, and to my grandpa **Lucio Morales**, *gracias por estar tan cerca de mí sin importar la distancia, por echarme porras y hacerme sentir apoyado*. Finally, thanks to the lovely persons who I already consider my family, **Cecilia Ávila**, and **Altaira Ávila**, *gracias por abrirme las puertas de sus casas, por preocuparse por mí y procurarme como a un hijo o un hermano*.

Thanks to my true friends, **Kattia Carpio** and **David Corro**, for keeping in touch with me and constantly remind me I have a friend regardless of the time and distance. And thanks to the best friend anyone could wish, **Christopher Bullé-Goyri**, who has never stopped believing in me and standing by my side, no matter what. I love you so much, brother; I will remember this year as one the most precious of my life, and it will be because you got happily married. I wish with all my heart I could have been with you...

Finally, thank you, **Andrea Ávila-Ávila**, for living this amazing part of my life with me. Thank you for your love that makes everything easier and reminds me what is the most important in my life. Thank you for laughing and crying with me, for resisting with me, for fighting next to me, and for helping me, and making me grow in ways you cannot even imagine. You are my best team and my best friend. I love you. Thanks to God that put you and everyone above in my way.

To the chemist from Cucuyulapa,
M.Ed. Anastasia Morales Hernández

To the geneticist from Teapa,
M.D. Luis Gómez Valencia

Index

Introduction	1
Preamble	2
Cancer and cell death	4
Cancer	4
Cell death	8
Types of cell death	8
Regulated cell death (RCD) mechanisms	9
Apoptosis: two canonical caspase-dependent cell death modalities	12
Regulated necrosis	14
<i>Role of Ca²⁺ signaling in cell death: link between extracellular and intracellular Ca²⁺</i>	15
a) Plasma membrane	15
b) Cytosolic calcium control by the endoplasmic reticulum	16
Caspase-independent, autophagy-dependent RCD	18
Immunogenic cell death	19
The thrombospondin-1–CD47 axis	21
Thrombospondins	21
Generalities of a matricellular protein	21
<i>Discovery of the thrombospondin protein superfamily</i>	22
<i>Complexity of multi-modular interactions</i>	23
TSPs and disease: the crucial role of the signature domain	25
<i>Structure of the thrombospondins' signature domain</i>	26
<i>The globular C-terminus: a ligand of CD47</i>	27

CD47	34
Generalities of its interactions	34
A therapeutic target in cancer	36
<i>Role of CD47 as an extracellular “don’t eat me” signal sender</i>	36
<i>CD47 outside-in signaling</i>	38
<i>CD47 outside-in signaling in erythrocytes</i>	39
<i>Integrin-associated CD47 outside-in signaling</i>	40
<i>Cardiovascular functions of CD47 outside-in signaling</i>	42
<i>CD47 outside-in signaling in T cells</i>	44
<i>CD47 and autophagy</i>	45
<i>CD47 activation by TSP1 can trigger RCD</i>	46
Triggering the TSP1-CD47 axis with therapeutic peptides	48
Justification	52
Hypotheses	56
Objectives	60
Results	63
CHAPTER 1. Study of the Mechanism of Immunogenic Cell Death induced by PKHB1 in T-cell leukemia	65
<i>Preamble</i>	66
1.1. Article 1: CD47 agonist peptide PKHB1 induces immunogenic cell death in T- cell acute lymphoblastic leukemia cells	68
Summary	69
Résumé de l’article 1	71
Resumen del artículo 1	72
Main manuscript	74
Supplementary Material	87

1.2. Article 2: PKHB1 tumor cell lysate induces antitumor immune system stimulation and tumor regression in syngeneic mice with tumoral T lymphoblasts	91
-----	-----
Summary -----	91
Résumé de l'article 2 -----	94
Resumen del artículo 2 -----	95
Main manuscript -----	97
Supplementary Material -----	108
 CHAPTER 2. Study of the Mechanism of Immunogenic Cell Death induced by PKHB1 in solid tumors	 110
<i>Preamble</i> -----	111
2.1. Article 3: PKHB1, a thrombospondin-1 peptide-mimic, induces antitumor effect through immunogenic cell death induction in breast cancer cells	112
-----	-----
Summary -----	112
Résumé de l'article 3 -----	116
Resumen del artículo 3 -----	118
Main manuscript -----	121
Supplementary Material -----	160
 CHAPTER 3. Optimization of the pharmacological properties of thrombospondin peptide mimics	 166
3.1. Article 4: Homotrimerization approach in the design of thrombospondin-1 mimetic peptides with improved potency in triggering regulated cell death of cancer cells	167
-----	-----
Summary -----	167
Résumé de l'article 4 -----	170
Resumen del artículo 4 -----	171
Main manuscript -----	173
Supplementary Material -----	187

Conclusions and perspectives	218
Cell death mechanism and immunogenicity of cell death induced by PKHB1	220
<i>Overall toxicity</i>	220
<i>Ca²⁺ regulation of cell death</i>	220
<i>Immunogenicity of cell death</i>	221
Relevance of optimizing TSP1 peptide mimics	222
<i>Homotrimeric peptides and cell death triggering mechanism</i>	222
<i>Potential of TSP-C-terminus peptide-mimics to induce cell death in cancer and non-resolving inflammatory cells</i>	224
<i>The future of therapeutic peptides</i>	224
References	227
Annex	251

Abstract

Our team developed PKHB1, a peptide mimic of TSP1 able to induce caspase independent and Ca^{2+} dependent cell death in chronic lymphocytic leukemia (CLL), involving the activity of $\text{PLC}\gamma 1$, which overexpression correlates with CLL progression. In the present thesis, the therapeutic potential of PKHB1 against T-cell acute lymphoblastic leukemia (T-ALL), breast, and lung cancer was assessed. PKHB1 induced Ca^{2+} dependent cancer cell death. PKHB1 was not toxic to human nor murine peripheral blood mononuclear cells, nor to mouse cells from primary or secondary lymphoid organs. In immunocompetent mice, PKHB1 reduced the growth of T-ALL and breast cancer as it promoted immune cell recruitment to the tumor site. PKHB1 induced immunogenic cell death, as demonstrated by the release of damage-associated molecular patterns by dying cells, mechanistic *ex vivo* experiments using co-cultures of PKHB1-killed cells, dendritic cells, and T cells, prevention of tumor establishment by prophylactic vaccination, remission in tumor-bearing mice after therapeutic vaccination with PKHB1-killed cells, and prevention of tumor establishment in mice in remission after rechallenged with viable cancer cells. Moreover, optimization of PKHB1 potency using a homotrimerization approach to mimic the homotrimeric nature of TSP1 was assessed. Structure-activity-relationship studies led to the discovery of a homotrimer, [PKT16]₃, ten times more potent than PKHB1 to induce Ca^{2+} -dependent cell death in CLL and lung cancer cells, proving that structural modifications can improve the potency of TSP1 peptide mimics.

Résumé

Notre équipe a développé peptide mimant de la TSP1, i.e. PKHB1, capable d'activer une mort caspases-indépendante et Ca^{2+} -dépendante de cellules de leucémie lymphoïde chronique (LLC). Le mécanisme implique la $PLC\gamma 1$ dont les niveaux d'expression corrént avec la progression de la maladie. Dans cette thèse, nous avons exploré le potentiel thérapeutique de PKHB1 contre la leucémie lymphoblastique aiguë à cellules T (T-ALL), le cancer du sein et du poumon. PKHB1 n'est pas toxique pour les cellules saines humaines ou murines et induit une mort des lignées tumorales Ca^{2+} -dépendante. Chez les souris immunocompétentes, PKHB1 réduit la masse des tumeurs (T-ALL et cancer du sein) en favorisant le recrutement des cellules immunitaires au niveau du site tumoral. PKHB1 induit une mort cellulaire immunogène, démontrée par la libération des «DAMPS» (ensemble de molécules relarguées par les cellules endommagées), par des études mécanistiques *ex vivo* utilisant des co-cultures des cellules cancéreuses tuées par PKHB1 (PKHB-1-TCL), des cellules dendritiques et de lymphocytes T, par la vaccination prophylactique avec PKHB1-TCL prévenant l'établissement des tumeurs, la rémission des tumeurs avec la vaccination thérapeutique par les PKHB1-TCL, et par la prévention de l'établissement des tumeurs chez la souris en rémission après une réexposition au cellules tumorales. De plus, une étude de relation structure-activité nous a permis d'optimiser nos peptides. Un analogue homotrimerique, [PKT16]₃, à l'image de la TSP1, s'est révélé dix fois plus puissant que PKHB1 pour induire la mort cellulaire dans la LLC et le cancer du poumon, démontrant que l'optimisation des mimes peptidiques de la TSP1 est possible.

Resumen

Nuestro equipo desarrolló PKHB1, un péptido mimético de la TSP1 capaz de inducir muerte celular independiente de caspasas y dependiente de Ca^{2+} en leucemia linfocítica crónica (CLL) que involucra la actividad de la $\text{PLC}\gamma 1$, cuya sobreexpresión correlaciona con la progresión de la CLL. En la presente tesis, se evaluó el potencial terapéutico de PKHB1 contra la leucemia linfoblástica aguda de células T (T-ALL), cáncer de mama y de pulmón. PKHB1 indujo la muerte de células cancerosas de manera dependiente de Ca^{2+} . PKHB1 no fue tóxico en células mononucleares de sangre periférica humana ni murina, ni en células de órganos linfoides primarios o secundarios de ratón. En ratones inmunocompetentes, PKHB1 redujo el crecimiento de tumores de T-ALL y de cáncer de mama, y promovió el reclutamiento de células del sistema inmune al sitio del tumor. PKHB1 indujo muerte celular inmunogénica, como lo demuestran la liberación de patrones moleculares asociados a daño por las células moribundas, experimentos mecanísticos *ex vivo* utilizando co-cultivos de células muertas por PKHB1, células dendríticas y células T, la prevención del establecimiento de tumores mediante vacunación profiláctica, la remisión en ratones portadores de tumores tras la vacunación terapéutica con células muertas con PKHB1, y la prevención del establecimiento de tumores en ratones en remisión después de un re-reto con células cancerosas viables. Además, se evaluó la optimización de la potencia de PKHB1 usando un enfoque de homotrimerización para imitar la naturaleza homotrimérica de TSP1. Estudios de relación estructura-actividad llevaron al descubrimiento de un homotrímero, $[\text{PKT16}]_3$, diez veces más potente que PKHB1 para inducir muerte celular dependiente de Ca^{2+} en células de CLL y de cáncer de pulmón, lo que demuestra que las modificaciones estructurales pueden mejorar la potencia de los péptidos miméticos de la TSP1.

Introduction

Preamble

Cancer accounts for the death of millions of people worldwide each year. This heterogeneous group of diseases are a result of both cell intrinsic and immunological processes that allow certain aberrant cell populations to grow uncontrolledly and escape from antitumor immune responses, among other characteristics. The increasing understanding of these processes has highlighted the limitations of classical therapies aiming to induce regulated cell death of cancer cells, but it has also pointed out their previously unidentified strengths while opening new avenues for overcoming resistance and novel therapies with less secondary effects.

During my thesis, I was involved in a collaborative project between Sorbonne University (LBM UMR 7203 – DRUG Lab/Kaybiotix) and the UANL (Laboratorio de Immunología y Virología–FCB) aimed to develop and evaluate the potency of peptide mimics of thrombospondin-1 (TSP1), a matricellular protein, high-affinity ligand of the cell receptor CD47. This receptor has attracted considerable interest as a therapeutic target in recent years, as its interaction with other of its ligands, SIRP α , represents an immune checkpoint susceptible of being targeted by blocking monoclonal antibodies. However, CD47 engagement by TSP1 controls signaling pathways relevant for therapeutic targeting, including the induction of regulated cell death. In this context, our group has developed peptide mimics of TSP1 with the implementation of a structure-activity relationship studies.

If small molecules have dominated the pharmaceutical world throughout the 20th century, the progress made over the past two decades in the field of peptides (syntheses on solid support, stability improvement, structure optimization, formulation, etc.) has made it possible to consider them as promising therapeutic tools. Indeed, overcoming the intrinsic problems of peptides has brought these molecules back to the forefront of research and discovery, determining the new generation of therapeutic molecules. These advances have enabled peptides to enter the pharmaceutical industry market.

In the following chapters, I will briefly describe the biology of cancer and its target opportunities, focusing regulated cell death induction, CD47 and TSP1. I will then define the objectives of my thesis around the evaluation of the potency of the first peptide mimic of TSP1 (i.e., PKHB1) to induce regulated cell death and awake antitumor immune responses against T cell acute lymphoblastic leukemia and breast cancer. Finally, I will describe a homotrimerization strategy used in a TSP1 peptide-mimic that significantly improved the cell binding and cell death-inducing ability of monomeric peptides.

Cancer and cell death

Cancer

Cancer is a group of diseases that account for the death of millions of people worldwide. It can occur in both sexes, in all ages, and despite advances achieved across the last years, to date, 50% of the people diagnosed with cancer die from it (Globocan, 2020). In 2020, 19.3 million people were diagnosed with cancer, and cancer was the cause of death of at least 10.0 million people the same year, being breast cancer the most diagnosed, and lung cancer the most lethal (**Figure 1**) (Globocan, 2020).

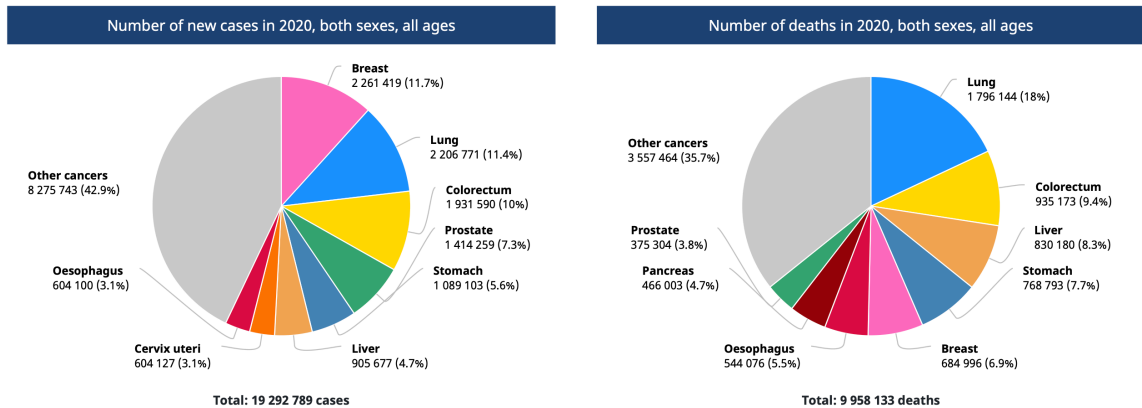


Figure 1. Worldwide cancer incidence and mortality in 2020. (Extracted from Globocan, 2020)

Hanahan and Weinberg summarized ten hallmarks that are common between the different types of cancer (**Figure 2**) (Hanahan and Weinberg, 2000, 2011). These qualities largely define cell intrinsic and immune processes that permit cancer development, survival and spreading, and therefore, they also represent target opportunities to combat the disease. One of them that is centrally related to this project, is their ability to resist cell death induction, as cell death induction is currently the main strategy to treat cancer this will be discussed in depth in the chapter dedicated to cell death.

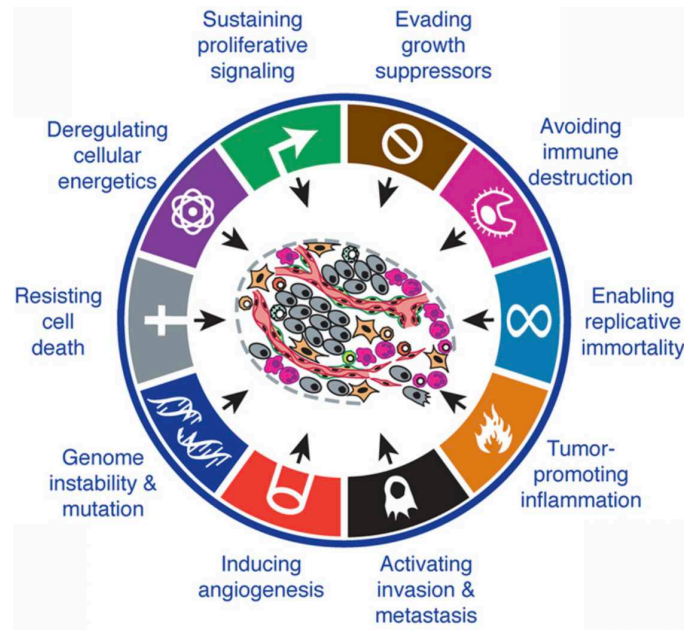


Figure 2. The hallmarks of cancer. (Adapted from Hanahan and Weinberg 2011)

The acceleration of angiogenesis and the invasion of other tissues by metastases also play key roles in cancer progression. Evidently, this anarchic cell reproduction is possible thanks to an energy metabolism adapted to their functioning but also thanks to the participation of the tumor microenvironment which will communicate with the cells to meet their energy needs while protecting them from current therapies. Among the other characteristics described by Hanahan and Weinberg, the lack of efficient recognition of tumor cells by the immune system present in the tumor microenvironment will lead to genomic instability and chronic inflammation participating in the initiation and progression of cancer.

Among the root causes of uncontrolled cell proliferation, mutations in tumor suppressor genes, also known as anti-oncogenes, prevent their function of inhibiting cell proliferation that negatively regulates the cell cycle or induces regulated cell death. The mutation or deletion of these genes leads to the loss or alteration of their function, giving these cells aberrant capacities that modulate their behavior. For example, the *TP53* gene, known as “the guardian of the genome”, is mutated in many cancers, and has functions that affect cell itself and its microenvironment (Amelio *et al.*, 2018).

The tumor microenvironment includes cellular and non-cellular components. Stromal cells of the microenvironment represent angiogenic vascular cells, immune cells and cancer associated fibroblasts (CAFs) while non-cellular components form the extracellular matrix (ECM). This includes the interstitial matrix and the basement membrane including secreted factors and matrix proteins such as collagen, proteoglycans, glycoproteins (Spaw, Anant and Thomas, 2017). The tumor microenvironment plays a key role in resistance to different therapies. Indeed, the environmental factors of the tumor are considered to be the main reasons for treatment failure and targeting the macrophages associated with cancer, CAFs or the signals they induce, may prove to be an effective strategy (Hirata and Sahai, 2017).

Likewise, cells of the innate and adaptive immune system present in tumors are therapeutic targets of interest and have become the main protagonists of new treatments based on immuno-oncology. Indeed, one of the most important challenges of tumorigenesis is to overcome a process called immune surveillance of tumors (Grivennikov, Greten and Karin, 2010). This process represents the ability of the immune system to recognize cancer cells as abnormal and to kill them by the action of lymphocytes. One of the anti-tumor therapeutic strategies then consists of stimulating the lymphocytes by removing checkpoints, responsible for their ineffectiveness. Targeting these checkpoints, including the CTLA-4 protein and the PD-1 / PD-L1 axis, is proving to be a powerful anti-tumor strategy that won scientists James Allison and Taku Honjo the Nobel Prize in medicine in 2018 (*James P. Allison – Facts – 2018 - NobelPrize.org*, no date).

Cells of the innate immune system are the most abundant in tumors, particularly macrophages. They are generally associated with a high resistance to treatment and therefore a poor prognosis of survival, which makes them targets of choice for the immunotherapeutic treatment of cancer. Macrophages, have a dual role in cancer: they are important mediators of phagocytosis of aged, damaged and cancer cells, but they can also promote tumor growth and metastasis helping the tumor escape immunosurveillance (Jaiswal *et al.*, 2010). The CD47 receptor is known to be one major source of tumor escape, by providing the anti-phagocytic “don’t eat me” signal to macrophages. Therefore,

it represents a new checkpoint of the innate immune system and offers the way for a new generation of checkpoint inhibitors (Matlung *et al.*, 2017). Nevertheless, CD47 plays crucial roles in the immune system as well, which widens its importance as a therapeutic target. This will be addressed later in the manuscript.

The main strategy to eliminate cancer cells from the body after tumor resection (when possible), consists in killing cancer cells. However, the development of compounds capable of effectively and selectively restoring cancer cell death is a major challenge in anticancer therapies. This issue becomes a real challenge when the approach aims to identify compounds capable of activating immunogenic death, which enables the destruction of tumors by the immune system and promote the long-term immune memory against the disease. This aspect will be presented in the following paragraphs, devoted to cell death.

Cell death

Certainly, scientific definition of biological life is at least complicated, especially considering the evolutionary origin of life on earth from prebiotic chemistry, RNA, and viruses (Lazcano and Miller, 1996). Indeed, although viruses are major biological entities, whether a virus is or not alive is an ongoing debate that does not seem to have a measurable scientific answer (Koonin and Starokadomskyy, 2016). In that sense, and despite the apparent simpleness of the task, scientific definition of “death” and its implications is not less complicated, as it is inexorably connected to life and its definition.

Keeping evident differences from viruses, it has been posited that the cell is the basic unit of life. Therefore, the cell membrane can constitute one of these limits. Having established this, it is possible to raise scientific questions around cell life and its death for practical means. In this way, cell death can be defined as the permanent ending of the cellular processes, which can be observed in cell traits and actions susceptible to being measured *in vitro* or *in vivo*. The Nomenclature Committee on Cell Death (NCCD) proposes that these attributes are met when (i) the integrity of the cell membrane has been lost, (ii) the cell or its nucleus have fragmented, and/or (iii) it has been phagocytosed by adjacent cells (Kroemer *et al.*, 2005).

Types of cell death

Cells can die by accident or in a regulated fashion (**Figure 3** left). Sudden changes alien to the cell, which nature can be mechanical (e.g., smearing), chemical (e.g., pH), or physical (e.g., temperature), can directly break the cell membrane and/or nucleus, without the need of any further cellular component, causing an accidental cell death (ACD), where the cell is incapable to adapt to these stimuli, and therefore, genetic, or pharmacologic interventions cannot prevent it. On the other hand, cells have evolved to sense less abrupt environmental changes that can be detrimental for the system they conform, and trigger regulated cell death (RCD; **Figure 3** right) using their own molecular machinery (Galluzzi *et al.*, 2014). As these processes require the availability of molecular sensors, second

messengers, and executioners which expression is internally modulated by the cell, genetic interventions or pharmacologic agents can affect the lethal outcome, whether by interfering with the signaling of certain components of the machinery, or with the ability of the cell to adapt to stress. In this way, RCD is necessary for life adaptation, species preservation, and evolution (Ameisen, 2002), and, playing crucial roles to contain local perturbations, and to recycle, remodel and repair tissues, RCD is necessary to maintain the hallmarks of health (López-Otín and Kroemer, 2021).

Many examples exist in which it has been demonstrated that RCD processes are “scheduled” since the cell’s birth. Such types of RCD processes are generally referred to as programmed cell death (PCD) (Galluzzi *et al.*, 2014). PCD is crucial during multicellular animal development to sculpt or delete structures, and in adulthood to moderate cell number during maintenance of tissues (Fuchs and Steller, 2011).

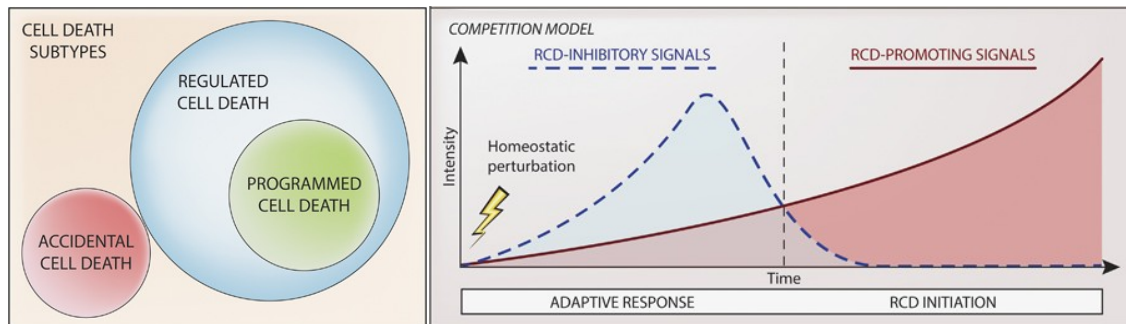


Figure 3. Types of cell death. Left. Different to accidental cell death (ACD), regulated cell death (RCD) uses the molecular machinery of the cell. Programmed cell death (PCD) refers to the types of RCD programmed since the birth of the cell to modulate the number of certain cell populations. Right. Generally, microenvironmental perturbations induce cell stress and promoting and inhibitory signals of RCD. If the cell does not achieve to adapt to stress, it can become engaged into an RCD process (Extracted from Galluzzi, et al. 2014).

RCD mechanism

RCD commence with inner or outer stimuli that activate an initiator mechanism. This in turn leads to the activation of mediator molecules and the production of modifiable

second messengers in the cell that lead to activation of executioner mechanisms (Vanden Berghe *et al.*, 2014; Galluzzi *et al.*, 2018). All of these signaling cascades can be inhibited by negative regulators of RCD at different steps, until surpassing certain boundaries after which death is imminent. These borders separating life-to-death decisions have been termed “points of no return” and are illustrated by the massive enhancement of molecular processes like caspase activation, mitochondrial outer membrane permeabilization (MOMP) and loss of its transmembrane potential ($\Delta\psi_m$), and exposure of phosphatidylserine (PS) residues to the outer face of the cell membrane as “eat me” signals for adjacent phagocytes (Kroemer *et al.*, 2005). Nevertheless, none of these processes have a unique irreversible lethal role by themselves, thus, only the observation of two or more of these criteria reassures that a cell is committed to die.

Therefore, only recently it has become clear that RCD is an interconnected circuitry of sensors and reactors with physiological roles (many of which are not directly related to death) that can gradually transition through points of no return. Thus, although several RCD subroutines with specific biochemical characteristics have been described, they all occur in precise circumstances, variables including the cell itself and the molecular machinery that they express, or are able to express, and the extracellular matrix and its components. In this way, all RCD subroutines are susceptible to the interference of other cellular pathways occurring concomitantly in varying circumstances (**Figure 4**).

Playing RCD decisive roles in the pathophysiology of a wide variety of diseases, identification of their characteristic biochemical criteria in particular cases has taken pivotal pharmacological relevance, as the evaluation of common points of no return help to identify in a first step discrete initiator or executioner mechanisms responsible of their delivery, and in a second step, the mediators and second messengers modulating the lethal response, all of which can be pharmacologically or genetically targeted or evaded. Such biochemical standards have replaced the traditional approaches classifying cell death as type I, II and III to refer to apoptotic, autophagic, and necrotic-like morphologies, respectively (Clarke, 1990). Indeed, diverse RCD products render a gradient of morphologies similar to these, and morphological classification is still used (Green and Llambi, 2015). However, substantial, clinically relevant biochemical differences conceal

within similar morphological outcomes (e.g., MPT-driven necrosis versus pyroptosis), and equally pertinent similarities may lay between two different ones (e.g., intrinsic versus extrinsic apoptosis). For this reason, the morphological classification should not be taken as anything but complementary to a biochemical definition.

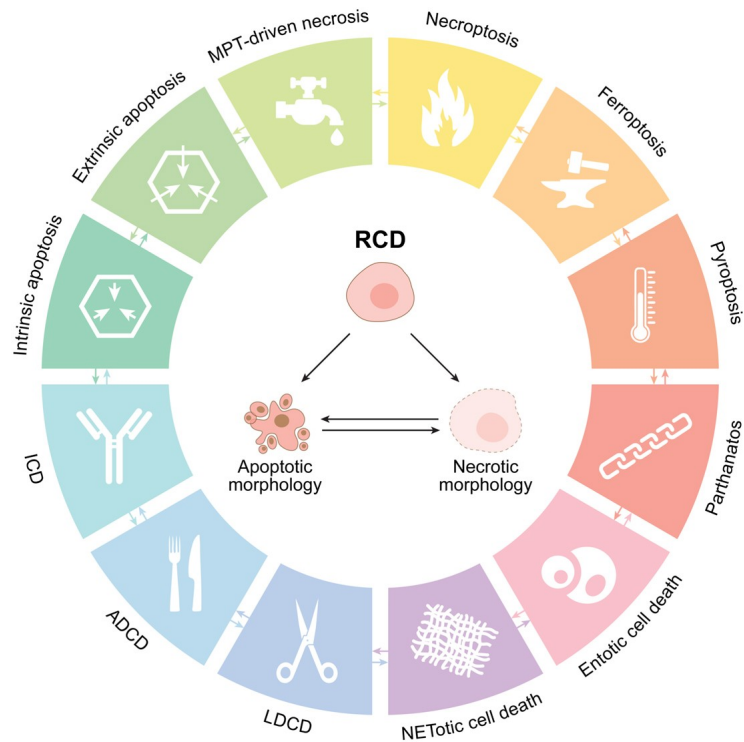


Figure 4. Known cell death subroutines. RCD implicate the participation of biochemical hallmarks that define certain types of cell death subroutines (indicated in different colors) in different cell types. These molecular actors will shape morphological features in the dying cell that will result in a varying range from fully apoptotic to fully necrotic morphology. As an interconnected network, the molecular actors of RCD may overlap in different situations. MPT, mitochondrial permeability transition; ICD, immunogenic cell death; ADCD, autophagy-dependent cell death; LDCD, lysosome-dependent cell death; NET, neutrophil extracellular traps (Adapted from Galluzzi *et al.*, 2018).

Apoptosis is a cell death program characterized by the broad participation of a type of cysteine proteases called caspases, which regulate an extremely controlled set of events that result in characteristic morphological features. Being the participation of caspases the main biochemical hallmark of apoptosis, for convenience of the present thesis I will subclassify RCD in two: a) apoptosis, as a canonical form of caspase-dependent RCD, and b)

regulated necrosis, as the exemplification of the interconnection between caspase-dependent and -independent RCD circuitry. Moreover, autophagy and immunogenicity of RCD will be mentioned as well, as examples (also convenient for the present thesis) of death-related cell adaptation to stress.

Apoptosis: two canonical caspase-dependent cell death modalities

Apoptosis can be triggered by intrinsic or extrinsic signals that lead to activation of different initiator mechanisms, being therefore considered two different RCD subroutines sharing some biochemical hallmarks and a characteristic morphology. While intrinsic apoptosis is triggered after inner sensing of a microenvironmental disturbance (e.g., DNA damage, ER stress, growth factor removal), extrinsic apoptosis is generally triggered after engagement of a death receptor with an agonistic ligand (e.g., tumor necrosis factor receptor 1, TNFR1, and TNF). In both cases, the different triggering mechanisms will generally provoke the activation of initiator caspases (e.g., caspase 8 in extrinsic apoptosis) and other signaling cascades that normally implicate the production and recruitment of proapoptotic BCL-2 family members, including BAX and BAK, that will mediate pore formation in the mitochondrial membrane, resulting in MOMP, $\Delta\psi_m$ dissipation, and release of intra-mitochondrial proapoptotic proteins like direct inhibitor of apoptosis (IAP) binding protein with low PI (DIABLO) and cytochrome C. The activation of executioner caspases (e.g., caspase 3 and caspase 7), which will accelerate cell-demolishing mechanisms that will shape higher degrees of their characteristic cell morphology (**Figure 5**) including pseudopod retraction, cell rounding, volume reduction, and membrane blebbing, chromatin condensation and nuclear fragmentation, irrelevant or null ultrastructural organelle modifications, and an intact plasma membrane until terminal stages (Galluzzi *et al.*, 2012, 2018).

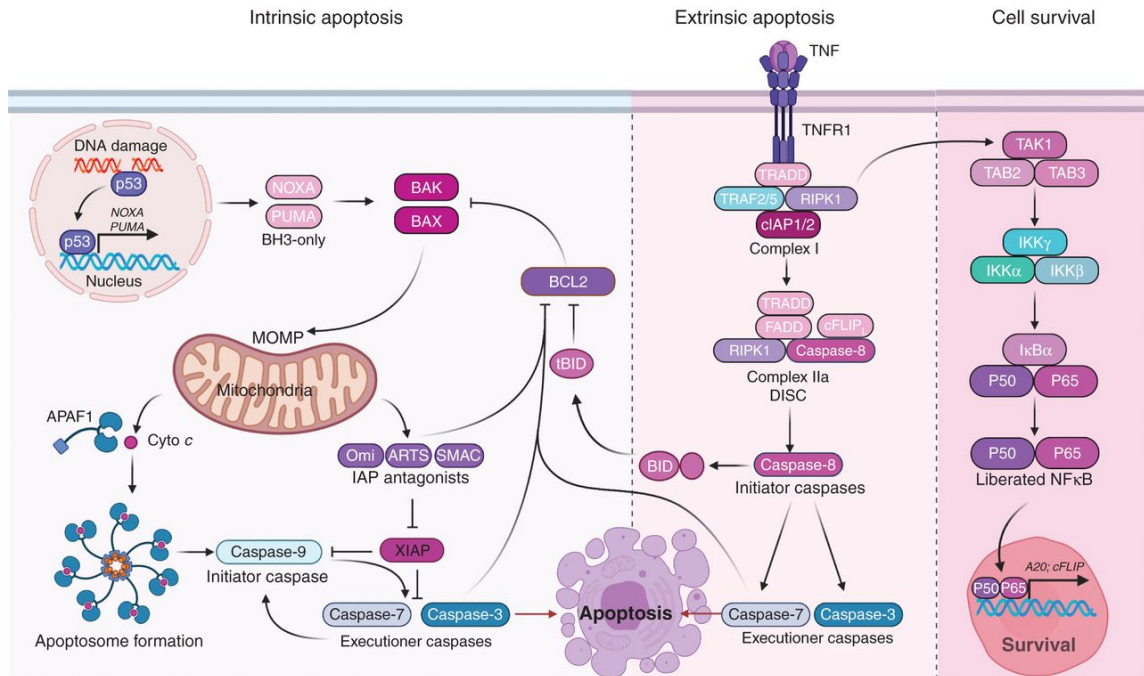


Figure 5. Extrinsic and intrinsic apoptosis circuitry. (Extracted from Koren and Fuchs, 2021)

The study of apoptosis laid bare the complexity of RCD mechanisms that can be triggered physiologically, in pathological processes, and the therapeutical opportunities to trigger or inhibit them. Indeed, although caspases characterize this type of RCD, they, can also trigger non-apoptotic RCD subroutines like necroptosis and pyroptosis (Vanden Berghe *et al.*, 2014; Galluzzi *et al.*, 2018), or even activities apparently unrelated to death, such as autophagy (Tsapras and Nezis, 2017), inflammation (Martinon and Tschopp, 2004; Van Opdenbosch and Lamkanfi, 2019) and cell differentiation (Lamkanfi *et al.*, 2007; Bell and Megeney, 2017). In the same way, several forms of RCD modalities do not rely on caspases, but on a large variety of initiators and executioners that have been described only recently and are subject of intense research currently (Vanden Berghe *et al.*, 2014; Galluzzi *et al.*, 2018).

Regulated necrosis

The word necrosis comes from the Greek “νεκρός” (nekrós), which means “death”. The term is generally used to refer to the death of animal tissues, and in cell biology to allude to type of cell death morphology characterized by rapid plasma membrane permeabilization, granulation of the cytosol and oncosis (swelling of organelles). Such morphological features of cell death can be observed in many types of RCD and in ACD. Therefore, an adequate differentiation between ACD and regulated forms of necrosis is imperative to study the implications in cell physiology of cell death modalities rendering such morphological attributes. In this way, regulated necrosis is defined as the different types of cell death subroutines that, under a genetically encoded cellular machinery, lead to a substantial necrotic morphology (Vanden Berghe et al., 2014).

Some types of regulated necrosis subroutines have been described in depth, many of these cell type-specific. Such subroutines include necroptosis, pyroptosis, pyronecrosis, ferroptosis, ETosis, NETosis, oxytosis, and parthanatos. Though, the list is not over, as more inductors and executioners that trigger RCD modalities that do not meet the biochemical criteria of the mentioned subroutines continue to be reported.

Interestingly, several components of the regulated necrosis machinery overlap at several points among different regulated necrosis subroutines and with those of apoptosis, advising the interconnection between both networks, and the possibility to activate similar executioners. Indeed, all types of regulated necrosis described to date share the participation of actors of the bioenergetic and redox metabolism. These weaponry control MOMP, lysosomal membrane permeability, oncosis, and plasma membrane permeability, classic in different types of regulated necrosis (**Figure 6**).

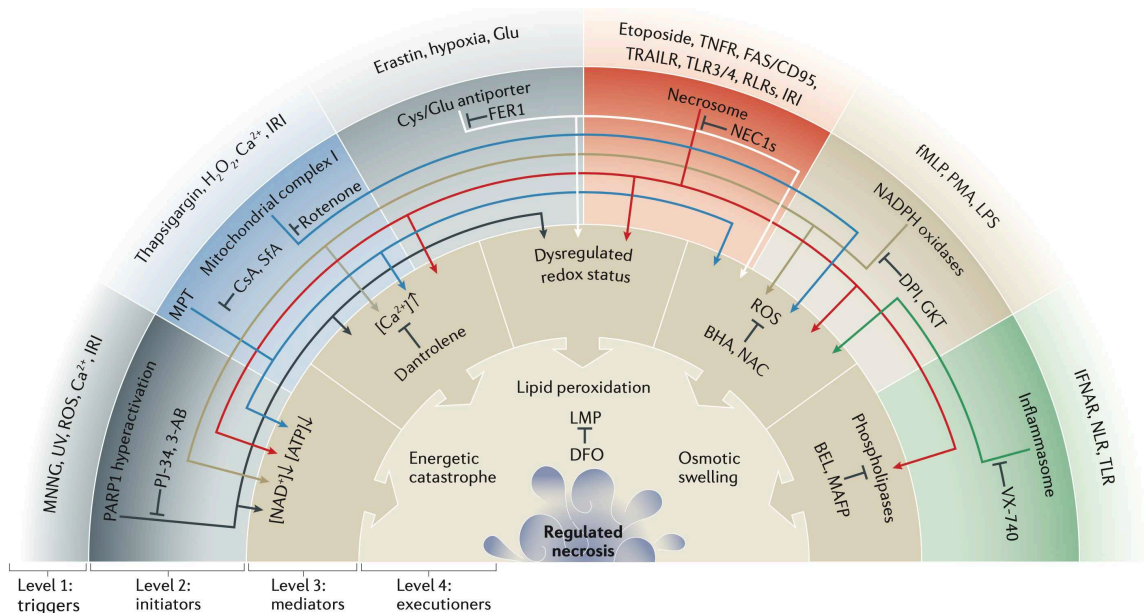


Figure 6. An integrated view of the emerging modes of regulated necrosis. (Extracted from Vanden Berghe *et al.*, 2014).

Role of Ca^{2+} signaling in cell death: link between extracellular and intracellular Ca^{2+}

a) Plasma membrane

The cell plasma membrane actively participates in RCD control. Plasma membrane is a semi-permeable phospholipid bilayer with embedded proteins that physically contains components necessary for cellular function and an adequate concentration of vital ions and organic molecules. This way, the permanent loss of its integrity is a sign of cell death (Kroemer *et al.*, 2005). Moreover, together with its selective permeability, expression of ion channels differentially controls the flux and inner concentration of certain organic molecules, sodium, potassium, and calcium ions, which directly regulate several executioner mechanisms of RCD (Cooper, 2000; Vanden Berghe *et al.*, 2014; Liu and Levine, 2015). As it is the contact site of the cell with its outer environment, through it travel biochemical signals from the outside to the inside of the cell, and vice-versa. Thus, in the tissue context, different components of the plasma membrane send direct signals that regulate phagocytic consumption, such as the expression of CD47 as “don’t eat me” signal (Jaiswal *et al.*, 2009) and calreticulin and phosphatidylserine exposure as “eat me”

signals (Gardai *et al.*, 2005; Kroemer *et al.*, 2005). Plasma membrane can also initiate RCD by sensing signals from the outside (e.g., TNF α or TSP1) via cell receptors (e.g., TNF α receptor, toll-like receptors or CD47 in certain scenarios) and associated complexes able transduce further signals that can be lethal in the adequate context. This can be dynamically regulated by cellular mechanisms that permit these receptors or their associated molecules to expose or internalize, or to undergo significant conformational changes that modulate their lethal signaling.

b) Cytosolic calcium control by the endoplasmic reticulum

Inside the cell, other membrane-enclosed structures modulate cell death. This is the case of the endoplasmic reticulum (ER), which control cellular processes of survival and responses to stress. Lipid biosynthesis, protein folding and transportation, as well as mitochondrial biogenesis occur at the ER. Being the major intracellular depository of calcium ions (Ca²⁺), it also participates in important cellular activities like cell proliferation, differentiation, motility, and death where intracellular Ca²⁺ signaling is crucial (Brini *et al.*, 2013; Plattner and Verkhratsky, 2016; Castillo, Chen and Jacobs, 2021). Cytosolic Ca²⁺ flux is extremely regulated. At physiological concentrations, it fluctuates around 0.1 μ M and can increase with ER Ca²⁺ release or via extracellular Ca²⁺ influx, where Ca²⁺ concentrations are higher (around 500 μ M and 1200 μ M respectively) (Berridge, Lipp and Bootman, 2000; Berridge, 2002; Plattner and Verkhratsky, 2016). Ca²⁺ is an exceptionally multifaceted ubiquitous second messenger, which roles variate depending on the intensity of cytosolic and intra-reticular fluctuations. As expected, cytosolic Ca²⁺ overload and intra-reticular Ca²⁺ exhaustion is detrimental for the cell and can be induced to provoke cell death, as evidenced by its participation in different RCD subroutines.

Intracellular flux of Ca²⁺ can be regulated by extracellular or intracellular mechanisms (**Figure 7**) (Martínez-Torres, 2013). Some extracellular agonist ligands can activate cognate membrane receptors (e.g., G-protein-coupled receptors), which will, by different means, induce phospholipase C (PLC) phosphorylation and the consequent conversion of membrane phosphatidyl-inositol diphosphate (PIP₂) to inositol triphosphate

(IP₃), a soluble second messenger that activates the IP₃ receptor (IP₃R) calcium channels at the ER. The activation of this channel moderately augments cytosolic Ca²⁺ concentration, which in turn activates a calcium-induced calcium release (CICR) mechanism. CICR activates more Ca²⁺ channels at the ER, principally the ryanodine receptors (RyR), which consequently increase the cytosolic Ca²⁺ concentration, and, if the mechanism progression is not prevented, the depletion intra-reticular Ca²⁺ (Berridge, Lipp and Bootman, 2000; Berridge, 2002).

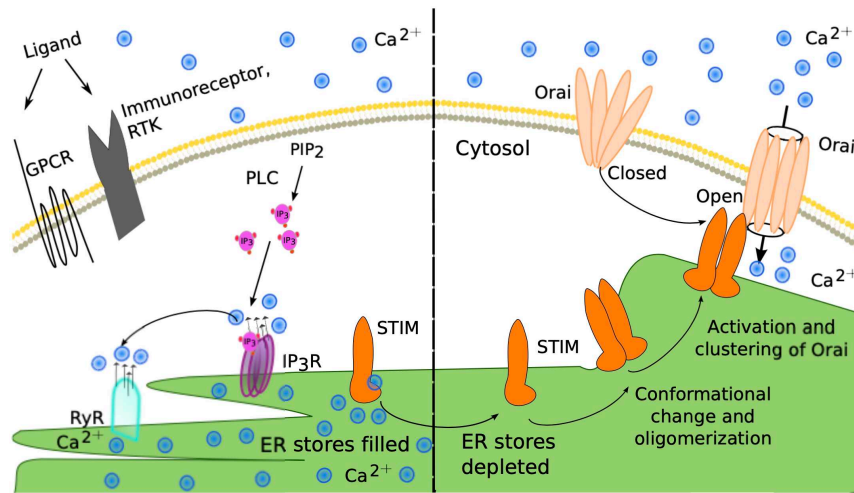


Figure 7. Store-operated Ca²⁺ entry. (Extracted from Martínez-Torres, 2013)

At this point, the intraluminal Ca²⁺-interacting trans-ER-membrane proteins stromal interaction molecule (STIM)-1 and/or STIM-2 sense Ca²⁺ store exhaustion at the ER lumen, undergoing conformational changes and associated oligomerization. This will also promote the oligomerized protein translocation to the contact sites of the ER with the plasma membrane, where the plasma membrane Ca²⁺ channel Orai (1, 2 and 3) proteins locate. Oligomerized STIMs Orai activation also activates other calcium release-activated calcium (CRAC) channels that mediate a massive cytosolic Ca²⁺ entry, and a physiologically relevant intracellular Ca²⁺ increase (Capiod, 2013; Pinto *et al.*, 2015; Xu *et al.*, 2015).

The different mechanisms of Ca²⁺ influx mediate important physiological tasks and are functionally regulated according to the cell type and its spatiotemporal situation, and

its deregulation has pathophysiological consequences. For example, kinases from Src and Ras family, which have been historically related to cancer development, can amplify PLC signaling (Rusanescu *et al.*, 1995; Bivona *et al.*, 2003; Stith, 2015). Indeed, overexpression and rearrangement of Ca²⁺ channels, pumps, and exchangers, as well as intermediate molecules like PLC, have been found to lead to elevated Ca²⁺ levels in cancer cells (Monteith *et al.*, 2007; Stewart, Yapa and Monteith, 2015), and these aberrations are generally associated with enhanced proliferation rates and treatment resistance (Orrenius, Zhivotovsky and Nicotera, 2003; Capiod *et al.*, 2007).

Caspase-independent, autophagy-dependent RCD

Autophagy is a regulated, multi-step, machinery of cell adaptation to stress in which the cell degrades itself. It is usually carried out as a mechanism of self-maintenance used during starvation for energy saving, and for the elimination of misfolded or pathogenic proteins or damaged organelles. Canonically, autophagy starts with a stress stimulus, such as starvation or rapamycin treatment, that indirectly triggers Beclin 1 phosphorylation (Kang *et al.*, 2011; Nazarko and Zhong, 2013) and the subsequent production of other products of the autophagy-related gene (Atg) family, which conjugate at the site of loose membranes to form double-membrane complexes called phagophores. This process can be mimicked by the cell-penetrating Beclin 1 peptide-mimic Tat-Beclin-1 (Shoji-Kawata *et al.*, 2013) and the ATG3-FLIP inhibitor Tat-vFLIP α 2 peptide (Lee *et al.*, 2009), which also initiate phagophore formation.

The phagophore matures with the help of the microtubule-associated protein 1A/1B-light chain 3 (LC3), capturing the intracellular entities while elongating until engulfing them in closed vesicles called autophagosomes. Normally, autophagosomes will fuse with cell-inner lysosomes to degrade their cargo, completing autophagy (Klionsky *et al.*, 2016). However, fusion mechanisms can be prevented (e.g., by Rubicon recruitment) and autophagosomes be involved in functions that lead to non-canonical outcomes (e.g., LC3-associated phagocytosis, LAP) (Martinez *et al.*, 2015; Wong, Sil and Martinez, 2018).

Most often, autophagy is cytoprotective. However, the molecular components of autophagy have been convincingly linked to RCD processes (Glick, Barth and Macleod, 2010; Nikolettou *et al.*, 2013; Galluzzi *et al.*, 2014; Mariño *et al.*, 2014). Autosis is probably currently the clearest example of a caspase-independent, autophagic machinery-dependent RCD subroutine (Liu and Levine, 2015). Autosis can be triggered by Tat-Beclin-1, starvation, and cerebral hypoxia-ischemia, causing cell death with characteristic morphological outcomes including enhanced adhesion of the cell to the substrate, focal ballooning of the perinuclear space, and endoplasmic reticulum dilation and fragmentation (Liu *et al.*, 2013). Autosis is not prevented by common pharmacological inhibitors of apoptosis or necroptosis, but pharmacological inhibitors of autophagy, as well as with cardiac glycosides or by the genetic inactivation of the Na⁺/K⁺-ATPase inhibit cell death (Liu *et al.*, 2013). Moreover, in these experiments, blockade of autophagosome/lysosome fusion did not prevent autosis of osteosarcoma cells, and recent studies provided genetic evidence in the same sense, showing that Rubicon upregulation promotes autosis during myocardial ischemia/reperfusion injury (Nah *et al.*, 2020), and suggesting that autosis is a non-canonical autophagy-related process.

Immunogenic cell death

Among the different types of regulated cell death, immunogenic cell death (ICD) has the particularity of being capable to activate an adaptive immune response against antigens of cellular (e.g., cancer antigens) or pathogenic (e.g., viral) nature, associated with dying cells (Galluzzi *et al.*, 2020). ICD is characterized by the exposure or release of endogenous immunogenic biomolecules, namely the damage-associated molecular patterns (DAMPs), which are sequentially produced following a state of stress, injury, or cell death (e.g., during cancer treatment). These released DAMPs bind to receptors located on immune cells, especially dendritic cells. Among different DAMPs, calreticulin (CRT) and other endoplasmic reticulum (ER) proteins such as heat shock proteins 70 and 90 (HSP70 and HSP90, respectively), ATP secretion, and the high mobility group box of non-histone chromatin protein 1 (HMGB1) are widely described. Collectively, DAMPs will recruit antigen presenting cells to the site of ICD induction and will stimulate uptake,

processing, and cross-presentation of dead-associated antigens, resulting in an adaptive immune response (**Figure 8**).

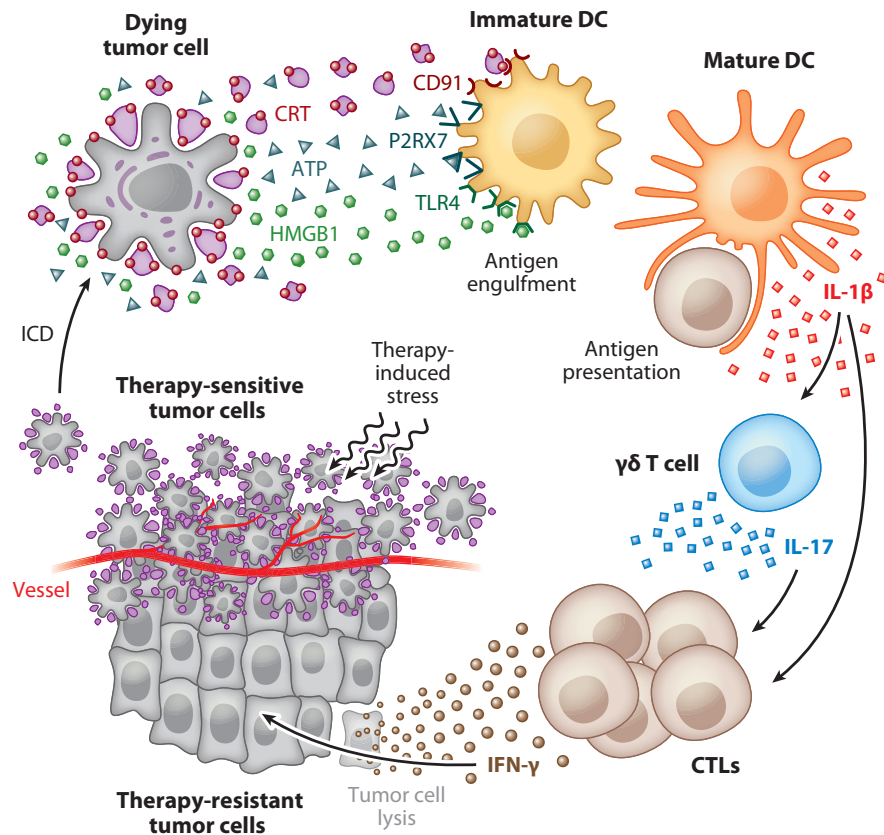


Figure 8. Immunogenic cell death in cancer treatment. Adapted from Kroemer & al. 2013.

With the aim of triggering immunogenic cell death, targeting the CD47-TSP1 axis might represent a promising strategy. If the TSP1-CD47 interaction has been reported to induce RCD, its possibility in inducing ICD has not received attention to date.

The thrombospondin-1–CD47 axis

Thrombospondins

Generalities of a matricellular protein

The ability of a tissue to adapt to enduring environmental challenges largely depends on the potential of local cells to modify their surroundings accordingly. Indeed, the extracellular matrix is constituted by molecules that cells produce and secrete locally to provide the tissues they conform structural and biochemical support (Frantz, Stewart and Weaver, 2010). Among these molecules, an important subset of non-structural, secreted, multi-domain, multifunctional proteins termed “matricellular proteins” can directly influence cell signaling in changing circumstances (Bornstein and Sage, 2002). Thrombospondins (TSPs), the first matricellular proteins to be described, are calcium-interacting matricellular glycoproteins that regulate a great variety of cellular functions during different stages of tissue remodeling events including development, aging and several pathophysiological processes (Adams and Lawler, 2011; Isenberg and Roberts, 2020).

Discovery of the thrombospondin protein superfamily

TSPs were discovered in platelet alpha granules as thrombin-sensitive proteins necessary for platelet aggregation (Baenziger, Brodie and Majerus, 1971). This first isolated TSP, thrombospondin-1 (TSP1, encoded by *THBS1*) was described to be a homotrimeric, multi-modular, calcium-sensitive protein encoded by a single gene (Phillips, Jennings and Prasanna, 1980; Margossian, Lawler and Slayter, 1981; Jaffe *et al.*, 1982). However, four more genes (*THBS2-5*) were later found to encode similar proteins in mammals (TSP2-5) (Bornstein *et al.*, 1991; Oldberg *et al.*, 1992; Vos *et al.*, 1992; Lawler *et al.*, 1993). These proteins are generally sub-classified as class A and class B TSPs, according to their tendency to oligomerize as homotrimers (TSP1 and TSP2) or homopentamers (TSP3, TSP4 and TSP5), respectively (**Figure 9**).

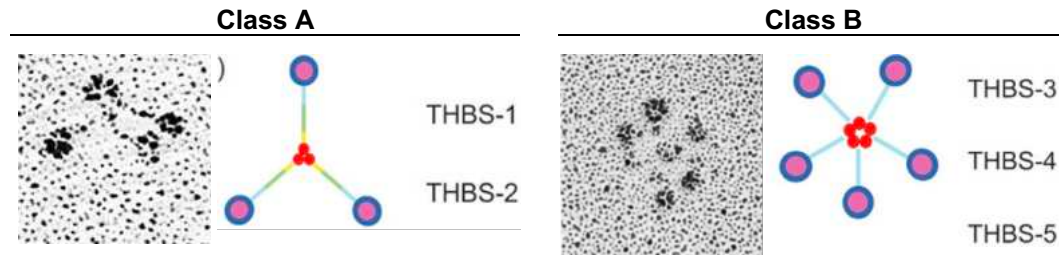


Figure 9. Classification of mammal's thrombospondins. Class A thrombospondins refer to TSP1 and TSP2, which naturally assemble as homotrimers. Class B thrombospondins refer to TSP3, TSP4, and TSP5/COMP, which assemble as pentamers. (Rotary shadowed microscopy images were taken from Lawler *et al.*, 1985, 1995 and illustrations from Carlson, Lawler and Mosher, 2008).

TSPs have been found to be extensively conserved across evolution, having apparently surged early in the evolution of animal multicellularity (Bentley and Adams, 2010; Adams and Lawler, 2011). Indeed, the emergence of a TSP superfamily at the origin of animal evolution has been recently proposed (Shoemark *et al.*, 2019) (**Figure 10**). This TSP superfamily is defined by the highly conserved C-terminal domain, generally referred to as the “signature domain”, which is composed by a globular carboxy-terminus, Ca^{2+} -interacting tandem repeats, and endothelial growth factor (EGF)-like modules. In this sense, the molecular architectures of all TSPs and TSP superfamily members are similar at the signature domain, but substantially differ as they approximate the N-terminal side. These differences consist in diverse modules that may or not be included in different TSPs (**Figure 10**), giving them tissue specificity while keeping their ability to interact with several proteic and non-proteic, cellular and extracellular matrix ligands in different spatiotemporal circumstances.

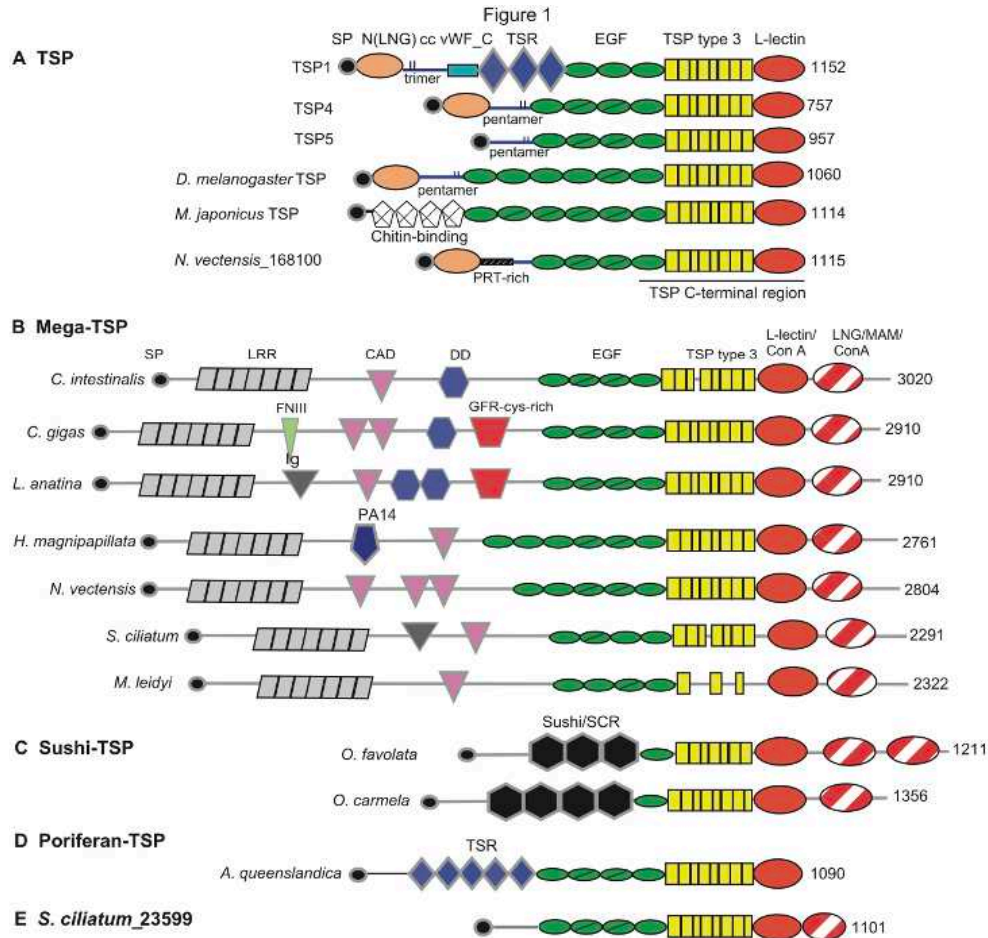


Figure 10. Domain architectures of the TSP family in mammals. (Extracted from Shoemark *et al.*, 2019)

Complexity of multi-modular interactions

Human TSPs have been the most largely studied to date and several cellular receptors and extracellular matrix ligands have been identified for each of their domains, although not for every TSP (**Figure 11**).

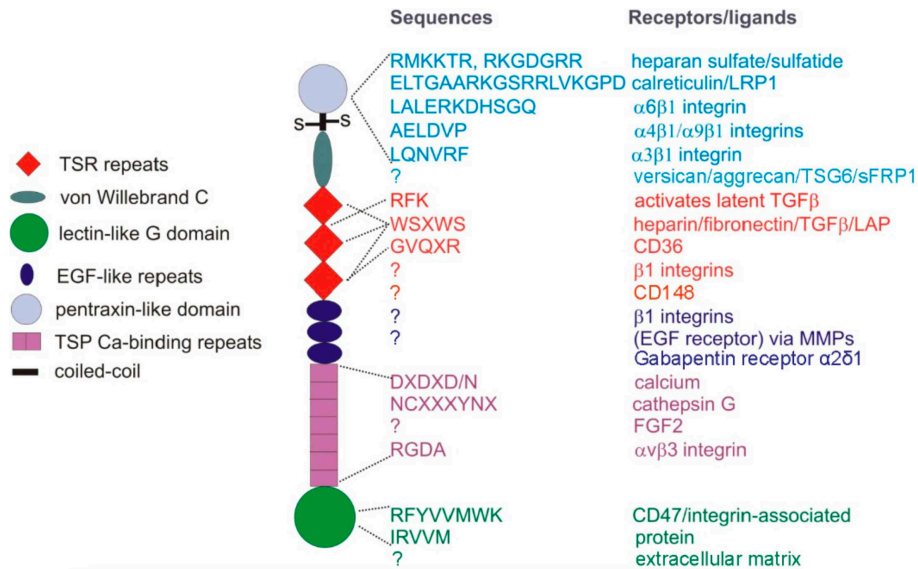


Figure 11. Class A TSP modules and their cell surface receptors or extracellular ligands. Class A TSPs contain all modules human, yet class B TSPs do not include all of them. The N-terminal pentraxin-like domain is not present in TSP5. The von Willebrand factor C and the type 1 TSP repeats (TSR) are only present in class A TSPs.

Together with their multi-ligand nature, their oligomerization ability supposes intricate interactions with cell receptor complexes in membranes of the same cell, but also with receptors in different cells and in different extracellular matrices. As a result of such complexity, there is not a unique role for a given TSP, in contrast, these vary in different tissues but even among cells according to their spatiotemporal circumstances, where different TSP receptors or ligands may or not be present (**Figure 12**).

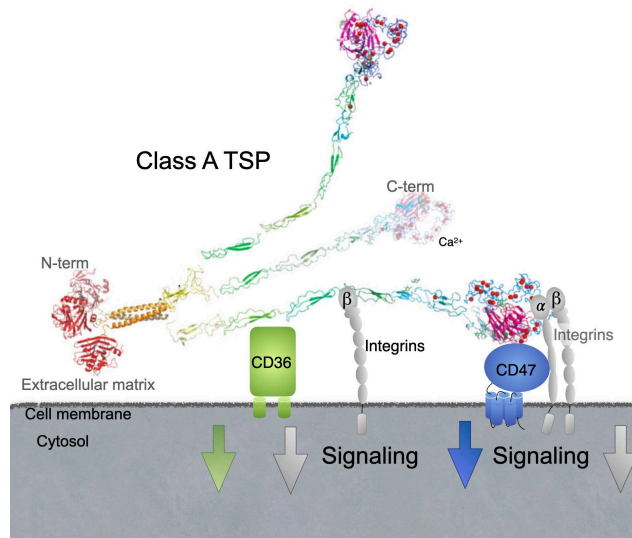


Figure 12. Complexity of simultaneous interactions of one TSP with several cell receptors. A class A TSP (Carlson, Lawler and Mosher, 2008), CD36, alpha and beta integrins and CD47 were chosen for cartoon exemplification.

TSPs and disease: the crucial role of the signature domain

The previous suggests different mechanisms for regulating TSP expression, and that dysregulation of any of these could lead to disease. Indeed, the expression of the different human TSPs varies in a multi-level, cell-specific, tissue-specific fashion within different stages of development, aging and pathophysiological processes including, cancer, inflammation, viral infection, wound healing, arterial injury, ischemia and reperfusion, heart hypertrophy, pulmonary arterial hypertension, Alzheimer's disease, diabetes and metabolic disorders, atherosclerosis, fibrosis, and skeletal and joints disorders (Stenina-Adognravi, 2014). However, the understanding of the mechanisms regulating their expression is largely incomplete to date.

Being TSP1 the first described TSP and playing determinant pathophysiological roles in the cancer microenvironment and during inflammation (Lopez-Dee, Pidcock and Gutierrez, 2011; Jeanne *et al.*, 2015; Huang *et al.*, 2017; Kaur *et al.*, 2021), compared to the other TSPs, the regulation of its expression has been the most studied to date. TSP1 expression is commonly associated to limiting cancer activities, as it is downregulated by

activated oncogenes and upregulated by various tumor suppressor genes (Insenberg and Roberts, 2020; Kaur *et al.*, 2021). Nevertheless, increasing evidence conversely depicts how TSP1 overexpression in the tumor microenvironment can play pro-tumorigenic roles via interaction with its receptors (Jeanne *et al.*, 2015; Huang *et al.*, 2017).

The opposing roles that TSP1 play in cancer illustrate the complex interplays that TSPs orchestrate during tissue remodeling, largely characterized by regulation of cell proliferation and death processes. Certainly, TSP1 deficiencies are also implicated in diseases associated to incorrect tissue development, remodeling, or repair, such as familial pulmonary artery hypertension, post-refractive surgery chronic ocular surface inflammation, familial premature myocardial infarction, and sickle cell disease (Insenberg and Roberts, 2020). Interestingly, ancient TSPs are also crucial for these processes in basal metazoan (e.g. TSP is crucial for hydra head regeneration) although they only share comparable signature domains with TSP1 (Shoemark *et al.*, 2019; **Figure 10**).

Moreover, many genetic alterations of other human TSPs that are associated to similar diseases occur within the signature domain (Adams & Lawler, 2008). Such is the case of *THBS5* gene, for example, for which >100 mutations in the signature domain are associated with the hereditary diseases pseudo-achondroplasia and multiple epiphyseal dysplasia (Posey *et al.*, 2004; Kennedy *et al.*, 2005). Another example is the increased risk to suffer familial premature coronary artery disease of patients with nonsynonymous single-nucleotide polymorphisms in the regions of *THBS1* and *THBS4* genes (Topol *et al.*, 2001). This poses a clear interest for this protein domain and its ligands in the field of medicine and drug development against cancer and diseases involving inflammation-related tissue remodeling processes.

Structure of the thrombospondins' signature domain

The signature domain of TSPs is composed of three modules: a globular lectin-like sequence at its C-terminus, aspartate-rich tandem repeats prompt to interaction with Ca²⁺ and one or several EGF-like modules at the N-terminus (**Figure 13A**). The crystal

structures of soluble recombinant signature domains of TSP1, TSP2 and TSP5/COMP have been solved, yet not all of them included the same modules. The crystal of TSP1 included the globular C-terminus and part of the calcium binding repeats (Kvansakul, Adams and Hohenester, 2004); the one of TSP2 comprised the globular C-terminus, all calcium binding repeats and the three EGF-like modules (Carlson *et al.*, 2005); and that of TSP5/COMP consisted of the globular C-terminus, the calcium-binding repeats and the last EGF-like repeats (Tan *et al.*, 2009). As expected from their highly conserved sequence identity, the three of them show a similar conformation, consisting of a prototypic globe that is semi-wrapped by a Ca^{2+} -binding wire and ends with an EGF-like stalk. (**Figure 13B**).

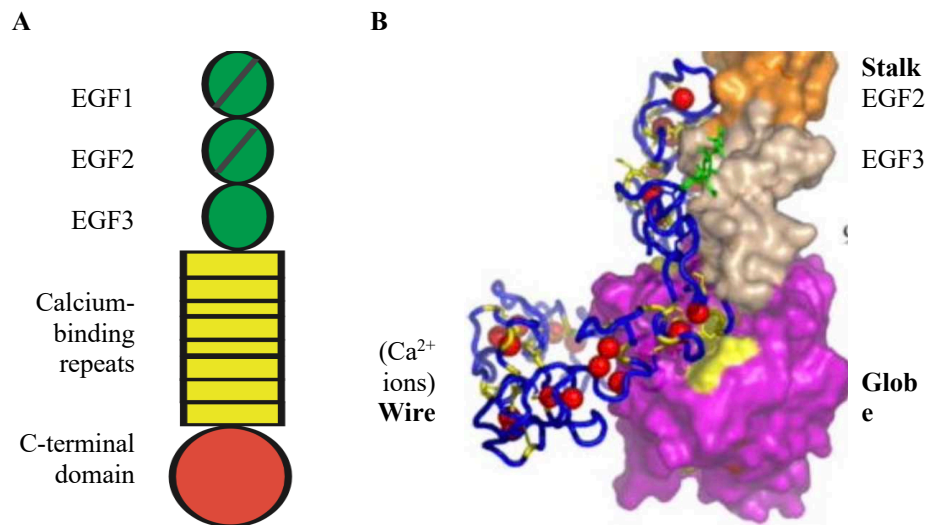


Figure 13. The thrombospondin signature domain. Schematic representation (A) and representative crystal structure (B) of the thrombospondin signature domain. C-terminus in magenta; Calcium binding wire in blue; EGF3 in beige and EGF2 orange; calcium ions are red spheres; note that there are calcium ions in the bottom of the globe). (Carlson, et al. Nat Struct Mol Biol, 2005).

The globular C-terminus: a ligand of CD47

Among the TSP signature domain substructures, the C-terminal globe is the most highly conserved across evolution (**Figure 14**). The globular C-terminus of TSPs is composed of two beta sheets with seven beta strands each, spaced by a small alpha helix

and folded in a wrapped candy-like fashion (Kvansakul, Adams and Hohenester, 2004; Carlson *et al.*, 2005; Tan *et al.*, 2009).

The transmembrane protein CD47 is the only known receptor for this domain (Gao *et al.*, 1996), and two peptide sequences termed 4N1 (RFYVVMWK) and 7N3 (FIRVVMYEGK), that constitute the last beta strands of each beta sheet, have been proposed to be responsible of the TSP1-CD47 interaction (Kosfeld and Frazier, 1993). Several lines of research have later provided immunoprecipitation and microscopical evidence of the TSP1-CD47 interaction (Kaur *et al.*, 2011, 2021; Martinelli *et al.*, 2013; Soto-Pantoja, Kaur and Roberts, 2015). However, long after its identification, a mystery prevails around its mechanics, as 4N1 and 7N3 strands are hidden within the three-dimensional structure of the TSP globe (Kvansakul, Adams and Hohenester, 2004; Carlson *et al.*, 2005; Tan *et al.*, 2009), and no crystal structure of the interaction with CD47 or any other protein is available to date. TSP1 requires the extracellular domain of CD47 to induce cell signaling (Mateo *et al.*, 2002), however surface plasmon resonance experiments using recombinant CD47 extracellular domain and TSP1 signature domain proteins did not reflect binding (Adams *et al.*, 2008). However, it was later found that detergent-stable, high affinity binding, necessary for immunoprecipitation of CD47 with TSP1, only occurs in a CD47 isoform containing an *o*-glycosaminoglycan modification in Ser64 (Kaur *et al.*, 2011).

Globular carboxy-terminus

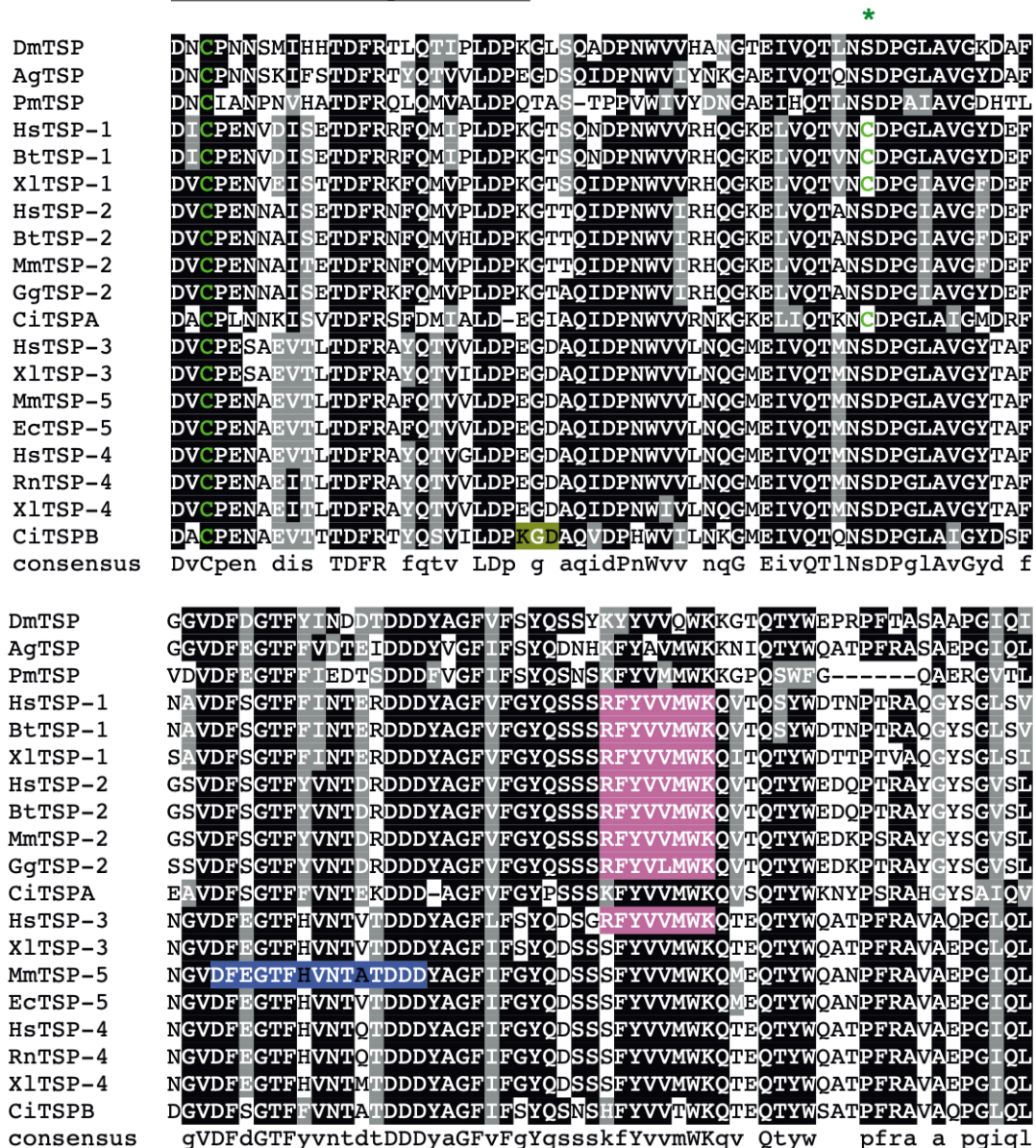


Figure 14. CLUSTAL W alignment of thrombospondins C-terminus. The alignment was prepared in CLUSTALW, and the 50% identity consensus is shown below the aligned sequences. Black highlighting indicates identical residues, grey indicates conserved similar residues and white background indicates unrelated amino acids. Cysteines are in green, with Cys 974 of TSP-1 indicated with an asterisk. KGD motifs in olive, the protease-binding motifs from TSP-1 in aquamarine, the collagen-IX binding motif from TSP-5 in blue and the CD47-binding motifs identified from TSP-1 peptides are in mauve.

(Continued in next page).

```

DmTSP      KLVNSTEGPGPMRNSLWHEGNTDGEARLLWKDPKNIAWKERTSYRWSLVHRPATGLIRL
AgTSP      KLINSATGPGEMLRNSLWHTGDTKGQVLLWKDPRNVGWTERAYRWLLLRHPKIGLIRL
PmTSP      KLIDSATGPGTALRDALWLTGSIITNOATLLWHDSSIGWTPKVAIRWLLHRPDIIGMRF
HsTSP-1    KVVNSTTGPGGELRNALWHTGNTSGQVRTLWHDPRHIGWKDFAYRWRLSHRPKTGFIRV
BtTSP-1    KVVNSTTGPGGELRNALWHTGNTSGQVRTLWHDPRHIGWKDFAYRWRLSHRPKTGFIRV
XlTSP-1    KVVNSTSGPGGELRNALWHTGNTSGQVRTLWHDPRHIGWKDFAYRWHLTHRPKTGFIRV
HsTSP-2    KVVNSTTGTGGEHLRNALWHTGNTSGQVRTLWHDPRNIGWKDYAYRWHLTHRPKTGYIRV
BtTSP-2    KVVNSTTGTGGEHLRNALWHTGNTSGQVRTLWHDPRNIGWKDYAYRWHLTHRPKTGYIRV
MmTSP-2    KVVNSTTGTGGEHLRNALWHTGNTSGQVRTLWHDPRNIGWKDYAYRWHLIHRPKTYMRV
GgTSP-2    KVVNSTTGTGGEHLRNALWHTGNTSGQVRTLWHDPRNIGWKDYAYRWHLIHRPKTGLIKV
CiTSPA     KVVNSTSGTG-EARNALWHTGDTKNEVRLTWYDDMCQGWDRDYAYRWHLQHRPETGFIRV
HsTSP-3    KAVTSVSGPGGELRNALWHTGHTPDQVRLWHDPRNVGWRDKTSYRWQLLRHPQVGYIRV
XlTSP-3    KAVKSTTGPGGELRNALWHTGHTPDQVRLWHDPRNVGWRDKTSYRWQLMRHPQVGYIRV
MmTSP-5    KAVKSSTGPGGELRNALWHTGHTPDQVRLWHDPRNVGWRDKTSYRWFLQHRPQVGYIRV
EcTSP-5    KAVKSSTGPGGELRNALWHTGHTPDQVRLWHDPRNVGWRDKTSYRWFLQHRPQVGYIRV
HsTSP-4    KAVKSKTGPGGELRNALWHTGHTPDQVRLWHDPRNVGWRDKVSYRWFLQHRPQVGYIRV
RnTSP-4    KAVKSKTGPGGELRNALWHTGHTPDQVRLWHDPRNVGWRDKVSYRWFLQHRPQVGYIRV
XlTSP-4    KAVKSKSGPGGELRNALWHTGHTPDQVRLWHDPRNVGWRDKVSYRWFLQHRPQVGYIRA
CiTSPB     KAVNSNKGPGERMRNALWHSGDITKDEVKVLWSDPMNQGWEDKTSYRWELQHRPQVGYIRI
consensus  KlvnSttGpGehlRnaLWhtG T qvrlLwkdPrnigWkdrtaYRW L HRP iGyirv

```

```

DmTSP      QMHEGNRLIFDSCNVFDSTLKGGRIGVFCFSQRMIIWSNLOYRCNRRVKPLIYNDLSDYLKTKVELQD
AgTSP      RIFDGDQMVADSGIFDITLKGGRIGVFCFSQEMI IWSDL YRCNDNVPESDLRAASEL
PmTSP      YLYQGNNQVIFDSCNIYDSTLKGGRIGLFCFSQKQI IWSNVKYS SDDVPQDMFNDLPTNLQTVLTS
HsTSP-1    VMYEGKKIMADSGPIYDKTYAGGRLGLFVFSQEMVFFSDLKYEGRDP-----
BtTSP-1    VMYEGKKIMADSGPIYDKTYAGGRLGLFVFSQEMVFFSDLKYEGRDS-----
XlTSP-1    VMYEGKRVADSGPIYDKTYAGGRLGLFVFSQEMVFFSDLKYEGRDS-----
HsTSP-2    LVHEGKQVMADSGPIYDQTYAGGRLGLFVFSQEMVYFSDLKYEGRDI-----
BtTSP-2    LVHEGKQVMADSGPIYDQTYAGGRLGLFVFSQEMVYFSDLKYEGRDV-----
MmTSP-2    LVHEGKQVMADSGPIYDQTYAGGRLGLFVFSQEMVYFSDLKYEGRDA-----
GgTSP-2    LVYEGKQVMVDSGPIYDTTFAGGRLGLFVFSQEMVYFSDLKYEGRDA-----
CiTSPA     TMYE-KDLLVDSGALYDKTFAGGRI GFFIFFSQEMVFFSDMEYMKDIT-----
HsTSP-3    KLYEGPQLVADSGVLIIDTSMRGGRLGVFCFSQENI IWSNLOYRCNDTVPEDFEPFRQLQGRV
XlTSP-3    KLYEGVDLVADSGVLIIDTSMRGGRLGVFCFSQENI IWSNLOYRCNDTIPEDFEPYRRLLDGKN
MmTSP-5    RFYEGPELVADSNVLDTSMRGGRLGVFCFSQENI IWANLRYRCNDTIPEDYESHRLQRV
EcTSP-5    RFYEGPELVADSNVLDTSMRGGRLGVFCFSQENI IWANLRYRCNDTIPEDYEQRLQQA
HsTSP-4    RFYEGSELVADSGVTIDTSMRGGRLGVFCFSQENI IWSNLKYRCNDTIPEDFQEFQTFQDFRDN
RnTSP-4    RFYEGSELVADSGVTIDTSMRGGRLGVFCFSQENI IWSNLKYRCNDTIPEDFQEFQTFQDFRDLN
XlTSP-4    RFYEGTELVADSGVTVDTSMRGGRLGVFCFSQENI IWSNLKYRCNDTIPEDFQAFQAQFSS
CiTSPB     RFRKSNMIADIGPVLDDTVKGGRLGVFCFSQENI IWSNLMYRCNDTLPESAVTSRPASREAV
consensus  myeg liaDsg ifDstlkGGRIGvFcFSQemiwsnlkYkCndsv

```

(Continues) Figure 14. CLUSTAL W alignment of thrombospondins C-terminus. Ag, Anopheles gambiae; Bt, Bos taurus; Ci, Ciona intestinalis; Dm, Drosophila melanogaster; Ec, Equus caballus; Gg, Gallus gallus; Hs, Homo sapiens; Mm, Mus musculus; Pm, Penaeus monodon; Rn, Rattus norvegicus; Xl, Xenopus laevis. (Continued in next page).

Unidentified protein folding mechanisms might explain TSP1 interaction with CD47. Molecular modeling studies have suggested that TSP1 globe undergoes discreet conformational changes when in close contact with the cell membrane, which allows exposure of the 4N1 peptide to the solvent (Figure 15) (Floquet *et al.*, 2008). Moreover,

higher content of beta sheets and solvent-accessible surface in the globe of a putative TSP1 signature domain in the absence of calcium were also predicted in another molecular modelling (Gupta *et al.*, 2017).

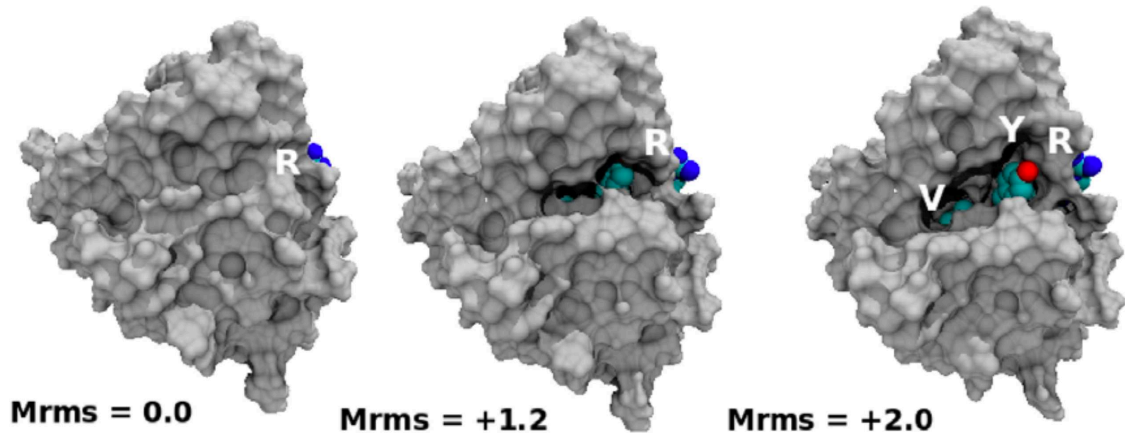


Figure 15. 4N1 cleft opening and exposure to the solvent. (Floquet *et al.* 2008)

Although these changes have not been measured experimentally, they provide an overview of this interaction (Figure 16), which accounting to its molecular complexity has not yet been crystallized.

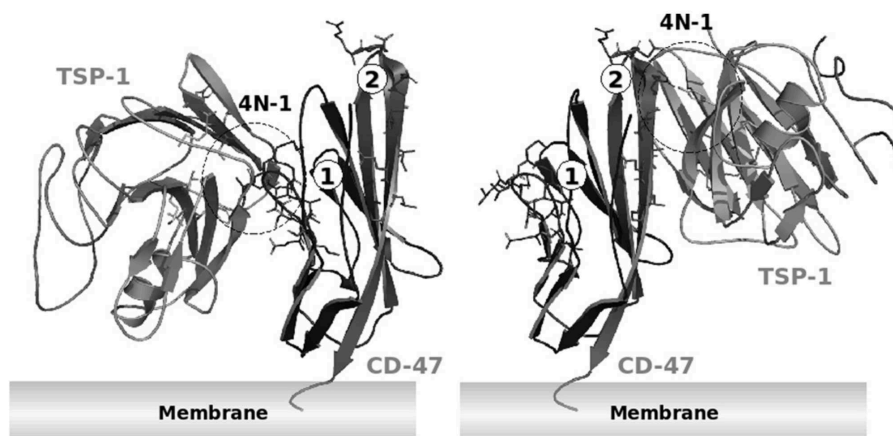


Figure 16. Putative TSP1-CD47 interaction regions. Two different regions of CD47 (1 and 2) proposed to interact with the 4N1 peptide (extracted from Floquet *et al.*, 2008).

Of note, although CD47 is not an evolutionarily ancient receptor of TSPs (Bentley and Adams, 2010), except for the arginine residue, the 4N1 sequence is extremely conserved across evolution (**Figure 14**). This is not the case of 7N3, which is only present in TSP1 (**Figure 14**). TSP1 is a better cell signal inducer than TSP2 and TSP4, yet all of them induce signaling (Jeff S Isenberg *et al.*, 2009), suggesting that 7N3 is important, yet dispensable for TSP binding to its receptor. Using structure-activity relationship (SAR) studies, our team recently identified that the highly conserved amino acid sequence part of 4N1 is necessary for efficient membrane binding and consequent cell death activity of 4N1-based peptide-mimics (Denèfle *et al.*, 2016). Similar studies have not been reported for 7N3. Moreover, recent studies using super-resolution fluorescence microscopy have evidenced co-localization of a 4N1-derived peptide construct with CD47 in membrane clusters (Wang *et al.*, 2020).

A DDD motif that is also highly conserved from basal metazoans to mammals (**Figure 14**) contains the only calcium ions that bind to the globe, and it is exposed to the surface of the crystal structures of TSP1 (Kvansakul, Adams and Hohenester, 2004), TSP2 (Carlson *et al.*, 2005) and TSP5/COMP (Tan *et al.*, 2009). Interestingly, this motif directly interacts with the lysine of the 4N1 strand (**Figure 17**), however, the role of this motif is largely unexplored.

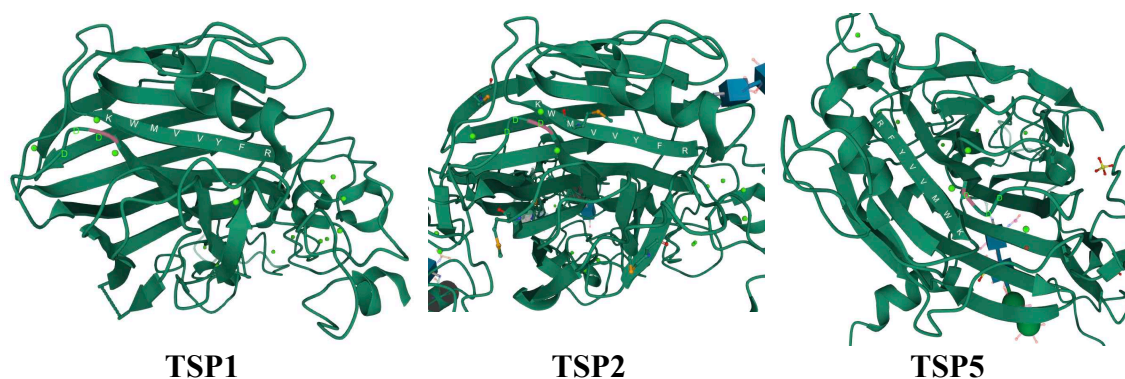


Figure 17. DDD-4N1 interaction. Crystal structures of the three TSP C-terminal domain available to date (TSP1, TSP2 and TSP5) show that a highly conserved DDD motif interacts with the 4N1 peptide within its three-dimensional structure. DDD motif and Ca^{2+} ions are shown in phosphorescent green; amino acids that conform the 4N1 beta strand are shown with white letters; the Asp residue responsible for the interaction is shown in pink.

The team of Dr. Adams, has suggested that this motif is involved in RGD-independent and CD47-independent cell attachment (Adams *et al.*, 2008). To assess this, they used a recombinant protein (termed Type3₅₋₇GCT) that incorporates the TSP1 globe and three last tandem repeats of the wire (thus, including both the DDD and an RGD motif), as well as VGD/RGD and AAA/DDD mutants of this protein with overall similar secondary structures to evaluate their attachment to cells coming from murine skeletal myoblasts (C2C12), human arterial smooth muscle, and murine dermal fibroblasts from wild-type and CD47 deficient (*Cd47^{tm1Fpl}*) mice. Cell attachment was drastically reduced in all cases where the plates were coated with the VGD/RGD or the AAA/DDD mutants, suggesting that the DDD motif is directly implicated in cell attachment.

Altogether, the previous evidence suggests the existence of a misunderstood, probably complex, protein folding mechanism in one or both proteins that surged during the evolution of vertebrates and enabled the TSP1 signature domain to interact with CD47, and therefore, probably with other unidentified transmembrane proteins evolutionarily related to this receptor, such as presenilins and immunoglobulins. However, as CD47 is the only known receptor and signal transducer of the TSP C-terminal domain, in the following pages, the known functions of CD47 will be described. Yet, similar to TSPs, which play diverse roles that are CD47-independent, CD47 has pharmacologically relevant, TSP1-independent functions that TSP1 regulate when competing for binding. These will be mentioned as well.

CD47

Generalities of its interactions

CD47 is a transmembrane glycoprotein member of the immunoglobulin superfamily that is expressed ubiquitously and plays several roles in the immune system of mammals. It is the only known cell receptor of the TSP1 C-terminal domain, and a counter-receptor of the signal-regulatory protein alpha (SIRP α) (Matozaki *et al.*, 2009). CD47 controls signaling pathways that modulate cell responses to stress and cell differentiation, as well as cellular functions including cell adhesion (e.g., platelet activation) and motility (e.g., leukocyte migration), principally through its interaction with TSP1 (Soto-Pantoja, Kaur and Roberts, 2015).

CD47 is composed of an extracellular immunoglobulin variable (IgV)-like N-terminus, five membrane-spanning domains with important presenilin homology, and an intracellular C-terminus where alternative splicing occurs, leading to four isoforms (Roberts *et al.*, 2012). Based its cloned sequence, it was predicted that the extracellular domain of CD47 contains seven N-glycosylation sites, and two functionally conserved disulfide bridges maintain the three-dimensional structure of the CD47 extracellular domain. One of these bonds locates near the N-terminus and links the extracellular domain with the extracellular part of the last (C-terminal) membrane-spanning domain (**Figure 18** left) (Brown and Frazier, 2001). Functional CD47–SIRP α interaction and mediated CD47 signaling in T cells depends on this bond (Rebres *et al.*, 2001). When the crystal structure of the CD47–SIRP α interaction was solved (Hatherley *et al.*, 2008), it was shown that the second bridge, which links Cys23 of the second C-terminal-most beta strand with the Cys96 of the rest of the domain, is important for correct folding of the contact site, and hence necessary for interaction with SIRP α (**Figure 18** right). Whether this long-distance disulfide bridge is necessary for TSP1 was not reported.

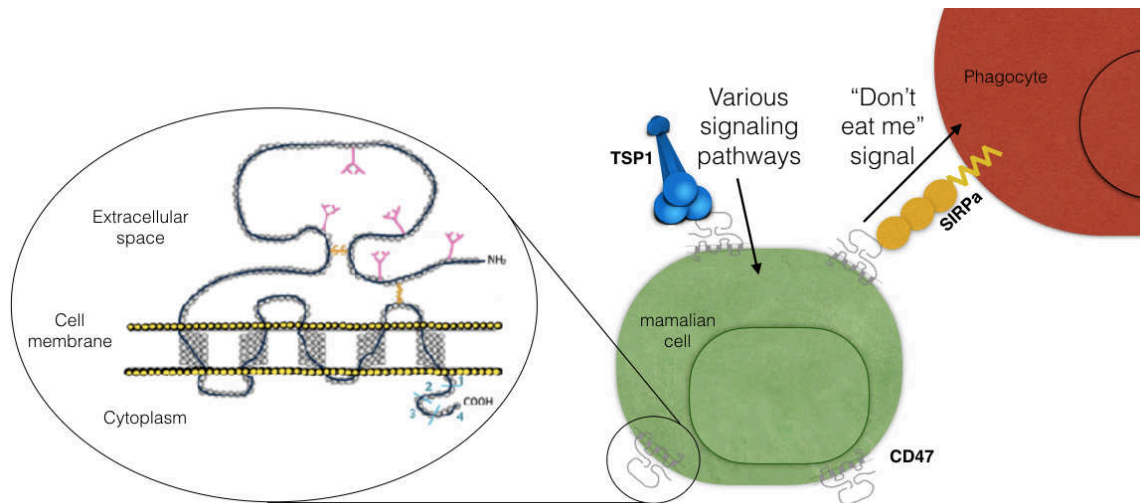


Figure 18. Ligands of CD47. Left. CD47 cartoon showing glycosylation sites (pink), disulfide bridges (yellow), and alternative splicing forms at the intracellular C-terminal domain. Right. In mammalian cells, CD47 can interact with the C-terminal domain of TSP1 (blue) and send “outside-in” signals. CD47 also serves as a counter-receptor for SIRP α . SIRP α is a transmembrane receptor mainly expressed in monocytes and macrophages, although it is also present at a lesser extent in dendritic and bone marrow progenitor cells, and in neurons, principally within the sites of synapsis (Barclay and Van den Berg, 2014). It consists of three connected extracellular domains and a unique transmembrane domain that links them to the intracellular domain. The extracellular domain that is most distal to the plasma membrane is of an IgV-type, and the remaining two that are closer to cell membrane are of an Ig constant-type. The intracellular domain of SIRP α contains four inhibitory motifs that are susceptible to interacting with phosphotyrosine phosphatases (dephosphorylation phosphoproteins) after extracellular stimulus by CD47 or anti-SIRP α antibodies that bind to the IgV-like domain. These stimuli regulate intracellular inhibition of phagocytosis cascade and is known as the “don’t eat me” signal (Barclay and Van den Berg, 2014).

Based on the contact sites of the CD47–SIRP α structure and the posttranslational modification of CD47 at Ser64, required for its immunoprecipitation TSP1 (Kaur *et al.*, 2011), it is predicted that the binding site of CD47 with TSP1 locates far from that of SIRP α . However, in Jurkat (and in CD47-defective JinB8) T cells, the whole TSP1 and the TSP1 signature domain, compete for binding with a recombinant SIRP α protein containing its three extracellular domains, and with the B6H12 anti-CD47 antibody (Isenberg *et al.*, 2009). Initial studies using full length CD47 in nanodisc membrane platforms have recently claimed to reach a 40 nM affinity with TSP1, for which cryo-EM

structure analysis is being pursued, yet no evidence is currently available to the public (Young *et al.*, 2020).

Interestingly, crystallization of CD47 IgV alone rendered CD47–CD47 complexes stabilized by a “strand swap” between two different molecules (Hatherley *et al.*, 2008). Before the interactions of this crystal was known, it had been proposed that CD47 from two different cells could interact homotypically (Rebres, Kajihara and Brown, 2005). Although CD47 IgV dimerization was considered to be artificial of the technique, a similar complex has been observed in crystals of CTLA-4, which is also a member of the immunoglobulin superfamily (Sonnen *et al.*, 2010). Moreover, it has been suggested that CD47 could undergo conformational changes that leads to differential interaction and signaling in erythrocytes (Burger *et al.*, 2012). An exciting speculation is that CD47 could undergo conformational changes when clustering, and that this could affect its interaction with TSP1, SIRP α , or even leading to interactions with other unknown ligands. However, this has not been sufficiently explored.

A therapeutic target in cancer

Role of CD47 as an extracellular “don’t eat me” signal sender

Although CD47 regulates outside-in signaling regulating several cellular functions in the cell that expresses it, it is most known for its passive role as an extracellular sender of “don’t eat me” signals when it interacts with SIRP α in the membranes of phagocytes (including, but not limited to macrophages and dendritic cells). This signal withholds phagocytosis and is largely regulated by differences in CD47 and SIRP α expression, which modulate the intensity of the signal (Barclay and Van den Berg, 2014). The pathways that control CD47 expression, however, are not completely understood, but several cytokines (e.g., TNF α , IFN γ , IL-6), oncogenes (e.g., HIF-1, MYC, NF κ B), micro RNAs (e.g., miR-708, miR-155, miR-200a), and enzymes (e.g., isoQC) can regulate CD47 expression at different levels in cancer (Huang *et al.*, 2020).

The “don’t eat me” signal is physiologically counter-regulated by the expression of “eat-me” signals, such as those sent by phosphatidylserine (PS) and calreticulin exposure. In erythrocytes, for example, high levels of CD47 are found in nascent and healthy, viable cells, but decreases with ageing and senescence; conversely, PS exposes with ageing, during infection, and in dying erythrocytes, enabling macrophages to recognize and eliminate them, dictating their lifespan (Arias and Arias, 2017). This also has pathophysiological implications in cancer. For example, circulating hematopoietic stem cells upregulate CD47 expression in their cell surface during their journeys through the bloodstream to avoid phagocytosis, and several types of leukemia do it as well, and CD47 overexpression correlates with their progression (Jaiswal *et al.*, 2009). Indeed, several types of solid and liquid cancers overexpress CD47, evading innate immune recognition, and clinically correlating with poor prognosis (Majeti *et al.*, 2009; M. P. Chao *et al.*, 2010; Chao, Weissman and Majeti, 2012; Willingham *et al.*, 2012). In many of these cases, CD47 expression seems to be a counterbalance of calreticulin exposure (Mark P Chao *et al.*, 2010). Therefore, it has been proposed that CD47 blockade with monoclonal antibodies can be a therapeutic strategy to disrupt this compensation and restore innate immune system-mediated phagocytosis of several types of cancers (Chao, Weissman and Majeti, 2012; Willingham *et al.*, 2012). However, innate responses are not sufficient to explain the antitumor effects of these strategies, as targeting CD47 with monoclonal antibodies in immunocompetent mice improves the outcome compared to immunodeficient mice by triggering adaptive immune system-mediated tumor destruction (Tseng *et al.*, 2013; Liu *et al.*, 2015). Based on the previous, CD47 represents an immune checkpoint for tumor evasion (**Figure 19**). Currently, several phase I and phase II clinical trials evaluate humanized monoclonal antibodies that block the CD47–SIRP α axis to treat a variety of cancers (Jalil, Andrechak and Discher, 2020), and other approaches based on recombinant proteins, peptides (Hazama *et al.*, 2020) and small molecules (Cabrales, 2019; Oronsky *et al.*, 2019, 2021; Lee *et al.*, 2021; Yu *et al.*, 2021) aiming to downregulate this interaction are also being assessed clinically and preclinically.

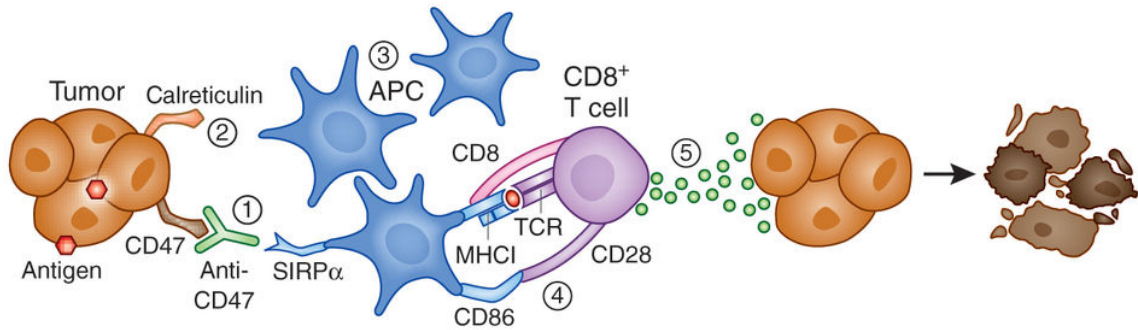


Figure 19. The CD47 immune checkpoint. CD47 blocking antibodies (1) and pro-phagocytic molecules such as calreticulin (2) cooperate to enhance tumor engulfment by APCs (3), enabling the processing and presentation of tumor antigens as peptides in the groove of MHC class I molecules (4) and the priming of CD8⁺ T cells specific for tumor antigens (5). MHC, major histocompatibility complex; TCR, T cell receptor. (Extracted from Vonderheide, 2015).

CD47 outside-in signaling

CD47 is more than a passive extracellular marker, and, although relevant in the cellular microenvironment, the sole differences in CD47 expression are largely insufficient to explain its pathophysiological roles. Indeed, CD47 controls a variety of intracellular signaling pathways that are activated by extracellular ligands. Some of these have been shown to be controlled by SIRP α , but the vast majority are largely governed by its interaction with TSP1 (**Figure 18**) and its lateral partners (Gardai *et al.*, 2005; Sarfati *et al.*, 2008; Murata *et al.*, 2014; Soto-Pantoja, Kaur and Roberts, 2015). Interaction of CD47 with its lateral partners is essential for some CD47 activities or the function of its partner, which expands the number of CD47-dependent signaling pathways.

Different to CD47, which is expressed ubiquitously, its lateral or intracellular binding partners are expressed differentially among cell types and particular spatiotemporal circumstances that regulate their expression and the expression of TSP1 in the microenvironment. This can directly regulate CD47 functions either by activating it or by perturbing its interactions with lateral partners and the signaling associated to them. I propose to call these CD47 “outside-in” signaling (as it is referred to integrin signaling after activation by ligands of the extracellular matrix) due to its functional similarities with integrin activation that regulate cell structural stability, motility, and responses to stress.

This has been previously proposed for G protein-coupled receptors (GPCRs) crosstalk with integrins (Shen, Delaney and Du, 2012), but, CD47 can regulate similar functions even in cells that do not express integrins, such as erythrocytes. In the following paragraphs a selection of signals with systemic implications will be presented.

CD47 outside-in signaling in erythrocytes

CD47 is necessary for correct erythrocyte physiology (Oldenborg, 2004, 2013; Kim *et al.*, 2018), where it is part of the Rhesus (Rh) antigen complex (Lindberg *et al.*, 1994). CD47 maintains erythrocyte stability within the band-3 based macrocomplex (Bruce *et al.*, 2003) via the protein 4.2, which links this complex to the erythrocyte skeleton (Dahl *et al.*, 2004). The stability of this complex is presumed to be regulated during erythropoiesis by the expression of different isoforms of the intracellular CD47 domain which will dictate their differentiation (Mordue *et al.*, 2017). This suggests that CD47-mediated intracellular signaling plays important roles in erythrocyte maturation.

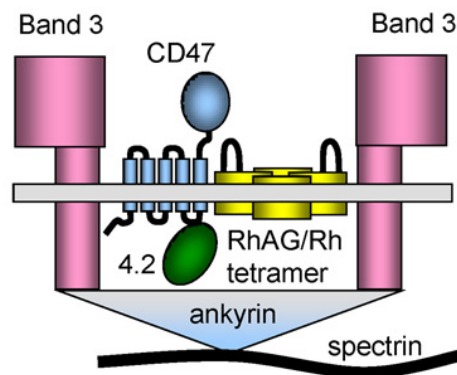


Figure 20. CD47 in the band 3 macrocomplex. (Adapted from Soto-Pantoja, Kaur and Roberts, 2015)

The role of CD47 as a “don’t eat me” signal was first proposed in erythrocytes, where it plays crucial roles preventing SIRP α -mediated macrophage erythrophagocytosis (Oldenborg *et al.*, 2000). However, it has been proposed that CD47 could undergo conformational changes during ageing that favor its interaction with TSP1, leading to converse, outside-in pro-phagocytic signals (Burger *et al.*, 2012). Recent evidence using

super-resolution fluorescence microscopy indicates that CD47 cluster formation augments in aged erythrocytes, enabling stronger interaction with TSP1 and a TSP1 peptide-construct based on 4N1K and provoking morphological changes in the erythrocyte (Wang *et al.*, 2020). The authors suggest that these interactions may compete with SIRP α , impairing “don’t eat me” signals and enabling phagocytosis of aged erythrocytes. Finally, another recent report shows that TSP1-mediated CD47 activation in erythrocytes induces a Ca²⁺ and nitric oxide influx that leads to cell deformability (Bissinger *et al.*, 2020). Therefore, in erythrocytes, CD47 is a structural molecule that crucially controls cell fate and lifespan.

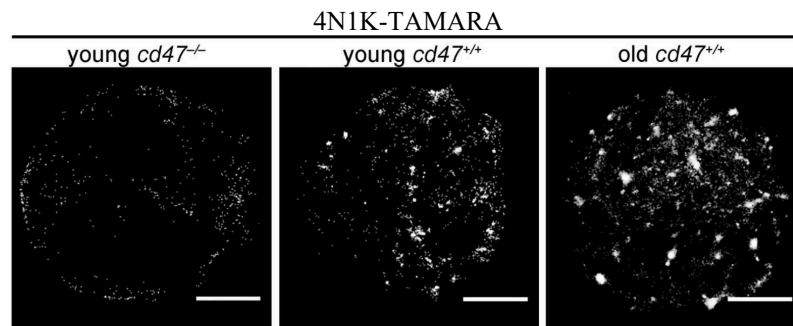


Figure 21. TSP1 peptide construct (4N1K-TAMARA) reveals CD47 cluster formation on aged erythrocytes. (Extracted from Wang *et al.*, 2020)

Integrin-associated CD47 outside-in signaling

Unlike erythrocytes, which do not express integrins, CD47-mediated signaling pathways in different cell types are related to its lateral interaction with integrins, owing to this its historical recognition as an integrin-associated protein (**Figure 22**) (Brown and Frazier, 2001). Lateral associations of CD47 with integrins are necessary in various cell types to induce TSP1-mediated CD47 signals regulating cell-cell and cell-matrix interactions. Indeed, CD47 was first described after immunoprecipitated with $\alpha_v\beta_3$ integrins, whose presence enhanced RGD-mediated neutrophil phagocytosis (Brown *et al.*, 1990). Later, CD47 was found to be physically and functionally associated to other integrins, including $\alpha_{IIb}\beta_3$, which is usually in complex with focal adhesion kinase (FAK), Syk, and Src (Chung, Gao and Frazier, 1997), $\alpha_2\beta_1$ (Wang and Frazier, 1998), and $\alpha_4\beta_1$ (Li *et al.*, 2002; Brittain *et al.*, 2004).

CD47 physically associates with β_3 integrins and heterotrimeric G_i proteins (Frazier *et al.*, 1999) in various cell types. In lipid rafts, this association requires the transmembrane and the intracellular domains, which regulate cell attachment in a way dependent on G_i signaling; but outside rafts, only the extracellular domain associates with integrins, and CD47 engagement indirectly leads to integrin clustering and associated Lyn, Src and SHP2 activation (McDonald, Dimitry and Frazier, 2003).

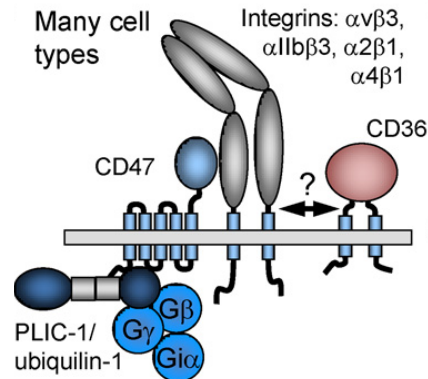


Figure 22. CD47: an integrin-associated protein. In many cell types, CD47 has been found to interact laterally with different integrins, which in turn may interact with CD36 (a complex containing the three receptors has not been directly reported, e.g., by immunoprecipitation, this uncertainty is denoted with a question mark), and intracellularly with PLIC-1/ubiquilin-1 and heterotrimeric G proteins. (Adapted from Soto-Pantoja, Kaur and Roberts, 2015)

Ubiquilin-1, first described as a protein linking CD47 with the cytoskeleton (abbreviated as PLIC-1), directly interacts with the intracellular domain of CD47 in this complex (Wu *et al.*, 1999). In Jurkat cells, exogenous overexpression of ubiquilin-1 inhibited CXCL12-mediated PLC activation and CXCR4 internalization, as well as G_i coupled receptor-mediated chemotaxis, and specific $G\beta\gamma$ -dependent intracellular Ca^{2+} influx, suggesting that ubiquilin-1 is a negative regulator of CD47 signaling (N'Diaye and Brown, 2003). Interestingly, a recent study demonstrated that CXCR4 ligation with CXCL12 controls CD47 turnover in mesothelioma and colon cancer (Mezzapelle *et al.*, 2021). An interesting question raising from this is whether differences in ubiquilin-1 or its related molecular signaling could control CD47 turnover during cancer progression.

Cardiovascular functions of CD47 outside-in signaling

Nitric oxide (NO) is central for correct control of vascular functions, hemostasis, muscle contractility regulation, tissue remodeling, and metabolism of cardiac and vascular tissue (Farah, Michel and Balligand, 2018). Therefore, deficiencies in NO signaling are associated to cardiac and vascular diseases such as coronary heart disease, coronary artery disease, myocardial infarction, erectile dysfunction, atherosclerosis, hypertension, cerebrovascular diseases and diabetic lesions (Cheng *et al.*, 2014, 2020; Farah, Michel and Balligand, 2018; Kamm *et al.*, 2019). On the contrary, a lack of regulation of NO signaling in vascular cells or neurons can lead to RCD by nitroxidative stress characteristic of Alzheimer's disease (Malinski, 2007), or to tissue remodeling and vasorelaxation necessary for cancer metastasis and angiogenesis (Jeff S. Isenberg *et al.*, 2009).

CD47 controls cardiovascular functions via the regulation of nitric oxide (NO), principally by its interaction with TSP1. Initial studies identified TSP1 as a potent negative regulator of NO signaling in endothelial cells (Isenberg *et al.*, 2005) and in vascular smooth muscle cells (Isenberg *et al.*, 2007). As CD36 was a known receptor of TSPs and a potent angiogenesis inhibitor with clear pharmaceutical interest (Silverstein *et al.*, 1992; Dawson *et al.*, 1997; Fortuna Haviv *et al.*, 2005) initial efforts focused in CD36 regulation of NO by TSP1. However, CD36 was soon found to be dispensable for TSP1-induced NO regulation, instead, CD47 dominant regulator of this process (Isenberg *et al.*, 2006).

NO is synthesized by three encoded NO synthases (NOS): inducible NOS (iNOS; produced during inflammatory conditions in leukocytes, endothelial cells, vascular smooth muscle cells, fibroblasts, nerve cells and cardiac myocytes), endothelial NOS (eNOS; produced by endothelial cells, cardiac myocytes, platelets, and erythrocytes) and neuronal NOS (nNOS; produced in autonomic cardiac neurons and ganglia, in cardiac myocytes and vascular smooth muscle cells) (Farah, Michel and Balligand, 2018). In endothelial cells, eNOS phosphorylation and activation is mediated by Akt, which activity is controlled by the vascular endothelial growth factor (VEGF) receptor-2 (VEGFR2). Canonically, the direct target of NO is soluble guanylyl cyclase (sGC), an enzyme that catalyzes guanosine-5'-triphosphate (GTP) conversion into cyclic guanosine monophosphate (cGMP), which, conjointly with hydrogen sulfide (H₂S), generate

paracrine signals that regulate vascular tone, blood pressure, and tissue perfusion (Roberts *et al.*, 2012; Farah, Michel and Balligand, 2018). CD47 redundantly inhibits this pathway at each step (**Figure 23**).

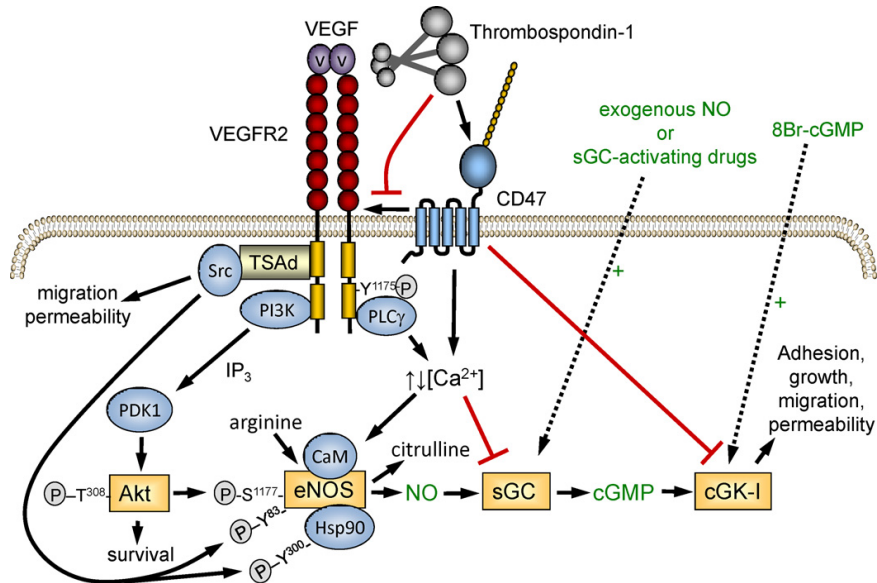


Figure 23. Redundant regulation of nitric oxide signaling by the TSP1-CD47 axis. (Adapted from Soto-Pantoja, Kaur and Roberts, 2015)

CD47 locates in close contact with VEGFR2 in endothelial (Kaur *et al.*, 2010) and T cells (Kaur *et al.*, 2014), and CD47 interaction with TSP1 displaces this complex and activates downstream VEGFR2 signaling. VEGFR2 signaling includes the activation of Src and Akt protein kinases (Kaur *et al.*, 2010, 2014), which in turn regulate eNOS activity (Montagnani *et al.*, 2001; Chen *et al.*, 2012). Moreover, CD47 activation by TSP1 directly inhibits acetylcholine-stimulated eNOS phosphorylation and activation of PLC γ and PI3K pathways, inducing intracellular Ca²⁺ increase (Bauer *et al.*, 2010). TSP1 is a potent inhibitor of sGC in endothelial cells, vascular endothelial muscle cells, T cells, and platelets (Isenberg *et al.*, 2005, 2008; Isenberg, Wink and Roberts, 2006; Ramanathan *et al.*, 2011). It has been suggested that TSP1-mediated CD47 signaling directly inhibits sGC (Miller, Isenberg and Roberts, 2010) via an increase of cytosolic Ca²⁺ influx that is also canonic of angiotensin II-mediated vasoconstriction pathway (Ramanathan *et al.*, 2011). CD47 activation pathway also redundantly inhibits GTP, GTPase activation (Rebres, Kajihara and

Brown, 2005; Chang and Blackstone, 2007). Finally, CD47 activation by TSP1 inhibits hydrogen sulfide signaling in activation of T cells (Miller *et al.*, 2013).

CD47 outside-in signaling in T cells

Together, the roles of CD47 as an extracellular sender of “don’t eat me” signals, a broad regulator of integrin functions, and a redundant director of vascular remodeling, make it a crucial participant for the correct functioning of the T cells, which implicate the entrance and exit of cells through the vasculature, and an adequate, safe cell motility throughout the long-distance travels. Indeed, CD47 is necessary for correct T cell trans-endothelial migration and recruitment to the site of inflammation *in vivo* (Azcutia *et al.*, 2012, 2013). But besides this, CD47 also plays anti-inflammatory roles. Activation of the T cell receptor (TCR) increases TSP1 production and reduces CD47-regulated T-cell motility (Bergström *et al.*, 2015). Conversely, TSP1 inhibits early T cell activation induced by ligation of the TCR with an anti-CD3 antibody in a way dependent on CD47, and this reduces CD47-induced pro-inflammatory interleukin (IL)-2 secretion and expression of the T cell activation marker CD69, while the 7N3 peptide impedes CD69 expression (Li *et al.*, 2001). Redundantly, SIRP α on the membrane of antigen presenting cells downregulate the expression of IL-12 receptor and reduces CD4⁺ and CD8⁺ cells responsiveness to IL-12 (Latour *et al.*, 2001). CD47 also mediates immunosuppressive activities via interaction with TSP1 and disruption of association with the VEGFR2 receptor (**Figure 24** left) (Kaur *et al.*, 2014), as in endothelial cells (**Figure 23**). The inhibitory role of TSP1 in T-cells requires the presence of an isoform of CD47 with a heparan sulfate modification at Ser64 (Kaur *et al.*, 2011). Finally, CD47 is also necessary for Fas-mediated apoptosis, where Fas ligation induces strong CD47 colocalization and caspase-dependent cell death (**Figure 24** right) (Manna *et al.*, 2005).

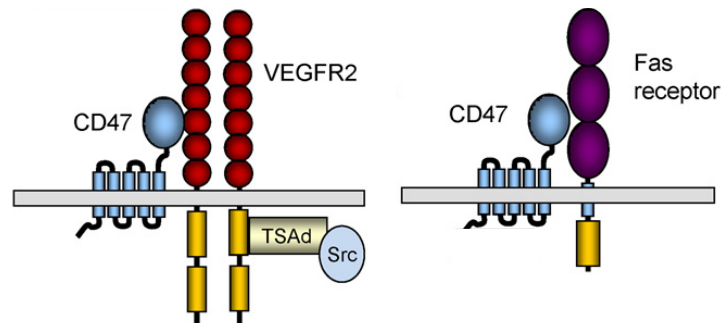


Figure 24. Known lateral partners of CD47 different to integrins in T cells. (Adapted from Soto-Pantoja, Kaur and Roberts, 2015)

CD47 and autophagy

CD47 has been proposed as a negative regulator of autophagy. Ionizing radiation was shown to induce autophagy in CD47-aberrant Jurkat (JinB8) cells but not in wild-type Jurkat cells, as demonstrated by electron microscopy images, LC3 staining by fluorescent microscopy, increased protein expression of BECN1, ATG5, ATG7, reduced expression of SQSTM1/p62 (Soto-Pantoja *et al.*, 2012). Consistently, genetic, or pharmacological blockade of CD47 in wild type Jurkat cells promotes cell survival, while exogenous induction of CD47 expression in JinB8 prevents autophagy. This is thought to be responsible of the systemic radioprotection that CD47 blockade provides to mice exposed to ionizing radiation (Soto-Pantoja *et al.*, 2013). After this, other groups have also found that CD47 deficiency or therapeutic blockade confers protection against stress in the heart, kidney and during anticancer therapy, via activation of autophagy (Sharifi-Sanjani *et al.*, 2014; Feliz-Mosquea *et al.*, 2018; El-Rashid *et al.*, 2019; Y. Li *et al.*, 2020). However, the mechanisms of CD47 control of autophagy remain largely unknown.

It has been suggested that CD47 activation by TSP1 can trigger autophagy in injured myocytes via a Ca^{2+} -regulated induction of histone deacetylase-3, as the TSP1 peptide mimic 7N3 increased LC3, ATG5, and ATG7 protein levels, while an anti-CD47 antibody (miap301) decreased their expression (Sharifi-Sanjani *et al.*, 2014). However, the autophagic flux was not measured. Others have drawn similar conclusions using the 4N1 strand in a Ras-expressing but not in wild type murine cancer cell line (Kalas *et al.*, 2013),

and in astrocytoma cells, but not in normal astrocytes (Sick *et al.*, 2011), yet with similar methodological shortage. Thus, TSP1 activation of CD47-mediated autophagy remains inconclusive.

Conversely, recent work reports that a recombinant SIRP α proteins (SIRP α -Fc, SIRP α D1-Fc, VEGFR1D2-SIRP α D1 bispecific fusion protein), together with pharmacological inhibition of autophagy potentiate the anticancer effects provided by CD47 blockade (Zhang *et al.*, 2017; Zhang, Chen, *et al.*, 2018; Zhang, Wang, *et al.*, 2018). This was proved in human and murine non-small cell lung cancer and glioblastoma cell lines, where treatment with recombinant SIRP α proteins triggered a time-dependent increase of the autophagic flux and inactivation of the Akt/mTOR signaling pathway, and combination with chloroquine treatment enhanced tumor reduction (Zhang *et al.*, 2017; Zhang, Chen, *et al.*, 2018; Zhang, Wang, *et al.*, 2018).

Although the role of CD47 in autophagy prevention is widely misunderstood, the current knowledge suggests that CD47 activity regulates signaling pathways that inhibit autophagy initiation via a consistent pathway involving Akt and Ca²⁺ signaling, and that the outcome of the autophagic flux depends on the cell type (and its differentiation stage), the nature of the stress signal (e.g., radiation, genotoxicity, genomic instability), and the nature stimulus activated by the CD47 ligand (i.e., SIRP α blockade, or TSP1, or TSP peptide-mimics-driven activation).

CD47 activation by TSP1 can trigger RCD

CD47 signaling can induce cell death. This process has been observed in different cell types and is consistently related to cancer and immune cells in the resolution phases of inflammation. Initial experiments showed that CD47 ligation by immobilized anti-CD47 antibodies (B6H12 and 2D3), TSP1 or TSP peptide-mimic 4N1K, induces caspase-independent cell death of chronic lymphocytic leukemia (CLL) cells (Mateo *et al.*, 1999). Later investigation confirmed these results and extended their observations to activated but not resting B cells, stem cells nor immature dendritic cells, and found that for cell

death to occur, CD47 crucially requires the correct expression of its transmembrane and extracellular domains (Mateo *et al.*, 2002).

A different group observed a similar outcome using soluble anti-CD47 antibodies (Ad22 and 1F7) in Jurkat cells, of T cell acute lymphoblastic leukemia (T-ALL), and in primary cells activated by an anti-CD3 antibody (OKT3), but not in resting T cells; while CD3-deficient Jurkat cells efficiently died after CD47 engagement (Pettersen *et al.*, 1999). Also in activated T cells and in T-ALL, treatment with the TSP peptide-mimic 4N1K or with 1F7 induced a similar type of cell death, regulated by $G_{i\alpha}$ proteins, which lowered intracellular cAMP levels, and reduced protein kinase A activity (Manna and Frazier, 2003). Moreover, using a yeast two-hybrid system with CD47 as bait, another group described that the Bcl-2 homology 3 (BH3)-only protein 19 kDa interacting protein-3 (BNIP3), a pro-apoptotic member of the Bcl-2 family, is a partner of CD47 that directly interacts with its intracellular domain to later induce mitochondrial damage and cell death of activated T cells (Lamy *et al.*, 2003).

In both CLL and T-ALL (and in activated T cells), it was observed that the cell death mechanism triggered by CD47 engagement is a caspase-independent process that induces a rapid phosphatidylserine exposure (2-6 h), with an almost simultaneous plasma membrane permeabilization. Later, consistent with the previous reports, it was demonstrated that CD47 engagement also induces the production of reactive oxygen species, and loss of $\Delta\psi_m$, but without the release of proapoptotic proteins nor AIF (which is generally related to caspase-independent RCD processes), or the induction of chromatin condensation or DNA fragmentation (Roué *et al.*, 2003). Similar traits were observed by different research groups in acute promyelocytic leukemia (NB4) cells after treatment with TSP1, the signature domain of TSP1, and 4N1K (Saumet *et al.*, 2005), and in breast cancer cells, after treatment with the TSP peptide-mimic 4N1K or the soluble anti-CD47 antibody 1F7, where, as in T-ALL, $G_{i\alpha}$ proteins reduced intracellular cAMP levels, and protein kinase A activity (Manna and Frazier, 2004). More recently, it was further reported that another soluble anti-CD47 antibody (CC2C6) was also able to induce cell death in Jurkat cells via a CD47-dependent RCD mechanism involving the Mcl-NOXA pathway and calcium increase that was dispensable for cell death (Leclair *et al.*, 2018).

Unfortunately, unlike for the previous reports, caspase dependence of cell death was not assessed, and it was only inferred from the absence of PARP-1 cleavage.

The molecular machinery activated after CD47 engagement in these situations is largely consistent with the non-lethal signaling pathways induced by TSP1-mediated CD47 activation in different cell types. Indeed, in agreement with the regulating anti-inflammatory effects of TSP1, mice deficient in CD47, TSP1 or TSP2 hold an inadequate resolution of pharmacologically induced inflammation (Lamy *et al.*, 2007). Of note, 4N1K only triggers the death of activated T cells from wild-type but not from CD47-deficient mice (Lamy *et al.*, 2007). Interestingly, for this type of RCD to occur, a “CD47-low” status (i.e., cells showing low antibody recognition by flow cytometry) on their cell surface is required (Van *et al.*, 2012), suggesting that during resolution of inflammation, this would additionally facilitate phagocytosis of dying T cells. Taken together, this suggests that CD47-induced cell death could constitute an RCD mechanism in T cells activated during contraction phases of the immune response and in T cell acute lymphoblastic leukemia (T-ALL). Recent studies elegantly demonstrated that activation of the TCR signaling pathway induces cell death in T-ALL through a molecular mechanism resembling the physiological process of negative selection of T lymphocytes (Trinquand *et al.*, 2016). An exciting question is whether CD47 is involved in such process of T cell development, and if alterations of CD47-mediated cell death pathways could have an impact in T-ALL development

Triggering the TSP1-CD47 axis with therapeutic peptides

Although targeting CD47 with TSP1-derived agonist peptide-mimics such as the 4N1K showed to induce signaling with therapeutic potential many years ago (Mateo *et al.*, 1999; Lamy *et al.*, 2007), surprisingly, the potential of their applications were largely unexplored, probably because of the major drawbacks that used to be generally associated with their use as therapeutic tools, such as poor metabolic stability, poor selectivity, poor oral bioavailability, immunogenicity and difficult syntheses (Danho *et al.*, 2009). While peptides have long been considered only as biological tools by major pharmaceutical

industries, many recent solutions have been developed in academia to overcome these limitations (Erak *et al.*, 2018). Indeed, as of 2017, 68 peptides had been approved in Europe, United States, and Japan, and 155 were under clinical investigation (Lau and Dunn, 2018), but by the time of writing, 75 are in the market, 160 in clinical trials. As the tendency keeps on raising, the therapeutic peptide market currently accounts for a well established market (Vlieghe *et al.*, 2010; Fosgerau and Hoffmann, 2015), expected to soon overpass the USD 50 billion mark (*Peptide Therapeutics Market To Reach USD 50.60 Billion By*, no date).

Knowing the therapeutic potential of targeting CD47 with TSP1 peptide-mimics, our group revisited the chemical structure of 4N1, the beta strand of the TSP1 described to be essential to interact with CD47. The poor solubility of 4N1, together with its substandard serum stability, which is even worse in 4N1K, were rapidly identified as major drawbacks for their therapeutic use. Therefore, using structure-activity relationship studies, the behavior of this type of peptides in aqueous solutions was described, being able to generate soluble peptides that resisted degradation by serum proteins. Further analyses let our team identify its pharmacophores and generate a first product: PKHB1, the first peptide-mimic of the TSP C-terminal domain (**Figure 25**), suitable for therapeutic use in vivo (Denèfle *et al.*, 2016).

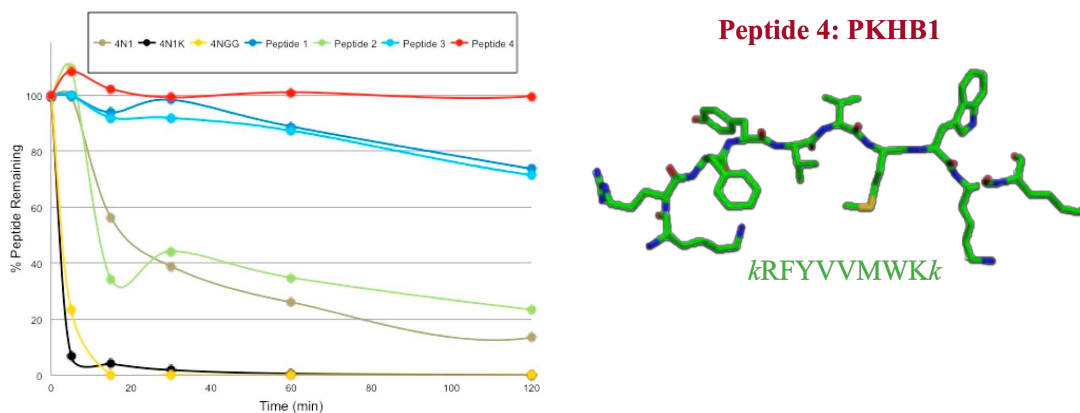


Figure 25. PKHB1 stability in serum. (Adapted from Denèfle *et al.* 2016)

Using this first peptide, termed PKHB1, it was found that, similar to 4N1K, TSP1, and anti-CD47 antibodies, it induced RCD in CLL (Martinez-Torres *et al.*, 2015). The cell

death mechanism triggered by PKHB1 in CLL also induces a rapid phosphatidylserine exposure and plasma membrane permeabilization independent of caspase activity, loss of mitochondrial membrane potential without the release of proapoptotic proteins nor AIF, induces the production reactive oxygen species, and does not induce chromatin condensation nor DNA fragmentation. Furthermore, it was found that the cell death mechanism induced by PKHB1 is regulated by an intracellular Ca^{2+} signaling controlled by PLC γ 1 activation (**Figure 26**), which overexpression was found to correlate with CLL progression, and which pharmacological or genetic inhibition in these cells prevent cell death (Martinez-Torres *et al.*, 2015).

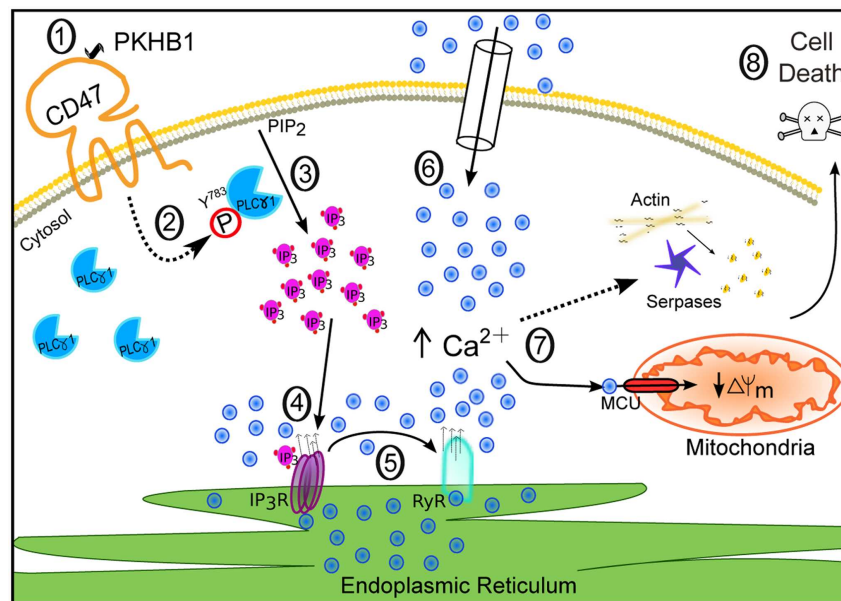


Figure 26. Molecular mechanism of cell death induced by PKHB1 in CLL cells. When PKHB1 engages to its target in CLL cell membranes, indirectly activates the overexpressed PLC γ 1, which cleaves PIP $_2$ into IP $_3$, a second messenger that opens calcium channels (IP $_3$ R) at the endoplasmic reticulum (ER). The sustained activation of PLC γ 1 in CLL, will lower levels of Ca^{2+} in the ER and result to the opening of further calcium channels (e.g., ryanodine receptors), which in turn will deplete Ca^{2+} stores from the ER and trigger the SOCE and CRAC mechanisms, leading to the entry of massive concentrations of Ca^{2+} into the cytosol that will activate serpases and induce mitochondrial damage (Extracted from Martinez-Torres *et al.*, 2015).

Justification

Justification

Cancer is a worldwide health problem, and many types of cancer are resistant to current therapies. Cancer therapy resistance and eventual relapse are in great part a result of cancer cell death evasion and immune escape, and therapy-induced immunogenic cell death is crucial for the long-lasting success of cancer therapies (Galluzzi *et al.*, 2020). The TSP1-CD47 axis plays an important role in the immune system of mammals and in the tumor microenvironment (Soto-Pantoja, Kaur and Roberts, 2015; Kaur *et al.*, 2021). In chronic lymphocytic leukemia, TSP1 and immobilized anti-CD47 antibody or the TSP C-terminal domain peptide-mimic 4N1K induces cell death (Mateo *et al.*, 1999). Rational structural modifications of 4N1K gave rise to PKHB1, a serum stable TSP C-terminal domain peptide-mimic for which pharmacophore have been identified (Denèfle *et al.*, 2016). Both PKHB1 and 4N1K trigger a particular type of caspase-independent cell death in CLL that induces calreticulin exposure and is regulated by calcium signaling, leading to tumor growth decrease in immunodeficient mice (Martinez-Torres *et al.*, 2015). Finally, first results from the laboratories hosting the present thesis work showed that PKHB1 kills cell lines from types of cancer besides CLL (Martínez-Torres, 2013; Denèfle *et al.*, 2016; Gómez-Morales, 2017), and that it can induce the complete tumor regression of T-ALL tumors in immunocompetent mice (Calvillo-Rodríguez 2018; Uscanga-Palomeque, 2019).

Hypotheses

Hypotheses

1. The RCD mechanism induced by PKHB1 is similar in different types of cancer
2. PKHB1 can induce immunogenic cell death in liquid (T-ALL) and solid (breast) cancer cells
3. Novel structural modifications can enhance the anti-tumor effects of PKHB1-derived analogs

Objectives

Objectives

The main goal of the present thesis was to evaluate the therapeutic potential of TSP C-terminal domain peptide-mimics that target the TSP1-CD47 axis in different types of cancer. Therefore, the specific aims of the present study were to:

- 1) Study PKHB1-induced cell death mechanism in cells from different types of cancer
- 2) Explore the implication of common actors of the anti-tumor immune response after PKHB1 treatment
- 3) Test the pharmaceutical potential of novel TSP C-terminal domain peptide-mimic designs

Results

CHAPTER 1

1. Study of the Mechanism of Immunogenic Cell Death induced by PKHB1 in T-cell leukemia

The results in the present chapters gave rise to a patent: **EP3650036A1**, held by Sorbonne Université and Universidad Autónoma de Nuevo León.

1.1. Article 1. CD47 agonist peptide PKHB1 induces immunogenic cell death in T-cell acute lymphoblastic leukemia cells

1.2. Article 2. PKHB1 tumor cell lysate induces antitumor immune system stimulation and tumor regression in syngeneic mice with tumoral T lymphoblasts

Preamble

Hematological malignancies, such as leukemia and lymphoma, are highly heterogeneous diseases that affect people of all ages and ethnicities and have long served as model diseases for cancer biology and treatment (Freireich, Wiernik and Steensma, 2014). Thanks to this, a great improvement in cancer treatment has been achieved in the past decades. However, challenges still exist to treat, for example, T-ALL, a rare, aggressive, highly heterogeneous type of leukemia that under currently available therapies in developed countries has a 5-year survival rate of ~50% in adults and ~70% in younger patients, but of <10% in patients with relapse (Marks and Rowntree, 2017). This is largely explained by the fact that in these cases where treatment fails, effective options are limited. Therefore, more effective therapies are needed.

Besides surgical resection, the main strategy to treat cancer has historically consisted in killing cancer cells (e.g., using radiotherapy or chemotherapies). With time, treatment effectiveness and specificity for these cells has improved with the understanding of cancer biology, which is now clear strongly depends on the development of aberrant capacities (e.g. neoantigens) that make some cancer cells incapable to correctly activate or execute cell death programs and/or to be recognized by the surveillant anti-tumor immune system, among other capacities (all of them famously reviewed by Hanahan and Weinberg, 2011).

Although every cell has a plethora of genetically encoded apparatus that could lead aberrant cells to self-destruct (Galluzzi *et al.*, 2018), many anticancer therapies induce apoptosis, a regulated cell death modality characterized by caspase dependency. However, activation of caspase-independent cell death mechanisms can be exploited as non-redundant therapies for cancer treatment (Bröker, Kruyt and Giaccone, 2005).

Based on the known implications of TSP1-CD47 axis in cell death of activated T-cells (see introduction) and the similar traits observed for PKHB1-induced cell death in CLL (including fast process of almost simultaneous phosphatidylserine exposure and plasma membrane permeability, caspase-independence, regulation of calcium signaling, induces mitochondrial damage), it was hypothesized that PKHB1 could activate molecular pathways in T-ALL similar to those in CLL, which seem to differ to those used by other therapies and could be useful even in cases where conventional therapies fail.

Moreover, the role that the immune system plays in the context PKHB1-based anticancer therapy had not been assessed. In CLL, PKHB1 induced calreticulin exposure (Martinez-Torres *et al.*, 2015), which leads cell death to awake immune responses (Obeid *et al.*, 2007). However, *in vivo* experiments were performed in severely immunodeficient (NSG) mice; thus, although PKHB1 induced the reduction of tumor growth, this strictly reflected direct tumor cytotoxicity but not indirect anti-tumor immune responses (Martinez-Torres *et al.*, 2015).

1.1. CD47 agonist peptide PKHB1 induces immunogenic cell death in T-cell acute lymphoblastic leukemia cells

Article published in “Cancer Science” on November 20th, 2018 (doi: 10.1111/cas.13885).

The data presented in this article were generated from a first hypothesis that PKHB1 could trigger regulated cell death in T-ALL as it does in CLL. To assess this, PKHB1 was manually synthesized using solid support, purified by HPLC, and >99% pure lyophilized peptide fractions (confirmed by LC/MS analyses) were used to study the effects of this peptide in T-ALL cell lines (CEM and MOLT-4) and a murine model of tumorigenic T-cell lymphoblasts (L5178Y-R), that was later used for experiments *in vivo*, using immunocompetent BALB/c mice.

Cells were cultured in presence of PKHB1, and cell death was analyzed by flow cytometry, measuring phosphatidylserine exposure and plasma membrane permeability using annexin-V-APC (Ann-V-APC) and propidium iodide (PI), respectively. In all cases the percentage of Ann-V-APC⁺ and PI⁺ cells augmented in a dose-dependent manner. Pre-incubation of cells with a pan-caspase inhibitor did not prevent PKHB1-induced cell death in any case, but extracellular calcium chelation did in all cases. In addition, PKHB1 induced the depolarization of the mitochondrial outer membrane, as observed by an increase of cells that lost staining with tetramethylrhodamine, ethyl, ester, measured by flow cytometry. Thus, PKHB1 triggered a caspase-independent cell death modality in T-ALL cells which execution required calcium uptake and caused mitochondrial damage.

In freshly isolated human and murine PBMCs, similar doses of PKHB1 did not change the proportion of cells stained with Ann-V-APC/PI, neither changed the proportion of CD4⁺ or CD8⁺ lymphocytes. PKHB1 did not reduce the viability (measured by MTT assays) of freshly isolated bone marrow, spleen, thymus, and lymph nodes cells neither, indicating a high selectivity to kill T-ALL cells but not other cells of the immune system.

In immunocompetent mice bearing L5178Y-R tumors, PKHB1 induced tumor remission. Histopathological and immunohistochemical analyses of tumor samples taken from PKHB1-treated mice before remission revealed the presence of giant cells

(presumably phagocytes), CD4⁺ and CD8⁺ cells inside the tumor. Cell counts of bone marrow, spleen and thymus were higher and cell counts of lymph nodes were lower in PKHB1-treated mice compared to non-treated mice. Lymphocyte cell count was also higher in PKHB1-treated compared to untreated mice. Altogether, the previous suggested that, besides direct cytotoxicity of cancer cells, the immune system participated in the tumor eradication induced by PKHB1 treatment.

We hypothesized that PKHB1-induced cell death was able to initiate immune responses against the tumor. As adjuvanticity is crucial for cell death immunogenicity, and DAMPs exposure largely provides such adjuvanticity, the ability of PKHB1 cytotoxicity to induce DAMPs in these cells was assessed. One of these DAMPs that is exposed during cell death and is determinant for immunogenicity is the exposure of calreticulin to the cell membrane (Obeid, et al. *Nat Med*, 2007), and PKHB1 induced calreticulin exposure in CLL (Martínez-Torres, et al. *Plos Med*, 2015). Therefore, the ability of PKHB1 to induce calreticulin exposure in T-ALL was evaluated using a phycoerythrin-tagged anti-calreticulin antibody (CRT-PE) and an homologous antibody with an irrelevant target (MOPC-PE). Fluorescent signal was higher in untreated and PKHB1-treated CEM, MOLT-4 and L5178Y-R cells marked with CRT-PE when compared to MOPC-PE. However, PKHB1 treatment increased CRT-PE fluorescence compared to the untreated controls in the three cases; this was corroborated by fluorescent microscopy, suggesting that calreticulin exposed to the cell membrane after treatment with PKHB1.

Besides calreticulin exposure, the release of other damage-associated molecular patterns (DAMPs) to the extracellular space such as ATP, HSP70, HSP90, and HMGB1 are also determinant adjuvants of cell death immunogenicity (Galluzzi, et al. 2017). Therefore, whole protein expression of calreticulin, HSP70, HSP90 and HMGB1 was measured in cell lysates and lyophilized supernatants of CEM, MOLT-4 and L5178Y-R cells cultured with or without PKHB1 treatment using western blot. Different patterns were observed among cell lines but, compared with untreated controls, expression of these proteins was lower in PKHB1-treated cell lysates and higher in PKHB1-treated supernatants. HMGB1 release was corroborated by an enzyme-linked immunosorbent assay. ATP release was evaluated by measuring luciferin-oxyluciferin conversion in the

supernatants of both control and PKHB1-treated cells; higher luminescence in PKHB1-treated cultures suggested ATP release. Altogether this indicates that PKHB1 treatment induced DAMPs exposure and release to the cell membrane and the extracellular space.

Together, the *in vivo* behavior and DAMPs release suggest that PKHB1 could induce ICD in T-ALL. Given the complexity of the cellular mechanisms that constitute anti-tumor immunity *in vivo*, the gold-standard to evaluate whether an anticancer treatment is able to induce ICD is the prophylactic vaccination of immunocompetent animals with cells killed by an ICD-inducer, which action would expose a variety of tumor antigens and generate adjuvants that initiate anti-tumor immune responses and generate immunological memory that is preventive of future tumor establishment.

For this reason, mice were immunized with increasing number of L5178Y-R cells (0=naïve, 1.5, 3 or 5 x10⁶ cells) killed by PKHB1. One week after, live L5178Y-R cells were inoculated in the naïve or immunized mice, and tumor growth was measured. While tumors grew normally in naïve animals, the number of immunized mice that did not develop the tumor augmented with the number of death cells that were immunized. Mice vaccinated with 5x10⁶ cells did not develop the tumor. This had an impact in survival, which augmented in vaccinated animals. Moreover, to test whether PKHB1 treatment rendered long-term immunological memory, mice that had undergone complete remission after PKHB1 treatment or naïve mice of similar age were challenged with L5178Y-R cells. The tumor only established in one out of six PKHB1-treated mice, while all six naïve mice developed the tumor.

Altogether, the data demonstrate that PKHB1 induces immunogenic cell death in T-ALL and suggests that PKHB1 could be a useful therapeutic tool against T-ALL.

Résumé de l'article 1


La leucémie lymphoblastique aiguë à cellules T (T-ALL) a un mauvais pronostic dérivé de son hétérogénéité génétique, qui se traduit par une résistance élevée aux chimiothérapies. Récemment, notre groupe de travail a conçu des peptides dérivés de la thrombospondine-1, agonistes de CD47 et a démontré leur capacité à induire la mort cellulaire dans la leucémie lymphoïde chronique. Encouragés par ces résultats prometteurs, nous avons évalué la mort cellulaire induite par PKHB1 (le premier peptide agoniste CD47 stable dans le sérum humain) sur des lignées cellulaires humaines CEM et MOLT-4 (T-ALL) et sur une ligne cellulaire tumorale de lymphoblastes T (L5178Y-R) murins, évaluant également la dépendance aux caspases et au calcium et le potentiel de membrane mitochondriale. De plus, nous avons évalué la sélectivité pour les lignées cellulaires cancéreuses en analysant la mort cellulaire et la viabilité des cellules non tumorales humaines et murines après l'activation de CD47. In vivo, nous avons déterminé que le traitement par PKHB1 de souris xénotransplantées par la lignée tumorale L5178Y-R augmentait le nombre de cellules leucocytaires dans le sang et les organes lymphoïdes tout en recrutant des leucocytes sur le site tumoral. Pour analyser si l'activation de CD47 induisait la mort cellulaire immunogène (MCI), nous avons identifié la présence de molécules caractéristiques libérées par les cellules tumorales endommagées (molécules qualifiées de DAMPs pour Damage-Associated Molecular Patterns en anglais), entre autres exposition de la calréticuline (CRT), libération d'ATP et de protéines de choc thermique HSP70 et HSP90, de la protéine HMGB1, et nous avons vacciné en prophylaxie les souris xénotransplantées par des cellules tumorales tuées par le peptide PKHB1. Nous avons ensuite évalué la mémoire immunologique. Nos données indiquent que PKHB1 induit un type de mort cellulaire indépendante des caspases et dépendante du calcium dans les cellules leucémiques, tout en épargnant les cellules non tumorales, murines et humaines. De plus, nos résultats montrent que PKHB1 déclenche une MCI dans les cellules leucémiques car il induit l'exposition de la CRT et la libération de DAMPs in vitro, et les vaccinations prophylactiques inhibent l'établissement de la tumeur in vivo. Ensemble, nos résultats améliorent la connaissance du potentiel des peptides agonistes de CD47 comme outils thérapeutiques pour traiter la leucémie lymphoblastique aiguë à cellules T.

Resumen del artículo 1

La leucemia linfoblástica aguda de células T (T-ALL) tiene un mal pronóstico debido a su heterogeneidad genética, lo que se traduce en una alta tasa de quimiorresistencia. Recientemente, nuestro grupo diseñó péptidos agonistas de CD47 derivados de la trombospondina-1 y demostró su capacidad para inducir la muerte celular en leucemia linfocítica crónica. Alentados por estos prometedores resultados, evaluamos la muerte celular inducida por el PKHB1 (el primer péptido agonista de CD47 estable en suero descrito) en líneas celulares de T-ALL humanas, CEM y MOLT-4 y en una línea celular de linfoblastos tumorales de células T murinos (L5178Y-R), evaluando la dependencia de caspasas, la dependencia de calcio y el potencial de la membrana mitocondrial. Además, evaluamos la selectividad para las líneas celulares cancerosas analizando la muerte celular y la viabilidad de las células no tumorales humanas y murinas después de la activación de CD47. In vivo, determinamos que el tratamiento con PKHB1 de ratones que portaban tumores con la línea celular L5178Y-R aumentó el recuento de células leucocitarias en sangre periférica y órganos linfoides, al mismo tiempo que se reclutaban leucocitos en el sitio del tumor. Para analizar si la activación de CD47 inducía muerte celular inmunogénica (MCI), evaluamos la exposición (calreticulina, CRT) y la liberación (ATP, proteínas de choque térmico 70 y 90, cuadro de grupo de alta movilidad 1, CRT) de patrones moleculares asociados a daño (DAMPs, del inglés *damage-associated molecular patterns*), y administramos una vacunación antitumoral profiláctica, determinante de la memoria inmunológica. Nuestros datos indican que el PKHB1 induce muerte celular independiente de caspasas y dependiente de calcio en las células leucémicas y no en células humanas y murinas no tumorales. Además, nuestros resultados demuestran que PKHB1 puede inducir MCI en células leucémicas, ya que induce la exposición de CRT y la liberación de DAMPs in vitro, y las vacunas profilácticas inhiben el establecimiento de tumores in vivo. En conjunto, nuestros resultados abonan al conocimiento del potencial que tienen los péptidos agonistas de CD47 como herramientas terapéuticas para tratar la leucemia.

Manuscript

CD47 agonist peptide PKHB1 induces immunogenic cell death in T-cell acute lymphoblastic leukemia cells

Ashanti Concepción Uscanga-Palomeque¹ | Kenny Misael Calvillo-Rodríguez¹ |
Luis Gómez-Morales¹ | Eva Lardé² | Thomas Denèfle² | Diana Caballero-Hernández¹ |
Hélène Merle-Béral³ | Santos A. Susin³ | Philippe Karoyan² |
Ana Carolina Martínez-Torres¹  | Cristina Rodríguez-Padilla¹

¹College of Biology Science, Laboratory of Immunology and Virology, Autonomous University of Nuevo Leon, San Nicolas de los Garza, Mexico

²CNRS, Biomolécules Laboratory, Superior Normal School, PSL University, Sorbonne University, Paris, France

³INSERM, UMRS 1138, Sorbonne University, University of Paris Descartes, Sorbonne Paris Cite, Center of Reserch of Cordeliers, Paris, France

Correspondence

Ana Carolina Martínez-Torres, Pedro de Alba s/n, Ciudad Universitaria, San Nicolás de los Garza, Nuevo León, México.
Email: ana.martinezto@uanl.edu.mx

Funding information

SEP-CONACYT-ECOS-ANUIES, Grant/Award Number: 291297; the Laboratory of Immunology and Virology of the College of Biological sciences; UANL

T-cell acute lymphoblastic leukemia (T-ALL) has a poor prognosis derived from its genetic heterogeneity, which translates to a high chemoresistance. Recently, our workgroup designed thrombospondin-1-derived CD47 agonist peptides and demonstrated their ability to induce cell death in chronic lymphocytic leukemia. Encouraged by these promising results, we evaluated cell death induced by PKHB1 (the first-described serum-stable CD47-agonist peptide) on CEM and MOLT-4 human cell lines (T-ALL) and on one T-murine tumor lymphoblast cell-line (L5178Y-R), also assessing caspase and calcium dependency and mitochondrial membrane potential. Additionally, we evaluated selectivity for cancer cell lines by analyzing cell death and viability of human and murine non-tumor cells after CD47 activation. In vivo, we determined that PKHB1-treatment in mice bearing the L5178Y-R cell line increased leukocyte cell count in peripheral blood and lymphoid organs while recruiting leukocytes to the tumor site. To analyze whether CD47 activation induced immunogenic cell death (ICD), we evaluated damage-associated molecular patterns (DAMP) exposure (calreticulin, CRT) and release (ATP, heat shock proteins 70 and 90, high-mobility group box 1, CRT). Furthermore, we gave prophylactic antitumor vaccination, determining immunological memory. Our data indicate that PKHB1 induces caspase-independent and calcium-dependent cell death in leukemic cells while sparing non-tumor murine and human cells. Moreover, our results show that PKHB1 can induce ICD in leukemic cells as it induces CRT exposure and DAMP release in vitro, and prophylactic vaccinations inhibit tumor establishment in vivo. Together, our results improve the knowledge of CD47 agonist peptides potential as therapeutic tools to treat leukemia.

KEYWORDS

acute lymphoblastic leukemia, cancer vaccine, CD47, DAMP, immunogenic cell death

Calvillo-Rodríguez and Gómez-Morales contibuted equally to this work. Martínez-Torres and Rodríguez-Padilla are co-senior authors.

This is an open access article under the terms of the Creative Commons Attribution-NonCommercial License, which permits use, distribution and reproduction in any medium, provided the original work is properly cited and is not used for commercial purposes.

© 2018 The Authors. *Cancer Science* published by John Wiley & Sons Australia, Ltd on behalf of Japanese Cancer Association.

1 | INTRODUCTION

Immunogenic cell death (ICD) is a type of regulated cell death that activates an adaptive immune response against dead-cell-associated antigens, inducing tumor cell immunogenicity.^{1,2} ICD is characterized by the exposure or release of endogenous immunogenic biomolecules, namely damage-associated molecular patterns (DAMP).³ In physiological conditions, DAMP are inside the cells, but when exposed or released, in case of stress, injury, or cell death, they bind receptors on immune cells.^{4,5} The main DAMP related to ICD exposed at the cell surface and/or released to the extracellular media are calreticulin (CRT)⁶⁻⁸ and other endoplasmic reticulum (ER) proteins such as heat shock proteins 70 and 90 (HSP70 and HSP90, respectively),^{9,10} secretion of ATP¹¹⁻¹³ and the non-histone chromatin protein high-mobility group box 1 (HMGB1).^{14,15} Collectively, these DAMP recruit antigen-presenting cells (APC) to ICD sites and stimulate the uptake, processing, and presentation of dead-cell-associated antigens, resulting in an adaptive immune response.^{1,16-18} However, DAMP release is not sufficient to determine whether a molecule will induce ICD; thus, *in vivo* vaccination experiments are the gold standard to identify ICD inducers.^{19,20}

A subset of chemotherapeutic agents including doxorubicin, mitoxantrone, oxaliplatin, bortezomib, cyclophosphamide, and anthracycline have the ability to trigger ICD,^{18,21} hence activating anticancer immune responses.¹ These drugs are used to treat different types of cancer, including hematological malignancies such as acute lymphoblastic leukemia (ALL).

Acute lymphoblastic leukemia is the most common type of childhood cancer, accounting for 80% of cases, and is the second most common acute leukemia in adults.²²⁻²⁴ The 5-year survival rate in adults is about 30%-50% compared to 90% in children.²⁵⁻²⁷ ALL can affect B cells (B-ALL) or T cells (T-ALL); T-ALL has a high risk of relapse as a result of acquired therapy resistance.²⁸ Chemoresistance is one of the most important reasons for failure in cancer treatments. Some cells are selected in a micro-evolutive process of survival after therapy induction, leading to the eventual relapse of nearly one case out of five.²⁹⁻³¹ Because treatment options are limited for these patients, their prognosis is poor. Thus, the development of new treatments able to stimulate the immune system, such as ICD-inducers, is important to fight chemoresistant malignancies.

CD47 is a potential therapeutic target for refractory hematological malignancies, by blocking its function using monoclonal antibodies³² or by its activation with peptides.^{33,34} CD47 is a transmembrane protein expressed ubiquitously and reported to be overexpressed in different types of hematological malignancies, including ALL.³⁵ CD47 plays many biological functions as a result of its interaction with at least two major ligands: signal-regulatory protein alpha (SIRP α) and the extracellular matrix protein, thrombospondin-1 (TSP1). SIRP α is present in APC such as macrophages and dendritic cells (DC), with which it controls a "don't eat me" signal that regulates programmed cell removal.³⁶ TSP1 mediates cell adhesion, migration, proliferation and death.³⁷ Thus, CD47 appears as a promising therapeutic target addressed by many approaches: for example, blockade of CD47-SIRP α interaction by monoclonal antibodies mediates innate,³² as well as adaptive, immune responses.³⁸ Additionally,

treatment with an anti-CD47 monoclonal antibody (CC2C6) has shown to induce caspase-independent cell death in T-ALL cell lines.³⁹

More recently, CD47 activation by peptides derived from the C-terminal domain of TSP-1 induces a caspase-independent and calcium-dependent cell death in different cancer cell lines.^{33,34,40,41} Indeed, CD47 engagement to PKHB1, the first-described serum-stable soluble CD47-agonist peptide, induced changes in ER morphology, CRT exposure, reactive oxygen species (ROS) production and dissipation of the mitochondrial membrane potential in cells from patients with CLL.³³

The present work is focused on determining whether PKHB1 is able to induce a selective ICD in T-ALL cell lines, while conserving the principal characteristics of CD47-mediated cell death.

2 | MATERIALS AND METHODS

2.1 | Blood and PBMC isolation

Peripheral blood was collected from 10 healthy volunteers after obtaining written informed consent. This study was approved by the Institutional Ethics Committee at the Universidad Autónoma de Nuevo León, College of Biological Sciences. The animal study was approved by the Animal Ethical Committee (CEIBA), Number: 01/2015. All experiments were conducted according to Mexican regulation NOM-062-ZOO-1999.

Blood from killed mice was obtained by cardiac puncture, whereas human blood was collected by venipuncture. PBMC isolation was carried out by density gradient centrifugation using Ficoll-Hypaque-1119 (Sigma-Aldrich, St Louis, MO, USA). White blood cells were obtained, washed and counted. Cells (4×10^5) were seeded in a 96-well plate with RPMI medium. CD4+/CD8+ determination was done using specific primary antibodies (CD4; MT310 sc-19641 and CD8; 32-M4 sc-1177; Santa Cruz Biotechnology, Dallas, TX, USA).

2.2 | Spleen, thymus, lymph node, and bone marrow cell extraction

Spleen, thymus, lymph node, and bone marrow cells were obtained from female BALB/c mice post-death. Spleen cells were obtained through perfusion, thymocytes and lymphatic node cells were obtained by maceration, and bone marrow cells (femur and tibia) were flushed with PBS. Every cell suspension was washed twice with PBS and counted using Trypan blue staining.

2.3 | Cell culture

CCRF-CEM ATCC CCL-119 and MOLT-4 ATCC CRL-1582 (human T-acute lymphoblastic leukemia, T-ALL), and L5178Y-R ATCC CRL-1722 (murine lymphoblastic T-cell line) were obtained from ATCC. Human and murine PBMC, human CD4+ and CD8+ T cells, and primary lymphoid organ's cells were obtained from healthy individuals. Cells were maintained in RPMI-1640 medium supplemented with 10% FBS, 2 mmol/L L-glutamine, 100 U/mL penicillin-streptomycin (GIBCO by Life Technologies, Grand

Island, NY, USA), and incubated at 37°C in a controlled humidified atmosphere with 5% CO₂. Cell count was carried out using Trypan blue (0.4% Sigma-Aldrich), a Neubauer chamber and an optic microscope (Zeiss Primo Star) as proposed by the ATCC's standard protocols.

2.4 | Flow cytometry, cell death induction, and inhibition

Annexin-V-allophycocyanin (Ann-V-APC 0.1 µg/mL; BD Pharmingen, San Jose CA, USA), propidium iodide (PI, 0.5 µg/mL; Sigma-Aldrich), and tetramethylrhodamine ethyl ester (TMRE, 20 nmol/L; Sigma-Aldrich) were used for phosphatidylserine exposure, cell viability, and mitochondrial transmembrane potential ($\Delta\Psi_m$) quantification, respectively, in a BD Accuri C6 flow cytometer (BD Biosciences, Franklin Lakes, NJ, USA) (total population 10 000 cells). Data were analyzed using FlowJo software (LLC, Ashland, OR, USA). Then, 1×10^6 cells/mL were treated for 2 hours with PKHB1 (as indicated). For the inhibition assays, calcium chelator, BAPTA (5 mmol/L, CalbioChem; Merck, Billerica, MA, USA) or the pan-caspase inhibitor Q-VD-OPH (QVD, 10 µmol/L; BioVision, Milpitas, CA, USA) was added 30 minutes before PKHB1.

2.5 | Complete blood count

Heparinized blood acquired from mice was assessed using the automatic Hematology Analyzer BC 7000 (KontroLab, Rome, Italy). Blood smears were carried out and fixed with methanol, stained with Wright's, and observed under the microscope to carry out differential blood white cell counts.

2.6 | Calreticulin exposure

Next, 1×10^6 cells/mL were plated, treated with PKHB1, and incubated for 2 hours. Cells were harvested, washed, and stained with Calreticulin-Phycoerythrin (FMC-75; Enzo Life Science, Farmingdale, NY, USA) antibody (1:1000) in FACS buffer. After 1 hour of incubation in darkness at room temperature, cells were washed and resuspended in 100 µL FACS buffer to be assessed by flow cytometry. For confocal microscopy (Olympus X70; Olympus, Tokyo, Japan), poly-L-lysine was added to sterile coverslips placed inside a six-well plate for 24 hours, then washed with PBS and 1×10^6 cells/mL were seeded. PKHB1 was added and incubated for 2 hours. Then, the cells were stained with Calreticulin-PE antibody (1:500) and Hoechst 33342 (Thermo Scientific Pierce, Rockford, IL, USA), incubated for 1 hour, and assessed by confocal microscopy.

2.7 | Western blot

In a serum-free culture medium, 1×10^6 cells/mL were seeded and treated with PKHB1 (CC₅₀ and CC₁₀₀ for each cell line) or left alone (control) for 2 hours. Supernatants were recovered and lysed with lysis buffer (20 mmol/L Tris pH 6.8, 2 mmol/L EDTA, 300 mmol/L NaCl and SDS 2%). Protein concentration was measured using the DC Protein

Assay kit (Bio-Rad, Hercules, CA, USA) and 50 µg protein was loaded into SDS-PAGE gels. After blotting, nitrocellulose filters were probed with primary antibodies (1:1000) against HMGB1 (HAP46.5: sc-56698), HSP70 (C92F3A-5: sc-66048), HSP90 (F-8: SC-13119) and Calreticulin (F-4: sc373863). Anti-mouse or anti-rabbit-HRP served as secondary antibodies (Santa Cruz Biotechnology). Visualization was carried out with ECL substrate system (Thermo Scientific, Waltham, MA, USA).

2.8 | ATP release assay

In this step, 1×10^6 cells/mL were treated with PKHB1 (CC₅₀ and CC₁₀₀ for each cell line) for 2 hours. Supernatants were used to assess extracellular ATP by a luciferase assay (ENLITEN kit, Promega, Madison, WI, USA) following the manufacturer's instructions. Bioluminescence was assessed in a microplate reader (Synergy HT, Software Gen5; BioTek, Winooski, VT, USA) at 560 nm.

2.9 | High-mobility group box 1 release assay

Supernatants of untreated and treated (PKHB1 CC₅₀ and CC₁₀₀ for each cell line) leukemic cells (1×10^6 cells/mL) were used to measure extracellular HMGB1 using the HMGB1 ELISA kit for CEM, MOLT-4 or L5178Y-R cells (BioAssay ELISA kit human or mouse, respectively; US Biological Life Science Salem, MA, USA), following the manufacturer's instructions. Absorbance was assessed at 450 nm.

2.10 | In vivo model

Six-to-eight-week-old BALB/c female mice were maintained in controlled environmental conditions (25°C and 12 hours light/dark cycle) and were supplied with rodent food LabDiet 5001 (LabDiet, St. Louis, MO, USA) and water ad libitum.

2.11 | Prophylactic vaccinations

L5178Y-R cells (1.5, 3, 5×10^6) were treated with 300 µmol/L PKHB1 (CC₁₀₀) for 2 hours. Cell death was confirmed using Trypan blue staining and flow cytometry. Treatment was carried out as follows: PKHB1-treated L5178Y-R cells were inoculated s.c. in 100 µL PBS into the left hind leg (day -7); 2×10^6 viable cells were inoculated into the right hind leg 7 days later⁴² (day 0). Tumors were measured three times per week until necropsy (day 60).

2.12 | Tumor establishment, drug administration and tumor measurement

Tumor was established by s.c. injection of 1×10^6 L5178Y-R cells in 100 µL PBS into the left hind leg. When the tumor reached 100 mm³, the first PKHB1 i.p. injection (200 µg) was applied (day 0). To reach complete remission, PKHB1 injection (200 µg) was applied once a week for 6 weeks (days 7, 14, 21, 28 and 35); mice in complete remission were used for long-term memory assay. Tumor volume and weight were measured three times per week using a caliper (Digimatic Caliper; Mitutoyo

Corporation, Kawasaki, Japan) and a digital scale (AWS-600-BLK American Weigh Scales Inc. Norcross, GA, USA). Tumor volume was determined with the formula: tumor volume (mm^3) = $4\pi/3 \times A \times B \times C$ where $4\pi/3$ is a mathematical constant, A= width, B= high, and C= depth.

2.13 | Long-term memory assay

Mice in complete remission after PKHB1 treatment were rechallenged with 2×10^6 cells in 100 μL PBS into the opposite limb, and tumor volume was measured as described above.

2.14 | Histology and immunohistochemistry

Tissues and organs were obtained and fixed in 10% neutral formalin, embedded in paraffin, sectioned (5 μm thickness) and stained with H&E (Sigma-Aldrich). Histopathological analysis was done by an external veterinarian pathologist (National professional certificate 2593012). Immunohistochemistry was done using CD4; MT310 sc-19641 and CD8; 32-M4 sc-1177 (Santa Cruz Biotechnology) primary antibodies, adding the universal biotinylated secondary antibody (VECTASTAIN Universal Quick HRP kit; Vector Laboratories, Burlingame, CA, USA)

following the manufacturer instructions, and developed with diaminobenzidine substrate (ImmPACT DAB; Vector Laboratories). Finally, hematoxylin-counterstained slides were coverslipped using resin as mounting solution and observed under the microscope.

2.15 | Statistical analysis

Mice were randomly assigned to different groups for all in vivo studies. Experiments were repeated three independent times. Mann-Whitney test and two-tailed unpaired Student's *t* test were carried out using GraphPad Prism Software (San Diego CA, USA) and presented as mean value \pm SD. *P*-values were considered significant as follows: *P* < .05; *P* < .01 and *P* < .001.

3 | RESULTS

3.1 | CD47 agonist peptide PKHB1 induces cell death in human and murine tumor lymphoblastic T-cell lines

The thrombospondin-1 mimetic peptide PKHB1 has shown cytotoxicity in several neoplastic cell lines.^{33,34} However, its effects on human

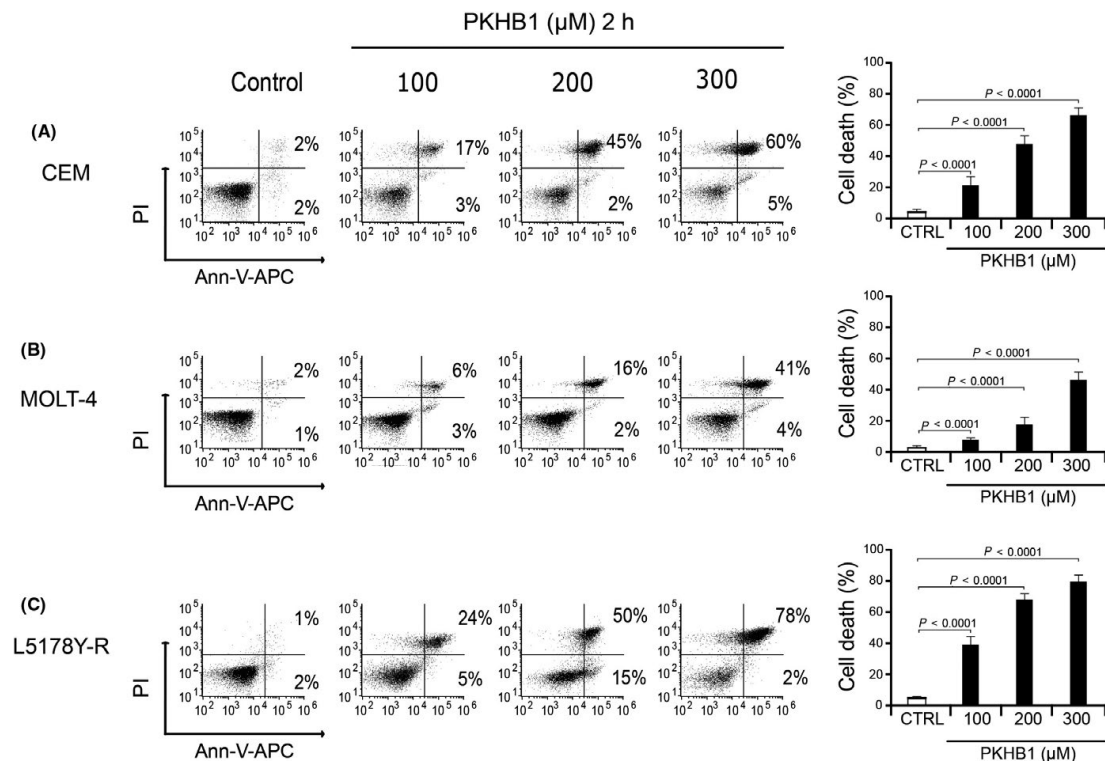


FIGURE 1 PKHB1 induces cell death in T-cell acute lymphoblastic leukemia cell lines. Cell death was measured by Annexin-V-allophycocyanin (Annexin-V-APC) and propidium iodide (PI) staining and graphed. Dot plots of (A) CEM, (B) MOLT-4 human leukemia cells, and (C) L5178Y-R murine cell line, without treatment (Control) and treated with 100, 200 and 300 $\mu\text{mol/L}$ PKHB1 for 2 h. Charts represent the means (\pm SD) of triplicates of at least three independent experiments (right side for each cell line)

ALL-derived CEM and MOLT-4 cell lines, as well as on the murine homologous L5178Y-R cell line (a murine T-cell lymphoblastic tumor cell line) has not been tested. Therefore, we assessed the effects of PKHB1 on these cells. PKHB1 induces cell death in a concentration-dependent way, because the cells incubated for 2 hours with increasing concentrations (100, 200 and 300 $\mu\text{mol/L}$) of PKHB1 showed an increase in the number of Ann-V-APC/PI positive CEM (Figure 1A), MOLT-4 (Figure 1B) and L5178Y-R (Figure 1C) cells. The cytotoxic concentration that induces approximately 50% of cell death (CC_{50}) in CEM is 200 $\mu\text{mol/L}$, in MOLT-4 is 300 $\mu\text{mol/L}$, and in L5178Y-R is 200 $\mu\text{mol/L}$.

3.2 | PKHB1 prompts caspase-independent but calcium-dependent cell death with loss of mitochondrial membrane potential in CEM, MOLT-4 and L5178Y-R cells

Once we determined that PKHB1 induces quick phosphatidylserine exposure and plasma membrane permeability in T-ALL cell

lines, we next assessed whether PKHB1-induced cell death in T-ALL cells shared the principal biochemical features previously described for CD47-mediated cell death; these include caspase independence,⁴³ a sustained calcium influx and mitochondrial membrane potential ($\Delta\Psi\text{m}$) loss.^{33,44} Thus, we preincubated the cells with a pan-caspase inhibitor (Q-VD-OPH) or an extracellular Ca^{2+} chelator (BAPTA) and cell death was tested. Caspase inhibition did not prevent PKHB1-induced killing of CEM (from 51% to 48%), MOLT-4 (from 57% to 51%), and L5178Y-R (from 52% to 49%) cells. Nevertheless, extracellular calcium chelation significantly reduced PKHB1-induced cell death in all cases: CEM (from 51% to 18%), MOLT-4 (from 57% to 38%), and L5178Y-R (from 52% to 21%) (Figure 2A). Calcium dependence for death induced by an immobilized anti-CD47 (B6H12) was also corroborated in CEM cells (Figure S1).

Treatment with the PKHB1 CC_{50} also induced loss of $\Delta\Psi\text{m}$ in T-ALL (Figure 2B) being 49% in CEM, 61% in MOLT-4, and of 51% in L5178Y-R.

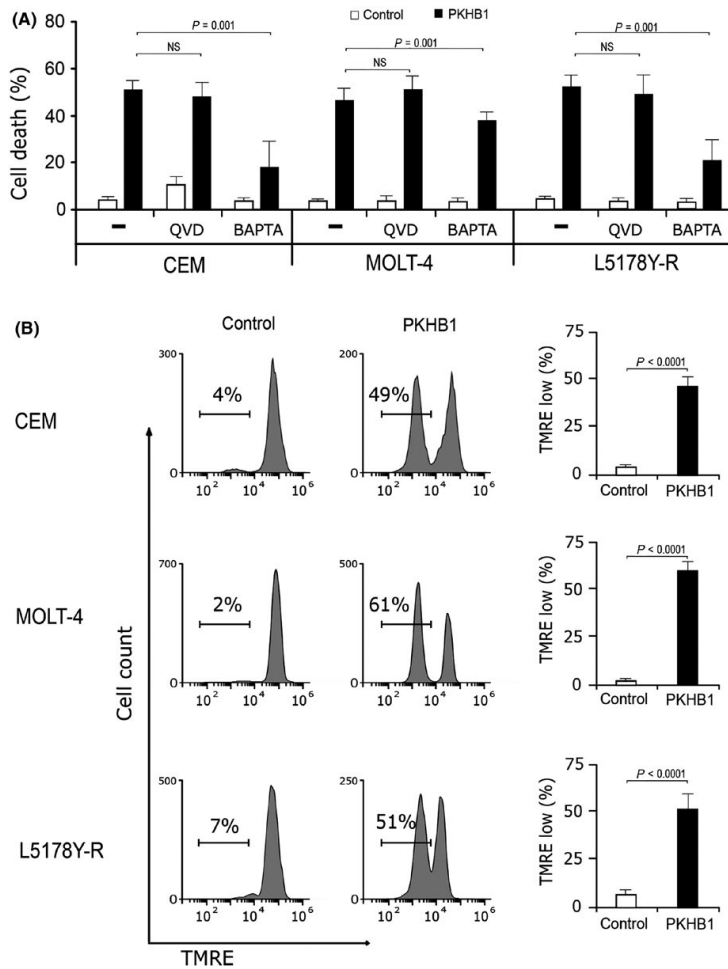


FIGURE 2 PKHB1 induces caspase-independent but calcium-dependent cell death and loss of mitochondrial membrane potential on leukemia cell lines. A, Graph represents cell death percentage of T-cell acute lymphoblastic leukemia (T-ALL) cells without treatment (Control) or treated with PKHB1 (200 $\mu\text{mol/L}$, 2 h) and left alone (-) or preincubated for 30 min with QVD (10 $\mu\text{mol/L}$) or Ca^{2+} chelator (BAPTA, 5 mmol/L) in the different cell lines tested. B, Loss of $\Delta\Psi\text{m}$ induced by PKHB1 (200 $\mu\text{mol/L}$, 2 h) was measured in T-ALL cells, and representative cytofluorometric plots are shown for each cell line tested. Charts (right) represent the means (\pm SD) of triplicates of at least three independent experiments. TMRE, tetramethylrhodamine ethyl ester. NS= Not significant

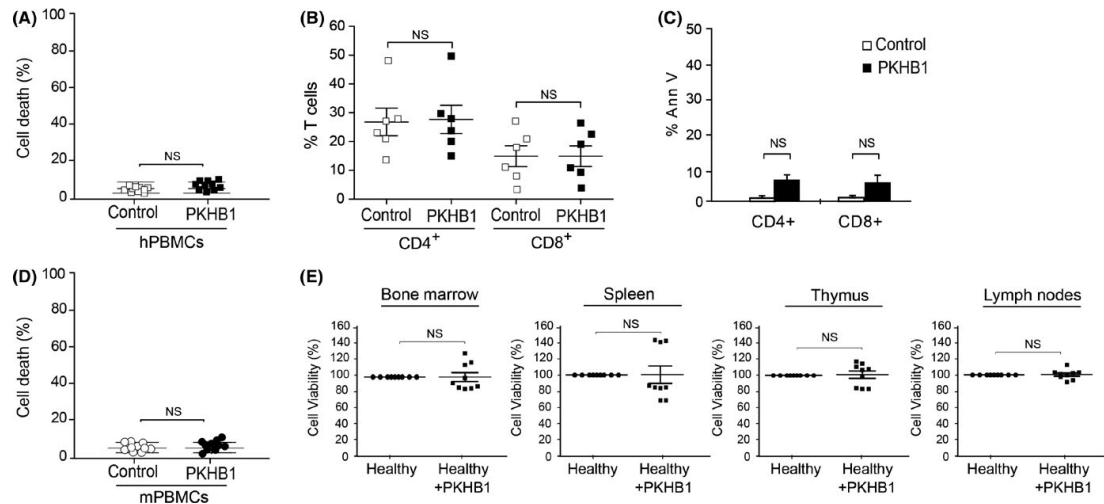


FIGURE 3 PKHB1 spares non-cancerous primary leukocytes from mice and humans in vitro. A, Cell death of total PBMC treated with PKHB1 was measured by Annexin-V/propidium iodide (PI) staining, and each donor is indicated as a square ($n = 10$ donors). B, Percentage of CD4⁺ and CD8⁺ T cells from each donor, left untreated (white square) or treated with PKHB1 (black square) ($n = 6$ donors). C, Cell death of CD4⁺ and CD8⁺ human cells was measured by Annexin-V-allophycocyanin (Annexin-V-APC) and graphed. D, Cell death of murine PBMC treated with PKHB1 was measured by Ann/PI staining. Each mouse is indicated as a circle ($n = 10$ mice). E, Cell viability of cells from bone marrow, spleen, thymus and lymph nodes from healthy mice (without tumor nor treatment) measured by MTT assays ($n = 9$ mice). NS= Not significant

3.3 | PKHB1 treatment spares non-cancerous primary leukocytes derived from humans and mice

Our workgroup previously reported that PKHB1 did not induce significant cell death in residual CD5⁻ B lymphocytes and T cells from CLL patients, and it neither induced kidney nor liver damage in mice.³³ Thus, we tested the selectivity of PKHB1 in human PBMC (Figure 3A) and CD4⁺ and CD8⁺ human T cells (Figure 3B,C) from healthy donors. Additionally, we tested PKHB1 selectivity in murine PBMC (Figure 3D) and primary cultures of bone marrow (BM), spleen, thymus, and lymph nodes of healthy (without tumor or treatment) BALB/c mice through indirect cell viability analysis (Figure 3E) through MTT analysis, as we wanted to determine general cell affection (cytotoxic, cytostatic, or antiproliferative effects). PKHB1 treatment did not significantly affect cell viability of human or murine non-cancerous cells (Figure 3), even though all organs expressed CD47 at a similar level to the neoplastic cells (Figure S2). These results showed the selectivity of PKHB1 to induce cell death in malignant cells only.

3.4 | L5178Y-R tumor-bearing BALB/c mice treated with PKHB1 show leukocyte infiltration to the tumor site and improved leukocyte cell number

After verifying that PKHB1 treatment did not affect healthy leukocytes in vitro, we assessed these effects in vivo. Immunocompetent female BALB/c mice were used to bear L5178Y-R tumor cells, and mice were treated weekly with 200 μ g PKHB1 i.p. After 18 days, all controls had

to be killed, and some PKHB1-treated mice were randomly selected to be killed for comparison. Tumors were dissected, and their morphological and cellular differences were analyzed (Figure 4A). The control group presented undifferentiated lymphoid cells, presumably L5178Y-R cells, some of them carrying out mitosis (Figure 4A left). Conversely, tumors in PKHB1-treated mice contained a mixture of lymphocytes and polymorphonuclear cells (PMN) (Figure 4A middle). Moreover, complete tumor regression in most of the mice was observed at day 30, where histological slides show what seems to be an antitumor immune response in the inoculation site (Figure 4A right). Because anticancer immune response is characterized by tumor infiltrating lymphocytes (TIL), we decided to carry out immunohistochemistry of tumor sections, which indicated the presence of CD4⁺ and CD8⁺ cells in PKHB1-treated mice (Figure 4B).

In addition, we carried out cell counts from lymphoid organs that belonged to control, PKHB1-treated or healthy mice. Noticeably, in PKHB1-treated mice, a significant increase in cell number of BM, spleen and thymus cells, and a significant decrease in cell number of lymph nodes were observed (Figure 4C). Moreover, cell number of the same organs in PKHB1-treated mice was similar to that of healthy mice. Additionally, the white blood cell (WBC) differential was carried out and showed no significant difference between healthy and PKHB1-treated mice, whereas untreated tumor-bearing mice presented a significant difference from the other two groups in all leukocyte types (Figure 4D). Altogether, the above suggests that PKHB1 improves the antitumor immune system of tumor-bearing mice and indicates possible participation of the immune system in complete tumor regression.

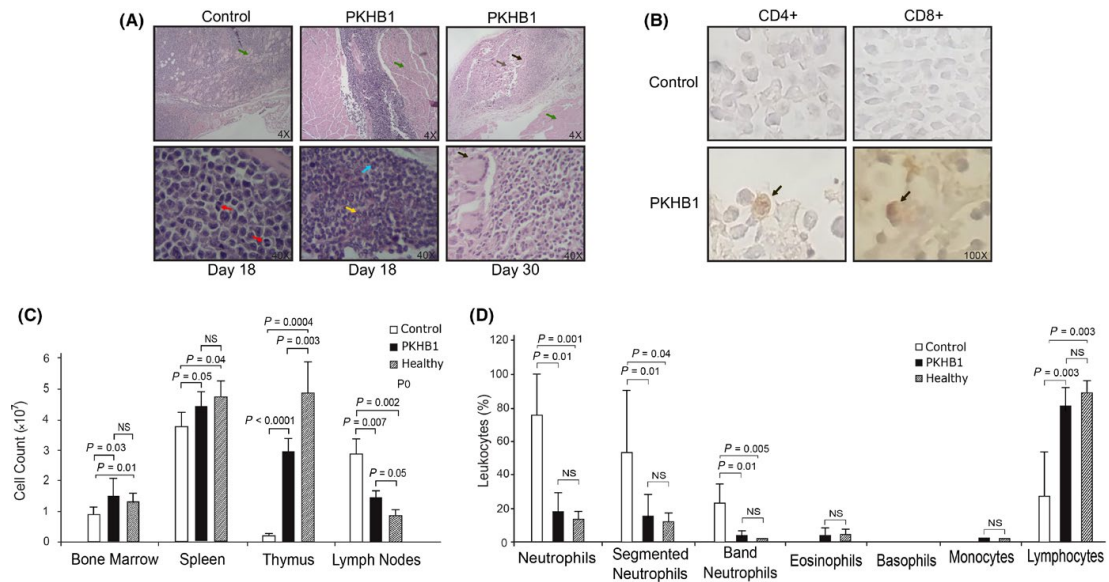


FIGURE 4 PKHB1-treatment of L5178Y-R tumor-bearing mice induces leukocyte infiltration to the tumor site and improves leukocyte cell number. A, Histology from tumors from control (day 18) and PKHB1-treated mice (days 18 and 30) stained with H&E. Mitotic cells (red arrow), lymphocytes (blue arrow), eosinophils (yellow arrow), giant cells (black arrow), necrosis (brown arrow) and, normal tissue (green arrow). B, For immunohistochemical staining, CD4⁺ and CD8⁺ cells were labeled in tumor tissue of control and PKHB1-treated mice. Arrows point to cells with positive labeling. C, Cell count of lymphoid organs from mice with tumor without treatment (Control), from mice with tumor treated with PKHB1 or from mice without tumor and without treatment (Healthy) was carried out using Trypan blue staining (n = 6 mice). D, Different types of leukocytes from control, PKHB1-treated and healthy mice are displayed in the graph, obtained using hematic biometry analysis. Results shown are representative of triplicates of at least three experiments. NS= Not significant

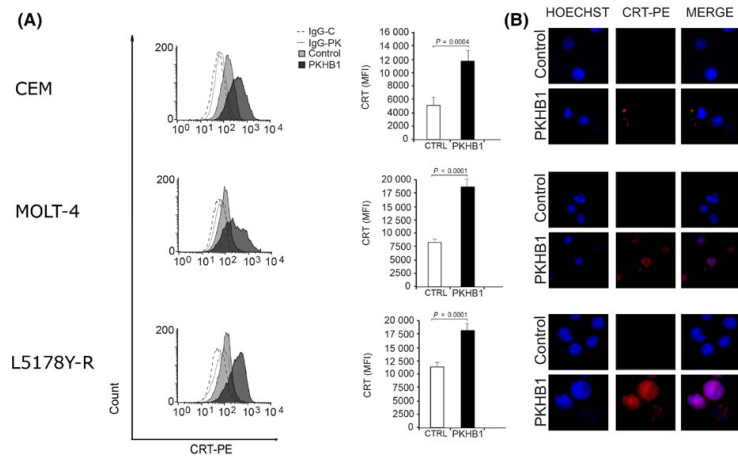


FIGURE 5 PKHB1 induces calreticulin exposure. A, Left charts are representative of surface calreticulin (CRT) detection in CEM (upper), MOLT-4 (middle) and L5178Y-R (bottom) cells using FACS. Negative controls, with IgG isotype antibodies, are shown in dotted (IgG-C) and solid (IgG-PK) lines, whereas gray (Control) is the basal CRT and black are cells treated (PKHB1). Right charts represent the means (\pm SD) of triplicates of at least three independent experiments. B, ECTO-CRT was observed in the cells treated with PKHB1 by CRT-PE staining and the nucleus was stained with Hoechst 33342 and visualized by confocal microscopy 40 \times (Mechanic zoom 7, Olympus X70; Olympus, Tokyo, Japan). Results shown are representative of triplicates of three independent experiments. CRT-PE = Calreticulin-PhycoErythrin

3.5 | PKHB1 treatment induces DAMP exposure and release in T-ALL cells

Previous results showed that PKHB1 could be an ICD inducer; thus, we assessed the exposure and release of several DAMP in T-ALL cells. In Figure 5, it can be observed that CEM, MOLT-4, and L5178Y-R cells incubated with the CC₅₀ of PKHB1 presented a significant increase in CRT exposure, analyzed by flow cytometry (Figure 5A), and confocal microscopy (Figure 5B).

Then, we measured the expression and release of HSP90, HSP70, CRT and HMGB1. The presence of these DAMP was determined by western blot in cellular lysates and supernatant of untreated cells and PKHB1-treated cells at CC₅₀ and CC₁₀₀ for each cell line tested.

Figure 6A shows the decrease in the expression of HSP90, HSP70, CRT, and HMGB1 in cellular lysates of cells treated with PKHB1. Conversely, expression of these DAMP increased in PKHB1-treated supernatants compared with the untreated cells (Figure 6B). These results indicate that PKHB1 treatment prompts the release of heat-shock proteins, CRT, and HMGB1 to the extracellular medium.

As HMGB1 release was barely detected by western blot, an ELISA assay was carried out. HMGB1 release varied depending on the cell line studied and on the concentration of PKHB1 used. Using PKHB1 CC₁₀₀ in CEM, MOLT-4 and L5178Y-R cell lines, HMGB1 release was sixfold, fourfold and twofold, respectively, compared to the untreated control, whereas using PKHB1 CC₅₀, MOLT-4 cells HMGB1 release was eightfold with respect to the control (Figure 7A).

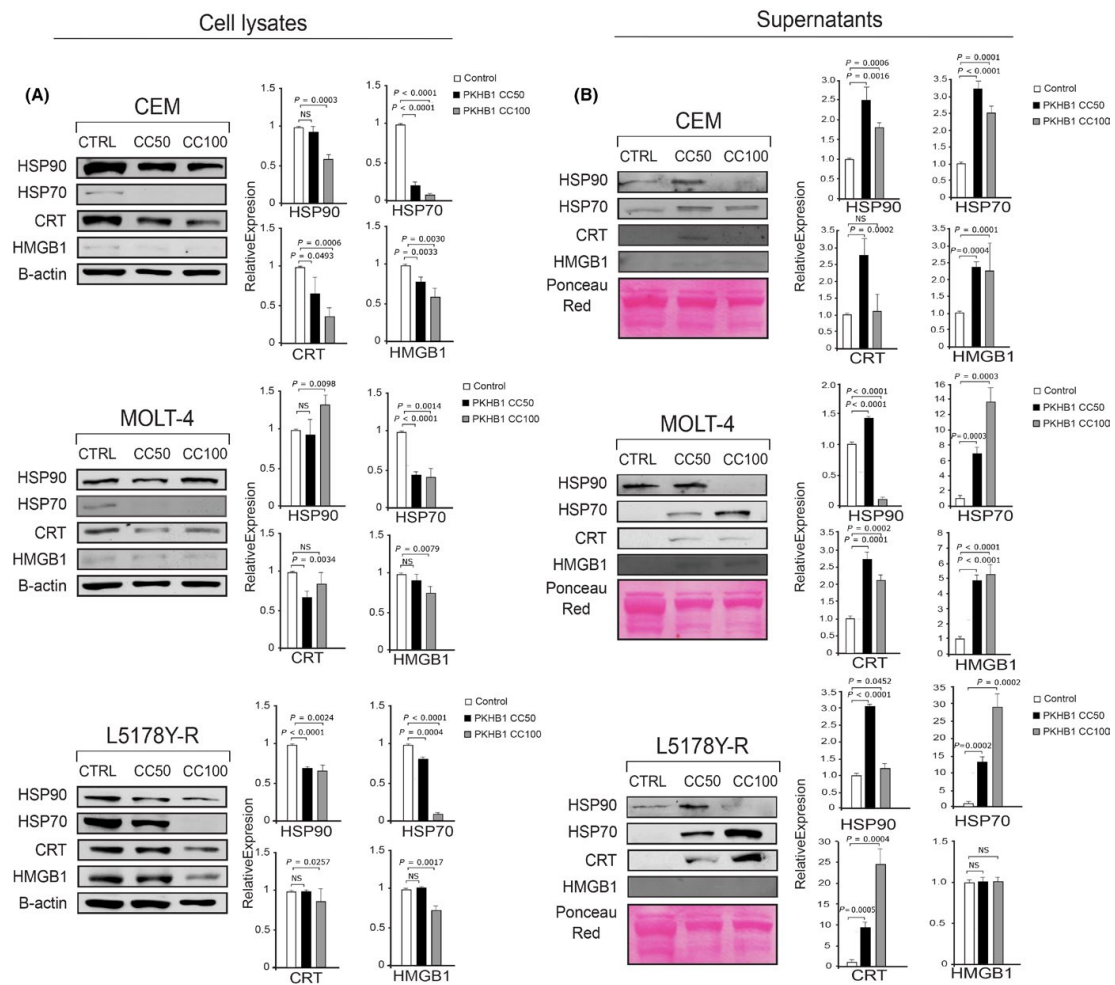


FIGURE 6 Heat shock protein (HSP)90, HSP70, calreticulin (CRT) and high-mobility group box 1 (HMGB1) protein expression and release in response to treatment with PKHB1. Western blot and densitometry analyses were carried out using cellular lysates (A) or supernatants (B) of CEM, MOLT-4 and L5178Y-R cells untreated and treated with two concentrations of PKHB1. Loading controls, β -actin, and Ponceau red were used to determine densitometry analyses of relative protein expression. Results shown are representative of triplicates of at least three independent experiments. NS= Not significant

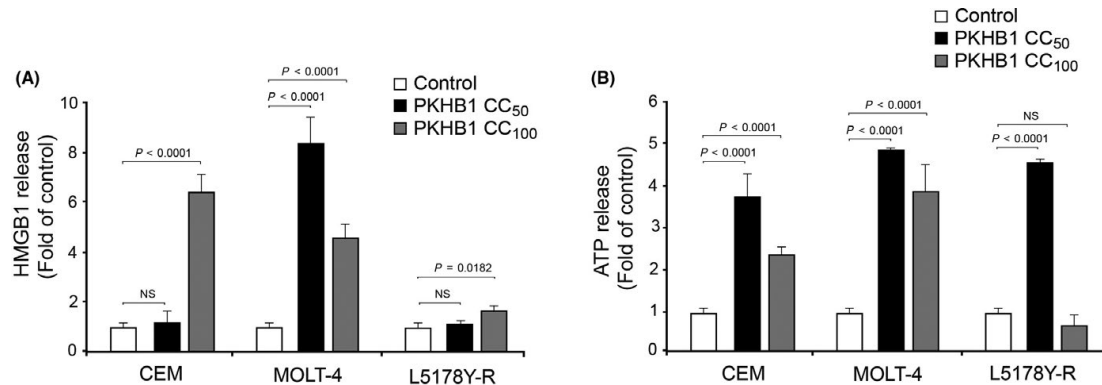


FIGURE 7 PKHB1 induces high-mobility group box 1 (HMGB1) and ATP release in CEM, MOLT-4 and L5178Y-R cell lines. Cells were treated with PKHB1 at CC₅₀ and CC₁₀₀ for 2 h, then 100 μ L supernatant of each sample was taken to measure HMGB1 release by ELISA (A) or ATP release through bioluminescence detection (B). Charts shown are means (\pm SD) of triplicates of three independent experiments. NS= Not significant

Another important indicator that immunogenic death is taking place is ATP-release. Therefore, a bioluminescence assay was carried out, finding that in supernatants of PKHB1-treated cells at CC₅₀ and CC₁₀₀, the presence of ATP significantly increased (Figure 7B).

3.6 | PKHB1-treated cells as prophylactic vaccine prevented tumor establishment of L5178Y-R cells

Considering the previous data, noting that PKHB1 treatment induces ICD, the next step was to carry out a prophylactic vaccination, which is the gold standard to confirm whether PKHB1 treatment induced ICD in vivo. The vaccine is based in the use of L5178Y-R cells treated in vitro with PKHB1 CC₁₀₀. Four groups of mice were used as follows: (i) control group without vaccine; (ii) 1.5M vaccine group, with 1.5×10^6 PKHB1-treated cells; (iii) 3M vaccine group, with 3×10^6 PKHB1-treated cells; and (iv) 5M vaccine group with 5×10^6 PKHB1-treated cells. Results showed that vaccination containing PKHB1-treated cells prevented the establishment of L5178Y-R tumor and a greater number of dead cells as a result of the peptide, and showed better response against tumor cells inoculated 7 days after receiving the vaccine (Figure 8). In the control group, six out of six mice (100%) developed tumor after inoculation with viable cells (Figure 8A top left), whereas three out of four mice (75%) developed tumor in the 1.5M vaccine group (Figure 8A top right), seven out of 14 mice (50%) developed tumor in the 3M vaccine group (Figure 8A lower left), and none of the mice (0%) in the 5M vaccine group developed the tumor (Figure 8A lower right). The 60-day survival rates of mice in each group were consistent with tumor growth, being 100% in the 5M vaccine group (Figure 8B).

3.7 | PKHB1-treatment induced long-term prevention of tumor establishment

Additionally, we assessed long-term tumor prevention in mice that presented complete tumor regression after PKHB1 treatment. In

these experiments one out of six mice (\approx 17%) rechallenged with 2×10^6 L5178Y-R viable cells developed tumor, whereas in the naïve control group, six out of six (100%) presented tumor growth (Figure 8C). Survival percentage was graphed using Kaplan-Meier curve, where rechallenged mice showed 90% survival (Figure 8D).

4 | DISCUSSION

There are few scientific reports on the use of synthetic peptides that can induce ICD.⁴⁵⁻⁴⁷ Herein, we assessed the ability of PKHB1, the first serum-stable CD47-agonist peptide: (i) to induce selective cell death in T-ALL cells with conserved characteristics of CD47-mediated cell death; and (ii) to determine whether this type of cell death is immunogenic. We observed that PKHB1 induced death in CEM, MOLT-4, and L5178Y-R cells (Figure 1), in a fast caspase-independent process that implicates phosphatidylserine exposure along with plasma membrane permeabilization, and loss of mitochondrial membrane potential (Figure 2) that is selective for malignant cells (Figure 3). These features have largely implicated CD47-induced cell death.^{33,34,39,40,44} In addition, we observed that calcium dependence for cell death induced by PKHB1 was conserved in T-ALL cells, as previously observed in CLL cells.³³

Our results showed that treatment with PKHB1 in tumor-bearing mice induces leukocyte infiltration to the tumor site and improves leukocyte cell number in different lymphoid organs (Figure 4). Increasing evidence suggests that ICD induces an antitumor immune response, increasing tumor infiltration of T cells. ICD stimulates the recruitment of DC through DAMP release. DC process tumor antigens and present antigens to T cells, helping to kill tumor cells. Thus, infiltration of T cells into the tumor site can be explained by exposure and secretion of CRT, and secretion of ATP and HMGB1 by the dying cells, which stimulate DC recruitment into the tumor microenvironment, antigen processing and presentation to T cells which then infiltrate the tumor site.^{48,49}

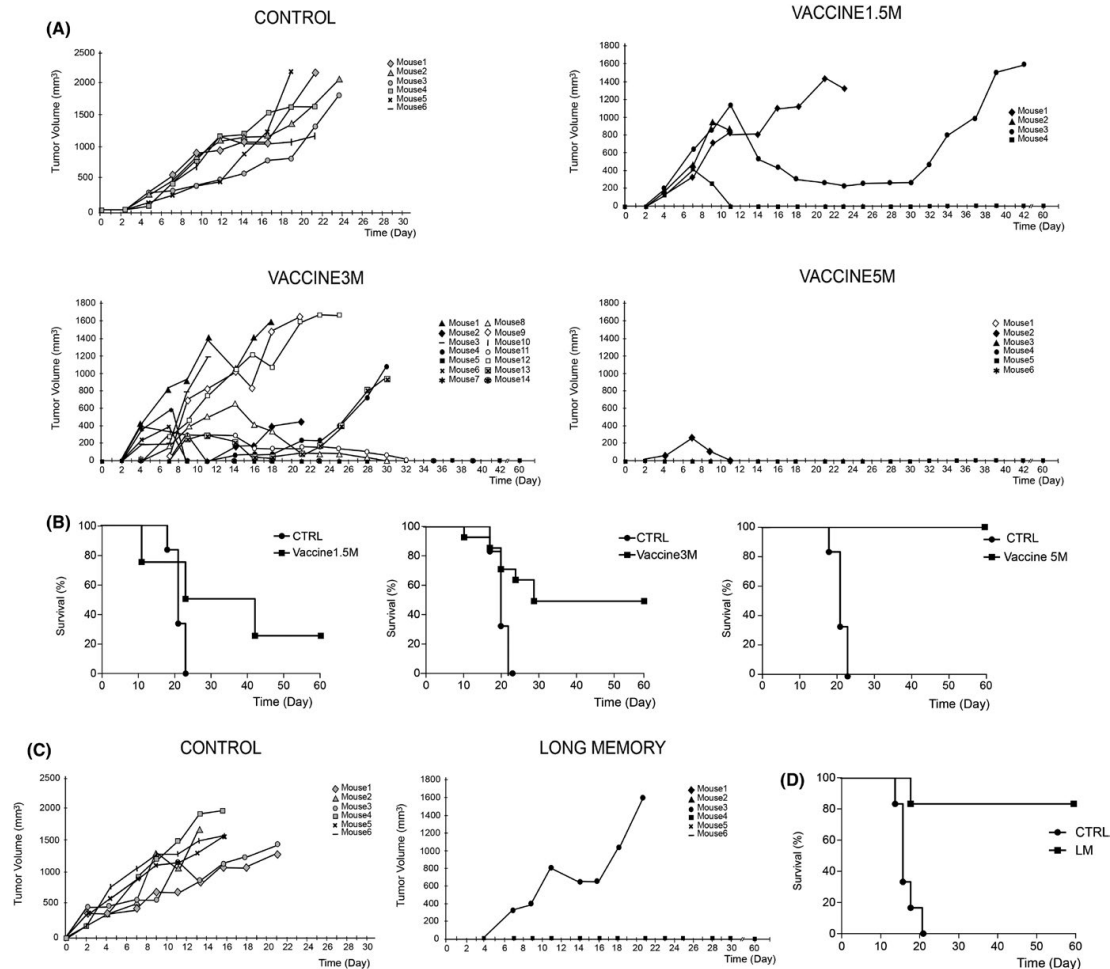


FIGURE 8 PKHB1 induces short- and long-term immunological memory through prophylactic vaccination or prior exposure to the tumor and treatment. A, Graphs indicate tumor growth in unvaccinated mice (Control; $n = 6$) or vaccinated with 1.5×10^6 (1.5M; $n = 4$), 3×10^6 (3M; $n = 8$) or 5×10^6 (5M; $n = 6$) CC₁₀₀ PKHB1-treated L5178Y-R cells and rechallenged with 2×10^6 living L5178Y-R cells. Each line represents one mouse. B, Survival in vaccinated mice over time. C, Long-term antitumor memory of mice in remission rechallenged with 3×10^6 viable L5178Y-R cells (control $n = 6$, PKHB1-treated $n = 6$). D, Survival in rechallenged mice over time. Survival is represented by the Kaplan-Meier graph

Indeed, PKHB1 prompted DAMP exposure and release on T-ALL cells. As CRT is one of the principal molecules necessary to determine that cell death is immunogenic,^{6,18} we demonstrated its exposure, by flow cytometry and confocal microscopy, on T-ALL after PKHB1 treatment (Figure 5). Diverse studies in the immunology field highlight the importance of CRT exposure as an "eat me" signal^{6,15,50,51} that helps antigen uptake by APC by binding to low-density lipoprotein receptor-related protein 1 (LRP1).⁷ There is a tight correlation between CRT and CD47 expression in cancer cells.⁵¹ Indeed, recently, it was determined that treatment of breast cancer cell lines with thrombospondin-1 (TSP-1) promoted interaction of TSP-1 with CRT and CD47 and induced cell autophagy and tumor growth inhibition in xenografted mice.⁵²

These results support the idea that TSP-1 or peptides derived from TSP-1 can induce cell death through CD47 activation and its correlation with CRT exposure. Also, HSP70 and HSP90, HMGB1 and ATP were released by PKHB1 treatment on CEM, MOLT-4 and L5178Y-R cell lines (Figures 6,7). Release of these molecules is involved in the activation of the immune system and induction of potent anticancer immunity.^{17,53,54}

However, DAMP release is not sufficient to ensure ICD induction, and in vivo vaccination is considered the gold standard.^{1,18,21} Our in vivo assays showed that PKHB1 activates short- and long-term immunological memory and induces a protective anticancer response in an immunocompetent murine model, as tumor

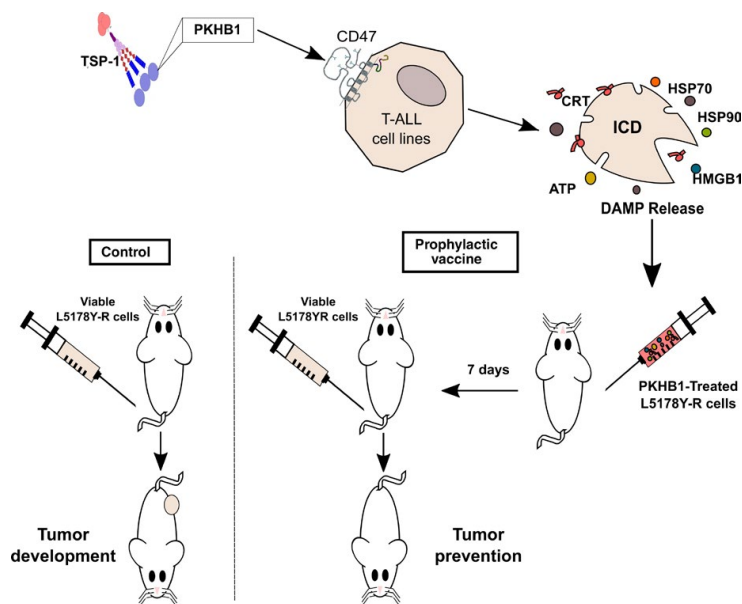


FIGURE 9 Schematic representation of CD47-mediated immunogenic cell death. PKHB1 induces fast immunogenic cell death in T-cell acute lymphoblastic leukemia cells (T-ALL) leading to damage-associated molecular patterns (DAMP) release. Giving prophylactic antitumor vaccine of tumor cells previously treated with PKHB1 prevented tumor establishment in vivo. CRT, calreticulin; HMGB1, high-mobility group box 1; HSP, heat shock protein; ICD, immunogenic cell death; TSP-1, thrombospondin-1

growth was prevented in most cases (Figure 9). We observed that increasing the number of PKHB1-treated cells in the vaccine improves its protective antitumor response (Figure 8). Previous reports using other ICD inducers also prevented tumor growth, such as in the case of melphalan, an alkylating agent used in melanoma treatment, where C57BL6 mice were injected with melphalan-killed murine B78 melanoma cells and rechallenged 10 days later with B78 viable cells, resulting in 40% of mice without tumor.⁵⁵ Similar results were obtained using doxorubicin in a mouse colon carcinoma (CT26) cell line.⁴² The use of this vaccine helps to stimulate anticancer immunity through the maturation of DC and cytotoxic T-cell activation⁵⁶ as well as enhancing NK cytotoxic activity.⁵⁷

Immunotherapy is a promising treatment option against cancer,⁵⁸ using host immune defenses against cancer and seeking to endow cancer cells with immunogenicity.⁵⁹ The increased immunogenicity of tumor cells triggers antitumor immune responses that could offer long-term therapeutic effects.¹ The finding that certain drugs are able to induce the awakening of the immune response by releasing DAMP and generating ICD triggered investigations to look for these types of agent.^{1,42,57,60} Anthracyclines, platinum derivatives, alkylating agents, and proteasome inhibitors are chemotherapeutic drugs with large amounts of evidence for triggering ICD.⁶¹ Other therapeutic modalities that show ICD induction are photodynamic therapy,⁶² radiotherapy,⁶³ oncolytic viruses,^{64,65} high hydrostatic pressure,⁶⁶ and other phytochemical agents such as shikonin^{67,68} and capsaicin.^{69,70}

Overall, our results highlight the advantages of the potential therapeutic use of targeting CD47 through peptide-based strategies, such as PKHB1, leading us to consider that this peptide

could be used in other types of cancer. However, the molecular pathway by which PKHB1 induces this type of death through CD47 signaling remains unclear, as does whether this type of treatment could be used therapeutically. Therefore, we believe that CD47 agonist peptides deserve further investigation, which might lead to the possibility of being scaled in the near future to clinical phases.


ACKNOWLEDGMENTS

We are grateful to Alejandra Elizabeth Arreola-Triana for article revision and editorial support for this manuscript. We thank the SEP-CONACYT-ECOS-ANUIES grant 291297 and the Laboratory of Immunology and Virology of the College of Biological Sciences, UANL, for the financial support and the facilities provided to achieve this work. ACUP, KMCR, and LGM thank CONACYT for their thesis grant. We also thank, for their financial support, Labex Michem (TD PhD thesis grant) and FNRS (EL PhD thesis grant). PK is grateful to Oncodesign for hosting the LBM DRUG lab.

CONFLICTS OF INTEREST

The patent applications PCT/EP2013/061727 and PCT/EP2014/077335 included results from this paper. A patent describing this work has been filed. No other competing interests exist.

ORCID

Ana Carolina Martínez-Torres  <https://orcid.org/0000-0002-6183-0089>

REFERENCES

- Kroemer G, Galluzzi L, Kepp O, Zitvogel L. Immunogenic cell death in cancer therapy. *Annu Rev Immunol*. 2013;31:51-72.
- Galluzzi L, Vitale I, Aaronson SA, et al. Molecular mechanisms of cell death: recommendations of the Nomenclature Committee on Cell Death 2018. *Cell Death Differ*. 2018;25(3):486-541.
- Land WG. The role of damage-associated molecular patterns (DAMPs) in human diseases: part II: DAMPs as diagnostics, prognostics and therapeutics in clinical medicine. *Sultan Qaboos Univ Med J*. 2015;15(2):e157.
- Rubartelli A, Lotze MT. Inside, outside, upside down: damage-associated molecular-pattern molecules (DAMPs) and redox. *Trends Immunol*. 2007;28(10):429-436.
- Garg AD, Dudek AM, Agostinis P. Cancer immunogenicity, danger signals, and DAMPs: what, when, and how? *BioFactors*. 2013;39(4):355-367.
- Obeid M, Tesniere A, Ghiringhelli F, et al. Calreticulin exposure dictates the immunogenicity of cancer cell death. *Nat Med*. 2007;13(1):54-61.
- Garg AD, Krysko DV, Verfaillie T, et al. A novel pathway combining calreticulin exposure and ATP secretion in immunogenic cancer cell death. *EMBO J*. 2012;31(5):1062-1079.
- Fucikova J, Kasikova L, Truxova I, et al. Relevance of the chaperone-like protein calreticulin for the biological behavior and clinical outcome of cancer. *Immunol Lett*. 2018;193:25-34.
- Spisek R, Charalambous A, Mazumder A, Vesole DH, Jagannath S, Dhodapkar MV. Bortezomib enhances dendritic cell (DC)-mediated induction of immunity to human myeloma via exposure of cell surface heat shock protein 90 on dying tumor cells: therapeutic implications. *Blood*. 2007;109(11):4839-4845.
- Garg AD, Galluzzi L, Apetoh L, et al. Molecular and translational classifications of DAMPs in immunogenic cell death. *Front Immunol*. 2015;6:588.
- Elliott MR, Chekeni FB, Trampont PC, et al. Nucleotides released by apoptotic cells act as a find-me signal to promote phagocytic clearance. *Nature*. 2009;461(7261):282.
- Aymeric L, Apetoh L, Ghiringhelli F, et al. Tumor cell death and ATP release prime dendritic cells and efficient anticancer immunity. *Cancer Res*. 2010;70(3):855-858.
- Martins I, Wang Y, Michaud M, et al. Molecular mechanisms of ATP secretion during immunogenic cell death. *Cell Death Differ*. 2014;21(1):79-91.
- Scaffidi P, Misteli T, Bianchi ME. Release of chromatin protein HMGB1 by necrotic cells triggers inflammation. *Nature*. 2002;418(6894):191-195.
- Inoue H, Tani K. Multimodal immunogenic cancer cell death as a consequence of anticancer cytotoxic treatments. *Cell Death Differ*. 2014;21(1):39-49.
- Tesniere A, Panaretakis T, Kepp O, et al. Molecular characteristics of immunogenic cancer cell death. *Cell Death Differ*. 2008;15(1):3-12.
- Krysko DV, Garg AD, Kaczmarek A, Krysko O, Agostinis P, Vandenabeele P. Immunogenic cell death and DAMPs in cancer therapy. *Nat Rev Cancer*. 2012;12(12):860.
- Bezu L, Gomes-da-Silva LC, Dewitte H, et al. Combinatorial strategies for the induction of immunogenic cell death. *Front Immunol*. 2015;6:187.
- Kepp O, Senovilla L, Vitale I, et al. Consensus guidelines for the detection of immunogenic cell death. *Oncoimmunology*. 2014;3(9):e955691.
- Garg AD, More S, Rufo N, et al. Trial watch: immunogenic cell death induction by anticancer chemotherapeutics. *Oncoimmunology*. 2017;6(12):e1386829.
- Galluzzi L, Buqué A, Kepp O, Zitvogel L, Kroemer G. Immunogenic cell death in cancer and infectious disease. *Nat Rev Immunol*. 2017;17(2):97-111.
- Jabbour E, O'Brien S, Konopleva M, Kantarjian H. New insights into the pathophysiology and therapy of adult acute lymphoblastic leukemia. *Cancer*. 2015;121(15):2517-2528.
- Terwilliger T, Abdul-Hay M. Acute lymphoblastic leukemia: a comprehensive review and 2017 update. *Blood Cancer J*. 2017;7(6):e577.
- National Cancer Institute. SEER cancer statistics review, 1975-2015. Leukemia, annual incidence rates (acute lymphocytic leukemia). <https://seer.cancer.gov/statfacts/html/aly1.html> Accessed August, 2018.
- McNeer JL, Bleyer A, Conter V, Stock W. Acute lymphoblastic leukemia. In: Bleyer A, Barr R, Ries L, Whelan J, Ferrari A, eds. *Cancer in Adolescents and Young Adults*. New York: Springer; 2017:151-175.
- McNeer JL, Bleyer A. Acute lymphoblastic leukemia and lymphoblastic lymphoma in adolescents and young adults. *Pediatr Blood Cancer*. 2018;65(6):e26989.
- Jaime-Pérez JC, Fernández LT, Jiménez-Castillo RA, et al. Age acts as an adverse independent variable for survival in acute lymphoblastic leukemia: data from a cohort in Northeast Mexico. *Clin Lymphoma Myeloma Leuk*. 2017;17(9):590-594.
- Li Y, Buijs-Gladdines JG, Canté-Barrett K, et al. IL-7 receptor mutations and steroid resistance in pediatric T cell acute lymphoblastic leukemia: a Genome Sequencing Study. *PLoS Med*. 2016;13(12):e1002200.
- Locatelli F, Schrappe M, Bernardo ME, Rutella S. How I treat relapsed childhood acute lymphoblastic leukemia. *Blood*. 2012;120(14):2807-2816.
- Pogorzala M, Kubicka M, Rafinska B, Wysocki M, Styczynski J. Drug-resistance profile in multiple-relapsed childhood acute lymphoblastic leukemia. *Anticancer Res*. 2015;35(10):5667-5670.
- Thompson PA, Tam CS, O'Brien SM, et al. Fludarabine, cyclophosphamide, and rituximab treatment achieves long-term disease-free survival in IGHV-mutated chronic lymphocytic leukemia. *Blood*. 2016;127(3):303-309.
- Majeti R, Chao MP, Alizadeh AA, et al. CD47 is an adverse prognostic factor and therapeutic antibody target on human acute myeloid leukemia stem cells. *Cell*. 2009;138(2):286-299.
- Martinez-Torres AC, Quiney C, Attout T, et al. CD47 agonist peptides induce programmed cell death in refractory chronic lymphocytic leukemia B cells via PLC γ 1 activation: evidence from mice and humans. *PLoS Med*. 2015;12(3):e1001796.
- Denèfle T, Bouillet H, Herbi L, et al. Thrombospondin-1 mimetic agonist peptides induce selective death in tumor cells: design, synthesis, and structure-activity relationship studies. *J Med Chem*. 2016;59(18):8412-8421.
- Chao MP, Alizadeh AA, Tang C, et al. Therapeutic antibody targeting of CD47 eliminates human acute lymphoblastic leukemia. *Cancer Res*. 2011;71(4):1374-1384.
- Barclay AN, van den Berg TK. The interaction between signal regulatory protein alpha (SIRP α) and CD47: structure, function, and therapeutic target. *Annu Rev Immunol*. 2014;32:25-50.
- Soto-Pantoja DR, Kaur S, Roberts DD. CD47 signaling pathways controlling cellular differentiation and responses to stress. *Crit Rev Biochem Mol Biol*. 2015;50(3):212-230.
- Liu X, Pu Y, Cron K, et al. CD47 blockade triggers T cell-mediated destruction of immunogenic tumors. *Nat Med*. 2015;21(10):1209-1215.
- Leclair P, Liu CC, Monajemi M, Reid GS, Sly LM, Lim CJ. CD47-ligation induced cell death in T-acute lymphoblastic leukemia. *Cell Death Dis*. 2018;9(5):544.
- Mateo V, Lagneaux L, Bron D, et al. CD47 ligation induces caspase-independent cell death in chronic lymphocytic leukemia. *Nat Med*. 1999;5(11):1277-1284.
- Sick E, Jeanne A, Schneider C, Dedieu S, Takeda K, Martiny L. CD47 update: a multifaceted actor in the tumour

- microenvironment of potential therapeutic interest. *Br J Pharmacol*. 2012;167(7):1415-1430.
42. Casares N, Pequignot MO, Tesniere A, et al. Caspase-dependent immunogenicity of doxorubicin-induced tumor cell death. *J Exp Med*. 2005;202(12):1691-1701.
 43. Oldenborg PA. CD47: a cell surface glycoprotein which regulates multiple functions of hematopoietic cells in health and disease. *ISRN Hematol*. 2013;2013:1-19.
 44. Manna PP, Frazier WA. The mechanism of CD47-dependent killing of T cells: heterotrimeric Gi-dependent inhibition of protein kinase A. *J Immunol*. 2003;170(7):3544-3553.
 45. Zhou H, Forveille S, Sauvat A, et al. The oncolytic peptide LTX-315 triggers immunogenic cell death. *Cell Death Dis*. 2016;7(3):e2134.
 46. Pasquereau-Kotula E, Habault J, Kroemer G, Poyet JL. The anti-cancer peptide RT53 induces immunogenic cell death. *PLoS ONE*. 2018;13(8):e0201220.
 47. Sakakibara K, Sato T, Kufe DW, VonHoff DD, Kawabe T. CBP501 induces immunogenic tumor cell death and CD8 T cell infiltration into tumors in combination with platinum, and increases the efficacy of immune checkpoint inhibitors against tumors in mice. *Oncotarget*. 2017;8(45):78277.
 48. Wang YJ, Fletcher R, Yu J, Zhang L. The immunogenic effects of chemotherapy-induced tumor cell death. *Genes Dis*. 2018;5:194-203.
 49. Lanitis E, Dangaj D, Irving M, Coukos G. Mechanisms regulating T-cell infiltration and activity in solid tumors. *Ann Oncol*. 2017;28(suppl_12):xii18-xii32.
 50. Gardai SJ, McPhillips KA, Frasch SC, et al. Cell-surface calreticulin initiates clearance of viable or apoptotic cells through trans-activation of LRP on the phagocyte. *Cell*. 2005;123(2):321-334.
 51. Chao MP, Jaiswal S, Weissman-Tsukamoto R, et al. Calreticulin is the dominant pro-phagocytic signal on multiple human cancers and is counterbalanced by CD47. *Sci Transl Med*. 2010;2(63):63-94.
 52. Chen Q, Fang X, Jiang C, Yao N, Fang X. Thrombospondin promoted anti-tumor of adenovirus-mediated calreticulin in breast cancer: relationship with anti-CD47. *Biomed Pharmacother*. 2015;73:109-115.
 53. Fucikova J, Kralikova P, Fialova A, et al. Human tumor cells killed by anthracyclines induce a tumor-specific immune response. *Cancer Res*. 2011;71(14):4821-4833.
 54. Rodríguez-Salazar MD, Franco-Molina MA, Mendoza-Gamboa E, et al. The novel immunomodulator IMMUNEPOTENT CRP combined with chemotherapy agent increased the rate of immunogenic cell death and prevented melanoma growth. *Oncol Lett*. 2017;14(1):844-852.
 55. Dudek-Perić AM, Ferreira GB, Muchowicz A, et al. Antitumor immunity triggered by melphalan is potentiated by melanoma cell surface-associated calreticulin. *Cancer Res*. 2015;75(8):1603-1614.
 56. Guo C, Manjili MH, Subjeck JR, Sarkar D, Fisher PB, Wang XY. Therapeutic cancer vaccines: past, present, and future. *Adv Cancer Res*. 2013;119:421-475.
 57. Showalter A, Limaye A, Oyer JL, et al. Cytokines in immunogenic cell death: applications for cancer immunotherapy. *Cytokine*. 2017;97:123-132.
 58. Papaioannou NE, Beniata OV, Vitsos P, Tsitsilonis O, Samara P. Harnessing the immune system to improve cancer therapy. *Ann Transl Med*. 2016;4(14):261.
 59. Li X. The inducers of immunogenic cell death for tumor immunotherapy. *Tumori J*. 2018;104(1):1-8.
 60. Pol J, Vacchelli E, Aranda F, et al. Trial Watch: immunogenic cell death inducers for anticancer chemotherapy. *Oncoimmunology*. 2015;4(4):e1008866.
 61. Vacchelli E, Aranda F, Eggermont A, et al. Trial Watch: tumor-targeting monoclonal antibodies in cancer therapy. *Oncoimmunology*. 2014;3(1):e27048.
 62. Tanaka M, Kataoka H, Yano S, et al. Immunogenic cell death due to a new photodynamic therapy (PDT) with glycoconjugated chlorin (G-chlorin). *Oncotarget*. 2016;7(30):47242-47251.
 63. Golden EB, Apetoh L. Radiotherapy and immunogenic cell death. *Semin Radiat Oncol*. 2015;25(1):11-17.
 64. Diaconu I, Cerullo V, Hirvonen ML, et al. Immune response is an important aspect of the antitumor effect produced by a CD40L-encoding oncolytic adenovirus. *Cancer Res*. 2012;72(9):2327-2338.
 65. Yamano T, Kubo S, Fukumoto M, et al. Whole cell vaccination using immunogenic cell death by an oncolytic adenovirus is effective against a colorectal cancer model. *Mol Ther Oncolytics*. 2016;3:16031.
 66. Fucikova J, Moserova I, Truxova I, et al. High hydrostatic pressure induces immunogenic cell death in human tumor cells. *Int J Cancer*. 2014;135(5):1165-1177.
 67. Lin TJ, Lin HT, Chang WT, et al. Shikonin-enhanced cell immunogenicity of tumor vaccine is mediated by the differential effects of DAMP components. *Mol Cancer*. 2015;14(1):174.
 68. Yin S, Yang NS, Lin TJ. Molecular basis of shikonin-induced immunogenic cell death: insights for developing cancer therapeutics. *Receptors Clin Investig*. 2016;3:1-5.
 69. D'Eliseo D, Manzi L, Velotti F. Capsaicin as an inducer of damage-associated molecular patterns (DAMPs) of immunogenic cell death (ICD) in human bladder cancer cells. *Cell Stress Chaperones*. 2013;18(6):801-808.
 70. Jin T, Wu H, Wang Y, Peng H. Capsaicin induces immunogenic cell death in human osteosarcoma cells. *Exp Ther Med*. 2016;12(2):765-770.

SUPPORTING INFORMATION

Additional supporting information may be found online in the Supporting Information section at the end of the article.

How to cite this article: Uscanga-Palomeque AC, Calvillo-Rodríguez KM, Gómez-Morales L, et al. CD47 agonist peptide PKHB1 induces immunogenic cell death in T-cell acute lymphoblastic leukemia cells. *Cancer Sci*. 2019;110:256-268. <https://doi.org/10.1111/cas.13885>

Supplementary material

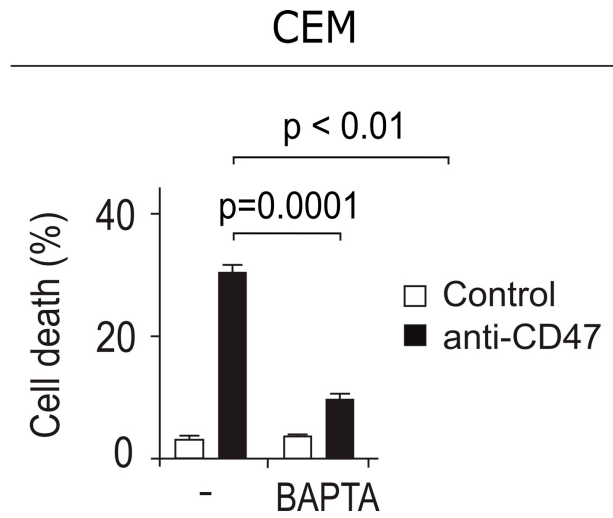


Figure S1. Calcium-dependence in immobilized B6H12-induced cell death. Cell death on CEM cells was measured by Annexin-V-APC and PI staining after calcium chelator (BAPTA) pre-incubation. Bar graphs represent the mean (\pm SD) of triplicates of at least three independent experiments.

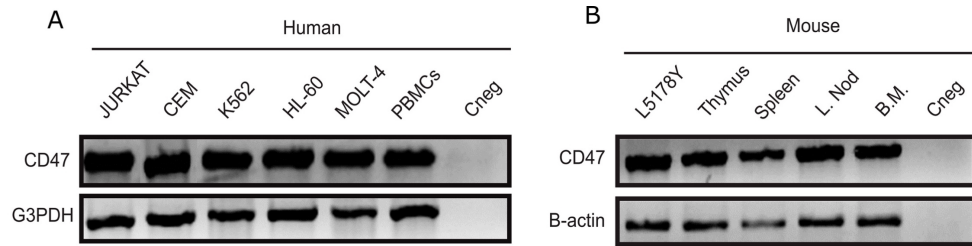


Figure S2. CD47 mRNA expression in cell lines and mouse organs. To confirm the presence of CD47 in **A.** the cell lines tested, as well as in **B.** mouse lymphoid organs, RT-PCR was performed using mRNA (5µg/µL). Every cell tested express CD47. G3PDH and β-actin were used as housekeeping genes.

1.2. PKHB1 tumor cell lysate induces antitumor immune system stimulation and tumor regression in syngeneic mice with tumoral T lymphoblasts

Article published in “Journal of Oncology” on June 4th, 2019 (doi: 10.1155/2019/9852361).

Based on the results obtained previously, showing that PKHB1 induces immunogenic cell death in T-ALL cells, it was evaluated whether cells killed by PKHB1 were able to induce according *ex vivo* immune responses.

First, PKHB1 and 4NGG (inactive control) peptides were manually synthesized using solid support, purified by HPLC, and >99% pure lyophilized peptide fractions were used this time to determine the minimal lethal dose (CC_{100}) of PKHB1 in L5178Y-R cells, measuring cell death by Ann-V-APC and PI staining using flow cytometry. At the PKHB1- CC_{100} (300 μ M), 4NGG did not augment L5178Y-R cell death with respect to untreated controls. As previously reported, extracellular calcium chelation but not caspase inhibition reduced PKHB1-induced cell death. Pharmacological inhibitors of reactive oxygen species production (N-acetyl cysteine), autophagy (spautin-1) or necroptosis (NEC-1) did not prevent cell death neither. Moreover, PKHB1 treatment increased the fluorescence of cells marked with CRT-PE (anti-calreticulin antibody) with respect to untreated cells. The previous confirmed that PKHB1 activates a particular caspase-independent RCD pathway in L5178Y-R cells that induces phosphatidylserine and calreticulin exposure, and suggests that this pathway is not regulated by the canonical initiators of autophagy or necroptosis.

To assess the ability of L5178Y-R cells killed by PKHB1 (PKHB1 tumor cell lysates, PKHB1-TCL) to induce immunogenic cell responses, activation of bone marrow-derived DCs by PKHB1-TCL was first tested. DCs were left alone or co-cultured with PKHB1-TCL for 24 h, washed, recovered, and stained with monoclonal antibodies against a DC maturation marker (anti-CD11c-AF488) and co-stimulatory molecules (anti-CD80-FITC or anti-CD86-APC). Compared to non-pulsed DCs, DCs pulsed with PKHB1-TCL had a similar levels of CD11c⁺ staining, but a higher levels of CD80 and CD86. Moreover, flow cytometry analysis showed that the supernatants of DCs pulsed with PKHB1-TCL had

higher levels of tumor necrosis factor alpha (TNF α). The previous suggests that PKHB1-TCL can induce the maturation of DCs.

To assess whether these PKHB1-TCL-pulsed DCs were able to prime T cells, CD3⁺ cells were obtained by positive selection of mouse PMBCs using magnet-activated cell sorting, and co-cultured with non-pulsed DCs, or with PKHB1-TCL-pulsed DC for four days.

On the one hand, flow cytometry evaluation of Th1/Th2-related cytokine (TNF α , IFN γ , IL-5 and IL-4) release showed that in the supernatants of T cells co-cultured with PKHB1-TCL-pulsed DC, there were significantly higher levels of TNF α , IFN γ and IL-2 compared to the supernatants of T cells co-cultured with non-pulsed DC, where there was a minor TNF α release, and no release IFN γ , IL-5 nor IL-4 nor IL-2. The pattern of cytokine production by theoretically primed T cells corresponds to an anti-tumor Th1 response phenotype.

On the other hand, it was evaluated whether hypothetically primed T cells matured to a L5178Y-R-cytotoxic phenotype. For this, L5178Y-R cells were stained with calcein-AM (which is fluorescent in metabolically active cells) and left alone or co-cultured with unprimed or with theoretically primed T cells. After 24 h, calcein-AM fluorescence in L5178Y-R cells was measured by flow cytometry. L5178Y-R cells cultured alone or co-cultured with unprimed T cells, did not lose calcein-AM fluorescence, while important populations (~75%) of calcein-AM negative L5178Y-R cells appeared when co-cultured with hypothetically primed T-cells, indicating T cell cytotoxicity to L5178Y-R cells. Altogether, the data suggests that L5178Y-R PKHB1-TCL activate the maturation of DC to a phenotype able to prime tumor-specific T cell responses without need of further adjuvanticity.

Given the strong immunogenicity of PKHB1-TCL, it was hypothesized that its application to established tumors could have an impact on tumor growth in vivo. Therefore, mice were inoculated with viable L5178Y-R cells, and waited for tumors to reach 100 mm³ before the first immunization with the PKHB1-TCL or with vehicle. Three more doses were administered 3, 6 and 9 days after. Contrary to controls, where tumor grew and killed all mice after 11 days, PKHB1-TCL significantly reduced tumor growth by the time of the last dose, when it reached its maximum volume (day 9), and after which

begun to decrease until 30 days after tumor establishment, improving overall survival. Mice that achieved remission and controls of similar age were (re-)challenged with L5178Y-R cells after >60 days post-remission. While tumor grew and killed all controls, none of the immunized mice developed the tumor and all survived re-challenge, confirming the long-term immunological memory provided by PKHB1-TCL treatment.

Résumé de l'article 2

La leucémie lymphoïde aiguë (LLA) est le cancer pédiatrique le plus courant. Actuellement, les traitements pour les patients atteints de LLA récidivante et réfractaire reposent principalement sur les immunothérapies. Cependant, les cancers hématologiques sont couramment associés à une faible immunogénicité et une faible tolérance immunitaire, ce qui peut contribuer à la rechute de la leucémie et aux difficultés associées au développement d'immunothérapies efficaces contre cette maladie. Nous avons récemment démontré que PKHB1, un peptide dérivé de TSP1 et agoniste de CD47, induisait une mort cellulaire immunogène (ICD) dans la LLA des cellules T (T-ALL). La mort cellulaire induite par PKHB1 sur les lignées T-ALL et leur homologue murin (L5178Y-R), induit l'exposition et la libération des molécules associées aux dommages cellulaires (DAMP). De plus, une vaccination prophylactique avec des cellules L5178Y-R traitées par PKHB1 prévient l'établissement de la tumeur *in vivo* dans tous les cas. En raison du potentiel immunogène des cellules traitées par PKHB1, nous avons évalué leur capacité à induire des réponses immunitaires antitumorales *ex vivo* et *in vivo* dans une tumeur établie. Nous avons d'abord confirmé la sélectivité de la mort cellulaire induite par PKHB1 sur les cellules tumorales L5178Y-R et observé qu'il y avait corrélation entre l'augmentation de l'exposition de la calréticuline et l'augmentation de la mort cellulaire. Ensuite, nous avons constaté que le lysat de cellules tumorales (TCL) obtenu à partir de cellules tumorales L5178YR traitées par PKHB1 (PKHB1-TCL) était capable d'induire, *ex vivo* la maturation des cellules dendritiques, la production de cytokines et les réponses antitumorales des cellules T. Enfin, nos résultats montrent que *in vivo*, le traitement par PKHB1-TCL induisait une régression tumorale chez les souris syngéniques transplantées avec des cellules L5178Y-R, augmentant leur survie globale et les protégeant de l'établissement des tumeurs après une rechallenge tumorale. Dans l'ensemble, nos résultats mettent en évidence l'immunogénicité de la mort cellulaire induite par PKHB1 et démontrent le potentiel thérapeutique de ce peptide pour surmonter la faible immunogénicité et la tolérance immunitaire dans la T-ALL.

Resumen del artículo 2

La leucemia linfocítica aguda (LLA) es el cáncer pediátrico más común. Actualmente, las opciones de tratamiento para pacientes con LLA en recaída y refractaria se basan principalmente en inmunoterapias. Sin embargo, los cánceres hematológicos se asocian comúnmente con una baja inmunogenicidad y tolerancia inmune, lo que puede contribuir a la recaída de la leucemia y las dificultades asociadas con el desarrollo de inmunoterapias efectivas contra esta enfermedad. Recientemente demostramos que PKHB1, un péptido agonista de CD47 derivado de la TSP1, induce la muerte celular inmunogénica (MCI) en la LLA de células T (LLA-T). La muerte celular inducida por PKHB1 en líneas celulares de LLA-T y su homólogo murino, L5178Y-R (línea celular de linfoblastos tumorales de células T murinas), indujo la exposición y liberación de patrones moleculares asociados al daño (DAMP). Además, una vacunación profiláctica con células L5178Y-R tratadas con PKHB1 impidió el establecimiento del tumor *in vivo* en todos los casos. Debido al potencial inmunogénico de las células tratadas con PKHB1, en este estudio evaluamos su capacidad para inducir respuestas inmunes antitumorales *ex vivo* e *in vivo* en un tumor establecido. Primero confirmamos la selectividad de la muerte celular inducida por PKBH1 en células tumorales L5178Y-R y observamos que la exposición a calreticulina aumentaba cuando aumentaba la muerte celular. Luego, descubrimos que el lisado de células tumorales (TCL) obtenido a partir de células tumorales L5178YR tratadas con PKHB1 (PKHB1-TCL) fue capaz de inducir *ex vivo* la maduración de las células dendríticas, la producción de citocinas y las respuestas antitumorales de las células T. Finalmente, nuestros resultados muestran que *in vivo*, el tratamiento con PKHB1-TCL induce la regresión tumoral en ratones singénicos trasplantados con células L5178Y-R, aumentando su supervivencia general y protegiéndolos del establecimiento tumoral tras la reexposición a células cancerosas viables. En conjunto, nuestros resultados destacan la inmunogenicidad de la muerte celular inducida por la activación de CD47 por PKHB1 como una herramienta terapéutica potencial para superar la baja inmunogenicidad y la tolerancia inmune en T-ALL.

Manuscript

Research Article

PKHB1 Tumor Cell Lysate Induces Antitumor Immune System Stimulation and Tumor Regression in Syngeneic Mice with Tumoral T Lymphoblasts

Ana Carolina Martínez-Torres ¹, Kenny Misael Calvillo-Rodríguez ¹,
Ashanti Concepción Uscanga-Palomeque ¹, Luis Gómez-Morales ^{1,2},
Rodolfo Mendoza-Reveles,¹ Diana Caballero-Hernández,¹
Philippe Karoyan ^{2,3,4} and Cristina Rodríguez-Padilla¹

¹Universidad Autónoma de Nuevo León, Facultad de Ciencias Biológicas, Laboratorio de Inmunología y Virología, Mexico

²Sorbonne Université, École Normale Supérieure, PSL University, CNRS, Laboratoire des Biomolécules, 75005 Paris, France

³Kayvisa, AG, Industriestrasse 44, 6300 Zug, Switzerland

⁴Kaybiotix, GmbH, Zugerstrasse 32, 6340 Baar, Switzerland

Correspondence should be addressed to Ana Carolina Martínez-Torres; ana.martinezto@uanl.edu.mx and Philippe Karoyan; philippe.karoyan@sorbonne-universite.fr

Received 27 December 2018; Revised 27 March 2019; Accepted 5 May 2019; Published 4 June 2019

Guest Editor: Shalini Gupta

Copyright © 2019 Ana Carolina Martínez-Torres et al. This is an open access article distributed under the Creative Commons Attribution License, which permits unrestricted use, distribution, and reproduction in any medium, provided the original work is properly cited.

Acute lymphocytic leukemia (ALL) is the most common pediatric cancer. Currently, treatment options for patients with relapsed and refractory ALL mostly rely on immunotherapies. However, hematological cancers are commonly associated with a low immunogenicity and immune tolerance, which may contribute to leukemia relapse and the difficulties associated with the development of effective immunotherapies against this disease. We recently demonstrated that PKHB1, a TSP1-derived CD47 agonist peptide, induces immunogenic cell death (ICD) in T cell ALL (T-ALL). Cell death induced by PKHB1 on T-ALL cell lines and their homologous murine, L5178Y-R (T-murine tumor lymphoblast cell line), induced damage-associated molecular patterns (DAMPs) exposure and release. Additionally, a prophylactic vaccination with PKHB1-treated L5178Y-R cells prevented tumor establishment *in vivo* in all the cases. Due to the immunogenic potential of PKHB1-treated cells, in this study we assessed their ability to induce antitumor immune responses *ex vivo* and *in vivo* in an established tumor. We first confirmed the selectivity of cell death induced by PKHB1 in tumor L5178Y-R cells and observed that calreticulin exposure increased when cell death increased. Then, we found that the tumor cell lysate (TCL) obtained from PKHB1-treated L5178YR tumor cells (PKHB1-TCL) was able to induce, *ex vivo*, dendritic cells maturation, cytokine production, and T cell antitumor responses. Finally, our results show that *in vivo*, PKHB1-TCL treatment induces tumor regression in syngeneic mice transplanted with L5178Y-R cells, increasing their overall survival and protecting them from further tumor establishment after tumor rechallenge. Altogether our results highlight the immunogenicity of the cell death induced by PKHB1 activation of CD47 as a potential therapeutic tool to overcome the low immunogenicity and immune tolerance in T-ALL.

1. Introduction

T cell acute lymphoblastic leukemia (T-ALL) is a hematological malignancy that affects mostly pediatric patients, as they account for 80% of the cases [1, 2]. It represents the second most common acute leukemia in adults, with

a 5-year survival rate of about 30-50% [3-5] with a high risk of relapse [6]. The use of nelarabine for relapsed and refractory T-ALL only results in responses in a substantial minority of patients [7]. Among other treatments, allogeneic hematopoietic cell transplantation (HCT) is proposed in patients with high-risk or relapsed/refractory disease, and

γ -secretase inhibitors for patients with NOTCH1 mutations are currently in clinical trials. Multiagent chemotherapy is proposed for older and unfit patients. However, T-ALL treatments have lagged behind those proposed for B-cell ALL, and the development of new therapeutic approaches against this aggressive malignancy remains a challenge. Since the T-ALL high risk of relapse has been attributed to its low immunogenicity and immune tolerance [6], the immune system stimulation able to induce immunological memory against tumor cells appears as a challenging but promising goal.

With this aim, whole tumor cell lysates (TCLs) have been shown to be able to prompt antitumor immune responses in preclinical murine models for glioblastoma, breast, and ovarian cancer and in clinical trials for melanoma, prostate, and ovarian cancer [8]. These immune responses are correlated with damage-associated molecular patterns (DAMPs) induction and the availability of the tumor neoantigens, both of which are promoted in accordance with the specific cell death inductor [9]. DAMPs interact with dendritic cells' (DCs) receptors (CD91, Toll-like receptor 4, purinergic receptors, among others), promoting their maturation and increasing antitumor activity [10]. Thus, TCL can be used to induce an immunogenic response from DCs against multiple tumor antigens, triggering a polyclonal tumor-specific T cell response [11].

Cancer treatment with DCs pulsed with tumor antigens has proved effective antitumor responses in mesothelioma, glioma, and breast cancer [12–14]. However, the use of TCL as therapeutic vaccines has been also shown to be a useful strategy to elicit antitumor immune responses, while overcoming immunosuppressive mechanisms of the tumor microenvironment [8]. TCLs hold more promises as cancer vaccines than individual tumor-associated antigens (TAAs) because they can elicit immune responses to multiple TAAs [15]. However, the availability and types of neoantigens, the amount of DAMPs released, and the overall immunogenicity of the TCL strongly rely on the cell death inductor [9]. Thus, it is important to find effective cell death inductors that are able to provide an immunogenic TCL able to induce antitumor immune responses.

CD47 activation through coated [16–18] or soluble anti-CD47 antibodies [19, 20], or immobilized [16] or soluble peptides derived from the C-terminal domain of thrombospondin-1 [21, 22], is an effective way to induce cell death in different types of cancerous cells, even in cells coming from patients that are resistant to chemotherapy [21, 22]. Thus, a TCL obtained through CD47 activation might help to understand the implications of CD47-mediated cell death in the activation of antitumor immune responses. Recently, we have shown that treatment of T-ALL cells with the CD47-agonist peptide, PKHBI, induced immunogenic cell death (ICD) [23]. ICD was induced by PKHBI in T-ALL cells, while it spares CD19 and CD3 lymphocytes [21], human and murine PBMCs, CD4 and CD8 T cells, and cells from murine lymphoid organs [23]. We found that PKHBI-treatment induces the exposure and release of several DAMPs (calreticulin (CRT), HSP70, HSP90, ATP, and HMGB1) in human T-ALL cell lines (CEM, MOLT-4

and their murine counterpart (L5178Y-R cells) [23]. *In vivo*, prophylactic vaccination experiments with PKHBI-treated cells prevented tumor establishment in immunocompetent BALB/c mice [23]. These results demonstrated that CD47 activation by PKHBI was able to induce DAMPs release and provide neoantigens able to elicit an antitumor immune response that prevented tumor establishment. However, the therapeutic potential of this type of ICD was not studied.

In the present work we focused on determining whether the induction of ICD by PKHBI has a therapeutic potential. Due to the immunogenicity of PKHBI-treated cells, we used the TCL obtained from PKHBI-treated L5178Y-R tumor cells (PKHBI-TCL) and focused on determining their ability to induce antitumor immune responses *ex vivo* and *in vivo* in an established L5178Y-R tumor developed in syngeneic BALB/c mice.

2. Material and Methods

2.1. T Cells and Dendritic Cells (DCs). This study was approved by the Animal Ethical Committee (CEIBA), of the School of Biological Sciences Number: 01/2015. All experiments were conducted according to Mexican regulation NOM-062-ZOO-1999.

The blood from sacrificed BALB/c mice was obtained by cardiac puncture. Peripheral blood mononuclear cells (PBMCs) isolation was performed by density gradient centrifugation using Ficoll-Hypaque-III19 (Sigma-Aldrich, St Louis, MO, USA). Murine CD3+ cells were isolated from total PBMCs by positive selection using magnetic-activated cell sorting (MACS) microbead technology with anti-CD3ε-biotin and anti-biotin microbeads (Miltenyi Biotec; >98% purity and >98% viability), as stated by manufacturer's instructions.

To obtain bone marrow-derived dendritic cells (DCs), after sacrifice, mice bone marrow was removed from femur and tibia of female BALB/c mice by flushing into RPMI-1640. Eluted cells were cultured for 5 days with 20 ng/mL of IL-4 and GM-CSF (R&D Systems, Minneapolis, MN, USA) until approximately 70% of the cells were CD11c+.

2.2. Cell Culture. L5178Y-R cell line (murine cancerous T lymphoblasts) was obtained from the ATCC. L5178Y-R, primary murine CD3+, and DCs were maintained in RPMI-1640 medium supplemented with 10% of fetal bovine serum, 2 mM L-glutamine, and 100U/mL penicillin-streptomycin (GIBCO by Life Technologies, Grand Island, NY, USA), and incubated at 37°C in a controlled humidified atmosphere with 5% CO₂. Cell count was performed using trypan blue (0.4% Sigma-Aldrich), a Neubauer chamber, and an optic microscope (Zeiss Primo Star) as proposed by the ATCC's standard protocols.

2.3. Cell Death Analysis. Annexin-V-allophycocyanin (Ann-V-APC 0.1µg/ml; BD Pharmingen, San Jose, CA, USA) and propidium iodide (PI, 0.5µg/ml Sigma-Aldrich) were used to assess phosphatidylserine exposure, cell death, and cell viability quantification, respectively, in a BD Accuri C6 flow cytometer (BD Biosciences, Franklin Lakes, NJ, USA) (total

population: 10,000 cells). Data was analyzed using FlowJo software (LLC, Ashland, OR, USA). 1×10^6 cells/mL were seeded and left untreated or treated for 2 h with 150 μ M or 300 μ M of PKHBI (KRFYVVMWKK) or 150 μ M of the control peptide 4NGG (KRFYGGMWKK) (as indicated) in serum-free media.

For cell death inhibitions we used the calcium chelator BAPTA (5mM), the antioxidant N-Acetyl Cysteine (NAC, 5mM), the pan-caspase inhibitors Q-VD-OPH (QVD, 10 μ M) and Z-VAD-FMK (Z-VAD, 50 μ M), the autophagic inhibitor Spautin-1 (SP-1, 15 μ M), and the necroptotic inhibitor Necrostatin-1 (Nec-1, 50 μ M). We pretreated the cells 30 minutes with the inhibitor before the treatment with PKHBI (150 μ M).

2.4. Calreticulin Exposure. L5178Y-R cells were plated (1×10^6 cells/mL), left untreated or treated with 300 μ M of 4NGG or 150 μ M or 300 μ M of PKHBI, and incubated for 2 h. Cells were harvested, washed, and stained with Calreticulin-Phycoerythrin (Calreticulin-PE, FMC-75; Enzo Life Science, Farmingdale, NY, USA) antibody (1:1000) in FACS buffer. After 1 h in darkness at room temperature (RT), cells were washed and resuspended in 100 μ L FACS buffer (PBS 1x and 2% of fetal calf serum) to be assessed by flow cytometry in a BD Accuri C6 flow cytometer (BD Biosciences) (total population: 10,000 cells). Data was analyzed using FlowJo software.

2.5. DCs Markers. DCs (1×10^6 cells/mL) were stained in 100 μ L of FACS buffer with the indicated antibodies at RT for 30 minutes and then washed twice with PBS. The cell surface markers were evaluated by flow cytometry with the fluorescent label-conjugated antibodies, anti-CD11c-Alexa-fluor 488 (R&D Systems), anti-CD80-FITC, and anti-CD86-APC, from BD Biosciences (San Jose, CA, USA).

2.6. Cocultures. DCs-PKHBI tumor cell lysate: DCs were resuspended in fresh medium at a concentration of 1×10^6 cells/mL. DCs were left untreated (control), or PKHBI-treated tumor cells were added at a concentration of 3×10^6 cells/mL to give a range of 1:3 DCs to PKHBI-treated tumor cells ratios. Coculture was left for 24 hours. Then the supernatant was removed, and the well was washed twice with PBS before doing the next coculture (with the addition of T-lymphocytes).

DCs-T-lymphocytes: Control DCs or DCs previously cocultured with PKHBI-TCL were maintained in fresh medium at a concentration of 1×10^6 cells/mL. Then, allogeneic BALB/c mCD3+ cells were added to each well at 3×10^6 cells/mL to give a range of 1:3 DC to CD3+ cells ratios. Coculture was left for 96 hours. Then, the lymphocytes were collected (by obtaining the supernatant), washed with PBS, and resuspended in fresh medium at a concentration of 5×10^6 cells/mL to be used in the next coculture (T- lymphocytes with cancer cells).

T-Lymphocytes-L5178Y-R cells: viable L5178Y-R cells were plated at a concentration of 1×10^5 cells/mL. Then, unprimed (previously cocultured with control DCs) or primed (previously cocultured with DCs-PKHBI-TCL) allogeneic BALB/c mCD3+ cells were added to each well at $5 \times$

10^5 cells/mL to give a range of 1:5 tumor to effector ratios. Coculture was left for 24 hours, before cytokine or calcein assessment.

2.7. Cytokine Release Assay. The supernatants from the indicated cultures were collected for IL-2, IL-4, IL5, and TNF α assessment (BD CBA Mouse Th1/Th2 Cytokine Kit, San Jose, CA, USA) by flow cytometry following manufacturer's instructions. IFN γ was assessed using an ELISA kit (Sigma-Aldrich) and using the Synergy HTTM (BioTek Instruments, Inc., Winooski, VT, USA) plate reader at 570 nm wavelength, following manufacturer's instructions.

2.8. Calcein Assay. L5178Y-R cells (1×10^6 cells/mL) were stained with (0.1 μ L/mL) of Calcein-AM from BD Biosciences (San Jose, CA) for 30 minutes and washed twice (PBS sterile). After this, T cells previously primed with DCs pulsed with PKHBI-TCL or with unpulsed DC were added in a 1:5 ratio. The L5178Y-R-T-lymphocytes' coculture was incubated at 37°C and 5% CO2 for 24 h. Finally, L5178Y-R-calcein negative cells were assessed in a BD Accuri C6 flow cytometer (BD Biosciences) (total population: 10,000 cells). Data was then analyzed using FlowJo software.

2.9. In Vivo Model. Six-to-eight-week-old BALB/c female mice were maintained in controlled environmental conditions (25°C and 12 h light/dark cycle) and were supplied with rodent food (LabDiet, St. Louis, MO, USA) and water *ad libitum*.

Tumor was established by subcutaneous injections of 2×10^6 L5178Y-R cells in 100 μ L PBS, in the left hind. Tumor volume and mice weight were measured three times a week using a caliper (Digimatic Caliper Mitutoyo Corporation, Japan) and a digital scale (American Weigh Scale-600-BLK, USA), respectively. Tumor volume was determined with the following formula: tumor volume (mm^3) = $4\pi/3 * A(\text{length}) * B(\text{width}) * C(\text{height})$. When the tumor reached 100 mm^3 , the first therapeutic vaccine of PKHBI-tumor cell lysate (PKHBI-TCL) was applied as follows:

L5178Y-R cells (5×10^6) were treated *in vitro* with 300 μ M PKHBI for 2 h (CC₁₀₀) in serum-free RPMI medium. Cell death was confirmed as previously indicated. Treated cells were inoculated subcutaneously in 100 μ L serum-free media, in the right hind, twice a week. Controls were treated with 100 μ L serum-free media.

For long memory assessment, we used six naïve mice (control) and six mice in complete remission after PKHBI-TCL treatment (tumor free >60 days). Both groups were injected with 2×10^6 living L5178Y-R cells in 100 μ L PBS, in the left hind. The latter group was named PKHBI-TCL-Rechallenge. We then assessed tumor volume and survival, as described previously.

2.10. Statistical Analysis. Mice were randomly assigned to different groups for all *in vivo* studies. At least three independent experiments were repeated three independent times. Mann-Whitney tests and two-tailed unpaired Student's *t*-tests were performed using GraphPad Prism Software (San Diego CA, USA) and presented as mean values \pm SD. The *p* values

were considered significant as follows: $p < 0.05$, $p < 0.01$, and $p < 0.001$.

3. Results and Discussion

3.1. Calreticulin Exposure Correlates with Cell Death Induced by PKHBI. ICD is characterized by DAMPs exposure or release, and anticancer immune memory generation [24]. CRT exposure has been continuously reported as one of the principal DAMPs necessary for the correct maturation of DCs and antigen presentation [25, 26]. The activation of CD47 by PKHBI induces CRT exposure in CLL cells [21]. Additionally, we recently reported that PKHBI induces immunogenic cell death with DAMPs release (CRT, HMGB1, HSP79, HSP90, and ATP) and CRT exposure in T-ALL human cell lines and their murine counterpart, the L5178Y-R cell line (a murine T cell lymphoblastic tumor cell line) [23]. However, correlation between CRT exposure and cell death induced by CD47 was not established; for that purpose, here we assessed this feature using the L5178Y-R cell line.

First, we assessed cell death induced by the control peptide 4NGG, which does not bind to CD47 [21], and cell death induced by different concentrations of PKHBI. We found that 4NGG (300 μM) was not able to induce cell death in L5178Y-R cells, while PKHBI induced a concentration-dependent cell death, reaching CC_{50} (cytotoxic concentration for 50% of the cells) at 150 μM and CC_{100} (cytotoxic concentration for 100% of the cells) at 300 μM .

Next, to evaluate the characteristics of the cell death induced by PKHBI, we used several cell death inhibitors. We have previously demonstrated that cell death induced through CD47 activation by PKHBI is a fast and atypical caspase-independent and calcium-dependent mechanism [21, 23]. Thus, we assessed cell death using the calcium chelator BAPTA, as positive control of cell death inhibition by PKHBI, and the antioxidant NAC (N-Acetyl Cysteine) which inhibits several cell death modalities that involve ROS production [27]; as apoptotic pan-caspase inhibitors we used Q-VD-OPH [28] and Z-VAD-FMK (which also inhibits pyroptosis, [29]); we also used the autophagic inhibitor Spautin-1 [30] and the necroptotic inhibitor Necrostatin-1 [31]. In Figure 1(c) we can observe that that only the calcium chelator, BAPTA, was able to inhibit PKHBI-cell death. Effectively cell death induced by CD47 activation seems to be mostly cytoplasmic and mediated by calcium augmentation [21, 23], and due to the velocity of the process it seems to be a different mechanism of cell death from the commonly described to date.

Using 300 μM of PKHBI for two hours induced 97% of cell death (defined as CC_{100}), and calreticulin exposure was observed for 90% of the cells. The PKHBI-tumor cell lysate of L5178Y-R cells (PKHBI-TCL) was generated with this CC_{100} . Figure 1 describes the PKHBI-induced CRT exposure in a PKHBI-concentration and cell death-dependent ways: indeed, the increasing number of Ann-V-APC/PI positive cells with increasing concentration of PKHBI (Figures 1(a) and 1(b)) is correlated with an increasing CRT exposure (Figures 1(d) and 1(e)).

Calreticulin exposure and cell death have been shown to be correlated when using various agents inducing ICD [26], such as IMMUNEPOTENT CRP [32] and shikonin [33]; however in some cases, CRT has been reported to be exposed pre-mortem [26]. We recently found that the CC_{100} was necessary for the highest release of HMGB1, HSP70, and HSP90 in L5178Y-R cells [23]. This observation led us to hypothesize that since the PKHBI-TCL is rich in DAMPs, it might induce DCs maturation and antigen presentation to T cells promoting antitumor responses.

3.2. PKHBI-TCL Induces Maturation of Bone Marrow-Derived DCs. To determine if PKHBI-TCL was able to induce the maturation of DCs, bone marrow-derived murine DCs were left untreated (control) or pulsed for 24 h with the previously obtained PKHBI-TCL. We assessed cytokine production by PKHBI-TCL, but we did not find a significant release of $\text{TNF}\alpha$, $\text{IFN}\gamma$, IL-5, IL-4, or IL-2 (Supplementary Table 1). After coculture, DCs were washed twice with PBS to remove any background noise given by the PKHBI-TCL. DCs cocultured with PKHBI-TCL show morphological changes (data not shown) and a significant increase in the expression of costimulatory molecules (CD80 and CD86) passing from 50% to 78%, while maintaining the expression of the DCs marker CD11c (Figures 2(a) and 2(b)). Furthermore, only DCs-PKHBI-TCLs show a significant increase in $\text{TNF}\alpha$ release in comparison with unstimulated DCs (Figure 2(c)).

Several types of TCL are able to induce DCs maturation at different degrees [8]; however most of them use LPS [33] or other adjuvants such as phytoextracts [34] and bacterial ghosts [35] in combination with the TCL. Our results show that PKHBI-induced cell death is able to promote DCs maturation and secretion of $\text{TNF}\alpha$, even in the absence of other immune-stimulants. The mature DC phenotype was characterized by the expression of the endocytic receptor CD11c [36], CD80, and CD86 [37], which increased significantly ($p = 0.0005$ and $p = 0.0066$, respectively) in DCs cocultured with PKHBI-TCL. We can observe a slight nonsignificant decrease in the expression of CD11c (Figures 2(a) and 2(b)); this differentiation marker can be downregulated by dendritic cells after their activation by TLR agonists [38]. The secretion of $\text{TNF}\alpha$ has been associated with a mature phenotype, as it acts as an autocrine maturation factor for DCs [37]. Several TCLs are able to induce its secretion at several degrees, ranging from 20 pg/mL to 250 pg/mL [39, 40]. Here we found that DCs pulsed with PKHBI-TCL induced the secretion of $\text{TNF}\alpha$ at a 270 pg/mL concentration, indicating the efficient maturation of DCs by PKHBI-TCL.

3.3. PKHBI-TCL Induces an Antitumor T Cell Response. Once we determined that PKHBI-TCL was able to induce DCs maturation, we assessed if the pulsed DCs (DCs-PKHBI-TCL) were able to prime T cells. First, CD3+ cells were cocultured for four days with pulsed or unpulsed DCs, and we assessed $\text{TNF}\alpha$, $\text{IFN}\gamma$, IL-5, IL-4, and IL-2 cytokine release. Table 1 shows that coculture of pulsed DCs with primary T-lymphocytes induces the release of $\text{TNF}\alpha$, $\text{IFN}\gamma$, and IL-2, while IL-5 and IL-4 release were not detected. The secretion

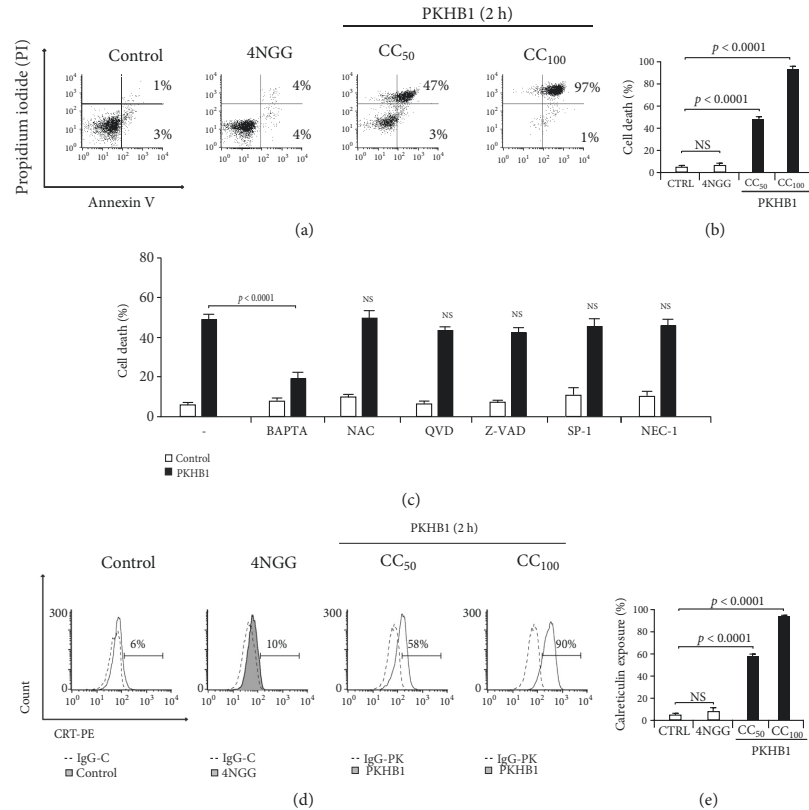


FIGURE 1: PKHBI induces cell death and calreticulin exposure in L5178Y-R cell line. (a) Cell death was measured by Annexin-V-allophycocyanin (Annexin-V-APC) and propidium iodide (PI) staining and graphed. Dot plots of L5178Y-R cells untreated (control) and treated with control peptide 4NGG (300 μ M) or CC₅₀ (150 μ M) and CC₁₀₀ (300 μ M) of PKHBI for 2 h. (b) Graph represents the means (\pm SD) of triplicates of three independent experiments obtained as in (a). (c) Cell death induced by PKHBI was assessed as in (a) with cells left without pretreatment (control) or pretreated (30 minutes) with BAPTA, N-Acetyl Cystein (NAC), Q-VD-OPH (QVD), Z-VAD-FMK (Z-VAD), Spautin-1 (SP-1), or Necrostatin-1 (Nec-1). (d) Calreticulin exposure induced by 4NGG (300 μ M) and PKHBI (CC₅₀ and CC₁₀₀, 2 h) was measured using FACS in L5178Y-R cell line, and representative histograms are shown. (e) Graph represents the means (\pm SD) of triplicates of three independent experiments obtained as in (c).

of TNF α , IFN γ , and IL-2 is associated with a Th1 phenotype [41], which promotes an antitumor immune response [42].

Next, primed (cocultured with pulsed DCs-PKHBI-TCL) or unprimed (cocultured with unpulsed DCs) T-lymphocytes were collected and cocultured during 24 h with L5178Y-R cells (previously stained with calcein-AM). After 24 h of coculture, supernatants were obtained, and we assessed IFN γ , IL-4, and IL-2 cytokine release. A significant increase in IL-2 and IFN γ release was observed in the supernatants of T-lymphocytes previously cocultured with DCs-PKHBI-TCL (Figure 3).

Once we observed that PKHBI-TCL induced IFN γ and IL-2 release, suggesting Th1 responses [41], we assessed antitumor cell cytotoxicity. For this purpose, we evaluated the loss of calcein in L5178Y-R cells. Results show that only T-lymphocytes cocultured with pulsed DCs-PKHBI-TCL induce a significant increase in the calcein negative L5178Y-R

cells, in comparison with the T-lymphocytes cocultured with control DCs (not pulsed with PKHBI-TCL) (Figure 4). This confirms the correct antigen presentation by DCs-PKHBI-TCL and the T cell cytotoxicity against L5178Y-R cancer cells.

Detection of IL-2, INF γ , and TNF α in supernatants of DCs and T cell cocultures indicates the establishment of an efficient anticancer immune response. These observations are in agreement with the results observed in our cocultures of T cells with DCs-PKHBI-TCL. The secretion of these cytokines suggests a Th1 phenotype [41] which was confirmed by the loss in cell viability of L5178Y-R cells cocultured with primed T cells.

Several cytotoxic agents have been demonstrated to induce *ex vivo* antitumor T cell responses, such as bortezomib in myeloma [43] and doxorubicin in colon carcinoma [44]. Also the allogeneic off-the-shelf dendritic cell vaccine,

TABLE 1: TNF α , IFN γ , IL-5, IL-4, and IL-2 cytokine release (pg/mL) in cocultures of T lymphocytes with control or pulsed DCs.

	TNF α (pg/mL)	IFN γ (pg/mL)	IL-5 (pg/mL)	IL-4 (pg/mL)	IL-2 (pg/mL)
DCs-Control + T-lymphocytes	38.9 \pm 14	0 \pm 0	0 \pm 0	0 \pm 0	0.2 \pm 0.2
DCs-PKHBI-TCL + T-lymphocytes	479.6** \pm 156	974.33* * \pm 115	0 \pm 0	0 \pm 0	3.5** \pm 0.7

Bone marrow-derived murine DCs were left with medium alone (DCs-control) or pulsed (DCs-PKHBI-TCL) during 24h with a PKHBI-TCL. Then, DCs were cocultured during 4 days with T-lymphocytes, and the supernatants were collected to quantify TNF α , IFN γ , IL-5, IL-4, and IL-2 release, by FACS. Numbers represent the means (\pm SD) of triplicates of three independent experiments. **p<0.01; * * p<0.001.

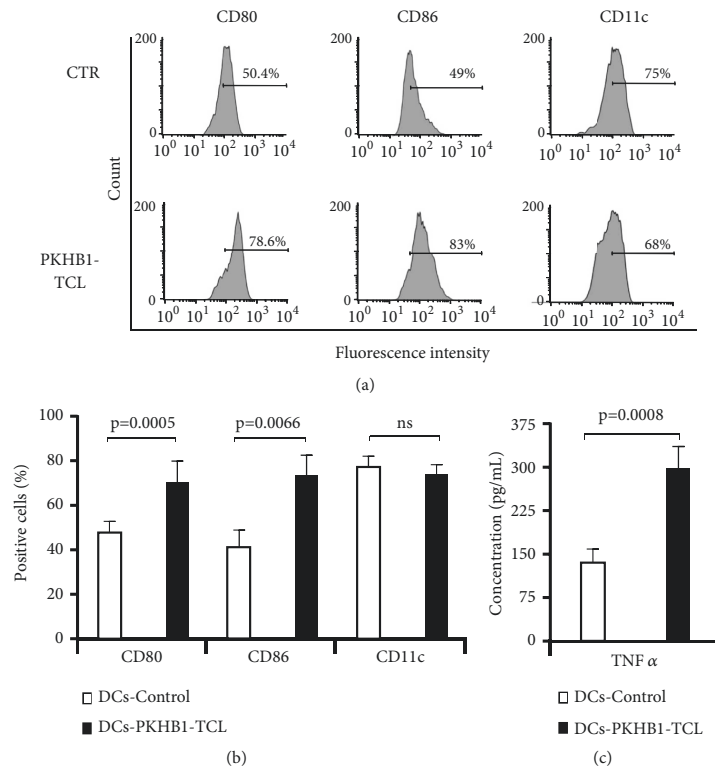


FIGURE 2: PKHBI-tumor cell lysate induces the maturation of bone marrow-derived dendritic cells. (a) Bone marrow-derived murine DCs were left only with medium (control) or pulsed during 24 h with a PKHBI-TCL. DCs were then stained to assess cell surface markers (CD11c, CD80, or CD86) by FACS, and representative histograms are shown. (b) DCs were treated as in (a) and the means obtained by FACS were graphed. (c) DCs were treated as in (a) and the supernatants were collected to quantify TNF α release, by FACS. Graphs represent the means (\pm SD) of triplicates of at least three independent experiments.

currently in clinical trials for acute myeloid leukemia [45], has demonstrated these responses *ex vivo* and *in vivo* in patients.

3.4. PKHBI-TCL Induces Tumor Regression. Once we established the *ex vivo* antitumor immune response induced by PKHBI-TCL, we assessed if the *in vivo* injection of PKHBI-TCL was able to diminish tumor growth and improve overall survival in syngeneic mice transplanted with L5178Y-R cells. First 2×10^6 L5178Y-R cells were inoculated in BALB/c mice.

When the tumor reached 100 mm^3 , a mice control-group was left without treatment (Control; $n = 7$), and a second group was treated with PKHBI-TCL two times per week (PKHBI-TCL; $n = 9$) (Figure 5(a)). Tumor growth was measured: we observed that PKHBI-TCL-treated mice showed significantly diminished tumor growth after day 10 (7 days after the first treatment), which continued to decrease until no tumor was detected by day 30 (Figure 5(b)). Tumor growth diminution was reflected in overall mice survival, as PKHBI-TCL-treated

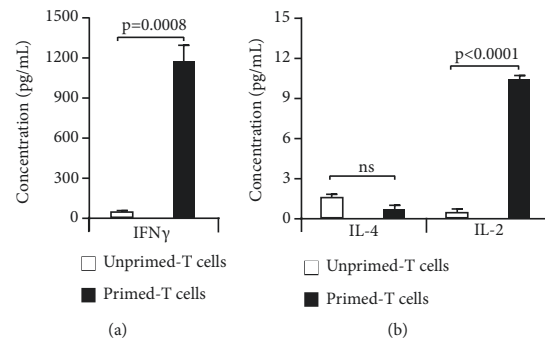


FIGURE 3: *IFN- γ* and *IL-2* secretion by unprimed or primed T cells cocultured with L5178Y-R cells. (a) L5178Y-R cells were cocultured with unprimed T-lymphocytes (previously cocultured with unstimulated DCs-Control) or primed T-lymphocytes (previously cocultured with pulsed DCs-PKHBI-TCL) in a 1:5 tumor to effector ratio, for 24 h, and the supernatants were collected and assayed for (a) *IFN- γ* release by ELISA and (b) *IL-4* and *IL-2* release by FACS. Graphs represent the means (\pm SD) of three experiments performed independently.

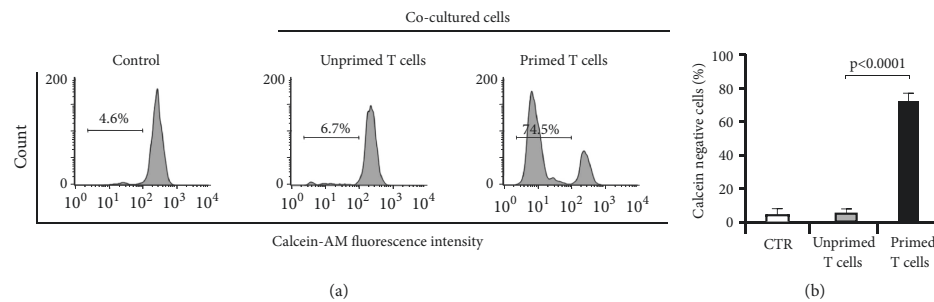


FIGURE 4: *Primed T cells' cytotoxicity in L5178Y-R cells.* (a) L5178Y-R cells were stained with calcein-AM and cocultured with unprimed T-lymphocytes (previously cocultured with unstimulated DCs-Control) or primed T-lymphocytes (previously cocultured with pulsed DCs-PKHBI-TCL) in a 1:5 tumor to effector ratio for 24 h. The percentage of L5178Y-R calcein negative cells was assessed by FACS; representative histograms are shown. (b) Graphs represent the means (\pm SD) of triplicates of three independent experiments obtained as in (a).

mice presented an 80% of survival over time (more than 150 days), while all control mice perished by day 11 (Figure 5(c)).

To assess immunological memory against tumor antigens after PKHBI-TCL-treatment, mice in complete remission (tumor free >60 days) were rechallenged with living L5178YR cells. Compared to naïve mice (control), in which a primary L5178YR cell challenge resulted in rapid tumor progression, those that were in remission were completely resistant to a rechallenge of L5178YR cells (Figure 6(a)). Furthermore, as no tumor developed, we observed a 100% of survival of the PKHBI-TCL-Rechallenged mice while all control mice perished by day 12 (Figure 6(b)).

It has been proved that other TCLs reduce tumor volume in different types of cancer, as, for example, combined with CpG in a glioblastoma mouse tumor model [46]. Additionally, in clinical trials TCLs have been tested in melanoma, prostate, mesothelioma, ovarian, and colorectal cancers [8]. These TCLs are usually produced using radiation, repeated freezing, and thawing, among others. Here we show that PKHBI-CD47 activation, which has been shown to effectively

induce cell death in different types of cancer [21, 22], including cells coming from refractory patients [21, 22], can provide an immunogenic TCL which is able to promote an antitumor immune response, even in the absence of adjuvants.

Interestingly, we observed that tumor volume began to diminish 7 days after the first administration of PKHBI-TCL reaching tumor regression by day 28 (Figure 5(c)). This waiting time corresponds with the time needed for T cells to expand and activate an antitumor immune response [47].

Other types of TCL have been able to induce tumor regression, increasing the survival rate in patients with melanoma and prostate cancer [8]; however, they do so only in combination with adjuvants, such as the case of CpG oligodeoxynucleotides, which are TLR9-agonist [46].

We recently demonstrated that PKHBI treatment of tumor-bearing mice induced long-term tumor prevention in 90% of the mice that presented complete tumor regression [23]. Here we demonstrated that PKHBI-TCL induces long-term immunological memory against tumor antigens, preventing tumor establishment in 100% of the mice after

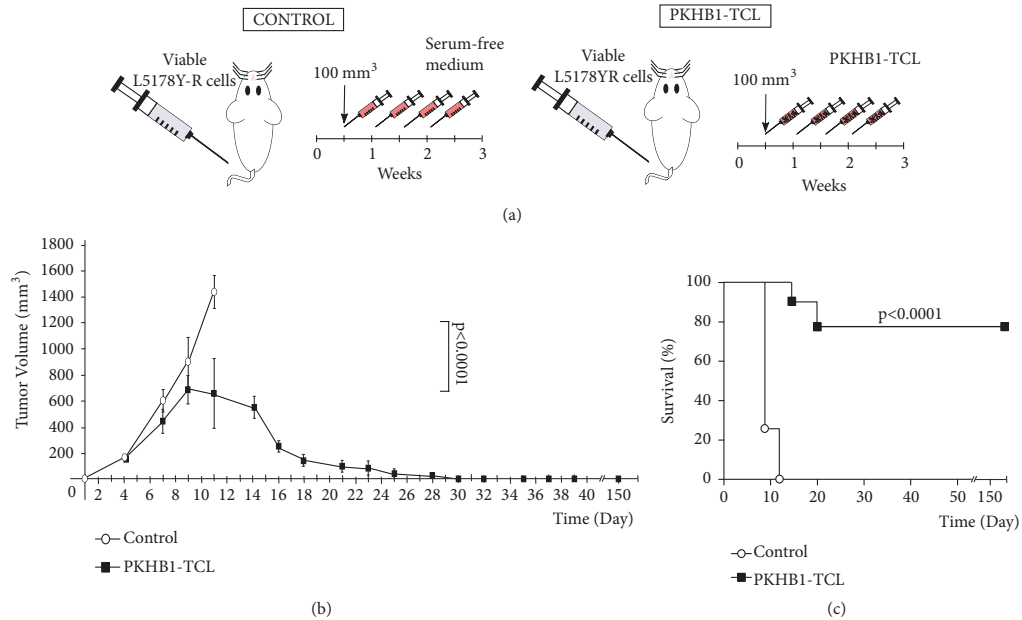


FIGURE 5: PKHBI-TCL treatment in L5178Y-R-tumor-bearing mice induce tumor regression. (a) Schema of PKHBI-TCL (5×10^6 CC₁₀₀ PKHBI-treated L5178Y-R cells) treatment started when tumor reached 100 mm³, and then PKHBI-TCL was administrated every 3 days for two weeks (for a total of four injections). (b) Graph indicates tumor volume (\pm SD) of untreated mice (control; n = 7) or PKHBI-TCL-treated mice (PKHBI-TCL; n = 9). (c) Kaplan-Meier survival curve of untreated mice (control; n = 7) or PKHBI-TCL-treated mice (PKHBI-TCL; n = 9) over time.

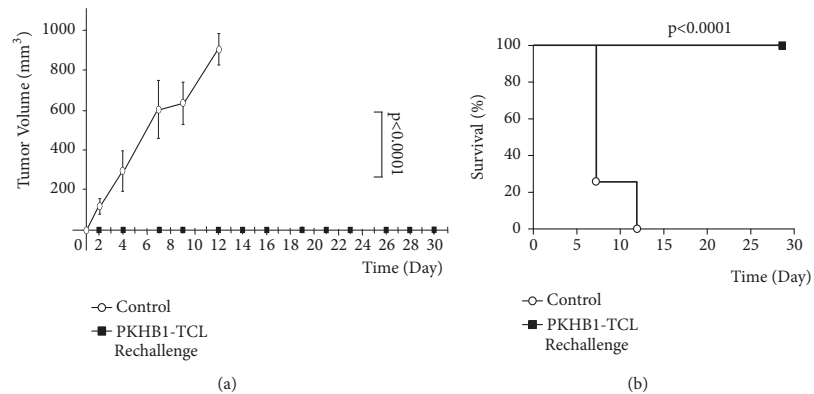


FIGURE 6: PKHBI-TCL therapeutic vaccination induces long-term antitumor memory. Mice in remission after therapeutic vaccinations were rechallenged with 2×10^6 L5178Y-R viable cells. (a) Graph indicates tumor growth in control mice (control, n = 6) or mice in remission after a previous treatment with PKHBI-TCL that were rechallenged with living L5178Y-R cells (PKHBI-TCL-Rechallenge, n = 6). (b) Kaplan-Meier survival graph of mice treated as in (a) over time. Control: n = 6; PKHBI-TCL-Rechallenge, n = 6.

L5178YR cells rechallenge (Figure 6). This underlines the immunogenicity of CD47-mediated cell death, when administering a CD47 agonist peptide or CD47-killed cells. This long lasting immunological memory has been promoted also by a TCL obtained by repeated freezing and thawing and

radiation-treated glioma cells, where nearly a 100% of survival was observed [48].

Although immunotherapy with pulsed DCs, primed T-lymphocytes, or CAR-T cells is the principal approach used to stimulate antitumor immune responses, here we demonstrate

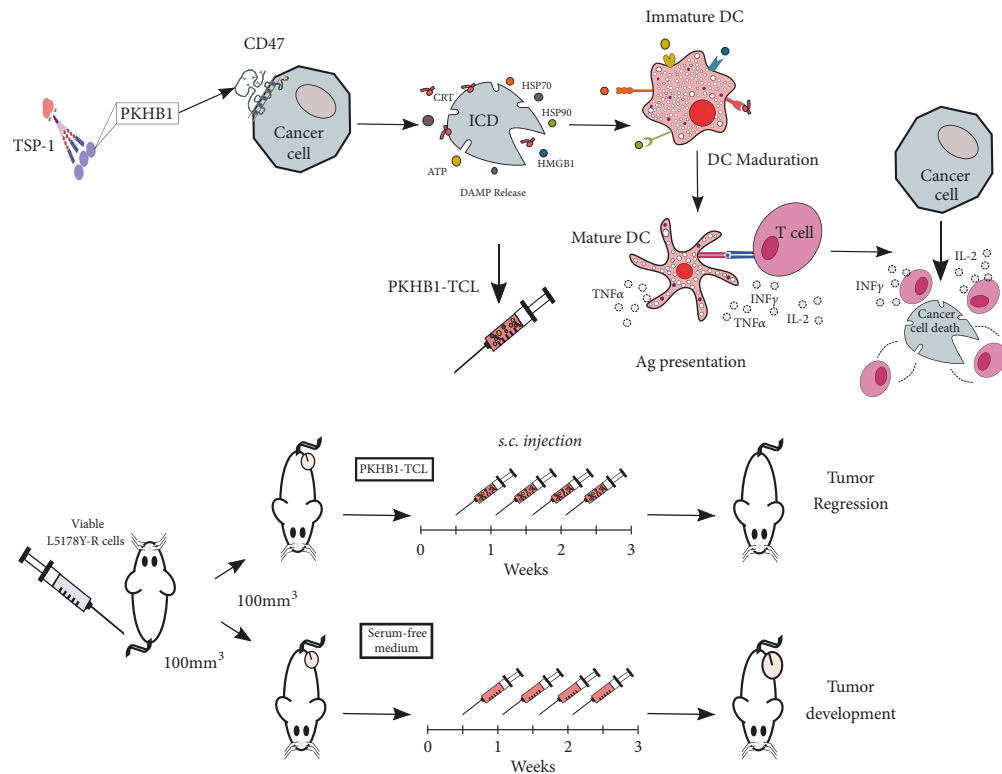


FIGURE 7: Schematic representation of CD47-mediated immunogenic cell death *in vitro*, *ex vivo*, and *in vivo*. PKHB1 induces selective ICD in L5178Y-R cell line leading to damage-associated molecular patterns (DAMP) release. DAMPs promote dendritic cell (DC) maturation and subsequent antigen presentation and T cell activation to induce cancer cell death. Moreover, PKHB1-treated cells administered as a therapeutic vaccine induce tumor regression in syngeneic mice bearing L5178Y-R tumors. CRT, calreticulin; HMGB1, high-mobility group box 1; HSP, heat shock protein; ICD, immunogenic cell death; TSP-1, thrombospondin-1.

that the crude TCL obtained from PKHB1 treatment is able to induce tumor regression in 80% of the mice, while preventing tumor establishment in 100% of the rechallenged mice that survived after PKHB1-TCL-treatment.

4. Conclusions

In this work we determined that the ICD induced by the CD47-agonist peptide, PKHB1, has a therapeutic potential, as the PKHB1-TCL was able to induce antitumor immune responses *ex vivo* and *in vivo* in an established L5178Y-R tumor. This was done by promoting the maturation of DCs, which trigger T cell antitumor effects, including INF γ release and L5178Y-R cell cytotoxicity, leading to tumor regression (Figure 7). Additionally, PKHB1-TCL-treated mice developed long-term immunological memory. These results highlight the immunogenicity of the cell death induced by CD47 activation by PKHB1 as a potential therapeutic tool to overcome the low immunogenicity of cancer cells, such as T-ALL.

Data Availability

The data used to support the findings of this study are available from the corresponding authors upon request.

Conflicts of Interest

The authors declare the following competing financial interest(s): a patent application including results from this paper has been filed. The authors declare that no other conflicts of interest exist.

Authors' Contributions

Ana Carolina Martínez-Torres and Kenny Misael Calvillo-Rodríguez are main authors and equally contributed to this work.

Acknowledgments

This work was supported by SEP-CONACyT-ECOS-ANUIES, Grant/Award Number: 291297; the Laboratory

of Immunology and Virology of the College of Biological Sciences, UANL; and Sorbonne Université, Laboratoire des Biomolécules. We thank the SEP-CONACyT-ECOS-ANUIES and the Laboratory of Immunology and Virology for the financial support and the facilities provided to achieve this work. Kenny Misael Calvillo-Rodríguez and Luis Gómez-Morales thank CONACyT for their scholarship. Luis Gómez-Morales thanks SU/LBM for scholarship. Philippe Karoyan is grateful to SATT Lutech, DGRIT from SU, Kayvisa, for financial support and to Oncodesign for hosting the LBM DRUG lab.

Supplementary Materials

Supplementary Table 1. TNF α , IFN γ , IL-5, IL-4, and IL-2 cytokine release by PKHB1-tumor cell lysate. L5178Y-R cells were treated for 2 h with PKHB1 (300 μ M) and the supernatants were collected to quantify TNF α , IFN γ , IL-5, IL-4, and IL-2 release, by FACS. (Supplementary Materials)

References

- [1] E. Jabbour, S. O'Brien, M. Konopleva, and H. Kantarjian, "New insights into the pathophysiology and therapy of adult acute lymphoblastic leukemia," *Cancer*, vol. 121, no. 15, pp. 2517–2528, 2015.
- [2] A. M. Noone, N. Howlander, M. Krapcho et al., *SEER Cancer Statistics Review, 1975-2015*, National Cancer Institute, Bethesda, MD, USA, 2018.
- [3] J. L. McNeer, A. Bleyer, V. Conter, and W. Stock, *Cancer in Adolescents and Young Adults*, 2017.
- [4] J. L. McNeer and A. Bleyer, "Acute lymphoblastic leukemia and lymphoblastic lymphoma in adolescents and young adults," *Pediatric Blood & Cancer*, vol. 65, no. 6, Article ID e26989, 2018.
- [5] J. C. Jaime-Pérez, L. T. Fernández, R. A. Jiménez-Castillo et al., "Age acts as an adverse independent variable for survival in acute lymphoblastic leukemia: data from a cohort in Northeast Mexico," *Clinical Lymphoma, Myeloma & Leukemia*, vol. 17, no. 9, pp. 590–594, 2017.
- [6] Y. Li, J. G. Buijs-Gladdines, K. Canté-Barrett et al., "IL-7 receptor mutations and steroid resistance in pediatric t cell acute lymphoblastic leukemia: a genome sequencing study," *PLoS Medicine*, vol. 13, no. 12, p. e1002200, 2016.
- [7] M. R. Litzow and A. A. Ferrando, "How I treat T-cell acute lymphoblastic leukemia in adults," *Blood*, vol. 126, no. 7, pp. 833–841, 2015.
- [8] C. L.-L. Chiang, G. Coukos, and L. E. Kandalaft, "Whole tumor antigen vaccines: Where are we?" *Vaccines*, vol. 3, no. 2, pp. 344–372, 2015.
- [9] B. Lucilla, C. Ligia, H. Dewitte et al., "Combinatorial strategies for the induction of immunogenic cell death," *Frontiers in Immunology*, 2015.
- [10] D. V. Krysko, A. D. Garg, A. Kaczmarek, O. Krysko, P. Agostinis, and P. Vandenabeele, "Immunogenic cell death and DAMPs in cancer therapy," *Nature Reviews Cancer*, vol. 12, no. 12, pp. 860–875, 2012.
- [11] R. Veronica, C. Martelli, L. Ottobriani et al., "Immunological characterization of whole tumour lysate-loaded dendritic cells for cancer immunotherapy," *PLoS ONE*, 2016.
- [12] J. G. J. V. Aerts, P. L. De Goeje, R. Cornelissen et al., "Autologous dendritic cells pulsed with allogeneic tumor cell lysate in mesothelioma: From mouse to human," *Clinical Cancer Research*, vol. 24, no. 4, pp. 766–776, 2018.
- [13] M. Eagles, F. Nassiri, J. Badhiwala et al., "Dendritic cell vaccines for high-grade gliomas," *Therapeutics and Clinical Risk Management*, vol. Volume 14, pp. 1299–1313, 2018.
- [14] M. Tomasicchio, L. Semple, A. Esmail et al., "An autologous dendritic cell vaccine polarizes a Th-1 response which is tumoricidal to patient-derived breast cancer cells," *Cancer Immunology, Immunotherapy*, vol. 68, no. 1, pp. 71–83, 2019.
- [15] F. E. González, A. Gleisner, F. Falcón-Beas, F. Osorio, M. N. López, and F. Salazar-Onfray, "Tumor cell lysates as immunogenic sources for cancer vaccine design," *Human Vaccines & Immunotherapeutics*, vol. 10, no. 11, pp. 3261–3269, 2014.
- [16] V. Mateo, L. Lagneaux, D. Bron et al., "CD47 ligation induces caspase-independent cell death in chronic lymphocytic leukemia," *Nature Medicine*, vol. 5, no. 11, pp. 1277–1284, 1999.
- [17] M. Bras, V. J. Yuste, G. Roué et al., "Drp1 mediates caspase-independent type III cell death in normal and leukemic cells," *Molecular and Cellular Biology*, vol. 27, no. 20, pp. 7073–7088, 2007.
- [18] H. Merle-Béral, S. Barbier, G. Roué, M. Bras, M. Sarfati, and S. A. Susin, "Caspase-independent type III PCD: A new means to modulate cell death in chronic lymphocytic leukemia," *Leukemia*, vol. 23, no. 5, pp. 974–977, 2009.
- [19] P. Leclair, L. Chi-Chao, M. Monajemi, S. Gregor Reid, M. Laura Sly, and L. Chinten James, "CD47-ligation induced cell death in T-acute lymphoblastic leukemia," *Cell Death & Disease*, vol. 9, no. 5, p. 544, 2018.
- [20] R. Puro, K. Liu, B. Capoccia et al., "Abstract 1765: A humanized anti-CD47 monoclonal antibody that directly kills human tumor cells and has additional unique functional characteristics," *Cancer Research*, vol. 78, no. 13 Supplement, pp. 1765-1765, 2018.
- [21] A. Martínez-Torres, C. Quiney, T. Attout et al., "CD47 agonist peptides induce programmed cell death in refractory chronic lymphocytic leukemia b cells via PLC γ 1 activation: evidence from mice and humans," *PLoS Medicine*, vol. 12, no. 3, p. e1001796, 2015.
- [22] T. Denèfle, H. Boulet, L. Herbi et al., "Thrombospondin-1 mimetic agonist peptides induce selective death in tumor cells: design, synthesis, and structure-activity relationship studies," *Journal of Medicinal Chemistry*, vol. 59, no. 18, pp. 8412–8421, 2016.
- [23] A. C. Uscanga-Palomeque, K. M. Calvillo-Rodríguez, L. Gómez-Morales et al., "CD 47 agonist peptide PKHB 1 induces immunogenic cell death in T-cell acute lymphoblastic leukemia cells," *Cancer Science*, vol. 110, no. 1, pp. 256–268, 2018.
- [24] W. G. Land, "The role of damage-associated molecular patterns (DAMPs) in human diseases part II: DAMPs as diagnostics, prognostics and therapeutics in clinical medicine," *Sultan Qaboos University Medical Sciences Journal*, vol. 15, no. 2, pp. e157–e170, 2015.
- [25] M. Obeid, A. Tesniere, F. Ghiringhelli et al., "Calreticulin exposure dictates the immunogenicity of cancer cell death," *Nature Medicine*, vol. 13, no. 1, pp. 54–61, 2007.
- [26] A. D. Garg, A. M. Dudek-Peric, E. Romano, and P. Agostinis, "Immunogenic cell death," *The International Journal of Developmental Biology*, vol. 59, no. 1-2-3, pp. 131–140, 2015.

- [27] A. C. Martínez-Torres, A. Reyes-Ruiz, M. Benítez-Londoño, M. A. Franco-Molina, and C. Rodríguez-Padilla, "IMMUNEPO-TENT CRP induces cell cycle arrest and caspase-independent regulated cell death in HeLa cells through reactive oxygen species production," *BMC Cancer*, vol. 18, no. 1, 2018.
- [28] T. M. Caserta, A. N. Smith, A. D. Gultice, M. A. Reedy, and T. L. Brown, "Q-VD-OPh, a broad spectrum caspase inhibitor with potent antiapoptotic properties," *Apoptosis*, vol. 8, no. 4, pp. 345–352, 2003.
- [29] Q.-R. Lin, C.-G. Li, Q.-B. Zha et al., "Gossypol induces pyroptosis in mouse macrophages via a non-canonical inflammasome pathway," *Toxicology and Applied Pharmacology*, vol. 292, pp. 56–64, 2016.
- [30] J. Liu, H. Xia, M. Kim et al., "Beclin1 controls the levels of p53 by regulating the deubiquitination activity of USP10 and USP13," *Cell*, vol. 147, no. 1, pp. 223–234, 2011.
- [31] Y. Cho, T. McQuade, H. Zhang, J. Zhang, F. K. Chan, and J. Alberola-Ila, "RIP1-dependent and independent effects of necrostatin-1 in necrosis and T cell activation," *PLoS ONE*, vol. 6, no. 8, p. e23209, 2011.
- [32] M. D. C. Rodríguez-Salazar, M. A. Franco-Molina, E. Mendoza-Gamboa et al., "The novel immunomodulator IMMUNEPO-TENT CRP combined with chemotherapy agent increased the rate of immunogenic cell death and prevented melanoma growth," *Oncology Letters*, vol. 14, no. 1, pp. 844–852, 2017.
- [33] H.-M. Chen, P.-H. Wang, S.-S. Chen et al., "Shikonin induces immunogenic cell death in tumor cells and enhances dendritic cell-based cancer vaccine," *Cancer Immunology, Immunotherapy*, vol. 61, no. 11, pp. 1989–2002, 2012.
- [34] W.-T. Chang, H.-M. Chen, S.-Y. Yin et al., "Specific dioscorea phytoextracts enhance potency of TCL-loaded DC-based cancer vaccines," *Evidence-Based Complementary and Alternative Medicine*, vol. 2013, Article ID 932040, 13 pages, 2013.
- [35] N. Dobrovolskienė, V. Pašukonienė, A. Darinskas et al., "Tumor lysate-loaded Bacterial Ghosts as a tool for optimized production of therapeutic dendritic cell-based cancer vaccines," *Vaccine*, vol. 36, no. 29, pp. 4171–4180, 2018.
- [36] M. F. Laursen, E. Christensen, L. L. T. Degn et al., "CD11c-targeted delivery of DNA to dendritic cells leads to cGAS- A Nd STING-dependent Maturation," *Journal of Immunotherapy*, vol. 41, no. 1, pp. 9–18, 2018.
- [37] A. M. Dudek, S. Martin, A. D. Garg, and P. Agostinis, "Immature, semi-mature, and fully mature dendritic cells: toward a DC-cancer cells interface that augments anticancer immunity," *Frontiers in Immunology*, vol. 4, article 438, 2013.
- [38] H. Singh-Jasuja, A. Thiolat, M. Ribon et al., "The mouse dendritic cell marker CD11c is down-regulated upon cell activation through Toll-like receptor triggering," *Immunobiology*, vol. 218, no. 1, pp. 28–39, 2013.
- [39] P. Chiarella, V. Reffo, J. Bruzzo, O. D. Bustuoabad, and R. A. Ruggiero, "Therapeutic anti-tumor vaccines: From tumor inhibition to enhancement," *Clinical Medicine: Oncology*, vol. 2, pp. 237–245, 2008.
- [40] C. L.-L. Chiang, L. E. Kandalaf, J. Tanyi et al., "A dendritic cell vaccine pulsed with autologous hypochlorous acid-oxidized ovarian cancer lysate primes effective broad antitumor immunity: From bench to bedside," *Clinical Cancer Research*, vol. 19, no. 17, pp. 4801–4815, 2013.
- [41] J.-F. Viillard, J. L. Pellegrin, V. Ranchin et al., "Th1 (IL-2, interferon-gamma (IFN- γ)) and Th2 (IL-10, IL-4) cytokine production by peripheral blood mononuclear cells (PBMC) from patients with systemic lupus erythematosus (SLE)," *Clinical & Experimental Immunology*, vol. 115, no. 1, pp. 189–195, 1999.
- [42] L. Jiang, Z. Yu, Y. Lin et al., "Low-molecular-weight polysaccharides from agaricus blazei Murrill modulate the Th1 response in cancer immunity," *Oncology Letters*, vol. 15, no. 3, pp. 3429–3436, 2018.
- [43] R. Spisek, A. Charalambous, A. Mazumder, D. H. Vesole, S. Jagannath, and M. V. Dhodapkar, "Bortezomib enhances dendritic cell (DC)-mediated induction of immunity to human myeloma via exposure of cell surface heat shock protein 90 on dying tumor cells: Therapeutic implications," *Blood*, vol. 109, no. 11, pp. 4839–4845, 2007.
- [44] N. Casares, M. O. Pequignot, A. Tesniere et al., "Caspase-dependent immunogenicity of doxorubicin-induced tumor cell death," *The Journal of Experimental Medicine*, vol. 202, no. 12, pp. 1691–1701, 2005.
- [45] A. A. van de Loosdrecht, S. van Wetering, S. J. A. M. Santegoets et al., "A novel allogeneic off-the-shelf dendritic cell vaccine for post-remission treatment of elderly patients with acute myeloid leukemia," *Cancer Immunology, Immunotherapy*, vol. 67, no. 10, pp. 1505–1518, 2018.
- [46] A. Wu, S. Oh, S. Gharagozlou et al., "In vivo vaccination with tumor cell lysate plus CpG oligodeoxynucleotides eradicates murine glioblastoma," *Journal of Immunotherapy*, vol. 30, no. 8, pp. 789–797, 2007.
- [47] S. M. Kaeck, E. J. Wherry, and R. Ahmed, "Effector and memory T-cell differentiation: implications for vaccine development," *Nature Reviews Immunology*, vol. 2, no. 4, pp. 251–262, 2002.
- [48] J. Belmans, M. Van Woensel, B. Creyns, J. Dejaegher, D. M. Bullens, and S. W. Van Gool, "Immunotherapy with subcutaneous immunogenic autologous tumor lysate increases murine glioblastoma survival," *Scientific Reports*, vol. 7, no. 1, Article ID 13902, 2017.

Supplementary material

Supplementary Material

	TNF α	IFN γ	IL-5	IL-4	IL-2
PKHB1-TCL	1.47 \pm 2.55	0.49 \pm 0.42	0 \pm 0	0.5 \pm 0.55	1.075 \pm 0.27

Supplementary Table 1. TNF α , IFN γ , IL-5, IL-4, and IL-2 cytokine release by PKHB1-tumor cell lysate. L5178Y-R cells were treated for 2h with PKHB1(300 μ M) and the supernatants were collected to quantify TNF α , IFN γ , IL-5, IL-4, and IL-2 release, by FACS.

CHAPTER 2

2. Study of the Mechanism of Immunogenic Cell Death induced by PKHB1 in breast cancer

The results in the present chapters gave rise to a patent: **EP3650036A1**, held by Sorbonne Université and Universidad Autónoma de Nuevo León.

2.1. Article 3. PKHB1, a thrombospondin-1 peptide-mimic, induces antitumor effect through immunogenic cell death induction in breast cancer cells

Preamble

Many therapies can activate molecular pathways in cancer cells that guide them to self-destruct in a regulated fashion. However, not all these therapies succeed to activate the host's anti-tumor immune system to combat the disease. These immunologically *silent* outcomes during cell death induction are largely responsible of the selective pressure in the tumor microenvironment that results in relapse of treatment-resistant cancer cell sub-clones.

In the opposite case, therapies able to lead cancer cells to additionally generate adjuvant molecules while dying (i.e., DAMPs) can generally awake the host's anti-tumor immune system to recognize these cells as antigenic, fight them, and generate immunological memory (Galluzzi *et al.*, 2016). Therapies able to trigger such ICD largely account for the long-term success of many anticancer treatments.

As mentioned in the previous chapter, our team had recently reported the ability of PKHB1, a serum-stable peptide-mimic of the thrombospondins C-terminus, to induce ICD in T-ALL, as proved *in vitro*, *ex vivo* and *in vivo*. The caspase-independent, calcium-dependent, regulated cell death mechanism activated by PKHB1 in T-ALL was similar to that described by the same peptide in chronic lymphocytic leukemia (Martinez-Torres *et al.*, 2015). Moreover, PKHB1 had demonstrated to efficiently kill cell lines from breast, lung and colon cancer (Denèfle *et al.*, 2016). Therefore, it was assessed whether PKHB1 could induce ICD in other, non-leukemic types of cancer as well.

2.1. PKHB1, a thrombospondin-1 peptide-mimic, induces antitumor effect through immunogenic cell death induction in breast cancer cells

Article to be submitted for publication at “Journal for Immunotherapy of Cancer” in July, 2021

Breast cancer is the most common type of cancer worldwide, and the triple-negative phenotype represents a highly aggressive and therapy-resistant type of cancer. To evaluate whether PKHB1 could induce ICD in breast cancer cells as it did in T-ALL, the human cell lines MCF7 and the triple-negative MDA-MB-231, as well as its murine homolog 4T1, were used. Breast cancer cells were cultured in presence of PKHB1, and different parameters related to cell death were assessed by flow cytometry, using fluorescent probes (Ann-V-APC for phosphatidylserine exposure; PI for plasma membrane permeability; TMRE, to stain mitochondria with intact membrane potential; hydroetidine for intracellular reactive oxygen species, ROS; and Fluo-4, intracellular calcium concentration). In the three cases PKHB1 induced dose-dependent cell death, as shown by an increased Ann-V-APC and PI staining. PKHB1-induced cell death provoked the loss of the mitochondrial membrane potential, ROS production, and increased intracellular calcium concentration, as shown by loss of TMRE staining, and high hydroetidine and Fluo-4 staining, respectively. Pharmacological inhibition of the molecular initiators of apoptosis (Z-VAD), necroptosis (NEC-1) or autophagy (SP-1) did not prevent cell death in any case. However, an extracellular calcium chelator (BAPTA) prevented cell death, and pre-incubation of cells with inhibitors of PLC (U73122) and intracellular calcium channels (dantrolene and 2-APB) significantly reduced cell death. Altogether this suggests that PKHB1 induces a regulated cell death subroutine similar to that induced in CLL and T-ALL.

To test the *in vivo* potential of PKHB1 treatment, 4T1 cells were implanted in immunocompetent (BALB/c) mice. Three days after inoculation, tumors reached 100 mm³ and mice were subjected to a daily treatment with vehicle (control group) or PKHB1, and tumor volume was measured until day 16, when the experiment was put to an end as mice in the control group needed to be euthanized. PKHB1 reduced tumor growth after one

week, and by the time of sacrifice tumor volumes were significantly reduced. Histopathology analyses showed that tumors in PKHB1-treated mice showed cell debris and immune cells infiltration. Compared to the control group, the blood of PKHB1-treated mice had a greater amount of T (CD3⁺) cells, maintaining a similar percentage of helper T (CD3⁺/CD4⁺) cells and a significantly higher amount of cytotoxic T (CD3⁺/CD8⁺) cells. All T cell populations were similar in the spleens of both groups. The lymph nodes of PKHB1-treated mice had significantly higher proportion of CD3⁺ cells, and although CD4⁺ populations were also higher, CD8⁺ populations were lower. Finally, more CD3⁺ cells were found in the tumors of PKHB1-treated mice, with significantly lower CD4⁺ populations and higher CD8⁺ populations.

Based on these previous results, it was hypothesized that PKHB1 could induce ICD in breast cancer cells as it does in T-ALL. To assess this, first, 4T1, MDA-MB-231 and MCF7 cells were cultured in presence of PKHB1, and production of DAMPs was evaluated. Exposure of calreticulin, HSP70 and HSP90 to the membranes of live cells was measured by flow cytometry, and in the case of calreticulin, confirmed by fluorescence microscopy. Release of HMGB1 and ATP was measured by ELISA and by luciferase assays, respectively, in cell-free supernatants. Compared to untreated and to IgG controls, 4T1, MDA-MB-231 and MCF7 cells treated with PKHB1 showed a significant increase in calreticulin-, HSP70- and HSP90-related fluorescence intensity, and supernatants of PKHB1-treated cells had significantly higher levels of HMGB1 and ATP, indicating that PKHB1 treatment induces DAMPs production in breast cancer cells.

Next, *ex vivo* experiments were performed. Mouse bone marrow-derived DC were cultured alone or co-cultured with 4T1 cells killed by PKHB1 (PKHB1-TCL). After 24 h co-culture, compared to non-exposed DC, DC exposed to PKHB1-TCL expressed significantly higher levels of maturation markers CD80 and CD86, maintaining DC marker CD11c levels. In addition, higher TNF α concentrations were found in supernatants of DC co-cultured with PKHB1-TCL, suggesting that DC pulsed with PKHB1-TCL matured to a pro-inflammatory phenotype.

The ability of PKHB1-TCL-pulsed DC to prime T cells, was evaluated in following experiments using T cells extracted from mouse blood, which were left alone (unprimed) or co-cultured with PKHB1-TCL-pulsed DC (primed). These T cells, were then co-

cultured with 4T1 cells to compare their cytokine release and cytotoxic activity. Compared to those of their unprimed counterparts, supernatants of 4T1 co-cultures with primed T cells had higher concentrations of IFN γ and IL-2, and similar IL-4 concentration, suggesting a Th1 response phenotype. To perform the T cell cytotoxicity experiments, viable 4T1 cells were stained with calcein and either left alone, or co-cultured with unprimed or primed T-cells. Compared to 4T1 cells cultured alone or co-cultured with unprimed T cells, a significantly higher proportion of 4T1 cells that were co-cultured with PKHB1-TCL-pulsed DC-primed T cells lost their calcein staining, indicating T-cell cytotoxicity against 4T1 tumor cells.

Prophylactic vaccination is the goldstandard to evaluate ICD (Galluzzi *et al.*, 2020). To this end, mice were immunized with tumor cell lysates (TCL) obtained by in vitro treatment with PKHB1 or with a known ICD inducer in breast cancer, epirubicin (EPI), used as positive control. One week after, mice were inoculated with viable cancer cells and tumor burden was monitored. The tumors grew in non-inoculated control mice, killing all of them in 20 around days. In contrast, immunizations with PKHB1-TCL or with EPI-TCL prevented correct tumor establishment in most mice, reflected in higher survival rates.

As we witnessed the strong immune responses triggered by the PKHB1-TCL, we wondered if using PKHB1-TCL as therapeutic cancer vaccine for mice that were already sick, could have an impact on tumor progression. To assess this, the mice were inoculated with viable cancer cells, and waited for tumors to reach 100 mm³, to then treat with vehicle, PKHB1-TCL or EPI-TCL. All mice being treated with vehicle had to be euthanized before day 23 as the disease progressed with tumor growth. Conversely, in mice treated PKHB1-TCL or with EPI-TCL, most of the tumors stopped growing after four applications of the therapeutic immunization, leading to cancer remission and an overall increased survival.

Finally, long-term immunological memory of immunized mice against 4T1 cells was assessed. For this, the mice that had undergone complete remission after prophylactic or therapeutic vaccination with PKHB1-TCL (>60 days of being tumor free), or naïve mice of similar ages (control), were (re)challenged with live 4T1 cells, and tumor growth was measured. In all controls, the tumors grew and mice died before day 23, while none of the immunized mice developed the tumors, reaching 100% 60-days survival after re-

challenge. Furthermore, 4T1 cells were stained with calcein and co-cultured with splenocytes obtained from naïve mice or from mice in remission, and after 24 h co-culture, there was a significantly higher ratio of calcein-negative 4T1 cells that were co-cultured with the long-immunized mice.

Altogether, these results demonstrate that PKHB1 induces ICD in breast cancer cells, and strongly support the use of PKHB1 and PKHB1-TCL as therapeutic tools to treat breast cancer, including the triple negative phenotype.

Résumé de l'article 3

État de l'art. Le cancer du sein est le cancer le plus fréquemment diagnostiqué et la principale cause de décès par cancer chez les femmes dans le monde. Les progrès récents dans le domaine de l'immuno-oncologie démontrent les effets immunostimulateurs bénéfiques de l'induction de la mort cellulaire immunogène (MCI). La MCI favorise l'infiltration tumorale par les cellules T et est associée à un meilleur pronostic chez les patientes atteintes d'un cancer du sein triple négatif (TNBC, Triple Negative Breast Cancer). Le but de cette étude était d'évaluer l'effet antitumoral du peptide PKHB1 sur les cellules cancéreuses du sein, et l'immunogénicité de la mort cellulaire induite par PKHB1 *in vitro*, *ex vivo* et *in vivo*.

Méthodes. Les caractéristiques de la mort cellulaire ont été évaluées par cytométrie en flux en utilisant des inhibiteurs de mort cellulaire. L'effet antitumoral de PKHB1 a été évalué en observant le volume de la tumeur, le poids et la distribution des lymphocytes (*in vivo*). Les caractéristiques de la mort cellulaire immunogène ont été évaluées, *in vitro*, par l'exposition ou la libération de modèles moléculaires associés aux dommages (DAMPs), et leur effet dans l'activation d'une réponse immunitaire antitumorale (*ex vivo*). De plus, *in vivo*, l'immunogénicité de la mort a été déterminée par l'évaluation de la capacité des cellules cancéreuses tuées par PKHB1 (PKHB1-TCL) à empêcher l'établissement de tumeurs des cellules cancéreuses du sein, ainsi que leur capacité à générer un mémoire immunologique anti-tumorale.

Résultats. Nos résultats ont montré que PKHB1 induit des altérations mitochondriales, la production de ROS, l'accumulation intracellulaire de Ca²⁺ ainsi que la mort cellulaire dépendante du calcium dans les cellules cancéreuses du sein, y compris les sous-types triple négatifs. Le traitement *in vivo* par PKHB1 induit une réduction du volume et du poids de la tumeur et favorise l'infiltration intratumorale des lymphocytes T CD8⁺. De plus, PKHB1 est capable d'induire une exposition de la calréticuline (CRT), une libération d'ATP et de HMGB1. Enfin, l'injection des cellules tumorales mortes après traitement par PKHB1 (PKHB1-TCL) induit la maturation des cellules dendritiques et la réponse

antitumorale des cellules T. Enfin, la réponse antitumorale liée à l'utilisation prophylactique et thérapeutique in vivo de PKHB1-TCL s'avère efficace dans le maintien d'une mémoire antitumorale à long terme.

Conclusions.

Le peptide PKHB1 a un effet antitumoral et active le système immunitaire par induction de la mort cellulaire immunogène dans les cellules cancéreuses du sein, favorisant également une mémoire immunogène à long terme.

Resumen del artículo 3

Antecedentes. El cáncer de mama es el cáncer que se diagnostica con más frecuencia y la principal causa de muerte por cáncer en mujeres en todo el mundo. Los avances recientes en el campo de la oncoinmunología demuestran los efectos inmunoestimuladores benéficos de la inducción de la muerte celular inmunogénica (MCI). La MCI aumenta la infiltración tumoral por las células T y se asocia con un mejor pronóstico en pacientes afectadas por cáncer de mama triple negativo con enfermedad residual. El objetivo de este estudio fue evaluar el efecto antitumoral del PKHB1, un péptido mimético de la trombospondina-1, contra células de cáncer de mama, y la inmunogenicidad de la muerte celular inducida por PKHB1 *in vitro*, *ex vivo* e *in vivo*.

Métodos. Las características de la muerte celular se evaluaron mediante citometría de flujo utilizando inhibidores de la muerte celular. Se evaluó el efecto antitumoral de PKHB1 observando el volumen tumoral, el peso y la distribución de linfocitos. La MCI se evaluó, *in vitro*, mediante la exposición o liberación de patrones moleculares asociados a daño (DAMPs) y su efecto en la activación de una respuesta inmune antitumoral (*ex vivo*). Además, *in vivo*, la inmunogenicidad de la muerte se determinó mediante la evaluación de la capacidad de las células cancerosas muertas por PKHB1 (PKHB1-TCL) para prevenir el establecimiento tumoral e inducir la regresión tumoral de las células de cáncer de mama trasplantadas, así como su capacidad para generar memoria inmunológica antitumoral a largo plazo.

Resultados. Nuestros resultados mostraron que PKHB1 induce alteraciones mitocondriales, producción de ROS, acumulación de Ca^{2+} intracelular y muerte celular dependiente de calcio en células de cáncer de mama, incluidos los subtipos triple negativos. PKHB1 tiene un efecto antitumoral *in vivo* que conduce a la reducción del volumen y peso del tumor y promueve la infiltración de células T CD8+ intratumoralmente. PKHB1 es capaz de inducir la exposición de calreticulina (CRT), HSP70 y HSP90, la liberación de ATP y de HMGB1. Además, PKHB1-TCL indujo la maduración de las células dendríticas y respuestas antitumorales de células T. Finalmente, PKHB1-TCL fue capaz de inducir una respuesta antitumoral contra las células de cáncer de mama *in vivo*, en una aplicación profiláctica, mientras que en un entorno terapéutico

indujo la regresión del tumor; ambas aplicaciones indujeron memoria antitumoral a largo plazo.

Conclusiones.

El péptido mimético de la trombospondina-1, PKHB1, tiene un efecto antitumoral in vivo e induce la activación del sistema inmunológico a través de la inducción de ICD en células TNBC.

Manuscript

**PKHB1, A THROMBOSPONDIN-1 PEPTIDE MIMIC, INDUCES ANTI-TUMOR
EFFECT THROUGH IMMUNOGENIC CELL DEATH INDUCTION IN
BREAST CANCER CELLS**

Kenny Misael Calvillo-Rodríguez^{1,2,3}, Luis Gómez-Morales^{1,2,3,4}, Rodolfo Mendoza-Reveles¹, Ashanti Concepción Uscanga-Palomeque¹, Philippe Karoyan^{2,3,4,5,6*}, Ana Carolina Martínez-Torres^{1*}, Cristina Rodríguez-Padilla^{1,7*}

1. Universidad Autónoma de Nuevo León, Facultad de Ciencias Biológicas, Laboratorio de Inmunología y Virología, Mexico.
2. Sorbonne Université, Ecole Normale Supérieure, PSL University, CNRS, Laboratoire des Biomolécules, LBM, 75005 Paris, France
3. Sorbonne Université, Ecole Normale Supérieure, PSL University, CNRS, Laboratoire des Biomolécules, DRUG Lab, Site OncoDesign, 25-27 Avenue du Québec, 91140 Les Ulis, France
4. Kaybiotix, GmbH, Zugerstrasse 32, 6340 Baar, Switzerland
5. Kayvisa, AG, Industriestrasse, 44, 6300 Zug, Switzerland
6. χ -Pharma, 25 Avenue du Québec, 91140 Les Ulis, France
7. LONGEVEDEN SA de CV, Monterrey, Mexico

*Co-senior authors

Corresponding Authors:

Ana Carolina Martínez-Torres. ana.martinezto@uanl.edu.mx

Philippe Karoyan. philippe.karoyan@sorbonne-universite.fr

Keywords: Breast cancer, immunogenic cell death, thrombospondin 1, PKHB1, tumor cell lysate, anticancer vaccine.

ABSTRACT

Background. Breast cancer is the most commonly diagnosed cancer and the leading cause of cancer death in women worldwide. Recent advances in the field of immuno-oncology demonstrate the beneficial immunostimulatory effects of immunogenic cell death (ICD) induction. ICD increases tumor infiltration by T cells and is associated with improved prognosis in patients affected by triple-negative breast cancer (TNBC) with residual disease. The aim of this study was to evaluate the antitumoral effect of PKHB1, a thrombospondin-1 peptide mimic, against breast cancer cells, and the immunogenicity of the cell death induced by PKHB1 *in vitro*, *ex vivo* and *in vivo*.

Methods. Characteristics of cell death were evaluated by flow cytometry using cell death inhibitors. The antitumoral effect of PKHB1 was evaluated observing the tumor volume, weight and lymphocytes distribution. Characteristics of immunogenic cell death were evaluated, *in vitro*, by the exposure or release of damage associated molecular patterns (DAMPs), and their effect in the activation of an antitumor immune response (*ex vivo*). In addition, *in vivo*, the immunogenicity of death was determined through the evaluation of the capacity of cancer cells killed by PKHB1 (PKHB1-TCL) to prevent tumor establishment of breast cancer cells, as well as their capacity to generate a long-term anti-tumor immunological memory.

Results. Our results showed that PKHB1 induces mitochondrial alterations, ROS production, intracellular Ca²⁺ accumulation as well calcium-dependent cell death in breast cancer cells, including triple-negative subtypes. PKHB1 has antitumor effect *in vivo* leading to tumor volume and weight reduction and promotes intratumorally CD8⁺ T cell infiltration. Furthermore, PKHB1 is able to induce calreticulin (CRT), HSP70 and HSP90

exposure, ATP and HMGB1 release. Additionally, the tumor cell lysate obtained by the treatment with PKHB1 induced dendritic cell maturation, and T cell antitumor responses. Finally, PKHB1-TCL *in vivo* was able to induce an antitumor response against breast cancer cells in a prophylactic application, whereas in therapeutic setting induced tumor regression and both applications induced long-term antitumor memory.

Conclusions.

PKHB1, a Thrombospondin-1 peptide mimic, has *in vivo* antitumor effect and induce immune system activation through immunogenic cell death induction in breast cancer cells.

BACKGROUND

Breast cancer is the most frequent type of cancer among women; its innate and acquired treatment-resistance to current therapies is the principal problem to treat it, causing the greatest number of cancer-related deaths. While systemic therapies have increased the survival rates of breast cancer patients, the dramatic variations in response rates of patients with distinct clinicopathologic parameters (Fortis *et al.*, 2017), as well as innate or acquired resistance to current therapies (Groenendijk and Bernards, 2014), make relevant the search for new effective treatments on the different molecular subtypes of breast cancer, in particular those associated with poor prognosis.

Recently several clinical studies have demonstrated the beneficial immunostimulatory effects of immunogenic cell death (ICD) induction (Garg *et al.*, 2017), recognized as a critical determinant for the efficiency of cancer therapies. Indeed, this peculiar cell death

type is capable of stimulating a long-term anti-tumor immune response against dead cancer cell antigens (Kroemer *et al.*, 2013). Additionally, inducing ICD increases tumor tissues infiltration by T cells, which plays an essential role in mediating a positive response to chemotherapy and is associated with improving clinical outcomes in all subtypes of breast cancer (Stanton and Disis, 2016; Garg *et al.*, 2017).

Recent reports by our group demonstrate that PKHB1, a peptide mimic of thrombospondin-1 (TSP-1), stable in the serum of mice and human, induces a cell death involving CD47 activation, in different cancer cells, especially in hematological malignancies (Martinez-Torres *et al.*, 2015; Denèfle *et al.*, 2016, 2019; Uscanga-Palomeque *et al.*, 2018). The ability of PKHB1 to induce cell death was also observed in leukemic cells from patients with aggressive and chemo-resistant phenotypes (Martinez-Torres *et al.*, 2015; Denèfle *et al.*, 2016, 2019; Uscanga-Palomeque *et al.*, 2018). Additionally, our group demonstrated that PKHB1 induces ICD in T cell acute lymphoblastic leukemia (Uscanga-Palomeque *et al.*, 2018), and that PKHB1-tumor cell lysate was able to induce complete tumor reduction and immunological memory against leukemic cells (Martínez-Torres *et al.*, 2019). However, little is known about the cell death mechanism, the immunogenicity and the antitumor effect of PKHB1 in solid cancers with different molecular characteristics and poor prognosis such as breast cancer (including the triple negative subtype).

Therefore, the aim of this study was to evaluate the antitumor potential of PKHB1 in breast cancer cells (*in vitro* and *in vivo*) including triple negative subtypes, and to determine if it induces anti-tumor immune system activation through ICD induction (*ex vivo* and *in vivo*).

METHODS

Peptide synthesis

PKHB1 and 4NGG peptides were synthesized manually, using Fmoc-protected amino acids and standard solid phase peptide synthesis (SPPS) methods, as described previously (6). The detailed methods are described in supplemental material and methods.

Cell culture.

MCF-7, MDA-MB-231 and 4T1 cell lines were obtained from the ATCC. MCF-7 and MDA-MB-231 cell lines were maintained in DMEM-F12 medium (GIBCO by Life Technologies, Grand Island, NY, USA), while 4T1 cell line was maintained in RPMI-1640 medium., both were supplemented with 10% of fetal bovine serum, 2mM L-glutamine, 100U/mL penicillin-streptomycin (GIBCO by Life Technologies, Grand Island, NY, USA), and incubated at 37°C in a controlled humidified atmosphere with 5% CO₂. Cell count was performed following the ATCC's standard protocols.

Cell death induction and inhibition analysis.

5×10^4 cells were plated in 24 wells dishes and left untreated or treated for 2h with 100 μ M, 200 μ M or 300 μ M of PKHB1 (KRFYVVMWKK) or 300 μ M of the control peptide 4NGG (KRFYGGMWKK). Annexin-V-allophycocyanin (Ann-V-APC 0.1 μ g/ml; BD Pharingen, San Jose CA, USA), and propidium iodide (PI, 0.5 μ g/ml Sigma-Aldrich) were used to assess phosphatidylserine exposure, cell death, and cell viability quantification, respectively, in a BD AccuryC6 flow cytometer (BD Biosciences, Franklin Lakes, NJ, USA) (total population 10,000 cells). Data was analyzed using FlowJo software (LLC, Ashland, OR, USA).

To decipher the cell death signaling pathway, the calcium chelator BAPTA (5 mM), the pan-caspase inhibitor Z- VAD-FMK (Z-VAD, 50 μ M), the antioxidant N-Acetyl Cysteine (NAC, 5 mM), the necroptotic inhibitor Necrostatin-1 (Nec-1, 50 μ M), the autophagic inhibitor spautin-1 (SP-1, 15 μ M), the PLC inhibitor U73122 (1.25 μ M) and the ER receptor inhibitors dantrolene (50 μ M) and 2-aminoethoxydiphenyl borate (2-APB, 40 μ M) were used. Cells were treated 30 minutes with the different inhibitors or the calcium chelator before treatment with PKHB1 (CC₅₀).

Intracellular Ca²⁺ levels assay.

5x10⁴ cells/well in 24 wells dishes (Life Science) were incubated 2h with PKHB1 (CC₅₀) or left untreated in complete medium. Then, cells were detached, washed with KREBS buffer, and resuspended in 200 μ L of RINGER buffer with 0.001 μ g/mL of Fluo-4 AM (Life Technologies) and 0.001 μ g/mL of Pluronic F-127 (Life Technologies), incubated 37°C for 30min. Next, cells were washed with RINGER buffer and assessed by BD Accury C6 flow cytometer (BD Biosciences, Franklin Lakes, NJ, USA) (total population 10,000 cells).

In vivo model.

This study was approved by the Animal Ethical Committee (CEIBA), of the School of Biological Sciences, number: CEIBA-2018-003. All experiments were conducted according to Mexican regulation NOM-062-ZOO-1999. Female BALB/c mice (six-to-eight-week-old; 22 \pm 2g weight) were maintained in controlled environmental conditions (25°C and 12 h light/dark cycle) and supplied with rodent food (LabDiet, St. Louis, MO,

USA) and water *ad libitum*, and they were monitored daily for health status. Mice were randomly assigned to different groups for all studies.

Tumor establishment.

5×10^5 live 4T1 cells in 100 μL of PBS were injected subcutaneously in the left hind. Tumor volume and mice weight were measured three times per week using a caliper (Digimatic Caliper Mitutoyo Corporation, Japan) and a digital scale (American Weigh Scale-600-BLK, USA), respectively. Tumor volume was determined with the formula: tumor volume (mm^3) = (Length x width²)/2. When tumor reached 100 mm^3 , mice were treated daily with 400 μg of PKHB1 in 200 μL of sterile water by intraperitoneal injection, control mice were treated with 200 μL of sterile water. Additionally, 16 days after tumor cells inoculation, mice were anaesthetized with an intraperitoneal injection of ketamine (80 mg/kg body weight) and xylazine (10 mg/kg body weight) and were euthanized by cervical dislocation, and tumors from Control or PKHB1 treated mice, were obtained and fixed in 3.7% neutral formalin, embedded in paraffin, sectioned (5 μm thickness) and stained with H&E (MERCK). Histopathological analyses were done by an external veterinarian pathologist (National professional certificate 2593012).

T cells evaluation.

16 days after tumor inoculation, mice treated or untreated were anaesthetized and sacrificed as described above. Blood was obtained by cardiac puncture and the peripheral blood mononuclear cells (PBMCs) isolation was performed by density gradient centrifugation using Ficoll-Hypaque-1119 (Sigma-Aldrich, St Louis, MO, USA). The spleen, lymph node and tumor were harvested and filtered through a cell strainer (70 μM)

with PBS (PBMCs were obtained from the spleen as described above), then 1×10^6 cells/mL were plated and the percent of CD3+, CD4+ and CD8+ T cells was observed by flow cytometry with the Mouse T lymphocyte subset antibody cocktail (from BD Bioscience), following the manufacturer's instructions.

Calreticulin, HSP70 and HSP90 exposure.

5×10^4 cells/well were plated in 24-well plates and treated with PKHB1 (CC_{50}) for 2h. Then, cells were detached, washed and incubated for 1h at (room temperature) RT with 2 $\mu\text{g/mL}$ of anti-Calreticulin (FMC-75, Enzo Life Science), 0.8 $\mu\text{g/mL}$ anti-HSP70 (F-3, Santa Cruz Biotechnology), 0.8 $\mu\text{g/mL}$ anti-HSP90 (F-8, Santa Cruz Biotechnology) in FACS buffer, cells were washed and incubated for 30 min in darkness at RT with goat anti-mouse IgG (Alexa Fluor 488) (H + L, Life Technologies) (1:1500) in FACS buffer, cells were then washed, resuspended in FACS buffer with 7-AAD (Life Technologies) (1:1000) and incubated in the dark for 10min at RT. The surface exposure of CRT, HSP70 and HSP90 was determined by flow cytometry among viable (7-AAD-negative) cells.

Immunofluorescence microscopy.

2.5×10^5 cells/well in a 6 well dishes were left untreated (Control) or treated with PKHB1 (CC_{50}) and incubated for 2h. Then, cells were washed with PBS and stained with Calreticulin-PE antibody (2 $\mu\text{g/ml}$) and Hoechst 33342 (0.5 $\mu\text{g/ml}$) (Thermo Scientific Pierce, Rockford, IL, USA), incubated for 1h in FACS buffer at RT, thus, cells were washed twice, maintained in PBS and assessed by confocal microscopy (Olympus X70; Olympus, Tokyo, Japan).

ATP and High-mobility group box 1 release assay.

2.5×10^5 cells/well in a 6 well dishes were left untreated (Control) or treated with PKHB1 (CC50) for 2h. Supernatants were recovered, centrifuged at 1600rpm/10 minutes and used to assess extracellular ATP by a luciferase assay (ENLITEN kit, Promega, Madison, WI, USA), or used to measure extracellular HMGB1 using the HMGB1 ELISA kit for MDA-MB-231, MCF-7 and 4T1 cells (BioAssay ELISA kit human or mouse, respectively; US Biological Life Science Salem, MA, USA) following the manufacturer's instructions. Bioluminescence was assessed in a microplate reader (Synergy HT, Software Gen5; BioTek, Winooski, VT, USA) at 560 nm, and absorbance was assessed at 450 nm.

T-cells isolation.

Mice were anaesthetized and sacrificed as described above, and blood was obtained by cardiac puncture. PBMCs isolation was obtained as described above. Murine CD3⁺ cells were isolated from total PBMCs by positive selection using magnetic-activated cell sorting (MACS) microbead technology with anti-CD3 ϵ -biotin and anti-biotin microbeads (Miltenyi Biotech; >98% purity and >98% viability), as stated by manufacturer's instructions.

Differentiation of bone marrow derived dendritic cells (BMDCs).

After sacrifice of anaesthetized mice, bone marrow was removed from femur and tibia by flushing into RPMI-1640. Eluted cells were cultured for 5 days with 20ng/mL of IL-4 and GM-CSF (R&D Systems, Minneapolis, MN, USA) until approximately 70% of the cells were CD11c⁺.

Evaluation of DCs maturation.

CD11c, CD80 and CD86 were evaluated by flow cytometry with the fluorescent label-conjugated antibodies, antiCD11c-Alexa-fluor 488 (R&D Systems), antiCD80-FITC and antiCD86-APC, from BD Biosciences (San Jose, CA, USA). 1×10^6 DCs /mL were stained in 100 μ L of FACS buffer with the indicated antibodies at RT for 30 minutes and then were washed twice with PBS, centrifugated at 1600rpm/10min and resuspended in 100 μ L of FACS buffer.

DCs + PKHB1 tumor cell lysate co-culture.

DCs were resuspended in fresh medium (1×10^6 cells/mL), left untreated (control) or incubated with 3×10^6 4T1 cells/mL of PKHB1-tumor cell lysate, to give a range of 1:3 (DCs to PKHB1-tumor cell lysate) and co-culture was left for 24 h. Then the supernatant was obtained, and the well was washed twice with PBS before the next co-culture.

DCs + T-lymphocytes co-culture.

Control DCs or DCs previously co-cultured with PKHB1-TCL were maintained in fresh medium at 1×10^6 cells/mL. Then, allogeneic BALB/c mCD3⁺ cells were added at 3×10^6 cells/mL to give a range of 1:3 (DCs to CD3⁺ cells), co-culture was left for 96 h. Then, lymphocytes were collected (in the supernatant), washed with PBS, and resuspended in fresh medium at 5×10^6 cells/mL for their use in the next co-culture.

T-Lymphocytes + 4T1 cells co-culture.

1×10^5 cells/mL viable 4T1 cells were plated. Then, allogeneic BALB/c mCD3⁺ cells were added to each well at 5×10^5 cells/mL, unprimed (previously co-cultured with control DCs) or primed (previously co-cultured with DCs-PKHB1-TCL) to give a range of 1:5 (tumor to effector). Co-culture was left for 24 h for cytokine or calcein assessment.

Cytokine release assay

Supernatants from the indicated co-cultures were obtained for the assessment of IL-2, IL-4, IL5, and TNF α (BD CBA Mouse Th1/Th2 Cytokine Kit, San Jose, CA, USA) by flow cytometry following manufacturer's instructions. IFN γ was assessed using an ELISA kit (Sigma-Aldrich) and the Synergy HTTM (BioTek Instruments, Inc., Winooski, VT, USA) plate reader at 570 nm wavelength, following manufacturer's instructions.

Calcein assay

4T1 cells (1×10^6 cells/mL) were stained with (0.1mL/mL) Calcein-AM from BD Biosciences (San Jose, CA) in FACS buffer at 37 °C and 5% CO₂ for 30 min, washed twice with PBS. Thus, T cells primed or unprimed were added in a 1:5 (tumor to effector) ratio. Co-culture was incubated at 37 °C and 5% CO₂ for 24 h. Finally, calcein positive or negative 4T1 cells were assessed in a BD AccuryC6 flow cytometer (BD Biosciences) (total population 10,000 cells). Data was then analyzed using FlowJo software.

PKHB1-TCL preparation

4T1 cells (1.5×10^6 cells/mL per mice) were plated and, after adherence, cells were then treated with 400 μ M of PKHB1 (CC₁₀₀) for 2 h, or EPI 10 μ M (CC₁₀₀) for 24 h. After

treatments, cells were obtained, centrifugated at 1600 rpm/10 min and resuspended in 100µL of serum free medium/mice. Cell death was confirmed using Trypan blue staining and flow cytometry. Finally, the PKHB1-TCL or EPI-TCL were inoculated by subcutaneous injection in the right flank.

Prophylactic vaccination

Vaccination was carried out as follows: PKHB1-TCL or EPI-TCL was inoculated s.c. in 100 µL of serum free medium into the right hind leg (day -7), seven days later viable (5×10^5) 4T1 cells were inoculated into the left hind leg (day 0). Tumor volume and weight were measured as described above.

PKHB1-TCL treatment

Tumor was established by subcutaneous injection of 5×10^5 4T1 cells in 100 µL of PBS, in the left hind. Tumor volume and mice weight were measured as described above. When tumor reached 100 mm³ the first treatment of PKHB1-TCL or EPI-TCL was applied. Tumor cell lysates were inoculated subcutaneously in 100 µl of serum free medium, in the right hind, twice a week for a total of four applications in a two-weeks period. Control mice were treated with 100 µl of serum free medium.

Long-term antitumor effect evaluation

Mice in complete remission after prophylactic or therapeutic 4T1-PKHB1-TCL application were re-challenged with 5×10^5 4T1 viable cells in 100 µL of PBS in the left hind and tumor volume was measured as described above.

Long-term splenocytes-cytotoxicity

Mice in complete remission after prophylactic or therapeutic PKHB1-TCL application were re-challenged with 5×10^5 4T1 viable cells in 100 μ L of PBS in the left hind. Three days after tumor inoculation mice were sacrificed, spleens were harvested, filtered through a cell strainer (70 μ M) with PBS, and PBMCs were obtained as described above. Splenocytes were recovered and co-cultured with 4T1 cells (previously stained with calcein-AM) at 44:1 ratio (respectively). Finally, calcein positive or negative cells were assessed as described above.

Statistical Analysis

Mice were randomly assigned to different groups for all *in vivo* studies. At least three independent experiments were repeated three independent times. Mann-Whitney tests and two-tailed unpaired Student's *t*-tests were performed using GraphPad Prism Software (San Diego CA, USA) and presented as mean values \pm SD. The *p* values were considered significant as follows: $p < 0.05$.

RESULTS

PKHB1 induces breast cancer cell death.

The potency of PKHB1 was previously demonstrated in hematopoietic malignancies (Martinez-Torres *et al.*, 2015; Uscanga-Palomeque *et al.*, 2018). Its effectiveness was not yet evaluated for solid tumors *in vivo*. Thus, after peptide synthesis and characterization

(Supplemental material and methods, table sup.1 and figure sup.1), we evaluated here its effect in two types of human breast cancer cell lines, I) MCF-7 (luminal subtype) and II) MDA-MB-231 (triple negative subtype), as well as on the murine 4T1 cell line (mimics triple negative subtype(Pulaski and Ostrand-Rosenberg, 2001)). We observed that PKHB1 induces cell death in a concentration-dependent way in MCF-7 (figure 1A), MDA-MB-231 (figure 1B) and 4T1 (figure 1C) cells, as they showed an increase in the percentage of double-positive Ann-V-APC/PI staining (figure sup. 2). We determined that the cytotoxic concentration that induces approximately 50% of cell death (CC_{50}) in MDA-MB-231 and MCF-7 is 200 μ M while in 4T1 is 300 μ M.

Next, we evaluated mitochondrial damage and cytosolic Ca^{2+} augmentation, and observed that PKHB1 (CC_{50}) induced loss of mitochondrial membrane potential (figure 1D), ROS production (figure 1E) and intracellular Ca^{2+} augmentation (figure 1F) in all cell lines. Afterwards, we searched to determine the cell death effectors and evaluated Ca^{2+} -dependence, ROS-dependence, and we used inhibitors of caspases (zVAD), necroptosis (Nec-1) and autophagy (SP-1) and assessed cell death. We found that PKHB1-induced cell death in all cells was only inhibited when using the calcium chelator BAPTA, as previously observed for leukemia cells (Martinez-Torres *et al.*, 2015; Uscanga-Palomeque *et al.*, 2018), suggesting a similar cell death mechanism and common signaling pathway among solid and liquid cancers. To assess this hypothesis, we used a PLC inhibitor (U73122) and ER receptor inhibitors (dantrolene, for ryanodine receptors, and 2-APB, for IP_3 receptors). We determined that PKHB1-cell death is inhibited when blocking the ER- Ca^{2+} -channels with U73122, dantrolene and 2-APB (figure 1J, K and L) in breast cancer cells, confirming our hypothesis.

PKHB1 has antitumor effects in breast cancer and promotes intratumorally CD8+ T cell infiltration.

To evaluate *in vivo* the potential antitumor effect of PKHB1, 4T1 breast cancer cells were grafted onto BALB/c mice. Daily treatments were initiated once the tumor volume reached 100 mm³, and 16 days after the cell transplant, tumor volume of the control mice had reached 1500 mm³ requiring the sacrifice of the animals, while the tumor volume of the PKHB1-treated mice reached a maximum volume of 890 mm³ (at day 8) which started to decrease, reaching a volume of 570 mm³ at day 16 (figure 2A). The decrease in tumor volume was correlated with the decrease in tumor weight, going from 1.5 grams in the controls to 0.40 grams in PKHB1-treated mice (figure 2B). The decrease in tumor volume in mice treated with PKHB1, led us to evaluate the involvement of T cells in the observed effect. First, we analyzed histological sections of tumors from control (figure 2C) or PKHB1-treated mice (figure 2D): results revealed that tumors from control mice showed tumor cells with moderate mitotic activity (blue arrows), whereas the PKHB1-treated mice showed sporadic mitotic activity, extensive necrosis with abundant accumulation of cellular debris (green arrows), and abundant inflammatory exudate, composed of polymorphonuclear elements, eosinophils and lymphoplasmacytic cells (red arrows).

Additionally, we evaluated if the cell number and distribution of T lymphocytes in peripheral blood, spleen, lymph nodes, and tumor site, changed after PKHB1 treatment. We observed (figure 2E) that the percentage of CD3+ cells increased in blood, lymph nodes, and tumors of PKHB1-treated mice, while it was maintained in spleen. When we assessed CD4+ cells, the percentage of cells significantly augmented in lymph nodes while it significantly diminished in the tumor site (figure 2F). Furthermore, CD8+ T cells

significantly increased in peripheral blood and specially in tumor site, while they significantly diminished in lymph nodes (figure 2G). Finally, we determined if splenocytes from PKHB1-treated mice could induce an antitumor cell cytotoxicity. For this purpose, we evaluated the decrease in calcein stained 4T1 cells after co-culture with splenocytes obtained from control or PKHB1-treated mice. In figure 2H, results show that splenocytes from PKHB1-treated mice induced a significant decrease in calcein stained 4T1 cells (75%) in comparison with control mice (40%).

PKHB1 induces DAMPs exposure and release in breast cancer cell lines.

As we observed that PKHB1 induced cell death in breast cancer cell lines and CD8+ T lymphocyte-recruitment in tumor site, we wondered if cell death induced by PKHB1 was able to induce DAMPs' exposure/release in breast cancer cells. The first step was to evaluate the exposure of CRT (the principal DAMP related with ICD). Our results show that PKHB1-treatment was able to induce 59%, 63%, and 50% of CRT positive cells in MCF-7 (figure 3A), MDA-MB-231 (figure 3B), and 4T1 (figure 3C) cells. The CRT exposure was confirmed by immunofluorescence microscopy and we observed that PKHB1 induced CRT exposure in all the cases (figure 3 D, E and F). Additionally, PKHB1-treatment induced 24 ± 3 , 3.2 ± 1.3 and 4.23 ± 2 -fold of HSP70 exposure (fig 3 G), 2 ± 0.6 , 2.7 ± 0.6 and 7 ± 1.85 -fold of HSP90 exposure (fig 3 H) in MCF-7, MDA-MB-231 and 4T1 cells, respectively when compared with untreated cells.

Finally, the presence of HMGB1 and ATP was assessed in the supernatants of treated and untreated breast cancer cells. In figure 3, results showed a significant release of HMGB1

(figure 3I) and ATP (figure 3J) in the supernatants of PKHB1-treated cells, when compared with untreated cells.

PKHB1-TCL induces maturation of bone marrow-derived DCs and anti-tumor T-cell responses.

To assess the immunogenicity of the dead cells obtained upon treatment with PKHB1, 4T1 cells were treated with CC_{100} of PKHB1. The PKHB1-tumor cell lysate (PKHB1-TCL) was then prepared as described in the methods section, and its ability to induce DCs maturation was evaluated. Thus, bone marrow-derived murine DCs were left untreated (Control) or pulsed for 24 h with the PKHB1-TCL. After co-culture, the DCs pulsed with PKHB1-TCL show a significant increase in the expression of co-stimulatory molecules CD80 and CD86 passing from 50% to 66% and 90%, respectively, while maintaining the expression of the DCs marker CD11c (figure 4A). Furthermore, DCs pulsed with PKHB1-TCL show a significant increase in $TNF\alpha$ release in comparison with unstimulated DCs (figure 4B). Once we determined that PKHB1-TCL was able to induce DCs maturation, we assessed if the pulsed DCs (DCs-PKHB1-TCL) were able to prime T cells. First, primary T lymphocytes ($CD3^+$ cells) were co-cultured for 96h with pulsed or unpulsed DCs and the release of $TNF\alpha$, $IFN\gamma$, IL-5, IL-4, and IL-2 was assessed. Results showed that co-culture of pulsed DCs with primary T lymphocytes induced the release of $TNF\alpha$, $IFN\gamma$, and IL-2, while IL-5 and IL-4 releases were not detected (table S2).

Next, primed (co-cultured with pulsed DCs-PKHB1-TCL) or unprimed (co-cultured with unstimulated DCs) T-lymphocytes were collected and co-cultured during 24h with viable 4T1 cells (previously stained with calcein-AM). Then a significant increase of IFN- γ and IL-2 release was observed in the supernatants of primed T-lymphocytes when being co-cultured with 4T1 cells, while no difference was observed in IL-4 release (figure 4 C and D). To assess antitumor cell cytotoxicity, we evaluated the decrease in calcein-stained 4T1 cells after co-culture with primed or unprimed T-lymphocytes. Results showed that only T-lymphocytes co-cultured with pulsed DCs-PKHB1-TCL induced a significant decrease in calcein stained 4T1 cells (figure 4E), in comparison with the 4T1 cells co-cultured with unprimed T lymphocytes (figure 4E).

Prophylactic vaccination with PKHB1-TCL prevented tumor establishment of 4T1 cells.

Considering that PKHB1 treatment induces tumor decline, infiltration of CD8⁺ cells into the tumor, DAMPs' exposure and release, and the antitumor immune response *ex vivo*, the next step was to carry out the *Gold Standard* of ICD (prophylactic vaccination) to confirm if PKHB1 induced ICD. The vaccine was based in the subcutaneous inoculation of the 4T1-PKHB1-TCL, 7 days before the transplantation of viable 4T1 cells, while mice were inoculated with 4T1-EPI-TCL used as a positive control, and controls without TCL were injected with serum-free medium (figure 5A). Results showed that vaccination with PKHB1-TCL prevented tumor establishment in 80% of mice compared to 70% for mice treated with EPI-TCL. 0% of survival was observed in the Control group inoculated with

serum-free medium (figure 5B). Additionally, survival rates of mice in each group were consistent with tumor growth, observing respectively 80% and 70% of survival in mice vaccinated with PKHB1-TCL and EPI-TCL by day 60, while control mice perished by day 21 (figure 5C).

Treatment with PKHB1-TCL induces tumor regression

After *ex-vivo* and *in vivo* results, we evaluated if the immunogenicity of PKHB1-TCL was able to diminish tumor growth and improve overall survival in syngeneic mice bearing 4T1 tumors. First, 4T1 viable cells were inoculated in BALB/c mice. When tumor reached 100 mm³, a control-group was treated with serum-free medium, a second group was treated with PKHB1-TCL and the third group was treated with EPI-TCL. All mice were treated two times per week for a total of four treatments (figure 5D). Tumor growth measurements show that PKHB1-TCL-treated mice had diminished tumor growth after day 10 (7 days after the first treatment), which continued to decrease until no tumor was detected by day 18, in the group of EPI-TCL the tumor diminished after day 10 (7 days after the first treatment) which continued to decrease until no tumor was detected by day 16 (figure 5E). Tumor growth diminution was reflected in overall mice survival, as PKHB1-TCL-treated mice presented a 78% of survival, while the EPI-TCL-treated mice presented 67% of survival, and all control mice perished by day 23 (figure 5F).

PKHB1-TCL prophylactic and therapeutic vaccinations induce long-term antitumor effect.

To assess the long-term antitumor effect response against 4T1 breast cancer cells induced by PKHB1-TCL in a prophylactic or therapeutic application, mice in complete remission (tumor free >60 days) were re-challenged with living 4T1 cells. Tumor volume analysis showed that, contrary to naïve mice (Control), which showed a correct 4T1 tumor establishment, mice in remission after PKHB1-TCL prophylactic or therapeutic application showed a slight increase in tumor volume at day 2, which immediately disappears by day 6 (figure 6A). These results correlate with mice's survival, where we observed that compared to naïve mice, in which a primary 4T1 cells challenge resulted in a 0% of survival by day 23, those that were in remission after prophylactic or therapeutic application of PKHB1-TCL were completely resistant to a re-challenge with 4T1 cells, resulting in a 100% of survival (figure 6B). Furthermore, we determined if splenocytes from re-challenged mice can induce an antitumor cell cytotoxicity. For this purpose, we evaluated the decrease in calcein stained 4T1 cells after co-culture with splenocytes obtained from naïve or re-challenged mice. In figure 6 D, results showed that splenocytes from re-challenged mice induced a significant decrease in calcein stained 4T1 cells (60%) in comparison with naïve mice (30%).

DISCUSSION.

Here we described for the first time the mechanism of cell death induced by PKHB1 in breast cancer cells, which conserves the principal molecular characteristics (caspase-independent, calcium-dependent, PLC-dependent and IP₃R and RYR receptors-dependent

cell death with the presence of ROS, loss of mitochondrial membrane potential and the intracellular accumulation of Ca^{2+}) reported mainly in leukemic cells (Martinez-Torres *et al.*, 2015; Uscanga-Palomeque *et al.*, 2018; Denèfle *et al.*, 2019; Martínez-Torres *et al.*, 2019). These results highlight the mechanism of cell death induced by PKHB1 as a conserved mechanism, especially among different types of tumor cells including the triple-negative phenotype. Additionally, we recently reported the overexpression of PLC γ 1 and its importance in the cell death induced by PKHB1 in CLL cells (6). Whereas, in breast cancer the PLC γ 1 is over-expressed in patients with poor clinical outcome (Lattanzio *et al.*, 2019). In this sense, the mechanism of PKHB1-cell death, might have an advantage in the cancer cells that overexpress PLC γ 1.

Our results also revealed the antitumor effect of PKHB1 against 4T1-breast cancer cells *in vivo*, as PKHB1-treatment diminished tumor volume and weight. Additionally, T cells distribution observed in PKHB1-treated mice suggests that PKHB1 promote an antitumor immune response, since it involves the increase of T-cells (in blood, lymph node and tumor), trafficking of CD4⁺ cells to lymph nodes, and tumor CD8⁺ cells infiltration (Krekorian *et al.*, 2019). Our results are promising due do it has been reported that extensive tumor infiltration by cytotoxic CD8⁺ T cells is strongly associated with patient's survival and response to therapy, even in different phenotypes of breast cancer (*The evaluation of tumor-infiltrating lymphocytes (TILs) in breast cancer: recommendations by an International TILs Working Group 2014*, no date; Catacchio *et al.*, 2019). Furthermore, splenocytes from PKHB1-treated mice were more cytotoxic against breast cancer cells than splenocytes from control mice, probably for the immunogenicity of the cell death triggered by PKHB1 (Krysko *et al.*, 2012; Krekorian *et al.*, 2019).

The low immunogenicity of tumor cells is a main obstacle of antitumor therapies, therefore a way to reactivate potent antitumor immune responses is through the emission of DAMPs (Abhishek D Garg *et al.*, 2015) and dead cells-derived antigens, which can be achieved in the ICD (Abhishek D. Garg *et al.*, 2015; Garg *et al.*, 2017). Here we demonstrated that PKHB1 is capable of inducing CRT, HSP70 and HSP90 exposure, HMGB1 and ATP release, which can promote the uptake of dying cells, and the recruitment, maturation and cross-presentation activity of antigen-presenting cells (APCs) (Krysko *et al.*, 2012; Galluzzi *et al.*, 2020). In these sense, we demonstrated that PKHB1-TCL is able to promote a mature phenotype of DCs (Dudek *et al.*, 2013) since this induced a significant increase in the co-stimulatory molecules CD80 and CD86, as well as the significant release of TNF α , such as different ICD-inductors (Montico *et al.*, 2018). Additionally, we observed that DCs pulsed with the PKHB1-TCL promote the antitumor specific cytotoxicity of T cells, which confirm the phenotypic and functional maturation of DCs.

On the other hand, vaccination assays involving syngeneic models are the gold standard to formally identify ICD inducers, since this demonstrates the tumor rejection capacity of the immunized host (Kepp *et al.*, 2014; Abhishek D Garg *et al.*, 2015). Our results show that the prophylactic application of EPI-TCL and PKHB1-TCL prevented tumor establishment and increased survival in 80% of the mice, without using adjuvants and with only one vaccination, in comparison with others ICD-inductors (---). Also, we used Epirubicin, a well-known ICD inductor with major side-effects in human (De Azambuja *et al.*, 2015; L. Li *et al.*, 2020; Reyes-Ruiz *et al.*, 2021) as a positive control, highlighting its ability to prevent the establishment of breast cancer in 70% of the mice. Our results are

in line with the protective potential of established ICD inducers including oxaliplatin, doxorubicin, iadurobicin, mitoxantrone and specific forms of radiotherapy (in colon cancer) which presented between 80%-90% of tumor-free mice (Obeid *et al.*, 2007; Tesniere *et al.*, 2010; Gorin *et al.*, 2014) while the antibody 7A7 (anti-EGFR) induced 50% of survival (lung cancer) (Garrido *et al.*, 2011), and especially with the fact that an ICD-inductor should display elevated tumor-free survival (>50%) (Humeau *et al.*, 2019). The therapeutic application of the dead cells killed by a potential ICD inducer can be used as a confirmatory trial for ICD inducers, to evaluate their ability to mediate therapeutic effects depending on the immune system against established neoplasms (Kepp *et al.*, 2014). In this sense, our results show that when we treated tumor bearing mice with only four applications of PKHB1-TCL, tumor volume decreased 7 days after the first administration, reaching tumor regression on day 18 in approximately 80% of mice, while in the group of EPI-TCL the tumor diminished 7 days after the first treatment which continued to decrease until tumor regression on day 16. Our results highlight the immunogenicity of the PKHB1-induced cell death, since the therapeutic application of the PKHB1-TCL induced tumor remission even in the absence of adjuvants. Additionally, we determined the therapeutic potential of the EPI-TCL for first time, as a novel strategy for the application of chemotherapy-ICD inducers. These results differentiate the PKHB1-TCL from other therapeutic strategies with tumor lysates against melanoma, prostate and ovarian cancer, which have been poorly evaluated and were mainly used in combination with adjuvants (Wu *et al.*, 2007; Chiang, Coukos and Kandalaft, 2015). The success of the therapeutic application of PKHB1-TCL in breast cancer was similar to the T-ALL model (Martínez-Torres *et al.*, 2019), despite their intrinsic molecular

differences (Pulaski and Ostrand-Rosenberg, 2001; Irvin *et al.*, 2002; McAndrew *et al.*, 2011; Abalsamo *et al.*, 2012).

The perspectives for cell therapy against cancer are based on the development of T cell responses, resulting in effective rejection of tumors and long-term protection (Henry *et al.*, 1999; Farkona, Diamandis and Blasutig, 2016). From this fact, the induction of ICD eventually results in long-lasting protective antitumor immunity (Zhou *et al.*, 2019). Our results demonstrate that PKHB1-TCL induces long-term antitumor effect since 100% of mice in remission after PKHB1-TCL prophylactic or therapeutic application survived at the re-challenge with 4T1 cells. Although immunotherapy with pulsed DCs, primed T lymphocytes or CAR-T cells is the main approach used to stimulate antitumor immune responses, they represent greater technical complexity, higher cost, among other disadvantages regarding the use of crude PKHB1-TCL (Papaioannou *et al.*, 2016; Lee Ventola, 2017; Calmeiro *et al.*, 2020).

Overall, our results demonstrate that PKHB1 is an ICD inducer in breast cancer cells and highlight a new approach for TSP-1 peptides mimic, which could induce ICD as a conserved mechanism of cell death in different types of tumor cells, including solid cancers, additionally, our results provide evidence for a novel strategy in the obtention and application of tumor cell lysates against cancer.

DECLARATIONS

Ethics approval.

The Animal Research and Welfare Ethics Committee (CEIBA), of the School of Biological Sciences approved this study: CEIBA-2018-003. All experiments were conducted according to Mexican regulation NOM-062-ZOO-1999.

Consent for publication.

Not applicable.

Availability of data and material.

The data used to support the findings of this study are available from the corresponding authors upon request.

Competing interest

The authors declare the following competing financial interest(s): a patent including results from this paper has been filed. The authors declare that no other competing interests exist.

Funding

This work was supported by SEP-CONACYT-ECOS-ANUIES, Grant/ Award Number: 291297; the Laboratory of Immunology and Virology of the College of Biological Sciences; UANL; Sorbonne-Université, Laboratoire des Biomolécules, DRUGLAB, Kaybiotix. KMCR and LGM hold a CONACyT scholarship. LGM hold a Kaybiotix grant.

Authors' contributions.

KMCR, ACUP and RMR carried out cell death, TMRE, and ROS assessment. KMCR and

RMR carried out Ca^{2+} assessment. LGM carried out peptide synthesis. KMCR performed *ex vivo* and *in vivo* experiments. ACMT and PK conceived and supervised the work. KMCR and ACMT prepared the figures and wrote the manuscript. KMCR, LGM, RMR, ACUP, PK, ACMT, and CRP designed experiments, analyzed and interpreted data, and read and approved the final manuscript.

Acknowledgments

We thank the SEP-CONACYT-ECOS-ANUIES grant 291297, the Laboratory of Immunology and Virology of the Faculty of Biological sciences, UANL, Kaybiotix and the DRUG Lab from Sorbonne University for the financial support and the facilities provided to achieve this work. KMCR, LGM, and ACUP thank CONACyT for their scholarship. LGM thanks SU/LBM/DRUG Lab/Kaybiotix for scholarship. PK is grateful to SATT-Lutech and DRI from SU, Kayvisa/Kaybiotix/ γ -Pharma for financial support and Oncodesign for hosting the LBM DRUG Lab. We thank Alejandra Reyes-Ruiz and Martin Herrick Ramón Kane for technical help, and Moises Armides Franco-Molina for the facilities and for his help.

REFERENCES

1. Fortis SP, Sofopoulos M, Sotiriadou NN, Haritos C, Vaxevanis CK, Anastasopoulou EA, et al. Differential intratumoral distributions of CD8 and CD163 immune cells as prognostic biomarkers in breast cancer. *J Immunother Cancer* [Internet]. 2017 Apr 18 [cited 2020 Jul 15];5(1):39. Available from: <http://jitc.bmj.com/lookup/doi/10.1186/s40425-017-0240-7>
2. Groenendijk FH, Bernards R. Drug resistance to targeted therapies: Déjà vu all over again [Internet]. Vol. 8, *Molecular Oncology*. Elsevier; 2014 [cited 2020 Jul 15]. p. 1067–83. Available from: [/pmc/articles/PMC5528618/?report=abstract](http://pmc/articles/PMC5528618/?report=abstract)
3. Garg AD, More S, Rufo N, Mece O, Sassano ML, Agostinis P, et al. Trial watch: Immunogenic cell death induction by anticancer chemotherapeutics. *OncoImmunology*. 2017.
4. Kroemer G, Galluzzi L, Kepp O, Zitvogel L. Immunogenic Cell Death in Cancer Therapy. *Annu Rev Immunol*. 2013;
5. Stanton SE, Disis ML. Clinical significance of tumor-infiltrating lymphocytes in breast cancer [Internet]. Vol. 4, *Journal for ImmunoTherapy of Cancer*. BioMed Central Ltd.; 2016 [cited 2020 Jul 15]. p. 59. Available from: <http://jitc.bmj.com/lookup/doi/10.1186/s40425-016-0165-6>
6. Martinez-Torres AC, Quiney C, Attout T, Bouillet H, Herbi L, Vela L, et al. CD47 Agonist Peptides Induce Programmed Cell Death in Refractory Chronic Lymphocytic Leukemia B Cells via PLC γ 1 Activation: Evidence from Mice and Humans. *PLoS Med*. 2015;
7. Denèfle T, Bouillet H, Herbi L, Newton C, Martinez-Torres A-C, Guez A, et al. Thrombospondin-1 Mimetic Agonist Peptides Induce Selective Death in Tumor Cells: Design, Synthesis, and Structure–Activity Relationship Studies. *J Med Chem* [Internet]. 2016 Sep 22 [cited 2018 Dec 21];59(18):8412–21. Available from: <http://pubs.acs.org/doi/10.1021/acs.jmedchem.6b00781>
8. Uscanga-Palomeque AC, Calvillo-Rodríguez KM, Gómez-Morales L, Lardé E, Denèfle T, Caballero-Hernández D, et al. CD 47 agonist peptide PKHB 1 induces immunogenic cell death in T-cell acute lymphoblastic leukemia cells. *Cancer Sci* [Internet]. 2018 Dec 14 [cited 2018 Dec 21];cas.13885. Available from: <https://onlinelibrary.wiley.com/doi/abs/10.1111/cas.13885>

9. Denèfle T, Pramil E, Gómez-Morales L, Levasseur MD, Lardé E, Newton C, et al. Homotrimerization Approach in the Design of Thrombospondin-1 Mimetic Peptides with Improved Potency in Triggering Regulated Cell Death of Cancer Cells. *J Med Chem* [Internet]. 2019 Sep 12 [cited 2019 Sep 26];62(17):7656–68. Available from: <https://pubs.acs.org/doi/10.1021/acs.jmedchem.9b00024>
10. Martínez-Torres AC, Calvillo-Rodríguez KM, Uscanga-Palomeque AC, Gómez-Morales L, Mendoza-Reveles R, Caballero-Hernández D, et al. PKHB1 Tumor Cell Lysate Induces Antitumor Immune System Stimulation and Tumor Regression in Syngeneic Mice with Tumoral T Lymphoblasts. *J Oncol* [Internet]. 2019 Jun 4 [cited 2019 Sep 23];2019:1–11. Available from: <https://www.hindawi.com/journals/jo/2019/9852361/>
11. Pulaski BA, Ostrand-Rosenberg S. Mouse 4T1 Breast Tumor Model. In: *Current Protocols in Immunology*. 2001.
12. Lattanzio R, Iezzi M, Sala G, Tinari N, Falasca M, Alberti S, et al. PLC-gamma-1 phosphorylation status is prognostic of metastatic risk in patients with early-stage Luminal-A and -B breast cancer subtypes. *BMC Cancer* [Internet]. 2019 Dec 30 [cited 2021 Mar 4];19(1):747. Available from: <https://bmccancer.biomedcentral.com/articles/10.1186/s12885-019-5949-x>
13. Krekorian M, Fruhwirth GO, Srinivas M, Figdor CG, Heskamp S, Witney TH, et al. Imaging of T-cells and their responses during anti-cancer immunotherapy [Internet]. Vol. 9, *Theranostics*. Ivyspring International Publisher; 2019 [cited 2020 Jul 15]. p. 7924–47. Available from: </pmc/articles/PMC6814447/?report=abstract>
14. Salgado R, Denkert C, Demaria S, Sirtaine N, Klauschen F, Pruneri G, et al. The evaluation of tumor-infiltrating lymphocytes (TILS) in breast cancer: Recommendations by an International TILS Working Group 2014 [Internet]. Vol. 26, *Annals of Oncology*. Oxford University Press; 2015 [cited 2021 Mar 9]. p. 259–71. Available from: </pmc/articles/PMC6267863/>
15. Catacchio I, Silvestris N, Scarpi E, Schirosi L, Scattone A, Mangia A. Intratumoral, rather than stromal, CD8+ T cells could be a potential negative prognostic marker in invasive breast cancer patients. *Transl Oncol* [Internet]. 2019 Mar 1 [cited 2020 Jul 15];12(3):585–95. Available from: </pmc/articles/PMC6350084/?report=abstract>

16. Krysko D V., Garg AD, Kaczmarek A, Krysko O, Agostinis P, Vandenabeele P. Immunogenic cell death and DAMPs in cancer therapy. *Nature Reviews Cancer*. 2012.
17. Garg AD, Dudek-Peric AM, Romano E, Agostinis P. Immunogenic cell death. *Int J Dev Biol* [Internet]. 2015 Sep 2 [cited 2018 Dec 21];59(1–3):131–40. Available from: <http://www.ncbi.nlm.nih.gov/pubmed/26374534>
18. Garg AD, Galluzzi L, Apetoh L, Baert T, Birge RB, Bravo-San Pedro JM, et al. Molecular and translational classifications of DAMPs in immunogenic cell death. *Front Immunol*. 2015;
19. Galluzzi L, Vitale I, Warren S, Adjemian S, Agostinis P, Martinez AB, et al. Consensus guidelines for the definition, detection and interpretation of immunogenic cell death [Internet]. Vol. 8, *Journal for ImmunoTherapy of Cancer*. BMJ Publishing Group; 2020 [cited 2020 Jul 21]. p. 70. Available from: <http://jitc.bmj.com/>
20. Dudek AM, Martin S, Garg AD, Agostinis P. Immature, Semi-Mature, and Fully Mature Dendritic Cells: Toward a DC-Cancer Cells Interface That Augments Anticancer Immunity. *Front Immunol* [Internet]. 2013 Dec 11 [cited 2018 Dec 21];4:438. Available from: <http://www.ncbi.nlm.nih.gov/pubmed/24376443>
21. Montico B, Nigro A, Casolaro V, Dal Col J. Immunogenic apoptosis as a novel tool for anticancer vaccine development [Internet]. Vol. 19, *International Journal of Molecular Sciences*. MDPI AG; 2018 [cited 2021 Jun 22]. Available from: [/pmc/articles/PMC5855816/](https://pubmed.ncbi.nlm.nih.gov/31555816/)
22. Kepp O, Tartour E, Vitale I, Vacchelli E, Adjemian S, Agostinis P, et al. Consensus guidelines for the detection of immunogenic cell death. *OncoImmunology*. 2014.
23. Li L, Li Y, Yang C, Radford DC, Wang J, Janát-Amsbury M, et al. Inhibition of Immunosuppressive Tumors by Polymer-Assisted Inductions of Immunogenic Cell Death and Multivalent PD-L1 Crosslinking. *Adv Funct Mater* [Internet]. 2020 Mar 3 [cited 2021 Mar 4];30(12):1908961. Available from: <https://onlinelibrary.wiley.com/doi/abs/10.1002/adfm.201908961>
24. Reyes-Ruiz A, Calvillo-Rodriguez KM, Martínez-Torres AC, Rodríguez-Padilla C. The bovine dialysable leukocyte extract IMMUNEPOTENT CRP induces immunogenic cell death in breast cancer cells leading to long-term antitumour memory. *Br J Cancer* [Internet]. 2021 Feb 3 [cited 2021 Mar 9];1–13. Available from: <https://www.nature.com/articles/s41416-020-01256-y>

25. De Azambuja E, Ameye L, Diaz M, Vandebossche S, Aftimos P, Hernández SB, et al. Cardiac assessment of early breast cancer patients 18 years after treatment with cyclophosphamide-, methotrexate-, fluorouracil- or epirubicin-based chemotherapy. *Eur J Cancer*. 2015 Nov 1;51(17):2517–24.
26. Tesniere A, Schlemmer F, Boige V, Kepp O, Martins I, Ghiringhelli F, et al. Immunogenic death of colon cancer cells treated with oxaliplatin. *Oncogene*. 2010;
27. Obeid M, Tesniere A, Ghiringhelli F, Fimia GM, Apetoh L, Perfettini J-L, et al. Calreticulin exposure dictates the immunogenicity of cancer cell death. *Nat Med* [Internet]. 2007 Jan 24 [cited 2018 Dec 21];13(1):54–61. Available from: <http://www.nature.com/articles/nm1523>
28. Gorin JB, Ménager J, Gouard S, Maurel C, Guilloux Y, Faivre-Chauvet A, et al. Antitumor immunity induced after α irradiation. *Neoplasia (United States)*. 2014;
29. Garrido G, Rabasa A, Sánchez B, López MV, Blanco R, López A, et al. Induction of Immunogenic Apoptosis by Blockade of Epidermal Growth Factor Receptor Activation with a Specific Antibody. *J Immunol*. 2011;
30. Humeau J, Lévesque S, Kroemer G, Pol JG. Gold standard assessment of immunogenic cell death in oncological mouse models. In: *Methods in Molecular Biology* [Internet]. Humana Press Inc.; 2019 [cited 2020 Jul 21]. p. 297–315. Available from: https://link.springer.com/protocol/10.1007/978-1-4939-8885-3_21
31. Chiang CL-L, Coukos G, Kandalaft LE. Whole Tumor Antigen Vaccines: Where Are We? *Vaccines* [Internet]. 2015 Apr 23 [cited 2018 Dec 21];3(2):344–72. Available from: <http://www.ncbi.nlm.nih.gov/pubmed/26343191>
32. Wu A, Oh S, Gharagozlou S, VEDI RN, Ericson K, Low WC, et al. In vivo vaccination with tumor cell lysate plus CpG oligodeoxynucleotides eradicates murine glioblastoma. *J Immunother*. 2007;
33. Irvin BJ, Williams BL, Nilson AE, Maynor HO, Abraham RT. Pleiotropic Contributions of Phospholipase C-gamma 1 (PLC-gamma 1) to T-Cell Antigen Receptor-Mediated Signaling: Reconstitution Studies of a PLC-gamma 1-Deficient Jurkat T-Cell Line. *Mol Cell Biol*. 2002;

34. McAndrew D, Grice DM, Peters AA, Davis FM, Stewart T, Rice M, et al. ORAI1-Mediated Calcium Influx in Lactation and in Breast Cancer. *Mol Cancer Ther.* 2011;
35. Abalsamo L, Spadaro F, Bozzuto G, Paris L, Cecchetti S, Lugini L, et al. Inhibition of phosphatidylcholine-specific phospholipase C results in loss of mesenchymal traits in metastatic breast cancer cells. *Breast Cancer Res.* 2012;
36. Henry F, Bretaudeau L, Hequet A, Barbieux I, Lieubeau B, Meflah K, et al. Role of antigen-presenting cells in long-term antitumor response based on tumor-derived apoptotic body vaccination. In: *Pathobiology.* 1999.
37. Farkona S, Diamandis EP, Blasutig IM. Cancer immunotherapy: The beginning of the end of cancer? *BMC Medicine.* 2016.
38. Zhou J, Wang G, Chen Y, Wang H, Hua Y, Cai Z. Immunogenic cell death in cancer therapy: Present and emerging inducers [Internet]. Vol. 23, *Journal of Cellular and Molecular Medicine.* Blackwell Publishing Inc.; 2019 [cited 2020 Jul 21]. p. 4854–65. Available from: </pmc/articles/PMC6653385/?report=abstract>
39. Calmeiro J, Carrascal MA, Tavares AR, Ferreira DA, Gomes C, Falcão A, et al. Dendritic cell vaccines for cancer immunotherapy: The role of human conventional type 1 dendritic cells [Internet]. Vol. 12, *Pharmaceutics.* MDPI AG; 2020 [cited 2020 Jul 22]. Available from: </pmc/articles/PMC7076373/?report=abstract>
40. Papaioannou NE, Beniata O V., Vitsos P, Tsitsilonis O, Samara P. Harnessing the immune system to improve cancer therapy [Internet]. Vol. 4, *Annals of Translational Medicine.* AME Publishing Company; 2016 [cited 2020 Jul 22]. Available from: </pmc/articles/PMC4971375/?report=abstract>
41. Lee Ventola C. Cancer immunotherapy, part 1: Current strategies and agents. *P T* [Internet]. 2017 Jun 1 [cited 2020 Jul 22];42(6):375–83. Available from: </pmc/articles/PMC5440098/?report=abstract>

FIGURE LEGENDS

Figure 1. PKHB1 induces cell death in breast cancer cell lines. Cell death analysis in (A) MCF-7, (B) MDA-MB-231 and (C) 4T1 cells, without treatment (Control), treated with the control peptide 4NGG or PKHB1 for 2h. (D) Representative graphs and quantification of the loss of $\Delta\Psi_m$ measured through TMRE, (E) ROS levels measured through Hydroethidine staining and intracellular Ca^{2+} by Fluo-4 staining, by flow cytometry in cells left alone or treated with PKHB1 for 2h. (F) Cell death induced by PKHB1 was assessed as in A, B and C in cells left without pre-treatment (-) or pre-treated (30 minutes) with BAPTA, Z-VAD-FMK (Z-VAD), N-Acetyl Cystein (NAC), Necrostatin-1 (Nec-1) or Spautin-1 (SP-1). Cell death induced by PKHB1 was assessed as in G, H and I in cells left without pre-treatment (-) or pre-treated (30 minutes) with dantrolene, 2-APB or U73122. Graph represents the means (\pm SD) of triplicates of three independent experiments. NS= Not significant.

Figure 2. PKHB1 treatment induces tumor reduction and T cells distribution. Mice were inoculated s.c. with 5×10^5 4T1 viable cells and when tumor reached 100mm^3 were treated with sterile water (Control, n=6) or PKHB1 (400 μ g of PKHB1 daily, n=6), tumor volume was measured three times per week. (A) Graphs indicate tumor growth in PBS-treated (Control) or PKHB1-treated mice (PKHB1). (B) Graphs indicate the tumor volume of control and treated mice at day 16. Histology from tumors of control or PKHB1-treated mice stained with H&E. Tumor cells (black arrows), mitotic cells (blue arrows), cellular debris (green arrows) and immune system cells infiltration (red arrows). (E, F and G) Graphs show the percent of CD3+, CD4+ and CD8+ cells in blood, spleen, lymph node and tumor of control or PKHB1-treated mice at day 16. (H) Graphs show the percent of calcein negative 4T1 cells after the co-culture with splenocytes of control (n=4), or PKHB1 treated mice (n=4). NS= Not significant.

Figure 3. PKHB1 induces exposure and release of DAMPs in breast cancer cells.

Representative FACS histograms of CRT exposure (filled histograms) and IgG isotype antibodies (open histograms) of 7-AAD negative (A) MCF-7, (B) MDA-MB-231 and (C) 4T1 cells, untreated (Control) or treated with PKHB1 for 2 h. Calreticulin exposure observed by confocal microscopy in (D) MCF-7, (E) MDA-MB-231 and (F) 4T1 cells untreated (Control) or treated with PKHB1 using CRT-PE staining and Hoechst 33342. Representative graphs of the ratio of HSP70 (G) or HSP90 (H) exposure of 7-AAD negative cells, untreated (Control) or treated with PKHB1 for 2h. Representative graphs of the (I) HMGB1 or (J) ATP release in the supernatants of control or PKHB1 treated cells. Graphs shown are means (\pm SD) of triplicates of three independent experiments. CRT-PE= Calreticulin-PhycoErythrin.

Figure 4. PKHB1-Tumor cell lysate induces antitumor immune response *ex vivo*. (A)

Representative histograms from flow cytometry analyses of CD80, CD86 or CD11c expression on DCs left with medium (CTR) or pulsed 24h with a PKHB1-TCL, graphs of the means obtained by FACS (right side). (B) DCs were treated as in A and the supernatants were collected to quantify TNF α release, by FACS. Supernatants of T lymphocytes+4T1 cells (unprimed or primed) co-culture were collected and assayed for IFN- γ (C), (D) IL-4 and IL-2 release. (E) Representative histograms from flow cytometry analyses of 4T1 cells stained with calcein-AM and co-cultured with T lymphocytes (unprimed or primed). Graphs shown are means (\pm SD) of triplicates of three independent experiments. NS= Not significant.

Figure 5. PKHB1-TCL induce tumor elimination in a prophylactic and therapeutic application.

(A) Schema of PKHB1-TCL or EPI-TCL prophylactic application. (B) Graph indicates the mean of the tumor growth in mice treated with serum-free medium (Control; n=10) or mice receiving a prophylactic vaccination with PKHB1-TCL (Prophylactic-PKHB1-TCL, n=10) or EPI-TCL

(Prophylactic-EPI-TCL, n=10). (C) Kaplan Meier survival graph of mice treated as in B over time. (D) Schema of PKHB1-TCL or EPI-TCL therapeutic application. (E) Graph indicates the mean of the tumor growth in mice treated with serum-free medium (Control; n=9), PKHB1-TCL (Therapeutic-PKHB1-TCL, n=9) or EPI-TCL (Therapeutic-EPI-TCL, n=9), arrows indicate days of TCL or serum free medium inoculation. (F) Kaplan Meier survival graph of mice treated as in E over time.

Figure 6. PKHB1-TCL prophylactic and therapeutic application induces long-term antitumor effect, schematic representation of the PKHB1-effect. Mice in remission (30 days) after PKHB1 prophylactic or therapeutic PKHB1-TCL application were re-challenged with 5×10^5 4T1 viable cells. (A) Graph indicates tumor growth in PBS-treated mice (Control; n=9), prophylactic re-challenged mice (Prophylactic remission-4T1 rechallenge, n=9) or therapeutic re-challenged mice (Therapeutic remission-4T1 rechallenge, n=9). Each line represents the mean of the tumor volume per group. (B) Kaplan Meier survival graph of mice treated as in A over time. (C) Graphs show the percent of calcein negative 4T1 cells after co-culture with splenocytes control (n=4), prophylactic (n=4) or therapeutic (n=4) rechallenged mice. (D) PKHB1 induces ROS production, intracellular Ca^{2+} accumulation, loss of mitochondrial membrane potential ($\Delta\Psi_m$), leading to DAMPs exposure and release in breast cancer cells. Neoantigens and DAMPs exposure/release induced by PKHB1 promotes DCs maturation, which triggers T-cell activation to induce cancer cytotoxicity. (E) On the other hand, PKHB1-treatment *in vivo* induces T-cells redistribution in lymph nodes, peripheral blood and intratumorally, leading to tumor reduction. (F) PKHB1-TCL prophylactic vaccination prevented tumor establishment. (G) PKHB1-TCL therapeutic application induced tumor remission. (H) PKHB1-treatment, PKHB1-TCL prophylactic or therapeutic application induced tumor-specific splenocytes' cytotoxicity.

FIGURE 1

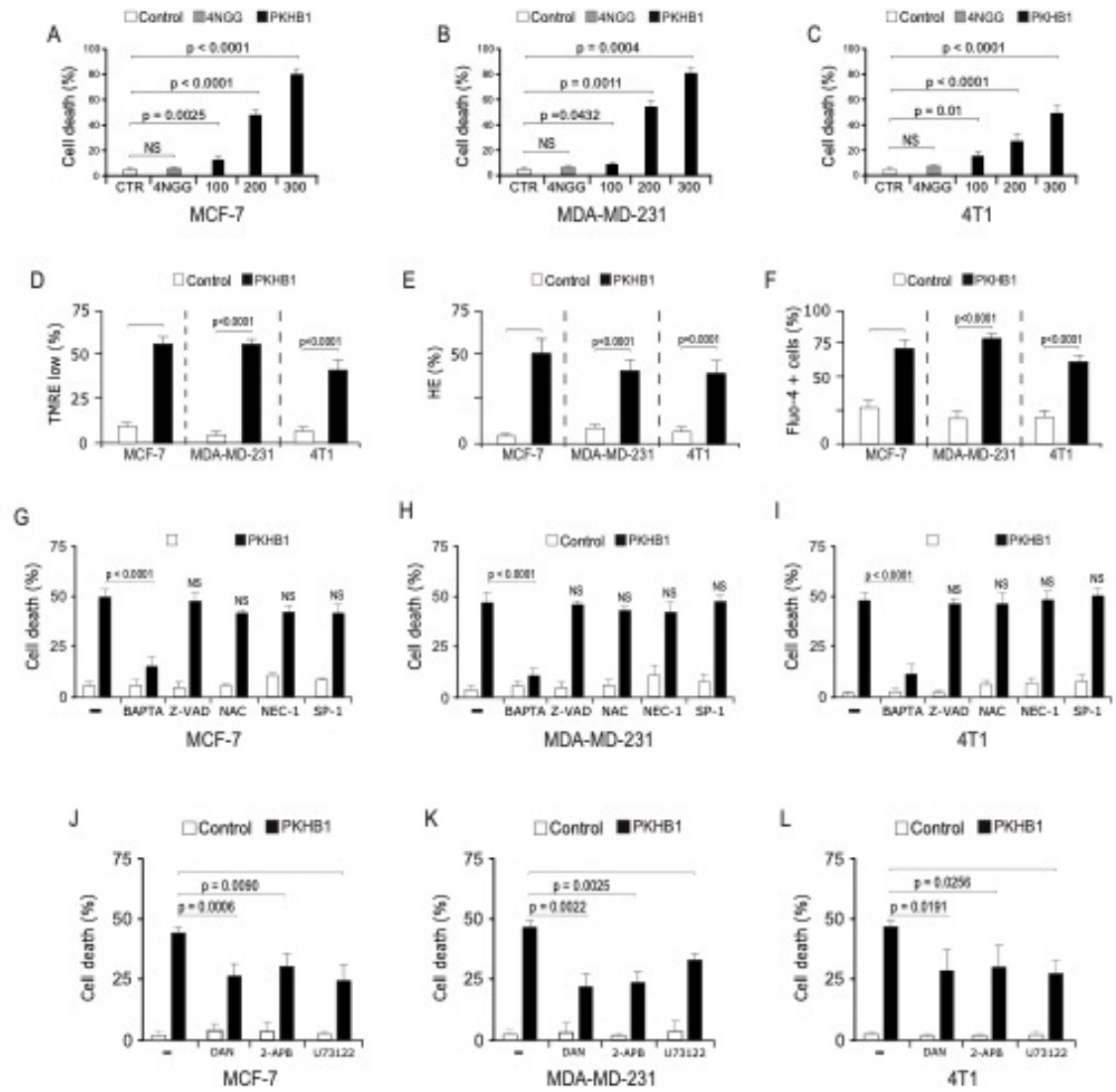


FIGURE 2

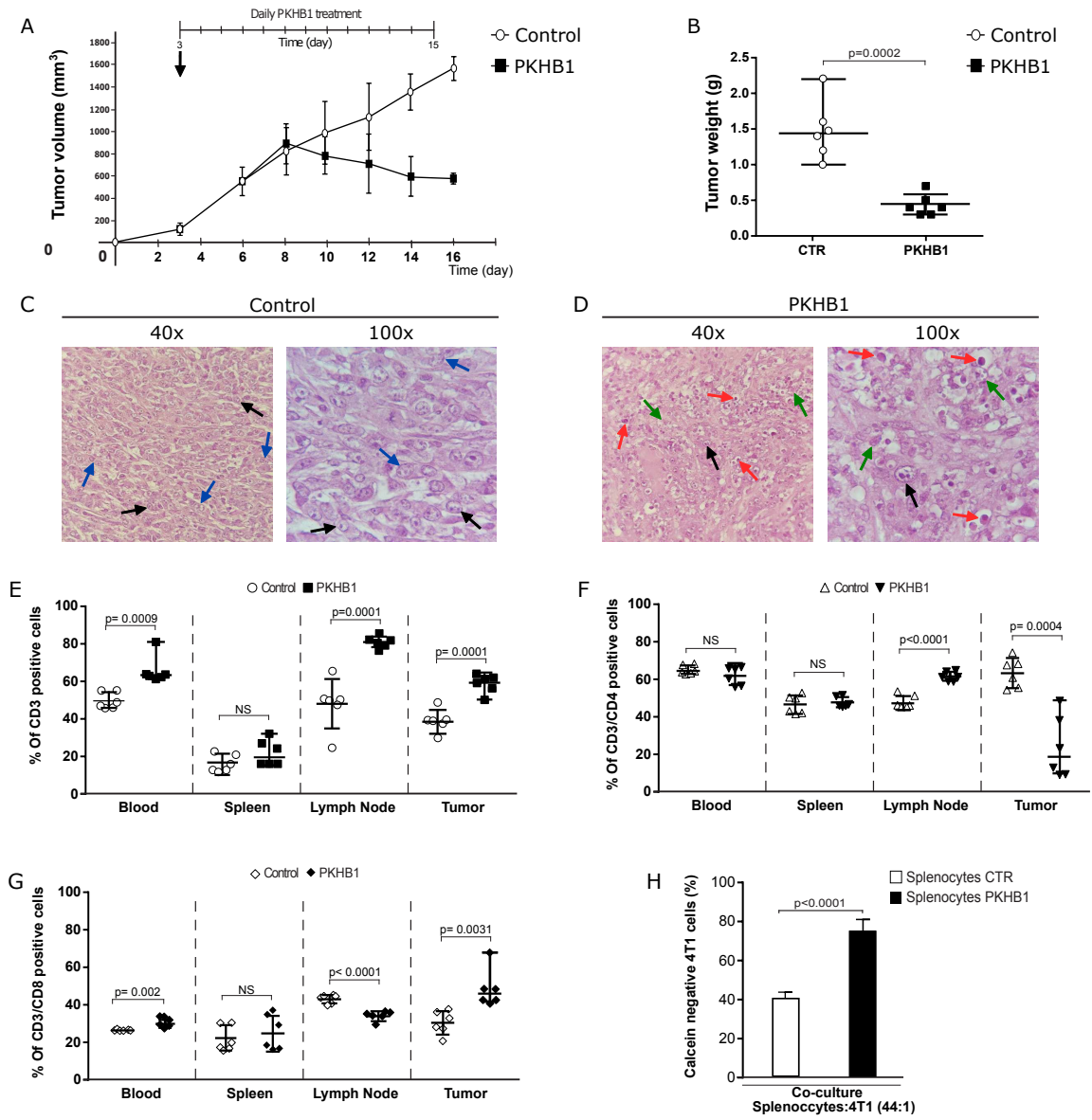


FIGURE 3

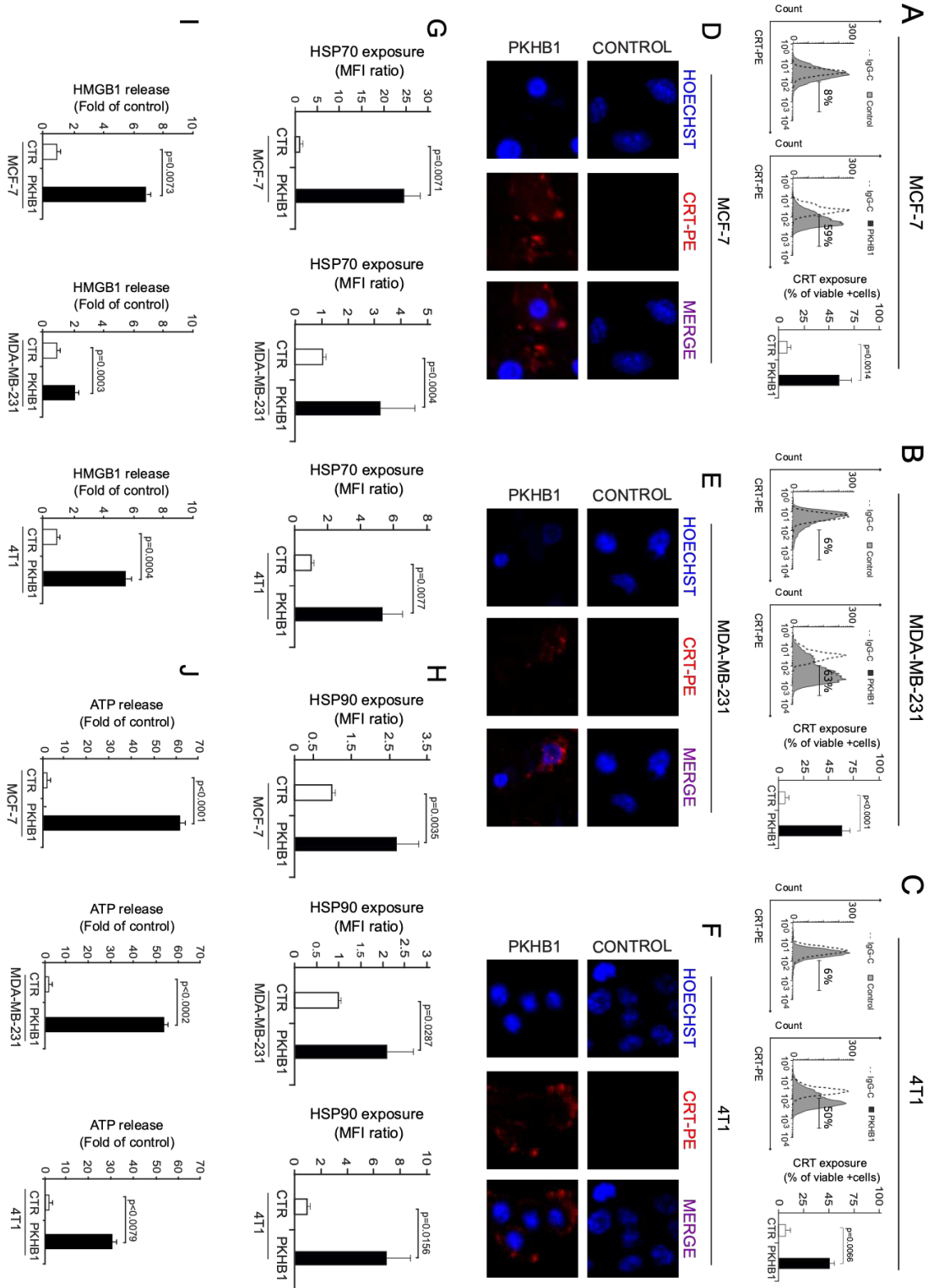


FIGURE 4

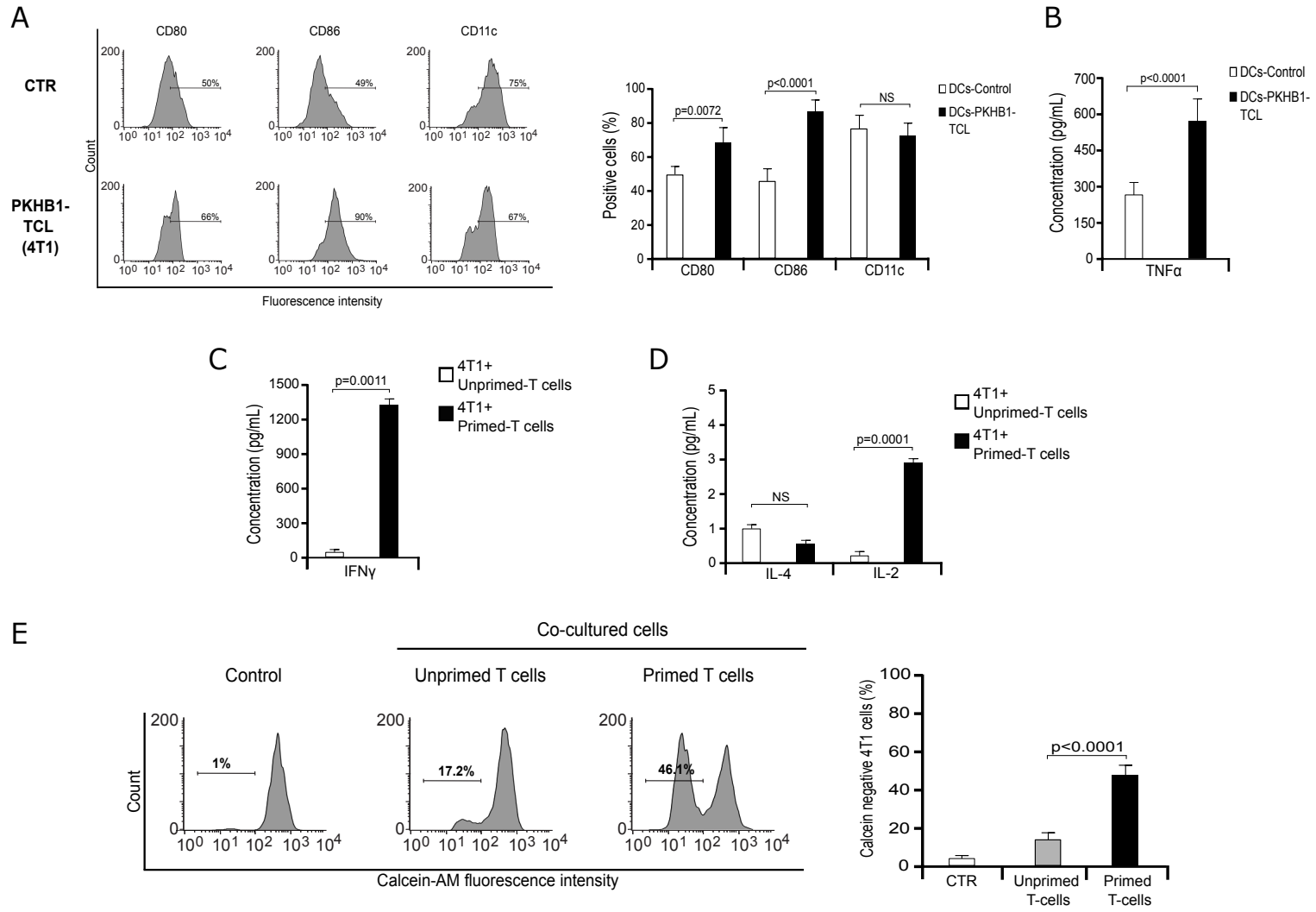


FIGURE 5

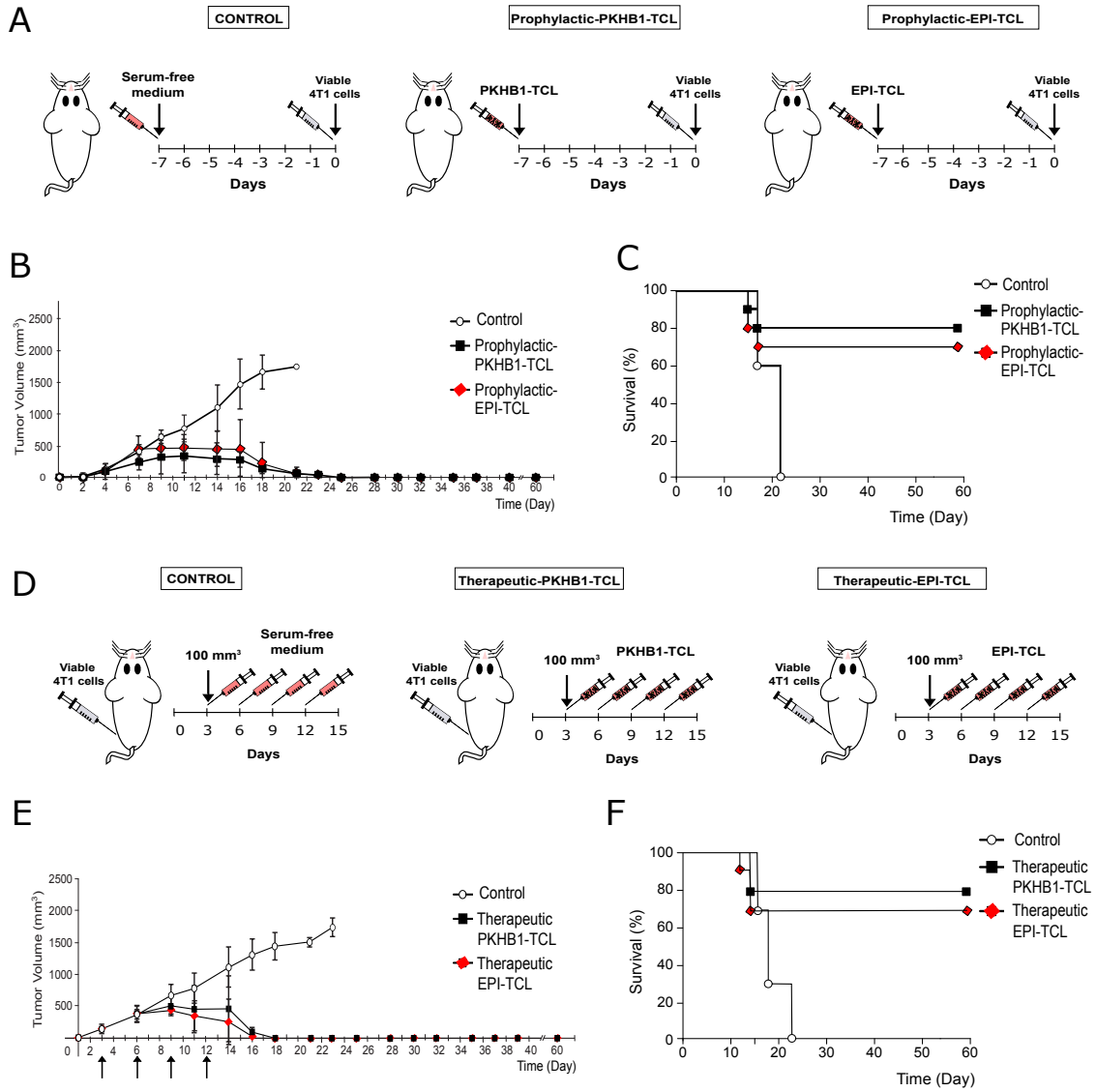
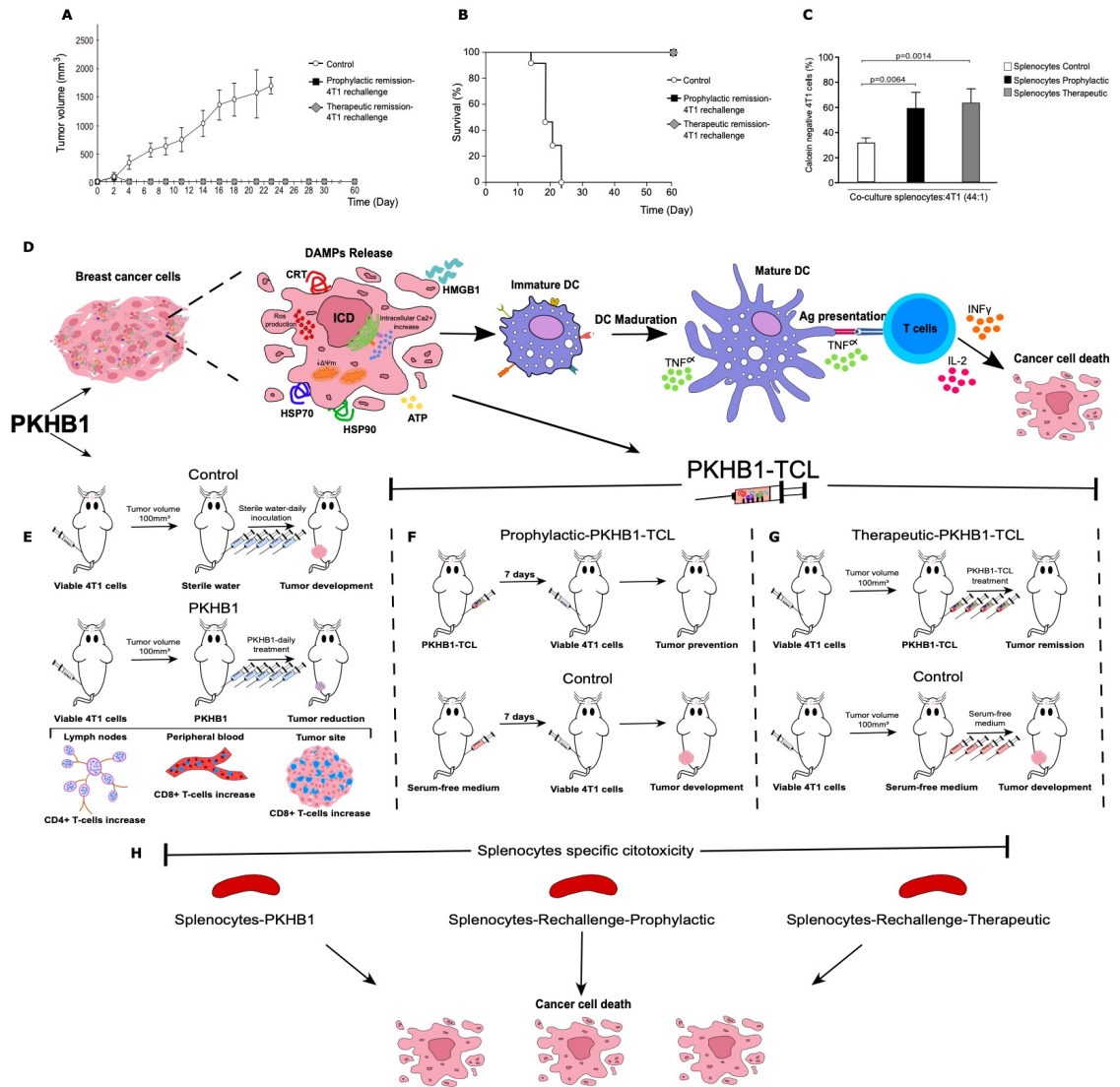


FIGURE 6



Supplementary material

Supplemental material and methods.

PKHB1 and 4NGG Syntheses and Characterizations

Both peptides were synthesized manually by solid-phase peptide synthesis on a Chlorotrytil resin (Merck Chemicals, Darmstadt, Germany) as described by Denèfle et al., 2016.

All commercial chemicals and solvents were reagent grade. All reactions performed in organic solvents were carried out with the use of standard techniques for the exclusion of moisture. All reactions were performed under argon or nitrogen in oven-dried glassware using anhydrous solvents and standard syringe techniques. All Fmoc carbamate protected amino acid derivatives; HBTU, HOBt and 2-CTC resin (100–200 mesh, loading 1.6 mmol/g) were purchased from Iris Biotech (Marktredwitz, Germany). Reagents such as DIEA, piperidine, DMF, IPA, Ac₂O, MeOH, TFA, and TIS were obtained from Sigma-Aldrich (St. Louis, MO, USA). The peptides PKHB1 and 4NGG were of >95% purity (determined by analytical reverse phase LC–MS).

Manual Loading of the First Amino Acid. Solid-phase peptide synthesis was performed in polypropylene Torviq syringes (20 mL). The 2-CTC resin was previously swelled in strictly anhydrous DCM (distilled) for 2 h. Side chain protected Fmoc-Aa-OH (0.30 mmol, 1 equiv) was coupled to 2-CTC resin (400 mg, loading 1.6 mmol/g) in the presence of DIEA (1.2 mmol, 4 equiv) in DCM (4 mL). The unreacted sites on the resin were capped by washing with a mixture of DCM/MeOH/DIEA (17:2:1) repeated 3 times. Thus, loading was reduced to 0.80 mmol/g for optimal peptide growth.

Manual Solid Phase Peptide Synthesis. Fmoc group was split off by treatment with piperidine/DMF (1:4) (1 × 1 min, 1 × 10 min). Activation step and coupling (4h for each step) were carried out with Fmoc-Aa-OH (1.2 mmol, 4 equiv), HBTU (1.2 mmol, 4 equiv) as coupling agent, HOBt (1.2 mmol, 4 equiv) as auxiliary nucleophile, and DIEA (2.4 mmol, 8 equiv) as base. When elongation of the peptide chain was completed, a washing step with MeOH was added after final N-terminal Fmoc removal in order to totally shrink the resin under vacuum.

Final Side Chain Deprotection and Cleavage from the Resin. The crude peptide was treated with the following cleavage cocktail: TFA/H₂O/TIS (95/2.5/2.5, 10 mL). The peptide was precipitated using cooled Et₂O (3 × 30 mL), and recovered after centrifugation (3 × 5 min, 7800 rpm). Diethyl ether was removed, and the peptide pellets were dried (under nitrogen flow). The resulting crude peptide was dissolved in aqueous 0.1% (v/v) TFA. Purification was conducted on reverse-phase HPLC Prep C18 column, eluting with 0.1% TFA in water (solvent A) and 0.1% TFA in acetonitrile (solvent B).

Purification. Preparative scale purification of peptides was performed by reverse phase HPLC on a Waters system consisting of a quaternary gradient module (Water 2535) and a dual wavelength UV/visible absorbance detector (Waters 2489), piloted by Empower Pro 3 software using the following columns: preparative Macherey- Nagel column (Nucleodur HTec, C18, 250 mm × 16 mm i.d., 5 μm, 110 Å) and preparative Higgins analytical column (Proto 200, C18, 150 mm × 20 mm i.d., 5 μm, 200 Å) at a flow rate of 14 mL/min and 20 mL/min, respectively. Small-scale crudes (<30 mg) were purified using semipreparative Ace column (Ace 5, C18, 250 mm × 10 mm i.d., 5 μm, 300 Å) at a flow rate of 5 mL/min. Purification gradients were chosen to get a ramp of approximately 1% solution B per minute in the interest area, and UV detection was done at 220 and 280 nm. Peptide fractions from purification were analyzed by LC–MS. All LC–MS or HPLC analyses were performed on C18 columns. The pure fractions were gathered according to their purity and then freeze-dried using an Alpha 2/4 freeze-dryer from Bioblock Scientific to get the expected peptide as a white powder. Final peptide purity (>95%) of the corresponding pooled fractions was checked by LC–MS.

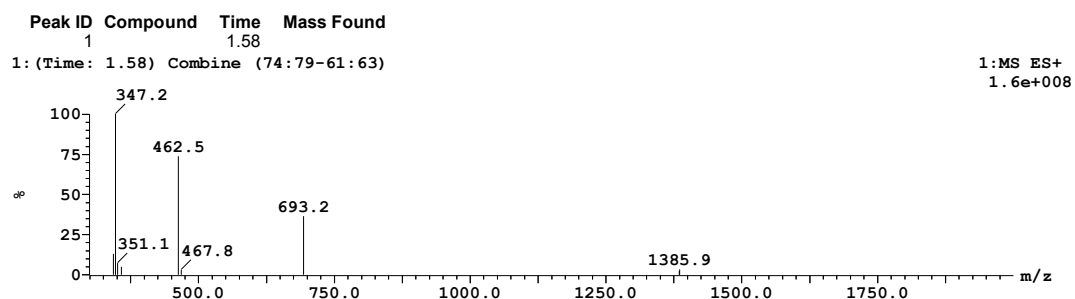
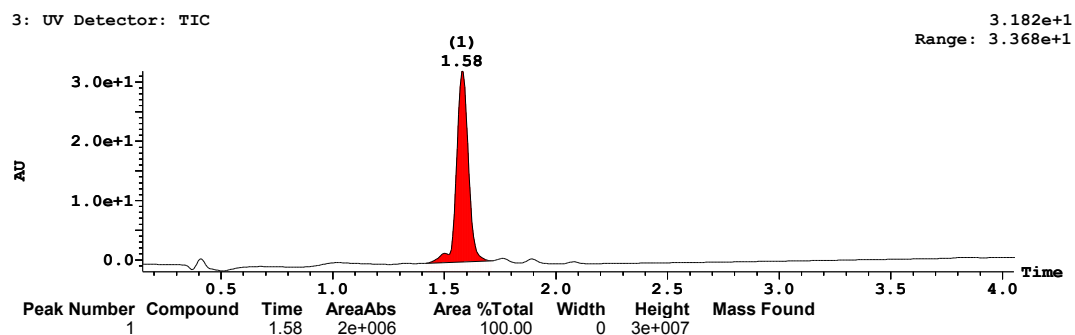
LC–MS analysis. Analytical HPLC was conducted on a X-Select CSH C18 XP column (30 mm × 4.6 mm i.d., 2.5 μm), eluting with 0.1% formic acid in water (solvent A) and 0.1% formic acid in acetonitrile (solvent B), using the following elution gradient: 0–3.2 min, 0–50% B; 3.2–4 min, 100% B. Flow rate was 1.8 mL/min at 40 °C. The mass spectra (MS) were recorded on a Waters ZQ mass spectrometer using electrospray positive ionization [ES⁺ to give (MH)⁺ molecular ions] or electrospray negative ionization [ES⁻ to give (MH)⁻ molecular ions] modes. The cone voltage was 20 V.

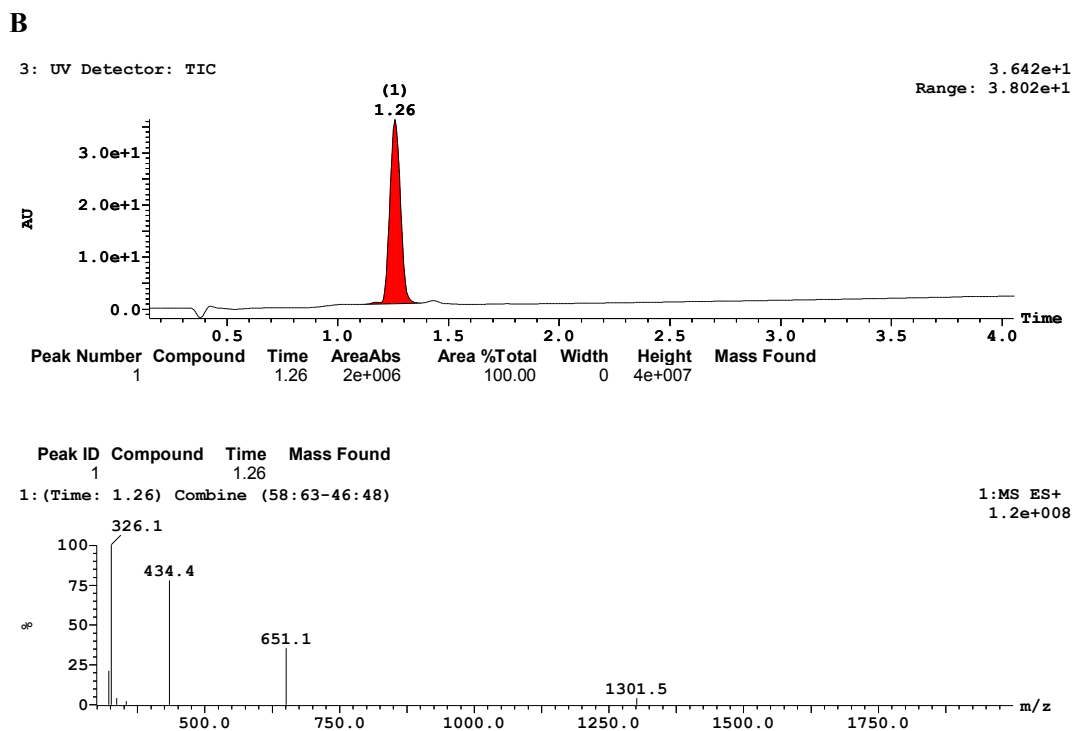
1) Peptides characterization

TABLE 1. SUMMARIZED ANALYTICAL DATA OF PKHB1 AND 4NGG.

PEPTIDE	MW (g/mol) ^a	<i>m/z</i> (ESI) ^b	<i>t_R</i> (min) ^c
PKHB1	1384.8	1385,9 [M+H] ⁺	1.58
		693.2 [M+2H] ²⁺	
		462.5 [M+3H] ³⁺	
		347.2 [M+4H] ⁴⁺	
4NGG	1300.6	1301,6[M+H] ⁺	1.26
		651.1 [M+2H] ²⁺	
		434.4 [M+3H] ³⁺	
		326.1 [M+4H] ⁴⁺	

a. Real molecular weight. **b.** Mass-to-charge ratio (*m/z*) observed by electrospray ionization (ESI) corresponding to total mass (M+H) and derived fractions. **c.** Retention times (*t_R*) observed using the method described above.





Supplementary Figure 1. LC-MS analysis of PKHB1 and 4NGG. Chromatograms (upper) of purified PKHB1 (A) and 4NGG (B) samples in water (5 mg/mL) show a single peak (1), representing 100% of the total area under the curve at $t_R=1.58$ min and $t_R=1.26$ min for PKHB1 and 4NGG respectively, under the conditions described above. Coupled mass spectrum (lower) show intense peaks at a mass-to-charge ratio (m/z) corresponding to the predicted total mass and mass fractions (summarized in Supplementary Table 1).

Supplementary Table 2. TNF α , IFN γ , IL-5, IL-4, and IL-2 cytokine release in co-cultures of T lymphocytes with control or pulsed DCs. Bone marrow-derived murine DCs were left with medium alone (DCs-Control) or pulsed (DCs-PKHB1-TCL) during 24h with a PKHB1-TCL. Then, DCs were co-cultured during 4 days with T-lymphocytes, and the supernatants were collected to quantify TNF α , IFN γ , IL-5, IL-4, and IL-2 release, by FACS. **p<0.01; ***p<0.001.

	TNFα (pg/mL)	IFNγ (pg/mL)	IL-5 (pg/mL)	IL-4 (pg/mL)	IL-2 (pg/mL)
DCs-Control	38.9	0	0	0	0.2
+ T-lymphocytes	± 14	± 0	± 0	± 0	± 0.2
DCs-PKHB1-TCL	335.17***	698.95 **	0	0	1.83*
+ T-lymphocytes	± 33.64	± 322.54	± 0	± 0	± 1.4

CHAPTER 3.

3. Optimization of the pharmacological properties of thrombospondin peptide mimics

3.1. Article 4. Homotrimerization approach in the design of thrombospondin-1 mimetic peptides with improved potency in triggering regulated cell death of cancer cells

3.1. Homotrimerization Approach in the Design of Thrombospondin-1 Mimetic Peptides with Improved Potency in Triggering Regulated Cell Death of Cancer Cells

Article published in the “Journal of Medicinal Chemistry” on August 12th, 2019 (doi: 10.1021/acs.jmedchem.9b00024).

Based on the natural homotrimeric assembly of TSP1, it was hypothesized that a homotrimeric variant of PKHB1 could have an improved potency. To achieve this, a click chemistry strategy was considered, using an azide-derivative of PKHB1 with an aminopentanoic acid spacer to bind a tertiary amine matrix. This peptide construct was synthesized on solid support, cleaved and, using copper-catalyzed azide–alkyne cycloaddition, the azido-derivative was attached to three-propargyl amine. Unfortunately, the resulting [PKHB1]₃ was not soluble in water, so, we went back to PKHB1 sequence to try to generate a more soluble monomer that we could potentially use to improve the solubility of the trimer as well.

As PKHB1 intends to mimic a beta strand, we thought that insolubility could be a result of beta strand stabilization and sheet nucleation, then, disrupting beta sheet stabilization could improve solubility. In peptides, it has been described that backbone amine methylations can improve solubility in this way. Thus, to improve PKHB1 solubility, variants containing N-methylated residues were generated and assessed in terms of affinity and cytotoxicity. Affinity was measured by bio-layer interferometry (BLI) assays, using cell membranes obtained from MEC-1 cells, a CLL cell line. The cytotoxic activity of the N-methylated peptides was measured in MEC-1 cells by flow cytometry, using Ann-V/PI staining. From the N-methylation scan we observed that the only residue in which N-methylation did not significantly affect the activity of the peptide was arginine (NMeR-PKHB1), and this was also accompanied by a slight but significant improvement in its affinity. Double N-methylation did not improve PKHB1 nor NMeR-PKHB1. And based on the previous work in the lab that led to the discovery of PKHB1, it was hypothesized that methionine or terminal end replacement could potentially improve the properties of NmeR-PKHB1. Thus, methionine was substituted by different

branched amino acids, including norleucine, an amino acid that is structurally very similar to methionine, but without the sulfur atom that is susceptible to oxidation. Norleucine replacement in this NmeR-PKHB1 gave rise to a peptide that was termed PKT16, with an improved affinity to its target compared to PKHB1, and as active as this last, but with improved solubility properties.

Using this non-aggregating peptide, PKT16, homotrimerization was achieved as planned for PKHB1, and the resulting [PKT16]₃ was soluble. Using biolayer interferometry, slower dissociation rates were observed for [PKT16]₃ compared to their monomeric predecessors, PKT16 and PKHB1, resulting a K_D in the nanomolar range. In terms of cell death induction, [PKT16]₃ at concentrations ten times lower than those of the monomeric predecessors kill the same amount of CLL cells. Thus, this peptide is more potent to bind to and kill CLL cells.

However, after substantial structural modifications, the mechanism of action of these new peptides had to be evaluated. To assess whether this was similar to PKHB1, cell death induction was measured, as in the previous chapters, in presence of pharmacological inhibitors of caspases (Q-VD-OPH), calcium (BAPTA), PLC γ 1 (U73122), or calcium channels in the endoplasmic reticulum (dantrolene and 2-APB), using PKHB1 as positive control. As expected, Q-VD-OPH did not prevent PKHB1-induced cell death, but BAPTA, U73122, dantrolene and 2-APB used alone or in combination, significantly inhibited cell death. Simultaneous experiments with PKT16 and [PKT16]₃, showed a very similar pattern, suggesting that [PKT16]₃, PKT16 and PKHB1 trigger a similar type of regulated cell death in CLL.

Finally, to evaluate whether this more potent peptide was also efficient in other types of cancer, its effects were evaluated in a lung cancer cell line, A549. And similar to MEC-1, cell death induced by [PKT16]₃, evaluated by Ann-V/PI staining, was ten times more potent than PKHB1 or the monomeric PKT16. A characteristic morphological feature of [PKT16]₃ was that it enhanced the attachment of dead cells to the plate, making harvesting difficult and potentially compromising the results observed by flow cytometry. To overcome this technical limitation, real-time cell analysis of cultures' electric impedance, which correlates to culture viability, was quantified. Impedance increased within the first hour of treatment but decreased with time, confirming the results obtained by flow

cytometry. Furthermore, the cell death induced by the trimer, PKT16 or PKHB1, was not inhibited by Q-VD-OPH, but BAPTA did prevent cell death. In the case of PKHB1 and PKT16, pharmacological inhibitors of PLC-regulated calcium signaling prevented cell death as in CLL. However, in the case of [PKT16]₃ only the simultaneous inhibition of the pathway reduced cell death significantly, suggesting that this pathway is only partially involved in the cell death induced by the trimer in these cells. We can conclude that [PKT16]₃, PKT16 and PKHB1 induce calcium-regulated cell death in lung cancer cells, as well as PKHB1 does in other types of cancer.

Résumé de l'article 4

Afin d'optimiser l'efficacité du premier peptide agoniste de CD47 stable dans le sérum (PKHB1) pour déclencher la mort sélectives des cellules cancéreuses, nous avons mis en place un programme de maturation visant à optimiser l'affinité du peptide pour son récepteur en mimant la structure trimérique de la thrombospondine-1. Tout d'abord, afin d'améliorer la solubilité, nous avons évalué les effets de la méthylation des amides (N-méthylation) sur le squelette peptidique de PKHB1. Des analyses structurales et pharmacologiques ont été réalisées pour évaluer l'impact desdites modifications chimiques sur la structure et l'activité biologique du peptide. Cette étude de relation structure-activité a conduit à la découverte d'un peptide N-méthylé très soluble que nous avons nommé PKT16. Ce monomère a été utilisé pour concevoir un peptide homotrimérique, [PKT16]₃, qui s'est avéré être dix fois plus puissant que son homologue monomérique. L'évaluation pharmacologique de la mort induite par [PKT16]₃ montre que ce peptide induit un type de mort cellulaire régulée par l'augmentation du calcium intracellulaire dans les cellules de leucémie lymphoïde chronique, similaire à celle précédemment rapportée avec PKHB1, mais aussi sur des lignées de cellules de cancer du poumon.

I. Resumen del artículo 4

Con el fin de optimizar la potencia del primer péptido agonista de CD47 estable en suero (PKHB1) para desencadenar la muerte celular regulada de células cancerosas, diseñamos un proceso de maduración de la afinidad del péptido por su ligando imitando la estructura trimérica de la trombospondina-1. Primero, con el fin de mejorar su solubilidad, evaluamos los efectos de la metilación de las amidas (N-metilaciones) en el esqueleto del péptido PKHB1. Se realizaron análisis estructurales y farmacológicos para evaluar el impacto conformacional de las modificaciones químicas mencionadas y la actividad biológica del péptido. Dicho estudio de relación estructura-actividad condujo al descubrimiento de un péptido N- metilado, altamente soluble que nombramos PKT16. Este monómero se utilizó para el diseño de un péptido homotrimérico, [PKT16]₃, que resultó ser diez veces más potente que su homólogo monomérico. La evaluación farmacológica de la muerte inducida por el [PKT16]₃ en líneas celulares adherentes (A549) y no adherentes (MEC-1) demuestra que este péptido induce un tipo de muerte celular regulada por el aumento de calcio intracelular, similar a lo reportado anteriormente con PKHB1 en MEC-1.

Manuscript

Homotrimerization Approach in the Design of Thrombospondin-1 Mimetic Peptides with Improved Potency in Triggering Regulated Cell Death of Cancer Cells

Thomas Denèfle,^{†,‡,◆} Elodie Pramit,^{†,‡,◆} Luis Gómez-Morales,^{†,‡,||,◆} Mikail D. Levasseur,^{†,‡,Ⓞ} Eva Lardé,^{†,‡} Clara Newton,^{†,‡} Kenny Herry,[⊥] Linda Herbi,[#] Yann Lamotte,[⊥] Estelle Odile,^{†,‡} Nicolas Ancellin,[⊥] Pascal Grondin,[⊥] Ana-Carolina Martinez-Torres,^{||} Fabrice Viviani,[⊥] Hélène Merle-Beral,[#] Olivier Lequin,^{†,Ⓞ} Santos A. Susin,[#] and Philippe Karoyan^{*,†,‡,§,∇,Ⓞ}

[†]Sorbonne Université, Ecole Normale Supérieure, PSL University, CNRS, Laboratoire des Biomolécules, LBM, 75005 Paris, France

[‡]Sorbonne Université, Ecole Normale Supérieure, PSL University, CNRS, Laboratoire des Biomolécules, LBM, Site OncoDesign, 25-27 Avenue du Québec, 91140 Les Ulis, France

[§]SiRIC CURAMUS (CANCER UNITED RESEARCH ASSOCIATING MEDICINE, UNIVERSITY & SOCIETY, Site de Recherche Intégrée sur le Cancer) IUC, AP-HP.6, Sorbonne Université 75005 Paris, France

^{||}Laboratory of Immunology and Virology, Autonomous University of Nuevo Leon, 66451 San Nicolas de los Garza, NL, Mexico

[⊥]OncoDesign, 25 Avenue du Québec, 91140 Les Ulis, France

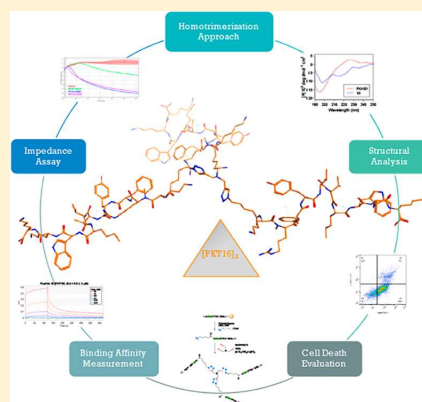
[#]Cell Death and Drug Resistance in Lymphoproliferative Disorders Team, Centre de Recherche des Cordeliers, INSERM UMRS 1138, 75006 Paris, France

[∇]Kayvisa AG, Industriestrasse, 44, 6300 Zug, Switzerland

[Ⓞ]Kaybiotix GmbH, Zugerstrasse 32, 6340 Baar, Switzerland

Supporting Information

ABSTRACT: In order to optimize the potency of the first serum-stable peptide agonist of CD47 (PKHB1) in triggering regulated cell death of cancer cells, we designed a maturation process aimed to mimic the trimeric structure of the thrombospondin-1/CD47 binding epitope. For that purpose, an N-methylation scan of the PKHB1 sequence was realized to prevent peptide aggregation. Structural and pharmacological analyses were conducted in order to assess the conformational impact of these chemical modifications on the backbone structure and the biological activity. This structure–activity relationship study led to the discovery of a highly soluble N-methylated peptide that we termed PKT16. Afterward, this monomer was used for the design of a homotrimeric peptide mimic that we termed [PKT16]₃, which proved to be 10-fold more potent than its monomeric counterpart. A pharmacological evaluation of [PKT16]₃ in inducing cell death of adherent (A549) and nonadherent (MEC-1) cancer cell lines was also performed.



INTRODUCTION

A potential goal in the therapy of cancer disease is the selective triggering of cancer cell death. With this aim, the CD47 receptor is attracting considerable attention. This membrane glycoprotein is involved in many biological functions that are sometimes antagonistic, depending on the spatiotemporal expression of the receptor and its identified ligands (at least thrombospondin-1 (TSP-1) and SIRP α) together with lateral interactions of CD47 with other membrane receptors.¹ On one hand, its binding to SIRP α on phagocytes serves as an inhibitor of phagocytosis.² As a result, cancer therapies using agents that disrupt the CD47:SIRP α interaction have been developed, and

some of them are currently under clinical investigation.³ On the other hand, some studies have focused on targeting the TSP-1:CD47 interaction, identified as a key signaling integrator of tumor progression.⁴ With this aim, TAX2, a peptide mimic of CD47 that targets TSP-1, was proven to display promising antiangiogenic, antitumor, and antimetastatic properties *in vivo* in preclinical mouse models of childhood neuroblastoma.⁵

Received: January 5, 2019

Published: August 12, 2019

We focused our attention on the reported ability of the TSP-1:CD47 ligation to induce regulated cell death (RCD)⁶ and recently described PKHB1,^{7,8} the first serum-stable agonist peptide mimicking the CD47 binding epitope (i.e., RFYVVMWK) of TSP-1. This peptide was proven to be efficient in triggering selective RCD of many adherent and nonadherent cancer cell lines while sparing normal cells. The molecular mechanism triggered by PKHB1 in chronic lymphocytic leukemia (CLL) cells (i.e., caspase-independent cell death mediated by sustained activation of PLC γ 1 leading to intracellular Ca²⁺ overload) was highlighted, and stimulation of CD47 appeared to be key to the cytotoxicity induced by this peptide since the disruption of the peptide:CD47 interaction by a fusion protein designed to specifically bind to CD47 led to inhibition of the cytotoxicity.⁷ The direct interaction between our peptide and CD47 in its native environment was studied using an active-site-directed covalent probe approach.^{8a} We also demonstrated its capacity to induce tumor regression in a xenografted immunodeficient NSG mice CLL model⁷ together with its ability to induce complete tumor remission in a BALB/c immunocompetent mice model, activating in the latter case immunogenic cell death.⁹ It was concluded from these experiments that PKHB1 treatment of tumors prolonged the life of the animals without affecting the vital and lymphoid organs. Collectively, these results highlight the potential of using peptide strategies to target the ubiquitous CD47 receptor and may appear as complementary to the use of monoclonal antibodies.⁷ However, even though PKHB1 appears to be a promising tool, we remain aware that optimization of its effectiveness could be an asset in order to reach the standardized requirements in terms of nanomolar potency in peptide-based drug development.¹⁰ Therefore, an affinity maturation process capable of increasing the potency of the peptide for its target would be invaluable. Since the X-ray structure of the TSP-1/CD47 complex has not been solved to date, the lead optimization of medicinal peptides remains a fastidious task involving a long and iterative strategy.¹¹ Nevertheless, the homotrimeric structure of TSP-1,¹² the multifunctional extracellular protein that we endeavor to mimic, prompted us to evaluate a homotrimerization strategy of our lead peptide, namely, PKHB1. The implication of polyvalent interactions for the design and use of multivalent ligands and inhibitors has been nicely reviewed and demonstrated elsewhere.¹³ Typically, a peptide homomultimerization approach may be relevant since multivalent interactions are much stronger than monovalent interactions.¹⁴ To this aim, the click chemistry cycloaddition¹⁵ of an azido derivative of PKHB1 was considered.¹⁶ This strategy was recently validated by Saludes and co-workers in the design of a bradykinin-derived peptide.¹⁷

Herein we first describe the structure–activity relationship (SAR) study that led to the discovery of a new monomeric peptide as potent as PKHB1 but with better solubility properties. Second, we discuss how we engaged this monomer through the homotrimerization process to yield a new, highly potent trimeric peptide. With regard to the efficacy of our peptides to trigger cell death, two techniques were used in parallel and correlated (in combination with microscopic observations), i.e., (1) classical flow cytometry (FCM), which combines the detection of phosphatidylserine (PS) exposure on early apoptotic cells using allophycocyanin-labeled annexin V (AnnV) and propidium iodide (PI) to distinguish dying cells from dead cells,¹⁸ and (2) a real-time cell analyzer (RTCA), a

technique using noninvasive electrical impedance monitoring that has been reported to quantify cancer cell proliferation, viability, invasion, and drug cytotoxicity in a label-free and real-time manner.¹⁹ The latter one was chosen to evaluate the efficacy of our compounds on an adherent cancer cell line (A549) because of its easy implementation, avoiding the cell-harvesting methods required in FCM that are known to affect the membrane integrity of adherent cancer cells and thus the proportion of apoptotic cells during detection.²⁰ Nevertheless, both techniques were used and showed good correlation in cell death detection. Although the design of our new peptide was based on PKHB1, we assumed that the homotrimeric nature of the peptide could trigger RCD that does not involve the same pathway. Thus, to get further information on the type of cell death triggered by our new peptides, experiments were realized in the presence of QVD.Oph (a broad-spectrum caspase inhibitor), BAPTA (an external calcium chelator), U73122 (a PLC γ 1 inhibitor), and 2-aminoethoxydiphenyl borate (2-APB) and dantrolene (intracellular calcium channel inhibitors). We report the results of these experiments that led to the discovery of two new and potent peptides, the monomer, which we termed PKT16, and its homotrimer [PKT16]₃.

RESULTS

We recently described the first serum-stable TSP-1:CD47 binding epitope peptide mimic, i.e., PKHB1, and its ability to trigger a caspase-independent Ca²⁺-mediated form of RCD on CLL cells from patients and MEC-1 cells, a nonadherent CLL cancer cell line, while sparing normal cells.^{7,8} The double AnnV/PI copositive staining and the swelling of the endoplasmic reticulum observed during the cell death induced by this peptide^{7,8} led us to classify it as a “programmed necrotic” cell death pathway.^{8,21} Although effective in inducing rapid and selective RCD of malignant cells, the potency of PKHB1 in terms of affinity and activity remained to be improved. To this end, a homotrimerization strategy was considered using a click chemistry approach, a tertiary amine as a matrix, and an aminopentanoic acid derivative as spacer.

Unfortunately, because of aggregation propensities observed with PKHB1 in some buffers, this peptide was not suitable for the design of the homotrimer. This phenomenon was attributed to the chaotropic effect of the buffer used to solubilize the peptide²² together with its β -strand structure, two parameters favoring the β -sheet nucleation. Thus, in order to limit this phenomenon, we went back to the PKHB1 sequence to first design a monomer devoid of aggregation properties. This goal was realized with the help of an *N*-methyl scan of the peptide backbone and SAR studies combining structural studies by NMR and circular dichroism (CD) spectroscopy, affinity measurement on MEC-1 cell membrane preparation using an Octet RED instrument as previously described,⁸ and AnnV/PI cytotoxicity assays henceforth coupled to RTCA investigations. *N*-Methylation of the backbone amides was chosen for its renowned ability to disrupt peptide:peptide interactions that promote aggregation.²³ Indeed, the replacement of the amide proton by a methyl group prevents the hydrogen-bonding interactions that normally stabilize β -sheet formation. In addition, *N*-methyl-amino acids prevent the close approach of β -strands because of steric hindrance and favor β -strand structure in the peptide itself by locally restricting the backbone conformation to extended structures.²⁴ Of importance, backbone methylations also contribute to enhanced resistance against proteolytic

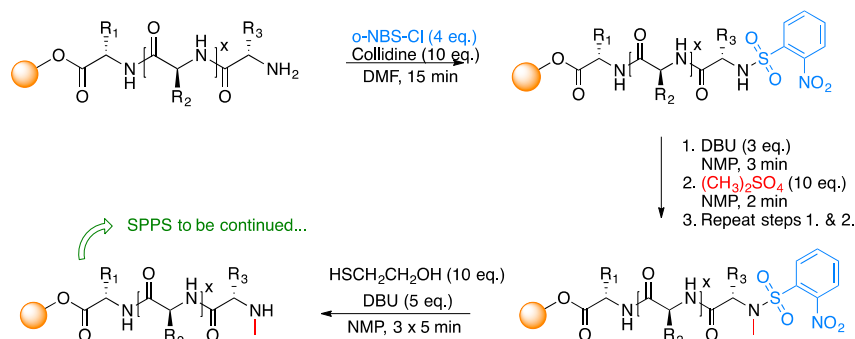


Figure 1. On-resin synthesis of backbone-N-methylated amino acids for the conception of an N-methyl library of PKHB1 analogues.

degradation.²⁵ N-Methylated amino acids have been used in several systems to control protein and peptide aggregation.^{26–28} A number of N-methylated peptides are currently being evaluated in clinical trials, displaying the promise of this chemical modification in delivering the next generation of peptide-based drugs.^{29–32} We based the setup of our N-Me sequence scan on the straightforward site-selective approach developed by Kessler and colleagues,³³ thus allowing fast access to iterative N-methylation of the backbone through the Fmoc/tBu solid-phase peptide synthesis (SPPS) technique. The complete methylation process was performed through a three-step methodology involving activation of the primary amine via sulfonylation followed by the so-called methylation using dimethyl sulfate and then elimination of the sulfonyl moiety with the help of β -mercaptoethanol (Figure 1).

Next, we carried out a SAR study by systematic biological evaluations of each methylated sequence (peptides 1 to 9) in terms of affinity and activity. As described in our earlier work,⁸ such rational design was enabled by the development of a binding assay using an MEC-1 cell membrane preparation in order to maintain the essential integrity of the targeted CD47 receptor.³⁴ Thus, the affinities reported as apparent K_d estimations and shown in Table 1 correspond to the measures of the peptide interactions with the membrane preparation containing CD47 under the described conditions. We assumed that all of our peptides were derived from PKHB1 and that any variations in their pharmacological profiles were due to variations in their interaction efficiency with the CD47 receptor since we had previously demonstrated that the disruption of this interaction by a fusion protein that specifically binds to CD47 led to inhibition of the cytotoxicity induced by PKHB1.⁷ In parallel to binding assay investigations, the ability of every peptide to selectively induce cell death was measured by AnnV/PI colabeling on the MEC-1 cancer cell line. The cytotoxicity activities are given as the mean \pm SD of the percentage of tumor cell death and refer to AnnV-positive cells (Table 1). Other modifications were also evaluated (peptides 10–16) to probe the potency of branched or aromatic side chains by substitution with Ile and Val or Tyr (Table 1). Both terminal ends were also modified to explore the impact of the extremities in terms of activity and affinity. To this end, C-terminal amino acids were replaced by a carboxamide moiety and N-terminal amines were capped through acetylation. Furthermore, additional terminal D-Lys residues were removed to evaluate their biological impact.

Table 1. Sequences, Affinities, and Activities of the Peptides Designed from the N-Me Scan and Optimization

peptide	sequence ^a	K_d (μ M) ^b	MEC-1 cell death (%), 200 μ M, 6 h ^c
PKHB1	kRFYVVMWk	43 \pm 21	67 \pm 8
Sp ^d	KWVKYRVMFK	NPD	NPD
1	k(NMeR)FYVVMWk	21 \pm 1	54 \pm 1
2	kR(NMeF)YVVMWk	NPD	NPD
3	kRF(NMeY)VVMWk	NPD	NPD
4	kRFY(NMeV)VMWk	36 \pm 4	11 \pm 0
5	kRFYV(NMeM)Wk	NPD	NPD
6	kRFYV(NMeE)Wk	NPD	11 \pm 1
7	kRFYV(NMeW)Wk	NPD	NPD
8	kRFYV(NMeK)Wk	48 \pm 12	20 \pm 1
9	k(NMeR) FYVVMW(NMeK)	38 \pm 20	19 \pm 1
10	k(NMeR)FYVVMWk	8.6 \pm 2	59 \pm 5
11	k(NMeR)FYVVLWk	15 \pm 4	26 \pm 8
12	k(NMeR)FYVVIWk	17 \pm 5	25 \pm 3
13	k(NMeR)FYVVWk	13 \pm 2	19 \pm 1
14	k(NMeR)FYVVVWk	9.5 \pm 3	23 \pm 0
15	Ac-(NMeR) FYVVMW-NH ₂	20 \pm 4	51 \pm 3

^aD-Amino acids are written in lower-case letters. X is the one-letter code for the norleucine residue. ^bBinding affinities were evaluated by biolayer interferometry using an Octet RED instrument. The reported apparent K_d values are averages of at least three independent experiments (standard deviations are indicated). NPD denotes nonpertinent data. ^cCell death induction was evaluated through cytotoxicity assays using AnnV/PI colabeling on MEC-1 cancer cells. The reported data are averages of at least three independent experiments (standard deviations are indicated). The sum of AnnV+/PI- and AnnV+/PI+ events were considered for cell death. ^dThe scrambled peptide (SP)³⁵ (see the Supporting Information) was evaluated at 300 μ M.

Among all of the peptides designed and evaluated, peptide 10 not only appeared to be the most soluble peptide but also presented a pharmacological profile very similar to that of PKHB1 with a slight (3-fold) improvement of its affinity. The conformational effects induced by N-methylation might explain this improvement. Thus, the secondary structure of peptide 10 was investigated, first by CD spectroscopy. Figure 2A shows the CD spectra of peptide 10 and the parent peptide PKHB1. The spectrum of PKHB1 is characteristic of a random-coil conformation with a negative minimum at 195 nm. The spectrum of peptide 10 exhibits a similar minimum

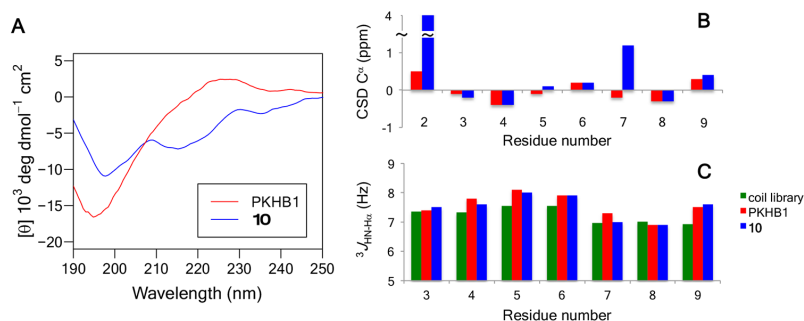


Figure 2. CD- and NMR-based conformational study of peptide **10** and PKHB1. (A) CD spectra of peptide **10** and PKHB1. (B) Chemical shift deviations (CSDs) from random coil values of $^{13}\text{C}\alpha$ resonances.³⁸ The same reference random coil values were used for the noncanonical amino acids of PKT16 (i.e., Arg and Met in place of NMeArg and Nle), explaining the larger CSDs observed for positions 2 and 7. (C) Comparison of $^3J_{\text{HN-H}\alpha}$ coupling constants with corresponding coil values.³⁶ The coil value for Met was used in place of that for Nle for peptide **10**. Nle is the three-letter code for the norleucine residue.

near 198 nm and another minimum around 215 nm. This additional contribution may be due to the presence of β -sheet conformers. Indeed, deconvolution of the CD spectrum allowed the estimation of a 14% population of β -sheet content in peptide **10**.

We next carried out NMR conformational studies to analyze the structural effects of N-methylation at the residue level. ^1H , ^{13}C , and ^{15}N resonances of peptide **10** were assigned and revealed the presence of two sets of chemical shifts. The main chemical shift differences involved the N-Me and CH α resonances of N-methyl-Arg2 (NMeArg2) and also the HN resonances of residues Phe3 up to Val6. This chemical shift heterogeneity was ascribed to cis–trans isomerism of the tertiary amide group between Lys1 and NMeArg2. The major form, whose population was estimated to be 91% on the basis of intensity ratios, corresponds to the trans isomer, as evidenced by a strong rotating-frame Overhauser effect (ROE) between the N-Me protons and H α of Lys1. The conformation of the major trans form was compared to that of PKHB1 by examining chemical shifts, J coupling constants, and ROEs. The structure of PKHB1 was previously shown to be highly flexible with some propensity to adopt extended backbone conformations for the FYVV segment containing aromatic and β -branched residues.⁸ The comparison of peptide **10** and PKHB1 showed that most of the residues have very similar chemical shifts, except for positions 2 and 7, corresponding to the N-methylation and Met-to-Nle substitution, respectively. The $^1\text{H}\alpha$ and $^{13}\text{C}\alpha$ chemical shifts marginally differ from random-coil values, indicating that peptide **10** does not adopt a stable regular secondary structure (Figure 2B). The four central residues FYVV exhibit $^3J_{\text{HN-H}\alpha}$ values that tend to be higher than coil values³⁶ (Figure 2C) and also have strong sequential H α –HN ROEs (data not shown), suggesting that extended conformations are significantly populated in this segment. The C-terminal part is characterized by lower-intensity sequential H α –HN ROEs and the presence of sequential HN–HN ROEs (residues 7/8 and 9/10), indicating that it explores less-extended conformations.

Altogether, these NMR parameters show that the conformational space of residues 3–10 is very similar in peptide **10** and PKHB1, a result that was somehow not inferred from the CD study. The differences observed in the CD spectra must therefore be related to local structural perturbations induced

by N-methylation and possibly changes in the CD spectroscopic properties of the tertiary amide bond.³⁷ We conclude that N-methylation restricts the backbone conformational space only locally around residues 1–2 and has no major effect on the global conformation of peptide **10** in segment 3–10. Overall, we observed that backbone N-methylation conferred very good solubility, and the peptide did not aggregate in water or in biological liquids (pure water, phosphate buffers, and human serum), thereby leading to promising physicochemical features.

Consequently, with this new peptide **10**, which we termed PKT16, we considered the homotrimerization approach in order to improve its pharmacological efficacy. The design and synthesis of the analogue were considered using a click chemistry strategy with a tertiary amine as a matrix and an aminopentanoic acid derivative as a spacer (Figure 3). On the basis of copper-catalyzed azide–alkyne cycloaddition (CuAAC) processes that have been smartly applied in the field of peptide therapeutics,⁴⁴ various reaction conditions were tested to implement a convenient trimerization strategy onto scaffold. Surprisingly, the only way to achieve this one-pot reaction was to use a methanol/acetonitrile mixture as the solvent and the tetrakis(acetonitrile) complex as the copper I source. In addition, the incorporation of tris[(1-benzyl-1H-1,2,3-triazol-4-yl)methyl]amine (TBTA) for copper(I) stabilization was crucial to properly conduct the homotrimer formation. For this purpose, the monomeric PKT16 (k-(NMeR)FYVVXWKK) sequence was synthesized on a solid support using standard Fmoc chemistry (see the Supporting Information) and coupled to the 5-azidopentanoic acid,⁴⁵ which was used as a spacer bearing the azido group for click chemistry (Figure 3). After cleavage and purification, the unprotected PKT16-N₃ peptide was used to perform the chemoselective click chemistry attachment onto the tripropargylamine matrix (see the Experimental Section for further explanations regarding detailed reaction conditions). Successfully, the homotrimer built around PKT16 was soluble in water and did not form insoluble aggregates over time, thus confirming the enhanced physicochemical features. We thereby started evaluation of the activity of this new trimeric peptide object, termed [PKT16]₃.

We first determined the affinity of [PKT16]₃ (on an MEC-1 cell membrane preparation containing CD47 receptor), which

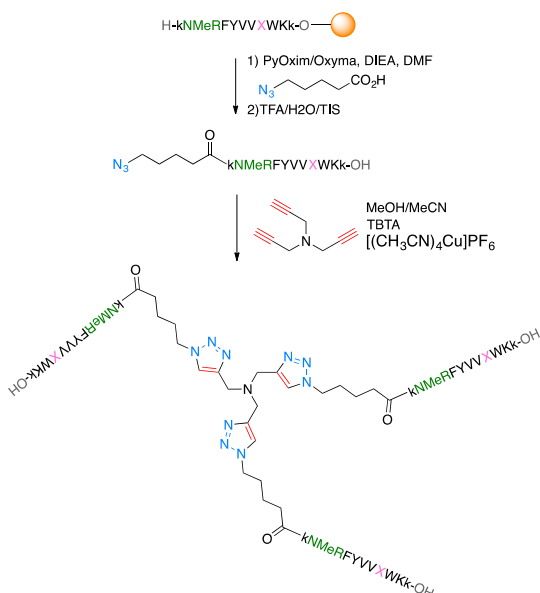


Figure 3. General scheme for the preparation of [PKT16]₃. Incorporation of the azido moiety was achieved via SPPS. Synthesis of the trimer was performed through a click chemistry reaction for attachment onto the trialkyne scaffold.

proved to be about 40-fold stronger than that of its monomeric precursor ($K_d([\text{PKT16}]_3) = 190 \pm 90 \text{ nM}$ vs $K_d(\text{PKT16}) = 8.6 \pm 2 \mu\text{M}$; see the Supporting Information). Its potency to induce cell death was evaluated on two different cancer cell lines: (i) the MEC-1 cell line, an established TP53 dysfunctional CLL cell line, and (ii) the adherent A549 nonsmall cell lung cancer cell line. Cell death was evaluated using classical FCM for MEC-1 cells (Figure 4) and A549 cells (Figure 5A–C). The RTCA technique was also used for the A549 cells (Figure 5D,E). The latter technique was chosen as a control because of its easy implementation for adherent cells that avoids the cell-harvesting methods required in FCM, which are known to affect the membrane integrity of adherent cancer cells and thus the proportion of apoptotic cells during detection.²⁰

In a first experiment, the efficiency of [PKT16]₃ was evaluated in a dose-dependent manner and compared with those of PKHB1 and PKT16 on MEC-1 cells, and the data are reported in Figure 4A. Moreover, although the design of this new peptide was based on PKHB1, for which we reported a caspase-independent Ca^{2+} -mediated form of RCD,^{7,8} we assume that the homotrimeric nature of the peptide could trigger a different RCD pathway. Indeed, microscopy observations of cells treated with the different peptides (Figure 4B) highlighted the ability of this new homotrimeric peptide to induce cell aggregation. This might be explained by its multivalency, which can promote simultaneous interactions with receptors of different cells. Thus, in order to highlight the cell death mechanism, in a second experiment cells were pretreated with Q-VD-OPH (a broad-spectrum caspase inhibitor), BAPTA (an extracellular calcium chelator), U73122 (a PLC γ 1 inhibitor), and 2-APB and dantrolene

(intracellular calcium channel inhibitors) before incubation with the peptides (Figure 4C and Table S4).

[PKT16]₃ was a much more potent RCD inducer than its monomeric counterpart PKT16 and PKHB1 in MEC-1 cells. Thus, its potency was also evaluated and compared to that of PKHB1 and PKT16 on the adherent human pulmonary alveolar epithelial cell line A549, and the data are reported in Figure 5A. Contrary to caspase inhibition, which had no effect on cell death induced by any of the three peptides, impairing Ca^{2+} signaling significantly decreased PKHB1-, PKT16- and [PKT16]₃-induced cell death in A549 cells as well (Figure 5B,C and Table S5).

Enhanced cell adhesion was also a relevant feature of [PKT16]₃-induced RCD in A549 cells, which strongly stuck to the well surface after treatment. In fact, cell collection from the well prior to cell death analysis was a highly challenging task, since trypsin was not very efficient at removing a subpopulation of cells with morphological features characteristic of [PKT16]₃-induced RCD (Figure S2). Therefore, the RTCA technique was used as a control to evaluate the cell death induced by our new peptide because of its easy implementation that avoids cell-harvesting methods, which are known to affect the membrane integrity of adherent cells and thus the proportion of dead and dying cells during detection.²⁰ In this way, the [PKT16]₃ efficacy was also characterized using RTCA with increasing peptide concentrations for up to 24 h (Figure 5D) together with measurement of the release of AK (Figure S5) and compared with those of known cytotoxic concentrations of PKHB1 and PKT16 (Figure 5E).

DISCUSSION AND CONCLUSIONS

The TSP-1:CD47 ligation was reported to induce RCD at least in CLL cells,⁶ and for the past few years we have focused our attention on the design of peptide mimics of the TSP-1:CD47 binding epitope. For that purpose, we implemented a SAR study aimed first to highlight the pharmacophores involved in this interaction. We reported that the crucial pharmacophores were not only restricted to the VVM motif but involved mainly the FYVV sequence.⁸ These studies led to the design of PKHB1, the first serum-stable agonist peptide^{7,8} mimicking the CD47 binding epitope (i.e., RFYVVMWK) of thrombospondin-1 (TSP-1). The PKHB1 sequence appeared to be key for its activity since a scrambled peptide (SP) (i.e., KWVKYRVMFK; see Table 1)³⁵ had no affinity for membrane preparation or cell death activity under the same conditions. PKHB1 was proven to be efficient in triggering cell death selectively in many adherent and nonadherent cancer cell lines while sparing normal cells. The molecular mechanism triggered by PKHB1 (caspase-independent cell death mediated by sustained activation of PLC γ 1 leading to intracellular Ca^{2+} overload) was highlighted, and stimulation of CD47 appeared to be key in the cytotoxicity induced by this peptide since disruption of the peptide:CD47 interaction by a fusion protein designed to specifically bind CD47 led to inhibition of the cytotoxicity.⁷ Its potency was also demonstrated in vivo in mice models at a dose of 10 mg/kg.^{7,9} However, even though PKHB1 appeared to be a promising tool, its high in vitro LC₅₀ (200 μM), which might be considered as a drawback in drug development, led us to design and explore an optimization process. Since the X-ray structure of the TSP-1/CD47 complex has not been solved to date, a multimerization approach was investigated, considering that the homotrimeric structure of

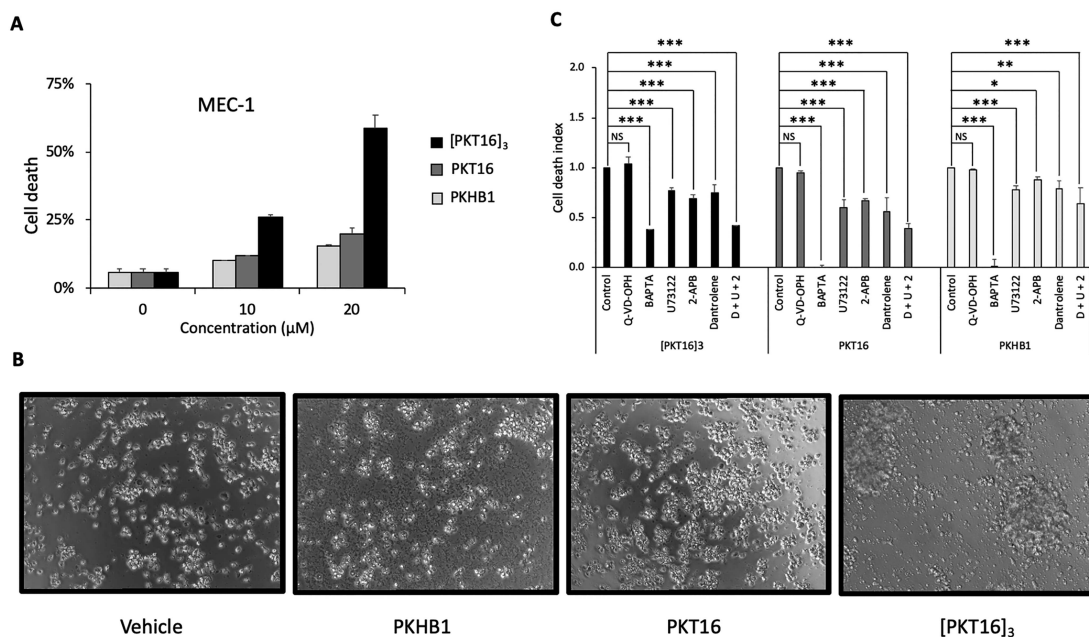


Figure 4. Low concentrations of [PKT16]₃ induce caspase-independent cell death regulated by Ca²⁺ in MEC-1 cells. (A) Comparison of cell death induction by different TSP-1-mimetic peptides. Cells were treated with the indicated peptide concentrations in complete medium, and cell death was analyzed by AnnV/PI staining. Histograms represent the mean \pm SD of two independent experiments. (B) Microscopy observations (20 \times) of cells treated with vehicle, PKHB1 (200 μM), PKT16 (200 μM), or [PKT16]₃ (20 μM). (C) Effect of pharmacological inhibition of caspases or calcium signaling in [PKT16]₃-induced cell death. Cells were preincubated with vehicle (Control), Q-VD-OPH (10 μM), BAPTA (3 mM), U73122 (400 nM), 2-APB (60 μM), dantrolene (80 μM), or a 1/3 combination of the last three (133 nM U73122, 20 μM 2-APB, 27 μM dantrolene) 1 h before treatment with [PKT16]₃ (5 μM), PKT16 (50 μM), or PKHB1 (50 μM) in serum-free medium to limit peptide interactions with albumin (see Figure S3). Cell death was analyzed by flow cytometry using AnnV/PI staining, and the cell death index was obtained by normalizing to 1.0 the cell death induced by each peptide with its corresponding control (see the Supporting Information). Histograms represent the mean \pm SD of at least two independent experiments. Two-way ANOVA: ***, $P \leq 0.0001$; **, $P \leq 0.001$; *, $P \leq 0.05$.

TSP-1 did not happen by accident but rather is linked to evolution enabling TSP-1 to interact simultaneously with multiple receptors.

The design of the homotrimer was first based on the PKHB1 structure (see the Supporting Information) but because of the aggregation propensities observed with PKHB1 and its trimer in some buffers, we concluded that this peptide was not suitable for our purpose. Thus, in order to limit this phenomenon, we went back to the PKHB1 structure and performed an *N*-methyl scan of its sequence since *N*-methylation of the backbone is known to disrupt peptide:peptide interactions that promote aggregation. The implementation of the *N*-Me scan enabled the identification of key positions for amide backbone modification (Table 1). First, we observed that some of the residues do not have the capacity to accept *N*-methylation. Notably, with regard to the FYVV segment, previously identified as the peptide pharmacophore,⁸ methylation of the backbone ultimately yielded a complete drop in activity, as observed with peptides 2, 3, 4, and 5, thus confirming that structural information included in this four-residue motif is crucial for CD47 engagement. Furthermore, we observed here that the only residue that can be methylated without a dramatic decrease in efficacy is Arg2, since peptide 1 retains full affinity and a range of activity similar to that of PKHB1. To evaluate the impact of multiple backbone

methylations, the data observed with peptides 1 and 8 led us to design the doubly *N*-methylated peptide 9. This peptide, which resulted from two successive *N*-methylations at Arg2 and Lys9, presented a pharmacological profile similar to that of peptide 8. This confirmed that unlike the suitable Arg2 position, *N*-methylation of Lys9 is deleterious, as observed with peptide 8. These data indicated that a single methylation might be sufficient to prevent peptide aggregation while maintaining efficiency. Actually, like the Pro residue, *N*-methylation is known to favor turn secondary structures in peptide sequences, thereby leading to disruption of the desired extended conformation.³⁹ According to the *N*-Me scan results, Arg2 was identified as the key amino acid to suitably accept backbone *N*-methylation. In addition, we also introduced chemical modifications into the sequence of peptide 1, for instance, replacement of Met7 with all-hydrocarbon counterpart Nle, as Met had previously been shown to be readily replaceable by Nle.⁸ This modification was proposed to avoid possible oxidation of the sulfur atom of the Met side chain, which might lead to decreased potency, as observed in the case of tachykinins.⁴⁰ This was demonstrated by the synthesis and biological evaluation of the sulfoxide and sulfone derivatives of PKHB1, which proved to be totally inactive (see the data related to PKHB1-SO and PKHB1-SO₂ given in the Supporting Information).

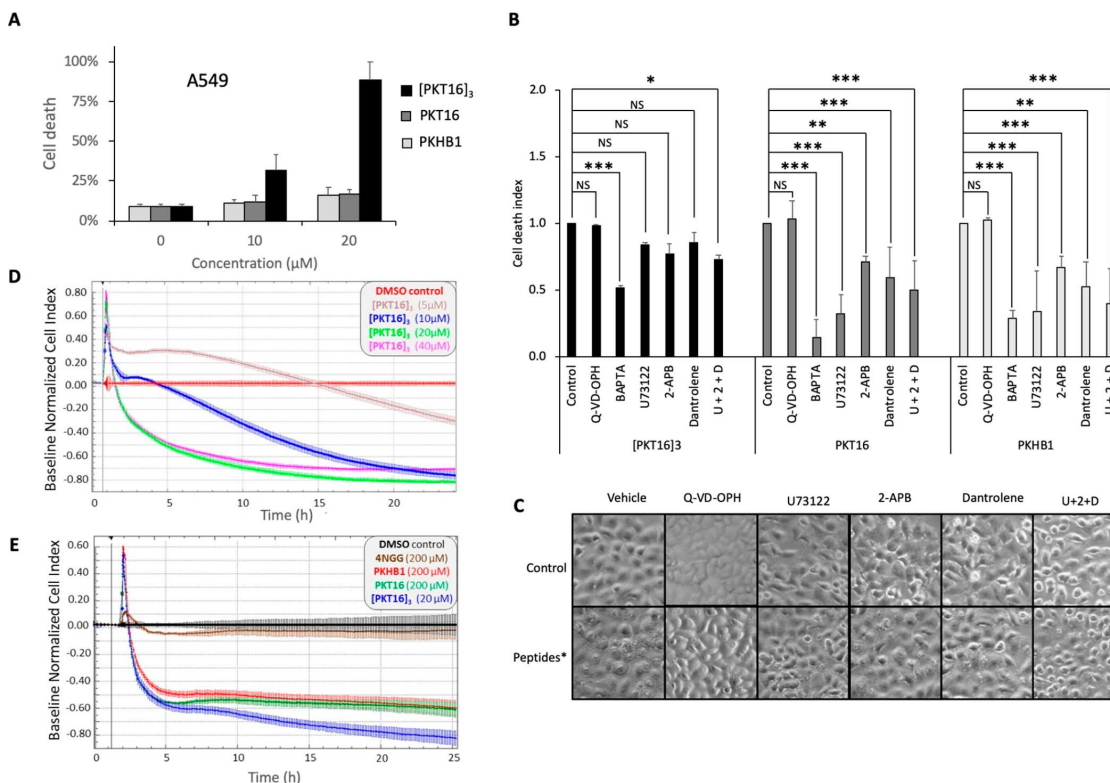


Figure 5. [PKT16]₃ induces caspase-independent cell death regulated by Ca²⁺ in A549 cells. (A) Comparison of cell death induction by different TSP-1-mimetic peptides. Cells were treated with the indicated peptide concentrations in complete medium, and cell death was analyzed by AnnV/PI staining. Histograms represent the mean ± SD of two independent experiments. (B) Effect of pharmacological inhibition of caspases or calcium signaling in [PKT16]₃-induced cell death. Cells were preincubated with vehicle (Control), Q-VD-OPH (10 μM), BAPTA (3 mM), U73122 (400 nM), 2-APB (60 μM), dantrolene (80 μM), or a 1/3 combination of the last three (133 nM U73122, 20 μM 2-APB, 27 μM dantrolene) 1 h before treatment with [PKT16]₃ (10 μM), PKT16 (100 μM), or PKHb1 (100 μM) in serum-free medium to limit peptide interactions with albumin (see Figure S3). Cell death was quantified by AnnV/PI and trypan blue staining, and the cell death index was calculated as in Figure 4C. Histograms represent the mean ± SD of two independent experiments. Two-way ANOVA: ***, $P \leq 0.0001$; **, $P \leq 0.001$; *, $P \leq 0.05$. (C) Microscopy observations (20X) of cells treated with the corresponding inhibitors alone (Control) or with TSP-1-mimetic peptides. *Similar morphology was observed irrespective of the peptide used ([PKT16]₃, PKT16, or PKHb1). (D) Full kinetics with cell index parameter on the A549 cell line with the control (0.4% DMSO) in red. (E) Comparison of the impedance signals of DMSO, 4NGG (negative control),^{7,8} PKHb1, PKT16, and [PKT16]₃ after incubation for 24 h at their respective LC₅₀ values.

With regard to the SAR study performed (i) to probe the potency of branched or aromatic side chains by substitution with Ile, Val, and Tyr and (ii) to explore the impact of the extremities in terms of activity and affinity (Table 1), the results showed that only amino acids presenting linear side chains are suitable to mimic Met7. Indeed, branched (Ile and Val) and aromatic (Tyr) residues are deleterious for peptide efficacy, as observed with peptides 11, 12, 13, and 14, suggesting that the CD47 binding pocket interacting with these side chains is rather small since it accepts only linear moieties. Nevertheless, these data have to be interpreted carefully since these modified peptides were prone to aggregation, as suggested by their more hydrophobic profiles. Chemical modifications of the extremities yielded the potent peptide 15, but this peptide was not suitable for the design of the homotrimer, which required a free amine function at the N-terminus.

Finally, peptide 10, in which Arg2 is N-methylated and Met7 is replaced by Nle, was chosen for further investigation because of (i) its structure suitable for further development, (ii) its potency similar to that of PKHb1, and (iii) its higher solubility in all of the buffers tested. This crucial point was confirmed during the structural analyses of peptide 10 realized by NMR and CD spectroscopy. Indeed, we observed by NMR spectroscopy that backbone N-methylation conferred very good solubility and that the peptide did not aggregate in either water or biological liquids (pure water, phosphate buffers, and human serum), thereby leading to promising physicochemical features.

Consequently, with peptide 10, which we termed PKT16, the homotrimerization was investigated using a click chemistry strategy with a tertiary amine as a matrix and an aminopentanoic acid derivative as a spacer (Figure 3). The synthesis was realized in a one-pot reaction for which the use of a

methanol/acetonitrile mixture as the solvent, the tetrakis(acetonitrile) complex as the copper(I) source, and incorporation of TBTA for copper(I) stabilization were revealed to be crucial to properly conduct the formation of the homotrimer, which we termed [PKT16]₃. Successfully, the homotrimer built using PKT16 was soluble in water and did not form insoluble aggregates over time, thus confirming the enhanced physicochemical features. We therefore started its pharmacological evaluation by first determining its affinity on an MEC-1 cell membrane preparation containing the CD47 receptor. Remarkably, we observed a significant synergistic effect that was not simply additive as a result of the 3-fold increased local concentration of PKT16 stretches. Indeed, the binding affinity of the [PKT16]₃ homotrimer (190 ± 90 nM) was about 40-fold stronger compared with its monomeric precursor (8.6 ± 2 μ M). Its potency in triggering cell death was evaluated first on MEC-1 cells and compared with those of monomeric PKHB1 and PKT16 in a dose-dependent manner (Figure 4A). The LC₅₀ was 20 μ M for the homotrimer, while a concentration of 200 μ M was required with the monomers to reach the same efficacy (see Table 1). Thus, the novel N-methylated trimer produces 10-fold higher induction of cell death, thereby confirming the synergistic effect allowed by multivalency. It should be noted that the observed discrepancy between activity and affinity is linked to the experimental conditions, which are different in the binding experiments and cell death experiments. The binding experiments were performed with a cell membrane preparation in simple phosphate-buffered saline (PBS), whereas the cell death experiments were performed with cells incubated in advanced RPMI medium containing albumin. Albumin binds low-molecular-weight molecules, including proteins and peptides, and thus affects the free peptide concentration required for cell death experiments (see Figure S3).⁴¹ The potency of the homotrimer to induce cell death was also evaluated on the adherent A549 cancer cell line (Figure 5). First, the potency was evaluated in a dose-dependent manner and compared with those of PKHB1 and PKT16 as for the MEC-1 cells, and the data are reported in Figure 5A. From these experiments, we can conclude that the homotrimer is much more potent than the monomers, with an LC₅₀ between 10 and 20 μ M. Furthermore, microscopy observations highlighted a peculiar behavior of the homotrimeric peptide (Figures 4B and S2). Indeed, compared with PKHB1 and PKT16 at 200 μ M, for which dead cells were observed without cell aggregation, the homotrimer peptide led to cell aggregates, which might be explained by its ability to establish multivalent interactions with receptors from different cells. Since this peculiar behavior might result in a different cell death mechanism than the one described for PKHB1,⁷ cells were preincubated with Q-VD-OPH, BAPTA (an external calcium chelator), U73122 (a PLC γ 1 inhibitor), and 2-APB and dantrolene (intracellular calcium channel inhibitors) before incubation with each of the three peptides PKHB1, PKT16, and [PKT16]₃ (Figures 4C and 5B). Together with Ca²⁺ chelation, inhibition of PLC γ 1 or the IP₃R or ryanodine receptors significantly diminished PKHB1- and PKT16-induced cell death in both cell lines. However, with [PKT16]₃, inhibition of PLC γ 1 or the calcium channels alone caused a significant decrease in cell death of MEC-1 cells but only a slight decrease that was not significant in A549 cells. However, combined inhibition of PLC γ 1-mediated calcium signaling significantly decreased cell death in all cases. These results suggest that PLC γ 1-mediated calcium overload is

crucial for [PKT16]₃ and its monomeric counterpart PKT16 to trigger RCD in the nonadherent MEC-1 cells, as already described for PKHB1. However, in the adherent lung cancer cells, this may also be true for the monomeric peptides PKHB1 and PKT16, but it is not the case for [PKT16]₃, in which PLC γ 1-mediated calcium signaling is only a partial modulator of RCD. Together with morphological observations, the double AnnV/PI copositive staining observed during MEC-1 cell death induced by [PKT16]₃ led us to classify it as a programmed necrotic cell death pathway similar to that reported for PKHB1.^{7,8,21} To go further, in the case of A549 cells, a type of RCD sharing some biochemical and morphological features of [PKT16]₃-induced RCD, such as caspase independence, ion-exchange dependence, enhanced cell–substrate adhesion, and focal ballooning of the perinuclear space, was recently reported under the name of autosis.⁴² Among other similar cellular stimuli, autotic cell death can be triggered by a cell-penetrating autophagy-inducing peptide (Tat-Beclin 1). Moreover, it has been recently demonstrated that targeting CD47 with a fusion protein approach (SIRP α D1-Fc) induces autophagy in non-small cell lung cancer cells, including the A549 cell line.⁴³ However, autosis is defined by autophagy triggering, and it is an autophagy-dependent cell death mechanism regulated by the Na⁺/K⁺-ATPase pump, which was not assessed in the present work. Thus, further analysis is needed to know whether [PKT16]₃ induces autosis in A549 cells. Altogether, our results showing pharmacological inhibition of TSP-1-mimetic peptides in MEC-1 and A549 cells highlight the molecular disparities among the two cell types, which come from two different diseases, and demonstrate that TSP-1-mimetic peptides can restore programmed cell death in both cases.

Since it was reported that the cell-harvesting methods required in FCM affect the membrane integrity of adherent cancer cells and thus the proportion of apoptotic cells during detection,²⁰ cell death induced by [PKT16]₃ was also evaluated using the RTCA technique in a dose-dependent manner (Figure 5D), and its cell index was compared with those of PKHB1 and PKT16 at their respective LC₅₀ values (Figure 5E). The cell index was continuously recorded every minute for 24 h, and treatments were realized 1 h after the beginning of the cell index recording (see the arrows in Figure 5D,E). For all of these experiments, the addition of peptide provoked first a large increase in the impedance signal that was attributed to the calcium burst we already observed through CD47 receptor activation with PKHB1 in CLL cells. In Figure 5D, the experiment realized in a dose-dependent manner (from 5 to 40 μ M) highlighted a rapid and profound diminution of the cell index upon 2 h treatments at peptide concentrations of 20 and 40 μ M. These observations correlate with those realized by FCM. Indeed, the maximum diminution of the cell index was observed from 20 μ M, corresponding to the approximate LC₅₀ estimated for this cell line using FCM. This ability of our peptide to induce profound diminution of the cell index was correlated to the loss of cell membrane integrity identified by measurement of the release of adenylate kinase (AK) (see Figure S5D). The loss of cell membrane integrity is also reflected by the double AnnV/PI staining in FCM. Finally, the impedance signals in cells treated with PKHB1, PKT16, or its trimer [PKT16]₃ were similar when the cells were treated with their respective LC₅₀'s (Figure 5E). Again, even for the PKHB1 and PKT16 monomers, the profound diminution of the cell index was correlated to the

loss of cell membrane integrity identified by measurement of the release of AK (see Figure S5E). This technique is therefore effective and powerful to quickly and simply evaluate the potency of our compounds on adherent cancer cell lines.

In conclusion, in this work we designed a new series of soluble peptides mimicking the action of the TSP-1 C-terminal binding domain, namely, the selective induction of RCD in tumors. We initiated rational SAR studies that led to the discovery of mimetic peptides, the monomer termed PKT16 and its trimeric analogue [PKT16]₃, both with improved pharmacological features, increased solubility, fitter structural properties, and higher efficacy. Such refinements were unlocked by scanning the entire sequence through amide backbone N-methylation and the judicious substitution of key amino acids. In order to further ameliorate our lead properties, we set up a multivalency strategy through homotrimerization of active peptide stretches mounted onto a rigid small-molecule scaffold. Preparation of the trimer object via click chemistry yielded a soluble biopolymer that presented deeply improved pharmacological parameters in terms of activity and affinity. To our knowledge, this trimeric peptide is the strongest-affinity and most active TSP-1 C-terminal binding domain-mimetic peptide in triggering RCD through CD47 engagement in tumors. Many pieces of evidence urge us to propose programmed necrotic cell death as the cell death mechanism triggered by our peptide. However, the behavior of our homotrimer led us to propose a death mechanism comparable to autosis, which, however, remains to be characterized here. Overall, this work provides several insights of major importance for identifying potent therapeutic strategies in the design of new TSP-1 C-terminal binding domain-mimetic peptides triggering RCD of cancer cells.

EXPERIMENTAL SECTION

1. General Chemistry. *1.1. Peptide Synthesis.* All of the peptides were manually synthesized from Fmoc-protected amino acids utilizing standard SPPS methods. SPPS was performed in polypropylene Torviq syringes (10 or 20 mL) fitted with a polyethylene porous disk at the bottom and closed with an appropriate piston. Solvent and soluble reagents were removed through back-and-forth movements. The appropriate protected amino acids were sequentially coupled using PyOxim/Oxyrna as coupling reagents. The peptides were cleaved from the chlorotriyl or Rink amide resin with a classical cleavage cocktail (95:2.5:2.5 TFA/TIS/H₂O). The crude products were purified using preparative-scale HPLC. The final products were characterized by analytical LC–MS and NMR spectroscopy. All of the tested compounds were TFA salts and were at least 95% pure. Detailed NMR studies were performed for the relevant peptides, and assignment tables are provided in the Supporting Information.

1.2. Site-Selective N-Methylation of the Amide Backbone. Residues were N-methylated on the solid phase through Kessler's methodology.³³ First, the free amino functionality was protected and activated with the *o*-nitrobenzenesulfonyl (*o*-NBS) group, then N-methylated using 1,8-diazabicyclo[5,4,0]undec-7-ene (DBU) and dimethyl sulfate (DMS), and finally deprotected (removal of *o*-NBS) by treating the resin with β -mercaptoethanol and DBU. For *o*-NBS activation, a solution of *o*-NBS-Cl (4 equiv) and collidine (10 equiv) in *N*-methylpyrrolidone (NMP) was added to the resin-bound free-amine peptides and shaken for 15 min at room temperature. The resin was washed with NMP (5 \times). For N-methylation with DBU and DMS, a solution of DBU (3 equiv) in NMP was added to the resin bound *o*-NBS-protected peptides, and the resulting mixture was shaken for 3 min. A solution of DMS (10 equiv) in NMP was added to the reaction mixture, which was then shaken for 2 min. The resin was filtered off and washed once with NMP, and the N-methylation procedure was repeated once more. The resin was washed with NMP

(5 \times). For *o*-NBS removal, the resin bound *N*-methyl-*N*-*o*-NBS peptides were treated with a solution of β -mercaptoethanol (10 equiv) and DBU (5 equiv) in NMP for 5 min. The deprotection procedure was repeated once more, and the resin was washed with NMP (5 \times).

1.3. Homotrimerization by Solution-Phase Click Chemistry. Typically, pure azido peptide derivative (36 mg, 19 μ mol, 3.6 equiv) was taken up in 750 μ L of MeOH that had previously been frozen, put on a vacuum pump to remove gas molecules, and then purged with N₂ for at least 30 min. To this mixture was added tripropargylamine (0.94 μ L, 6.7 μ mol, 1 equiv) in 250 μ L of MeOH, followed by the addition of TBTA (21 mg, 40 μ mol, 6 equiv) and tetrakis(acetonitrile)copper(I) hexafluorophosphate, [(CH₃CN)₄Cu]PF₆ (78 mg, 203 μ mol, 30 equiv). To this mixture was added MeCN dropwise (around 20 drops) to bring everything into solution, and the reaction was allowed to proceed in a round-bottom flask at room temperature under a flow of nitrogen with constant stirring for a maximum of 72 h. The sample was quenched with 5 mL of H₂O, frozen, and then lyophilized. The dried crude product was resuspended in 0.1 M EDTA (3 \times 5 mL to rinse the tube), loaded on a 1.6 g Zeoprep 90 C18 cartridge (particle size 40–63 μ m), and sequentially eluted with 15 mL of H₂O, 1:1 H₂O/MeCN, and MeCN. Each fraction was collected in a round-bottom flask and analyzed by LC–MS (method A). The EDTA, H₂O, and H₂O/MeCN fractions were concentrated to dryness, resuspended in H₂O, filtered with a 0.22 μ m filter, and purified as described earlier to isolate the peptide homotrimer.

1.4. Analytics. All of the analytical data are given in the Supporting Information. Two methods were conducted for LC–MS analysis.

Method A: Analytical HPLC was conducted on an X-Select CSH C18 XP column (30 mm \times 4.6 mm i.d., 2.5 μ m), eluting with 0.1% formic acid in water (solvent A) and 0.1% formic acid in acetonitrile (solvent B) using the following elution gradient: 0–3.2 min, 0–50% B; 3.2–4 min, 100% B. The flow rate was 1.8 mL/min at 40 $^{\circ}$ C. The mass spectra were recorded on a Waters ZQ mass spectrometer using electrospray positive ionization (ES+) mode to give [M + H]⁺ molecular ions or electrospray negative ionization (ES–) mode to give [M – H][–] molecular ions. The cone voltage was 20 V.

Method B: Analytical HPLC was conducted on an X-Select CSH C18 XP column (30 mm \times 4.6 mm i.d., 2.5 μ m), eluting with 0.1% formic acid in water (solvent A) and 0.1% formic acid in acetonitrile (solvent B) using the following elution gradient: 0–3.2 min, 5–100% B; 3.2–4 min, 100% B. The flow rate was 1.8 mL/min at 40 $^{\circ}$ C. The mass spectra were recorded on a Waters ZQ mass spectrometer in ES+ or ES– mode. The cone voltage was 20 V.

1.5. Purification. Preparative-scale purification of peptides was performed by reversed-phase HPLC on a Waters system consisting of a quaternary gradient module (Waters 2535) and a dual-wavelength UV/vis absorbance detector (Waters 2489), piloted by Empower Pro 3 software using the following columns: a preparative Macherey-Nagel column (Nucleodur HTec, C18, 250 mm \times 16 mm i.d., 5 μ m, 110 Å) and a preparative Higgins analytical column (Proto 200, C18, 150 mm \times 20 mm i.d., 5 μ m, 200 Å) at flow rates of 14 and 20 mL/min, respectively. Small-scale crudes (<30 mg) were purified using a semipreparative Ace column (Ace 5, C18, 250 mm \times 10 mm i.d., 5 μ m, 300 Å) at a flow rate of 5 mL/min. Purification gradients were chosen to get a ramp of approximately 1% solution B min^{–1} in the interest area, and UV detection was done at 220 and 280 nm. Peptide fractions from purification were analyzed by LC–MS (method A or B depending on the retention time) or by analytical HPLC on a Dionex system consisting of an automated LC system (Ultimate 3000) equipped with an autosampler, a pump block composed of two ternary gradient pumps, and a dual-wavelength detector, piloted by Chromeleon software. All of the LC–MS and HPLC analyses were performed on C18 columns. The pure fractions were gathered according to their purities and then freeze-dried using an Alpha 2/4 freeze-dryer (Bioblock Scientific) to get the expected peptide as a white powder. The final peptide purity of the corresponding pooled fractions (>95%) was checked by LC–MS using method A.

2. Peptide Stability Studies. *2.1. Degradation Assays in Human Serum and Mouse Plasma.* To a mixture of 250 μL of human serum or mouse plasma and 750 μL of RPMI 1640 medium was added 20 μL of the peptide DMSO stock solution at 10 mM. The mixture was incubated at 37 $^{\circ}\text{C}$, and 100 μL aliquots were removed from the medium at different times, mixed with 100 μL of TCA solution (6%), and incubated at 4 $^{\circ}\text{C}$ for at least 15 min to precipitate all of the serum proteins. After centrifugation at 12 000 rpm for 2 min, 50 μL of the supernatant was transferred to an injection vial and analyzed by HPLC with a linear gradient of MeCN in water (5 to 95% + 0.1% TFA). The relative concentrations of the remaining soluble peptides were calculated by integration of the absorbance at 220 nm as a function of the retention time (peak area).

2.2. Stability under Chymotrypsin and Trypsin Incubation. A 0.6 mL microcentrifuge tube was charged with 180 μL of phosphate buffer (pH 7.4), 10 μL of enzyme (0.05 mg/mL stock solution in pH 7.4 phosphate buffer), and 10 μL of peptide (10 mM stock solution in DMSO). The resulting reaction mixture was capped and incubated at room temperature for 3 h. A 20 μL aliquot of the crude reaction mixture was quenched by addition of 180 μL of 1:1 water/acetonitrile, and the resulting mixture was subjected to LC-MS analysis.

3. Structural Analyses. *3.1. CD Spectroscopy.* CD experiments were performed on a Jasco J-815 CD spectropolarimeter with a Peltier temperature-controlled cell holder (30 $^{\circ}\text{C}$) over the wavelength range 190–270 nm. Peptide samples were prepared at a concentration of 50 μM in 10 mM sodium phosphate buffer (pH 7.4) using a quartz cell with a path length of 1 mm. Measurements were taken every 0.2 nm at a scan rate of 10 nm/min.

3.2. NMR Spectroscopy. Lyophilized PKT16 peptide was dissolved at 1 mM concentration in 550 μL of $\text{H}_2\text{O}/\text{D}_2\text{O}$ (90:10 v/v). Sodium 4,4-dimethyl-4-silapentane-1-sulfonate- d_6 (DSS) (Sigma-Aldrich) was added at a final concentration of 0.11 mM for chemical shift calibration. NMR experiments were recorded on a Bruker Avance III 500 MHz spectrometer equipped with a TCI $^1\text{H}/^{13}\text{C}/^{15}\text{N}$ cryoprobe with Z-axis gradient. NMR spectra were processed with TopSpin 3.2 software (Bruker) and analyzed with the NMRFAM-SPARKY program.³⁸ ^1H , ^{13}C , and ^{15}N resonances were assigned using 1D ^1H WATERGATE, 2D ^1H - ^1H TOCSY (DIPS1-2 isotropic scheme of 80 ms duration), 2D ^1H - ^1H ROESY (300 ms mixing time), 2D ^1H - ^{13}C HSQC, 2D ^1H - ^{15}N HSQC, and 2D ^1H - ^{13}C HMBC spectra recorded at 25 $^{\circ}\text{C}$. ^1H chemical shifts were referenced against the DSS ^1H signal, and ^{13}C and ^{15}N chemical shifts were referenced indirectly. The chemical shift deviations were calculated as the differences between the observed ^1H and ^{13}C chemical shifts and random coil values.⁴⁶ $^3J_{\text{HN-H}\alpha}$ coupling constants were measured by 1D ^1H WATERGATE experiments recorded at 5 or 25 $^{\circ}\text{C}$ or 1D rows extracted from 2D TOCSY spectra acquired with high resolution.

4. Biological Assays. *4.1. Binding Affinity Measurements by Biolayer Interferometry.* The binding affinities of peptides for a membrane preparation from MEC-1 cells were measured by biolayer interferometry on an Octet RED96 System (Pall FortéBio Corp., Menlo Park, CA). This system monitors interference of light reflected from two sources (an internal reflection surface and the liquid–solid interface of a fiber optic sensor) to measure the rate of binding of molecules to the biosensor surface. MEC-1 cell membrane preparations were biotinylated with an EZ-Link NHS-PEG4-Biotin kit from Thermo Scientific. Biotinylated membranes were then loaded onto SuperStreptavidin (SSA) biosensors (Pall FortéBio Corp.) at empirically determined concentrations. All of the affinity measurements were carried out in assay buffer (PBS with 0.2% bovine serum albumin (BSA) and 1% DMSO) at 30 $^{\circ}\text{C}$. The assay protocols are further detailed in the Supporting Information.

4.2. Cell Death Induction and Pharmacological Inhibition. MEC-1 cells (an established CLL cell line with dysfunctional TP53) and A549 cells (human alveolar basal epithelial adenocarcinoma cells) were maintained in complete medium (Advanced RPMI 1640 supplemented with 10% fetal calf serum, 2 mM L-glutamine, and 100 units/mL penicillin–streptomycin). Cell death was induced by

treating MEC-1 cells for 2 h or A549 cells for 6 h with the indicated peptide concentrations. Etoposide (200 μM , 24 h) was used as a positive control for p53- and caspase-dependent apoptosis. Cell death was measured by flow cytometry using AnnV-APC (0.1 $\mu\text{g}/\text{mL}$; BD Biosciences) and PI (0.5 $\mu\text{g}/\text{mL}$; Sigma-Aldrich) staining or by the automated counting of trypan-blue-stained cells (Beckman Vi-CELL XR cell viability analyzer). Q-VD-OPH (BioVision, Milpitas, CA, USA), BAPTA (CalbioChem; Merck, Billerica, MA, USA), U73122 (Sigma-Aldrich), 2-APB (Sigma-Aldrich), and dantrolene (Sigma-Aldrich) were used as indicated in the figure legends. Two-way ANOVA was performed using GraphPad Prism 8.0 software for statistical analysis.

4.3. Cell Viability Evaluation by Impedance Measurement. The xCELLigence system (ACEA Biosciences Inc.) monitors cellular events in real time without the incorporation of labels. The system measures the electrical impedance across interdigitated micro-electrodes integrated on the bottom of tissue culture E-Plates (16-well). The impedance measurement provides quantitative information about the biological status of the cells, including cell number, viability, and morphology. With regard to cell culture, A549 cells were grown in RPMI 1640 medium supplemented with 10% fetal bovine serum and 2 mM L-glutamine. The peptide incubations were performed in RPMI-1640 medium supplemented with 2 mM L-glutamine and 0.2% BSA (incubation medium). For our experiments, 50 μL of growth medium was added to each well of the 16-well E-plate to measure background levels of impedance. Then 150 μL of cell suspension was added to reach a cell density of 20 000 cells/well. Cells were allowed to seed at room temperature for 30 min and then placed in the reader at 37 $^{\circ}\text{C}$ and 5% CO_2 for real-time recording of the cell index. The following day, the growth medium was removed and replaced with 100 μL of the incubation medium. After stabilization of the impedance signal for 2 h, 100 μL of incubation medium containing 2-fold peptide concentrations was added to the cells in order to reach the desired concentration in the well (direct addition of DMSO caused stress and damaged the cells). Negative controls were treated with the vehicle (DMSO at 0.4% final concentration). Each condition was tested in triplicate or quadruplicate and in two independent experiments. The cells were monitored every minute until 24 h after treatment.

■ ASSOCIATED CONTENT

5 Supporting Information

The Supporting Information is available free of charge on the ACS Publications website at DOI: 10.1021/acs.jmedchem.9b00024.

Additional experimental details concerning (1) synthesis and characterization of the peptides, (2) stability studies, (3) structural analyses, (4) binding affinity measurements, (5) cell viability evaluation through impedance, (6) flow cytometry, (7) cell death induction, and (8) cancer cell lines used for *in vitro* experiments (PDF) Molecular SMILES strings (CSV)

■ AUTHOR INFORMATION

Corresponding Author

*E-mail: philippe.karoyan@sorbonne-universite.fr. Phone: +33 1 44274469.

ORCID

Mikail D. Levasseur: 0000-0003-4228-0875

Olivier Lequin: 0000-0001-5307-3068

Philippe Karoyan: 0000-0003-1525-6474

Author Contributions

◆T.D., E.P., and L.G.-M. contributed equally. T.D., M.D.L., C.N., E.L., and L.G.-M. performed all of the peptide syntheses. T.D. performed the binding and impedance experiments (with P.G. and E.L. for binding by Octed Red and with K.H. and

N.A. for the impedance). O.L. performed the structural studies and analyses. K.H. and L.G.-M. performed the in vitro PCD studies with the A549 cell line. L.G.-M., E.P., and L.H. performed the in vitro PCD studies with the MEC-1 cell line. P.K., H.M.-B., and S.A.S. supervised the cell death experimental work. P.K. conceived and supervised this project, designed all of the mimetic peptides and the experiments, interpreted all of the data, and wrote the draft of the manuscript. P.K. wrote the manuscript with contributions from T.D. and L.G.-M. and review by the coauthors.

Notes

The authors declare the following competing financial interest(s): Patent applications PCT/EP2013/061727, PCT/EP2014/077335, and PCT/EP2017/061223 included results from this paper.

ACKNOWLEDGMENTS

This work was supported by the Labex Michem (Ph.D. thesis grant to T.D.), the IPV Program (Ph.D. thesis grant to E.P.), the French National Cancer Institute (Grant INCa-5839), ECOS Nord (M17S01), and Curamus (08ACUR2018). P.K. is grateful to SATT Lutec and DGRIT from Sorbonne Université for helpful logistical and financial support and to Philippe Gene, Fabrice Viviani, and Alexis Denis from Oncodesign for hosting the LBM team.

ABBREVIATIONS USED

AnV, annexin-V; BALB/c mice, Bagg albino mice; CD47, cluster of differentiation 47; CLL, chronic lymphocytic leukemia; CSD, chemical shift deviation; FCM, flow cytometry; MEC-1, chronic B cell leukemia; LC₅₀, lethal concentration of drug leading to death of 50% of cells; NSG mice, NOD scid gamma mice; PI, propidium iodide; RCD, regulated cell death; ROE, rotating-frame Overhauser effect; RTCA, real-time cell analyzer; SPPS, solid-phase peptide synthesis; TSP-1, thrombospondin-1

REFERENCES

- (1) Soto-Pantoja, D. R.; Kaur, S.; Roberts, D. D. CD47 Signaling Pathways Controlling Cellular Differentiation and Responses to Stress. *Crit. Rev. Biochem. Mol. Biol.* **2015**, *50* (53), 212–230.
- (2) Oldenborg, P. A.; Zheleznyak, A.; Fang, Y. F.; Lagenaur, C. F.; Gresham, H. D.; Lindberg, F. P. Role of CD47 as a Marker of Self on Red Blood Cells. *Science* **2000**, *288*, 2051–2054.
- (3) (a) Chao, M. P.; Alizadeh, A. A.; Tang, C.; Myklebust, J. H.; Varghese, B.; Gill, S.; Jan, M.; Cha, A. C.; Chan, C. K.; Tan, B. T.; Park, C. Y.; Zhao, F.; Kohrt, H. E.; Malumbres, R.; Briones, J.; Gascoyne, R. D.; Lossos, I. S.; Levy, R.; Weissman, I. L.; Majeti, R. Anti-CD47 Antibody Synergizes with Rituximab to Promote Phagocytosis and Eradicate Non-Hodgkin Lymphoma. *Cell* **2010**, *142*, 699–713. (b) Chao, M. P.; Weissman, I. L.; Majeti, R. The CD47-SIRP α Pathway in Cancer Immune Evasion and Potential Therapeutic Implications. *Curr. Opin. Immunol.* **2012**, *24*, 225–232. (c) Willingham, S. B.; Volkmer, J.-P.; Gentles, A. J.; Sahoo, D.; Dalerba, P.; Mitra, S. S.; Wang, J.; Contreras-Trujillo, H.; Martin, R.; Cohen, J. D.; Lovelace, P.; Scheeren, F. A.; Chao, M. P.; Weiskopf, K.; Tang, C.; Volkmer, A. K.; Naik, T. J.; Storm, T. A.; Mosley, A. R.; Edris, B.; Schmid, S. M.; Sun, C. K.; Chua, M.-S.; Murillo, O.; Rajendran, P.; Cha, A. C.; Chin, R. K.; Kim, D.; Adorno, M.; Raveh, T.; Tseng, D.; Jaiswal, S.; Enger, P. Ø.; Steinberg, G. K.; Li, G.; So, S. K.; Majeti, R.; Harsh, G. R.; van de Rijn, M.; Teng, N. N. H.; Sunwoo, J. B.; Alizadeh, A. A.; Clarke, M. F.; Weissman, I. L. The CD47-Signal Regulatory Protein Alpha (SIRP α) Interaction is a Therapeutic Target for Human Solid Tumors. *Proc. Natl. Acad. Sci. U. S. A.* **2012**, *109* (17), 6662–6667. (d) Soto-Pantoja, D. R.; Stein, E. V.; Rogers,

- N. M.; Sharifi-Sanjani, M.; Isenberg, J. S.; Roberts, D. D. Therapeutic Opportunities for Targeting the Ubiquitous Cell Surface Receptor CD47. *Expert Opin. Ther. Targets* **2013**, *17*, 89–103. (e) Tseng, D.; Volkmer, J. P.; Willingham, S. B.; Contreras-Trujillo, H.; Fathman, J. W.; Fernhoff, N. B.; Seita, J.; Inlay, M. A.; Weiskopf, K.; Miyaniishi, M.; Weissman, I. L. Anti-CD47 Antibody-Mediated Phagocytosis of Cancer by Macrophages Primes an Effective Antitumor T-Cell Response. *Proc. Natl. Acad. Sci. U. S. A.* **2013**, *110* (27), 11103–11108. (f) Gholamin, S.; Mitra, S. S.; Feroze, A. H.; Liu, J.; Kahn, S. A.; Zhang, M.; Esparza, R.; Richard, C.; Ramaswamy, V.; Remke, M.; Volkmer, A. K.; Willingham, S.; Ponnuswami, A.; McCarty, A.; Lovelace, P.; Storm, T. A.; Schubert, S.; Hutter, G.; Narayanan, C.; Chu, P.; Raabe, E. H.; Harsh, G. T.; Taylor, M. D.; Monje, M.; Cho, Y. J.; Majeti, R.; Volkmer, J. P.; Fisher, P. G.; Grant, G.; Steinberg, G. K.; Vogel, H.; Edwards, M.; Weissman, I. L.; Cheshier, S. H. Disrupting the CD47-SIRP α Anti-Phagocytic Axis by a Humanized Anti-CD47 Antibody is an Efficacious Treatment for Malignant Pediatric Brain Tumors. *Sci. Transl. Med.* **2017**, *9* (381), eaf2968. (g) Buatois, V.; Johnson, Z.; Salgado-Pires, S.; Papaioannou, A.; Hatterer, E.; Chauchet, X.; Richard, F.; Barba, L.; Daubeuf, B.; Cons, L.; Broyer, L.; D'Asaro, M.; Matthes, T.; LeGallou, S.; Fest, T.; Tarte, C.; Clarke Hinojosa, R. K.; Genescà Ferrer, E.; Ribera, J. M.; Dey, A.; Bailey, K.; Fielding, A. K.; Eissenberg, L.; Ritchey, J.; Rettig, M.; Dipersio, J. F.; Kosco-Vilbois, M. H.; Masternak, K.; Fischer, N.; Shang, L.; Ferlin, W. G. Preclinical Development of a Bispecific Antibody that Safely and Effectively Targets CD19 and CD47 for the Treatment of B-Cell Lymphoma and Leukemia. *Mol. Cancer Ther.* **2018**, *17* (8), 1739–1751. (h) Advani, R.; Flinn, I.; Popplewell, L.; Forero, A.; Bartlett, N. L.; Ghosh, N.; Kline, J.; Roschewski, M.; LaCasce, A.; Collins, G. P.; Tran, T.; Lynn, J.; Chen, J. Y.; Volkmer, J. P.; Agoram, B.; Huang, J.; Majeti, R.; Weissman, I. L.; Takimoto, C. H.; Chao, M. P.; Smith, S. M. CD47 Blockade by Hu5F9-G4 and Rituximab in Non-Hodgkin's Lymphoma. *N. Engl. J. Med.* **2018**, *379*, 1711–1721. (i) Russ, A.; Hua, A. B.; Montfort, W. R.; Rahman, B.; Riaz, I. B.; Khalid, M. U.; Carew, J. S.; Nawrocki, S. T.; Persky, D.; Anwer, F. Blocking “Don't Eat Me” Signal of CD47-SIRP α in Hematological Malignancies, an In-Depth Review. *Blood Rev.* **2018**, *32*, 480–489.
- (4) Sick, E.; Jeanne, A.; Schneider, C.; Dedieu, S.; Takeda, K.; Martiny, L. CD47 Update: a Multifaceted Actor in the Tumour Microenvironment of Potential Therapeutic Interest. *Br. J. Pharmacol.* **2012**, *167*, 1415–1430.
- (5) Jeanne, A.; Martiny, L.; Dedieu, S. Thrombospondin-Targeting TAX2 Peptide Impairs Tumor Growth in Preclinical Mouse Models of Childhood Neuroblastoma. *Pediatr. Res.* **2017**, *81* (3), 480–488.
- (6) (a) Mateo, V.; Lagneaux, I.; Bron, D.; Biron, G.; Armant, M.; Delespesse, G.; Sarfati, M. CD47 Ligation Induces Caspase-Independent Cell Death in Chronic Lymphocytic Leukemia. *Nat. Med.* **1999**, *5* (11), 1277–1284. (b) Lih, C. J.; Wei, W.; Cohen, S. N. Tbx1: a Transcriptional Regulator of Thrombospondin-1 that Modulates Cellular Sensitivity to Taxanes. *Genes Dev.* **2006**, *20*, 2082–2095. (c) Lamy, L.; Foussat, A.; Brown, E. J.; Bornstein, P.; Ticchioni, M.; Bernard, A. Interactions Between CD47 and Thrombospondin Reduce Inflammation. *J. Immunol.* **2007**, *178*, 5930–5939. (d) Calippe, B.; Augustin, S.; Beguier, F.; Charles-Messance, H.; Poupel, L.; Conart, J. B.; Hu, S. J.; Lavalette, S.; Fauvet, A.; Rayes, J.; Levy, O.; Raoul, W.; Fitting, C.; Denèfle, T.; Pickering, M. C.; Harris, C.; Jorieux, S.; Sullivan, P. M.; Sahel, J. A.; Karoyan, P.; Sapièha, P.; Guillonéau, X.; Gautier, E. L.; Sennlaub, F. Complement Factor H Inhibits CD47-Mediated Resolution of Inflammation. *Immunity* **2017**, *46* (2), 261–272.
- (7) Martinez-Torres, A. C.; Quiney, C.; Attout, T.; Boulet, H.; Herbi, L.; Vela, L.; Barbier, S.; Chateau, D.; Chapiro, E.; Nguyen-Khac, F.; Davi, F.; Le Garff-Tavernier, M.; Moumne, R.; Sarfati, M.; Karoyan, P.; Merle-Beral, H.; Launay, P.; Susin, S. A. CD47 Agonist Peptides Induce Programmed Cell Death in Refractory Chronic Lymphocytic Leukemia B Cells via PLCG γ Activation: Evidence from Mice and Humans. *PLoS medicine* **2015**, *12* (3), No. e1001796.

- (8) (a) Karoyan, P.; Gomes-Morales, L.; Bellier, J.; Pramill, E.; Denèfle, T.; Rademaker, G.; Lardé, E.; Malgorn, C.; Kaminska, M.; Linhart, V.; Grillot, D.; Thai, R.; Merle-Beral, H.; Dedobbeleer, M.; Agirman, F.; Bellhacène, A.; Grondin, P.; Ancelin, N.; Martínez-Torres, A.-C.; Susin, S.; Devel, L.; Castronovo, V. PKHB1, a TSP-1 Peptide Mimic, Interacts with CD47, Triggers Regulated Cell Death with Potent Anti-Cancer Activities in Vivo. Unpublished Results. (b) Denèfle, T.; Boulet, H.; Herbi, L.; Newton, C.; Martínez-Torres, A. C.; Guez, A.; Pramill, E.; Quiney, C.; Pourcelot, M.; Levasseur, M. D.; Lardé, E.; Moumné, R.; Ogi, F. X.; Grondin, P.; Merle-Beral, H.; Lequin, O.; Susin, S. A.; Karoyan, P. Thrombospondin-1 Mimetic Agonist Peptides Induce Selective Death in Tumor Cells: Design, Synthesis, and Structure-Activity Relationship Studies. *J. Med. Chem.* **2016**, *59* (18), 8412–8421.
- (9) (a) Uscanga-Palomeque, A. C.; Calvillo-Rodríguez, K. M.; Gómez-Morales, L.; Lardé, E.; Denèfle, T.; Caballero-Hernández, D.; Merle-Beral, H.; Susin, S. A.; Karoyan, P.; Martínez-Torres, A.-C.; Rodríguez-Padilla, C. CD47 Agonist Peptide PKHB1 Induces Immunogenic Cell Death in T-Cell Acute Lymphoblastic Leukemia Cells. *Cancer Sci.* **2019**, *110* (1), 256–268. (b) Martínez-Torres, A. C.; Calvillo-Rodríguez, K. M.; Uscanga-Palomeque, A. C.; Gómez-Morales, L.; Mendoza-Revelles, R.; Caballero-Hernández, D.; Karoyan, P.; Rodríguez-Padilla, C. PKHB1 Tumor Cell Lysate Induces Antitumor Immune System Stimulation and Tumor Regression in Syngenic Mice with Tumoral T Lymphoblasts. *J. Oncol.* **2019**, *2019*, 9852361.
- (10) (a) Diao, L.; Meibohm, B. Pharmacokinetics and Pharmacokinetic-Pharmacodynamic Correlations of Therapeutic Peptides. *Clin. Pharmacokinet.* **2013**, *52* (10), 855–868. (b) Di, L. Strategic Approaches to Optimizing Peptide ADME Properties. *AAPS J.* **2015**, *17* (1), 134–143.
- (11) (a) Henninot, A.; Collins, J. C.; Nuss, J. M. The Current State of Peptide Drug Discovery: Back to the Future? *J. Med. Chem.* **2018**, *61* (4), 1382–1414. (b) Tsomaia, N. Peptide Therapeutics: Targeting the Undruggable Space. *Eur. J. Med. Chem.* **2015**, *94*, 459–470. (c) Angell, Y.; Holford, M.; Moos, W. H. Building on Success: A Bright Future for Peptide Therapeutics. *Protein Pept. Lett.* **2018**, *25* (12), 1044–1050.
- (12) (a) Lawler, J. The Functions of Thrombospondin-1 and-2. *Curr. Opin. Cell Biol.* **2000**, *12* (5), 634–640. (b) Anilkumar, N.; Annis, D. S.; Mosher, D. F.; Adams, J. C. Trimeric Assembly of the C-Terminal Region of Thrombospondin-1 or Thrombospondin-2 Is Necessary for Cell Spreading and Fascin Spike Organisation. *J. Cell Sci.* **2002**, *115* (11), 2357–2366. (c) Kvensakul, M.; Adams, J. C.; Hohenester, E. Structure of a Thrombospondin C-Terminal Fragment Reveals a Novel Calcium Core in the Type 3 Repeats. *EMBO J.* **2004**, *23* (6), 1223–1233. (d) Adams, J. C.; Bentley, A. A.; Kvensakul, M.; Hatherley, D.; Hohenester, E. Extracellular Matrix Retention of Thrombospondin 1 is Controlled by its Conserved C-Terminal Region. *J. Cell Sci.* **2008**, *121* (6), 784–795.
- (13) Mammen, M.; Choi, S. K.; Whitesides, G. M. Polyvalent Interactions in Biological Systems: Implications for Design and Use of Multivalent Ligands and Inhibitors. *Angew. Chem., Int. Ed.* **1998**, *37* (20), 2754–2794.
- (14) (a) Cwirła, S. E.; Balasubramanian, P.; Duffin, D. J.; Wagstrom, C. R.; Gates, C. M.; Singer, S. C.; Davis, A. M.; Tansik, R. L.; Matheakis, L. C.; Boytos, C. M.; Schatz, P. J.; Baccanari, D. P.; Wrighton, N. C.; Barrett, R. W.; Dower, W. J. Peptide Agonist of the Thrombopoietin Receptor as Potent as the Natural Cytokine. *Science* **1997**, *276* (5319), 1696–1699. (b) Morcos, S. K. Contrast Media and Modern Imaging. *Eur. J. Radiol.* **2006**, *60* (3), 305–306.
- (15) Meldal, M.; Tornøe, C. W. Cu-Catalyzed Azide–Alkyne Cycloaddition. *Chem. Rev.* **2008**, *108* (8), 2952–3015.
- (16) Karoyan, P.; Launay, P.; Merle-Beral, H.; Susin, S. A. Method and Pharmaceutical Composition for Use in the Treatment of Cancer. WO 2013182650 A1, 2013.
- (17) Saludes, J. P.; Morton, L. A.; Coulup, S. K.; Fiorini, Z.; Cook, B. M.; Beninson, L.; Chapman, E. R.; Fleschner, M.; Yin, H. Multivalency Amplifies the Selection and Affinity of Bradykinin-Derived Peptides for Lipid Nanovesicles. *Mol. Biosyst.* **2013**, *9* (8), 2005–2009.
- (18) (a) Vermes, I.; Haanen, C.; Reutelingsperger, C. Flow cytometry of apoptotic cell death. *J. Immunol. Methods* **2000**, *243*, 167–190. (b) Crowley, L. C.; Scott, A. P.; Marfell, B. J.; Boughaba, J. A.; Chojnowski, G.; Waterhouse, N. J. Measuring Cell Death by Propidium Iodide Uptake and Flow Cytometry. *Cold Spring Harbor Protoc.* **2016**, *2016* (7), 647–651.
- (19) (a) Giaever, I.; Keese, C. R. Monitoring Fibroblast Behavior in Tissue Culture with an Applied Electric Field. *Proc. Natl. Acad. Sci. U. S. A.* **1984**, *81* (12), 3761–3764. (b) Scott, C. W.; Peters, M. F. Label-Free Whole-Cell Assays: Expanding the Scope of GPCR Screening. *Drug Discovery Today* **2010**, *15* (17–18), 704–716. (c) Webling, K.; Groves-Chapman, J. L.; Ruesson, J.; Saar, I.; Lang, A.; Sillard, R.; Jakovenko, E.; Kofler, B.; Holmes, P. V.; Langel, U. Pharmacological Stimulation of GAL1R But Not GAL2R Attenuates Kainic Acid-Induced Neuronal Cell Death in the Rat Hippocampus. *Neuropeptides* **2016**, *58*, 83–92. (d) Türker Şener, L.; Albeniz, G.; Dinç, B.; Albeniz, I. iCELLigence Real-Time Cell Analysis System for Examining the Cytotoxicity of Drugs to Cancer Cell Lines. *Exp. Ther. Med.* **2017**, *14* (3), 1866–1870. (e) Ke, N.; Wang, X.; Xu, X.; Abassi, Y. A. The xCELLigence System for Real-Time and Label-Free Monitoring of Cell Viability. *Methods Mol. Biol.* **2011**, *740*, 33–43. (f) Xing, J. Z.; Zhu, L.; Jackson, J. A.; Gabos, S.; Sun, X. J.; Wang, X. B.; Xu, X. Dynamic Monitoring of Cytotoxicity on Microelectronic Sensors. *Chem. Res. Toxicol.* **2005**, *18* (2), 154–161.
- (20) (a) Yan, G.; Efferth, T. Cell Harvesting Methods Affect Cellular Integrity of Adherent Cells During Apoptosis Detection. *Anticancer Res.* **2018**, *38* (12), 6669–6672.
- (21) Galluzzi, L.; Vitale, I.; Aaronson, S. A.; Abrams, J. M.; Adam, D.; Agostinis, P.; Alnemri, E. S.; Altucci, L.; Amelio, I.; Andrews, D. W.; Annicchiarico-Petruzzelli, M.; Antonov, A. V.; Arama, E.; Baehrecke, E. H.; Barlev, N. A.; Bazan, N. G.; Bernassola, F.; Bertrand, M. J. M.; Bianchi, K.; Blagosklonny, M. V.; Blomgren, K.; Borner, C.; Boya, P.; Brenner, C.; Campanella, M.; Candi, E.; Carmona-Gutierrez, D.; Cecconi, F.; Chan, F. K.; Chandel, N. S.; Cheng, E. H.; Chipuk, J. E.; Cidlowski, J. A.; Ciechanover, A.; Cohen, G. M.; Conrad, M.; Cubillos-Ruiz, J. R.; Czabotar, P. E.; D'Angiolella, V.; Dawson, T. M.; Dawson, V. L.; De Laurenzi, V.; De Maria, R.; Debatin, K. M.; DeBerardinis, R. J.; Deshmukh, M.; Di Daniele, N.; Di Virgilio, F.; Dixit, V. M.; Dixon, S. J.; Duckett, C. S.; Dynlacht, B. D.; El-Deiry, W. S.; Elrod, J. W.; Fimia, G. M.; Fulda, S.; García-Sáez, A. J.; Garg, A. D.; Garrido, C.; Gavathiotis, E.; Golstein, P.; Gottlieb, E.; Green, D. R.; Greene, L. A.; Gronemeyer, H.; Gross, A.; Hajnóczky, G.; Hardwick, J. M.; Harris, I. S.; Hengartner, M. O.; Hetz, C.; Ichijo, H.; Jaattela, M.; Joseph, B.; Jost, P. J.; Juin, P. P.; Kaiser, W. J.; Karin, M.; Kaufmann, T.; Kepp, O.; Kimchi, A.; Kitsis, R. N.; Klionsky, D. J.; Knight, R. A.; Kumar, S.; Lee, S. W.; Lemasters, J. J.; Levine, B.; Linkermann, A.; Lipton, S. A.; Lockshin, R. A.; Lopez-Otin, C.; Lowe, S. W.; Luedde, T.; Lugli, E.; MacFarlane, M.; Madeo, F.; Malewicz, M.; Malorni, W.; Manic, G.; Marine, J. C.; Martin, S. J.; Martinou, J. C.; Medema, J. P.; Mehlen, P.; Meier, P.; Melino, S.; Miao, E. A.; Molkentin, J. D.; Moll, U. M.; Munoz-Pinedo, C.; Nagata, S.; Nunez, G.; Oberst, A.; Oren, M.; Overholtzer, M.; Pagano, M.; Panaretakis, T.; Pasparakis, M.; Penninger, J. M.; Pereira, D. M.; Pervaiz, S.; Peter, M. E.; Piacentini, M.; Pinton, P.; Prehn, J. H. M.; Puthalakath, H.; Rabinovich, G. A.; Rehm, M.; Rizzuto, R.; Rodrigues, C. M. P.; Rubinsztein, D. C.; Rudel, T.; Ryan, K. M.; Sayan, E.; Scorrano, L.; Shao, F.; Shi, Y.; Silke, J.; Simon, H. U.; Sistigu, A.; Stockwell, B. R.; Strasser, A.; Szabadkai, G.; Tait, S. W. G.; Tang, D.; Tavernarakis, N.; Thorburn, A.; Tsujimoto, Y.; Turk, B.; Vanden Berghe, T.; Vandenabeele, P.; Vander Heiden, M. G.; Villunger, A.; Virgin, H. W.; Vousden, K. H.; Vucic, D.; Wagner, E. F.; Walczak, H.; Wallach, D.; Wang, Y.; Wells, J. A.; Wood, W.; Yuan, J.; Zakeri, Z.; Zhivotovskiy, B.; Zitvogel, L.; Melino, G.; Kroemer, G. Molecular Mechanisms of Cell Death: Recommendations of the Nomenclature Committee on Cell Death 2018. *Cell Death Differ.* **2018**, *25* (3), 486–541.

- (22) Long, F. A.; McDevit, W. F. Activity Coefficients of Nonelectrolyte Solutes in Aqueous Salt Solutions. *Chem. Rev.* **1952**, *51* (1), 119–169.
- (23) (a) Chatterjee, J.; Gilon, C.; Hoffman, A.; Kessler, H. N-Methylation of Peptides: a New Perspective in Medicinal Chemistry. *Acc. Chem. Res.* **2008**, *41* (10), 1331–1342. (b) Chatterjee, J.; Rechenmacher, F.; Kessler, H. N-Methylation of Peptides and Proteins: an Important Element for Modulating Biological Functions. *Angew. Chem., Int. Ed.* **2013**, *52* (1), 254–269.
- (24) (a) Tonelli, A. E. Conformational characteristics of L-proline oligomers. *J. Am. Chem. Soc.* **1970**, *92* (21), 6187–6190. (b) Tonelli, A. E. On the Stability of Cis and Trans Amide Bond Conformations in Polypeptides. *J. Am. Chem. Soc.* **1971**, *93* (26), 7153–7155. (c) Tonelli, A. E. Conformational Characteristics of Polypeptides Containing Isolated L-Proline Residues with Cis Peptide Bonds. *J. Mol. Biol.* **1974**, *86* (3), 627–635. (d) Vitoux, B.; Aubry, A.; Cung, M. T.; Marraud, M. N-Methyl Peptides VII. Conformational Perturbations Induced by N-Methylation of Model Dipeptides. *Int. J. Pept. Protein Res.* **1986**, *27* (6), 617–632.
- (25) Marelli, U. K.; Ovadia, O.; Frank, A. O.; Chatterjee, J.; Gilon, C.; Hoffman, A.; Kessler, H. Cis-Peptide Bonds: A Key for Intestinal Permeability of Peptides? *Chem. - Eur. J.* **2015**, *21* (43), 15148–15152.
- (26) Rajarathnam, K.; Sykes, B. D.; Kay, C. M.; Dewald, B.; Geiser, T.; Baggiolini, M.; Clark-Lewis, I. Neutrophil Activation by Monomeric Interleukin-8. *Science* **1994**, *264* (5155), 90–92.
- (27) Hughes, E.; Burke, R. M.; Doig, A. J. Inhibition of Toxicity in the Beta-Amyloid Peptide Fragment Beta-(25–35) Using N-Methylated Derivatives: a General Strategy to Prevent Amyloid Formation. *J. Biol. Chem.* **2000**, *275* (33), 25109–25115.
- (28) Kokkonen, N.; Stott, K.; Amijee, H.; Mason, J. M.; Doig, A. J. N-Methylated Peptide Inhibitors of Beta-Amyloid Aggregation and Toxicity. *Biochemistry* **2006**, *45* (32), 9906–9918.
- (29) Brogini, M.; Marchini, S. V.; Galliera, E.; Borsotti, P.; Tarabozzi, G.; Erba, E.; Sironi, M.; Jimeno, J.; Faircloth, G. T.; Giavazzi, R.; D'Incalci, M. Aplidine, A New Anticancer Agent of Marine Origin, Inhibits Vascular Endothelial Growth Factor (VEGF) Secretion and Blocks VEGF-VEGFR-1 (flt-1) Autocrine Loop in Human Leukemia Cells MOLT-4. *Leukemia* **2003**, *17* (1), 52–59.
- (30) Kindler, H. L.; Tothy, P. K.; Wolff, R.; McCormack, R. A.; Abbruzzese, J. L.; Mani, S.; Wade-Oliver, K. T.; Vokes, E. E. Phase II Trials of Dolastatin-10 in Advanced Pancreaticobiliary Cancers. *Invest. New Drugs* **2005**, *23* (5), 489–493.
- (31) Tamura, K.; Nakagawa, K.; Kurata, T.; Satoh, T.; Nogami, T.; Takeda, K.; Mitsuoka, S.; Yoshimura, N.; Kudoh, S.; Negoro, S.; Fukuoka, M. Phase I Study of TZZT-1027, a Novel Synthetic Dolastatin 10 Derivative and Inhibitor of Tubulin Polymerization, which was Administered to Patients with Advanced Solid Tumors on Days 1 and 8 in 3-Week Courses. *Cancer Chemother. Pharmacol.* **2007**, *60* (2), 285–293.
- (32) Mas-Moruno, C.; Rechenmacher, F.; Kessler, H. Cilengitide: the First Anti-Angiogenic Small Molecule Drug Candidate Design, Synthesis and Clinical Evaluation. *Anti-Cancer Agents Med. Chem.* **2010**, *10* (10), 753–768.
- (33) Biron, E.; Chatterjee, J.; Kessler, H. Optimized Selective N-Methylation of Peptides on Solid Support. *J. Pept. Sci.* **2006**, *12* (3), 213–219.
- (34) Rebres, R. A.; Vaz, L. E.; Green, J. M.; Brown, E. J. Normal Ligand Binding and Signaling by CD47 (Integrin-Associated Protein) Requires a Long Range Disulfide Bond Between the Extracellular and Membrane-Spanning Domains. *J. Biol. Chem.* **2001**, *276* (37), 34607–34616.
- (35) The scramble peptide was designed using a scrambler tool, available at <https://peptidexus.com/article/sequence-scrambler> (accessed Feb 10, 2019).
- (36) Avbelj, F.; Grdadolnik, S. G.; Grdadolnik, J.; Baldwin, R. L. Intrinsic Backbone Preferences are Fully Present in Blocked Amino Acids. *Proc. Natl. Acad. Sci. U. S. A.* **2006**, *103* (5), 1272–1277.
- (37) (a) Gordon, D. J.; Sciarretta, K. L.; Meredith, S. C. Inhibition of Beta-Amyloid (40) Fibrillogenesis and Disassembly of Beta-Amyloid (40) Fibrils by Short Beta-Amyloid Congeners Containing N-Methyl Amino Acids at Alternate Residues. *Biochemistry* **2001**, *40* (28), 8237–8245. (b) Sciarretta, K. L.; Boire, A.; Gordon, D. J.; Meredith, S. C. Spatial Separation of β -Sheet Domains of β -Amyloid: Disruption of Each β -Sheet by N-Methyl Amino Acids. *Biochemistry* **2006**, *45* (31), 9485–9495.
- (38) Lee, W.; Tonelli, M.; Markley, J. L. NMR-FAM-SPARKY: Enhanced Software for Biomolecular NMR Spectroscopy. *Bioinformatics* **2015**, *31* (8), 1325–1327.
- (39) Sagan, S.; Karoyan, P.; Lequin, O.; Chassaing, G.; Lavielle, S. N- and C-Alpha-Methylation in Biologically Active Peptides: Synthesis, Structural and Functional Aspects. *Curr. Med. Chem.* **2004**, *11* (21), 2799–2822.
- (40) Sagan, S.; Karoyan, P.; Chassaing, G.; Lavielle, S. Further Delineation of the Two Binding Sites (R*) Associated with Tachykinin Neurokinin-1 Receptors Using [3-Prolinomethionine¹¹]-SP Analogues. *J. Biol. Chem.* **1999**, *274* (34), 23770–23776.
- (41) Plum, A.; Bjerring Jensen, L.; Bøggild Kristensen, J. In Vitro Protein Binding of Liraglutide In Human Plasma Determined by Reiterated Stepwise Equilibrium Dialysis. *J. Pharm. Sci.* **2013**, *102* (8), 2882–2888.
- (42) Liu, Y.; Shoji-Kawata, S.; Sumpter, R.-M.; Wei, Y.; Ginot, V.; Zhang, L.; Posner, B.; Tran, K. A.; Green, D. R.; Xavier, R. J.; Shaw, S. Y.; Clarke, P. G. H.; Puyal, J.; Levine, B. Autosis is a Na⁺,K⁺-ATPase-Regulated Form of Cell Death Triggered by Autophagy-Inducing Peptides, Starvation, and Hypoxia–Ischemia. *Proc. Natl. Acad. Sci. U. S. A.* **2013**, *110* (51), 20364–20371.
- (43) Zhang, X.; Fan, J.; Wang, S.; Li, Y.; Wang, Y.; Li, S.; Luan, J.; Wang, Z.; Song, P.; Chen, Q.; Tian, W.; Ju, D. Targeting CD47 and Autophagy Elicited Enhanced Antitumor Effects in Non-Small Cell Lung Cancer. *Cancer Immunol. Res.* **2017**, *5* (5), 363–375.
- (44) (a) Li, H.; Aneja, R.; Chaiken, I. Click Chemistry in Peptide-Based Drug Design. *Molecules* **2013**, *18* (8), 9797–9817. (b) Angell, Y. L.; Burgess, K. Peptidomimetics via Copper-Catalyzed Azide-Alkyne Cycloadditions. *Chem. Soc. Rev.* **2007**, *36* (10), 1674–1689. (c) Schellinger, J. G.; Danan-Leon, L. M.; Hoch, J. A.; Kassa, A.; Srivastava, I.; Davis, D.; Gervay-Hague, J. Synthesis of a Trimeric gp120 Epitope Mimic Conjugated to a T-Helper Peptide to Improve Antigenicity. *J. Am. Chem. Soc.* **2011**, *133* (10), 3230–3233. (d) Byrne, C.; McEwan, P. A.; Emsley, J.; Fischer, P. M.; Chan, W. C. End-Stapled Homo and Hetero Collagen Triple Helices: a Click Chemistry Approach. *Chem. Commun.* **2011**, *47* (9), 2589–2591.
- (45) Fernandez-Llamazares, A. I.; Garcia, J.; Adan, J.; Meunier, D.; Mitjans, F.; Spengler, J.; Albericio, F. The Backbone N-(4-Azidobutyl) Linker for the Preparation of Peptide Chimera. *Org. Lett.* **2013**, *15* (17), 4572–4575.
- (46) Wishart, D. S.; Bigam, C. G.; Holm, A.; Hodges, R. S.; Sykes, B. D. ¹H, ¹³C and ¹⁵N Random Coil NMR Chemical Shifts of the Common Amino Acids. I. Investigations of Nearest-Neighbor Effects. *J. Biomol. NMR* **1995**, *5* (1), 67–81.

Supplementary material

SUPPORTING INFORMATION

Homotrimerization Approach in the Design of Thrombospondin-1 Mimetic Peptides with Improved Potency in Triggering Regulated Cell Death of Cancer Cells

Thomas Denèfle^{†,‡,◆}, Elodie Pramit^{†,‡,#,◆}, Luis Gómez-Morales^{†,‡,||,◆}, Mikail D. Levasseur^{†,‡}, Eva Lardé^{†,‡}, Clara Newton^{†,‡}, Kenny Herry[⊥], Linda Herbi[#], Yann Lamotte[⊥], Estelle Odile^{†,‡}, Nicolas Ancellin[⊥], Pascal Grondin[⊥], Ana-Carolina Martinez-Torres^{||}, Fabrice Viviani[⊥], Hélène Merle-Beral[#], Olivier Lequin[†], Santos A. Susin[#] and Philippe Karoyan^{*,†,‡,§,∇,◦}

◆Equal contribution

† Sorbonne Université, École Normale Supérieure, PSL University, CNRS, Laboratoire des Biomolécules, LBM, 75005 Paris, France

‡ Sorbonne Université, École Normale Supérieure, PSL University, CNRS, Laboratoire des Biomolécules, LBM, Site OncoDesign, 25-27 Avenue du Québec, 91140 Les Ulis, France

§ SiRIC CURAMUS (CANCER UNITED RESEARCH ASSOCIATING MEDICINE, UNIVERSITY & SOCIETY, Site de Recherche Intégrée sur le Cancer) IUC, AP HP.6, Sorbonne Université 75005 Paris, France

|| Laboratory of Immunology and Virology, Universidad Autónoma de Nuevo León, 66451 San Nicolas de los Garza, NL, Mexico

⊥ OncoDesign, 25 Avenue du Québec, 91140 Les Ulis, France

Cell Death and Drug Resistance in Lymphoproliferative Disorders Team, Centre de Recherche des Cordeliers, INSERM UMRS 1138, 75006 Paris, France

∇ Kayvisa AG, Industriestrasse, 44, 6300 Zug, Switzerland

◦ Kaybiotix GmbH, Zugerstrasse 32, 6340 Baar, Switzerland

Contents

1. Synthesis and characterization of the peptides
2. Stability studies
3. Structural analyses
4. Binding affinity measurements
5. Cell culture
6. Cell death induction and inhibition
7. Cell viability evaluation through impedance
8. Molecular formula strings

1. Synthesis and characterization of the peptides

General methods:

Chemicals: All commercial chemicals and solvents were reagent grade and were used without further purification unless otherwise specified. All reactions except those in aqueous media were carried out with the use of standard techniques for the exclusion of moisture. All reactions were performed under argon or nitrogen in oven-dried glassware using anhydrous solvents and standard syringe techniques. Peptide synthesis transformations and washes were performed at room temperature. All Fmoc carbamate protected amino acid derivatives, coupling reagents (PyOxim/Oxyma Pure), Fmoc-Rink Amide (200-400 mesh, loading 0.62 mmol/g) and 2-CTC resin (100-200 mesh, loading 1.6 mmol/g) were purchased from Iris Biotech (Marktredwitz, Germany). Reagents such as DIEA, piperidine, DMF, IPA, Ac₂O, MeOH, TFA and TIS were obtained from Sigma-Aldrich (Saint Louis, USA). Compounds molecular weights were calculated using ChemBioDraw® Ultra 12. All final products were of > 95% purity unless otherwise indicated (determined by analytical reverse phase LC-MS). Analytical data are given in Table S1.

Analytics: Two methods were conducted for LC-MS analysis. Method A: analytical HPLC was conducted on a X-Select CSH C18 XP column (30 × 4.6 mm id, 2.5 μm) eluting with 0.1% formic acid in water (solvent A) and 0.1% formic acid in acetonitrile (solvent B), using the following elution gradient 0 - 3.2 min: 0% to 50% B, 3.2 - 4 min 100% B, at a flow rate of 1.8 mL/min at 40 °C. The mass spectra (MS) were recorded on a Waters ZQ mass spectrometer using electrospray positive ionisation [ES⁺ to give (MH)⁺ molecular ions] or electrospray negative ionisation [ES⁻ to give (MH)⁻ molecular ions] modes. The cone voltage was 20 V. Method B: analytical HPLC was conducted on a X-Select CSH C18 XP column (30 × 4.6 mm id, 2.5 μm) eluting with 0.1% formic acid in water (solvent A) and 0.1% formic acid in acetonitrile (solvent B), using the following elution gradient 0 - 3.2 min: 5% to 100% B, 3.2 - 4 min: 100% B, at a flow rate of 1.8 mL/min at 40 °C. The mass spectra (MS) were recorded on a Waters ZQ mass

spectrometer using electrospray positive ionisation [ES+ to give (MH)⁺ molecular ions] or electrospray negative ionisation [ES- to give (MH)⁻ molecular ions] modes. The cone voltage was 20 V.

Purification: Preparative scale purification of peptides was performed by reverse phase HPLC on a Waters system consisted of a quaternary gradient module (Water 2535) and a dual wavelength UV/Visible Absorbance detector (Waters 2489), piloted by Empower Pro 3 software using the following columns: preparative Macherey-Nagel column (Nucleodur HTec, C18, 250 × 16 mm id, 5 µm, 110 Å) and preparative Higgins Analytical column (Proto 200, C18, 150 × 20 mm id, 5 µm, 200 Å) at a flow rate of 14 mL/min and 20 mL/min respectively. Small- scale crudes (< 30 mg) were purified using semi-preparative Ace column (Ace 5, C18, 250 × 10 mm id, 5 µm, 300 Å) at a flow rate of 5 mL/min. Purification gradients were chosen to get a ramp of approximately 1% solution B per minute in the interest area and UV detection was done at 220 nm and 280 nm. Peptide fractions from purification were analyzed by LC-MS (method A or B depending of retention time) or by analytical HPLC on a Dionex system consisted of an automated LC system (Ultimate 3000) equipped with an auto sampler, a pump block composed of two ternary gradient pumps and a dual wave-length detector, piloted by Chromeleon software. All LC-MS or HPLC analyses were performed on C18 columns. The pure fractions were gathered according to their purity and then freeze-dried using an Alpha 2/4 freeze dryer from Bioblock Scientific to get the expected peptide as a white powder. Final peptide purity (> 95%) of the corresponding pooled fractions was checked by LC-MS using method A.

Manual loading of the first amino acid:

Solid-phase peptide syntheses were performed in polypropylene Torviq syringes (10 or 20 mL) fitted with a polyethylene porous disc at the bottom and closed with an appropriate piston. Solvent and soluble reagents were removed through back and forth movements. The 2-CTC resin was previously swelled in strictly anhydrous DCM (distilled) for 2 h. Side-chain protected Fmoc-Aa-OH (0.30 mmol, 1 eq.) was coupled to 2-CTC resin (400 mg, loading 1.6 mmol/g) in the presence of DIEA (1.2 mmol, 4 eq.) in

DCM (4 mL). The unreacted sites on the resin were capped by washing with a mixture of DCM/MeOH/DIEA (17:2:1) repeated 3 times. Thus loading was reduced to 0.80 mmol/g for optimal peptide growth. In the case of Rink Amide resin, swollen in DCM was done similarly in 2 h (500 mg, loading 0.62 mmol/g). However, first coupling was directly performed with protected Fmoc-Aa-OH (1.2 mmol, 4 eq.), PyOxim (1.2 mmol, 4 eq.), Oxyma Pure (1.2 mmol, 4 eq.) and DIEA (2.4 mmol, 8 eq.) without loading decreasing.

Manual solid phase peptide synthesis:

In all syntheses the scale was 0.30 mmol. Fmoc group was split off by treatment with piperidine/DMF (1:4) (1 × 1 min, 1 × 10 min). Washing steps between deprotection and coupling were carried out with DMF (3 × 1 min), IPA (3 × 1 min) and DMF (3 × 1 min). Activation step was carried out with Fmoc-Aa-OH (1.2 mmol, 4 eq.), PyOxim (1.2 mmol, 4 eq.) as coupling agent, Oxyma Pure (1.2 mmol, 4 eq.) as auxiliary nucleophile, and DIEA (2.4 mmol, 8 eq.) as base. The activated amino acid is then transferred to the resin where the coupling was performed for 1 to 18 h. Supported coupling reactions were monitored by classical Kaiser test (solution kit from Sigma-Aldrich). When elongation of the peptide chain was completed, a MeOH washing step was added after final N-terminal Fmoc removal for complete shrinkage of the resin under vacuum.

Site-selective N-Methylation of peptide backbone:

Residue was N-methylated on solid-phase through Kessler's methodology: first, the free amino functionality was protected and activated with the o-nitrobenzenesulfonyl (o-NBS) group, then N-methylated using 1,8-diazabicyclo[5,4,0]undec-7-ene (DBU) and dimethylsulfate (DMS), and finally deprotected (removal of o-NBS) by treating the resin with β-mercaptoethanol and DBU.

- o-NBS Activation: A solution of o-NBS-Cl (4 eq.) and collidine (10 eq.) in NMP was added to the resin-bound free amine peptides and shaken for 15 min at room temperature. The resin was washed with NMP (5×).
- N-Methylation with DBU and DMS: A solution of DBU (3 eq.) in NMP was added to the resin bound o-NBS-protected peptides and shaken for 3 min. A solution of dimethylsulfate (10 eq.) in NMP was then added to the reaction mixture and shaken for

2 min. The resin was filtered off, washed once with NMP and the N-methylation procedure repeated once more. The resin was washed with NMP (5×).

- o-NBS Deprotection: The resin bound N α -methyl-N α -o-NBS-peptides was treated with a solution of β -mercaptoethanol (10 eq) and DBU (5 eq) in NMP for 5 min. The deprotection procedure was repeated once more and the resin was washed with NMP (5×).

Homotrimerization by solution phase click chemistry (CuAAC):

Typically, pure PKT16-N3 TFA salts (47,1 mg, 24 μ mol, 3.6 eq.) was taken up in 750 μ L MeOH that was frozen and put on a vacuum pump to remove gas molecules and then purged with N₂ for at least 30 min. To this mixture was added tripropargylamine (0.94 μ L, 6.7 μ mol, 1 eq.) in 250 μ L MeOH, followed by the addition of Tris[(1-benzyl-1H-1,2,3-triazol-4-yl)methyl]amine (TBTA, 21 mg, 40 μ mol, 6 eq.) and Tetrakis (acetonitrile)copper(I) hexafluorophosphate [(CH₃CN)₄Cu]PF₆, 78 mg, 203 μ mol, 30 eq.). To this mixture was added MeCN dropwise (around 20 drops) to bring everything into solution, and the reaction was allowed to proceed in a round-bottom flask at room temperature under nitrogen flow with constant stirring for 72 h. The sample was quenched with 5 mL H₂O, frozen, and then lyophilized. The dried crude product was re-suspended in 0.1 M EDTA (3×5 mL to rinse the tube), loaded on a 1.6 g zeo prep 90 C18 (part. size 40-63 μ m) cartridge, and sequentially eluted with 25 mL H₂O, 1:1 H₂O/MeCN, and MeCN. Each fraction was collected in a round-bottom flask and analyzed by LCMS (method A). The EDTA, H₂O and H₂O/MeCN fractions were concentrated to dryness, re-suspended in H₂O, filtered with 0.22 μ m filter and purified as described earlier to obtain [PKT16]₃ as a white powder (depending on experiments: 5 – 15% yield).

Final side-chain deprotection and cleavage from the resin:

The crude peptides were treated with the following cleavage cocktail: TFA/H₂O/TIS (95/2.5/2.5, 10 mL). The syringes were shaken for 3 h and then precipitated 3 times using cooled Et₂O (3 × 30 mL), recovered after centrifugations (3 × 5 min, 7800 rpm), diethyl ether was removed (3 times), and then the peptide pellets were dried (under nitrogen flow). The resulting crude peptide was dissolved in aqueous 0.1% (v/v) TFA.

Purification was conducted on reversed-phase HPLC Prep C18 column, eluting with 0.1% TFA in water (solvent A) and 0.1% TFA in acetonitrile (solvent B) as described earlier.

Analytical data of synthesized peptides

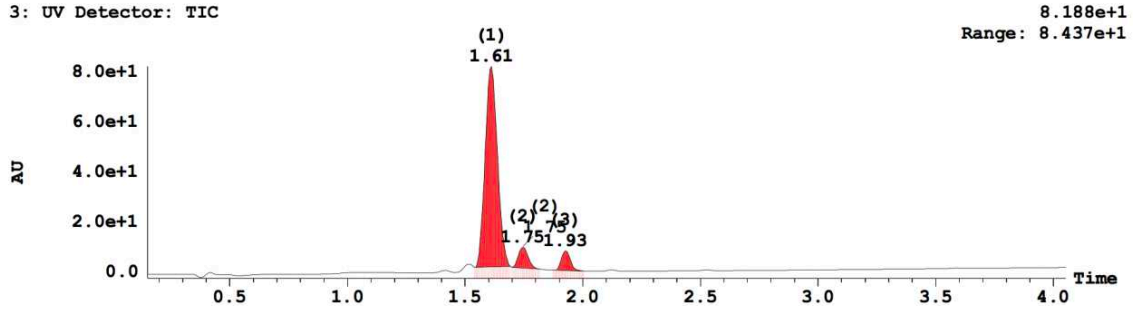
Table S1. Analytical data for the all synthesized peptides.

peptide	Mw (g·mol ⁻¹)	<i>m/z</i> (ESI)	t _R (min)
5	1398.8	1399.8 [M+H] ⁺ 700.2 [M+2H] ²⁺ 467.1 [M+3H] ³⁺ 350.6 [M+4H] ⁴⁺	1.70
4	1398.8	1399.8 [M+H] ⁺ 700.2 [M+2H] ²⁺ 467.1 [M+3H] ³⁺ 350.6 [M+4H] ⁴⁺	1.66
3	1398.8	1399.7 [M+H] ⁺ 700.1 [M+2H] ²⁺ 467.1 [M+3H] ³⁺ 350.6 [M+4H] ⁴⁺	1.74
2	1398.8	1399.7 [M+H] ⁺ 700.1 [M+2H] ²⁺ 467.1 [M+3H] ³⁺ 350.6 [M+4H] ⁴⁺	1.71
1	1398.8	1399.6 [M+H] ⁺ 700.1 [M+2H] ²⁺ 467.1 [M+3H] ³⁺ 350.6 [M+4H] ⁴⁺	1.61
7	1398.8	1399.7 [M+H] ⁺ 700.1 [M+2H] ²⁺ 467.1 [M+3H] ³⁺ 350.6 [M+4H] ⁴⁺	1.65
6	1398.8	1399.7 [M+H] ⁺ 700.1 [M+2H] ²⁺ 467.1 [M+3H] ³⁺ 350.5 [M+4H] ⁴⁺	1.67
8	1398.8	1399.8 [M+H] ⁺ 700.1 [M+2H] ²⁺ 467.1 [M+3H] ³⁺ 350.6 [M+4H] ⁴⁺	1.67
9	1412.8	1413.8 [M+H] ⁺ 707.1 [M+2H] ²⁺ 471.1 [M+3H] ³⁺ 354.1 [M+4H] ⁴⁺	1.67
10 (PKT16)	1380.8	1381.8 [M+H] ⁺ 691.1 [M+2H] ²⁺ 461.0 [M+3H] ³⁺ 346.0 [M+4H] ⁴⁺	1.69
11	1380.8	691.1 [M+2H] ²⁺ 461.0 [M+3H] ³⁺ 346.0 [M+4H] ⁴⁺	1.68

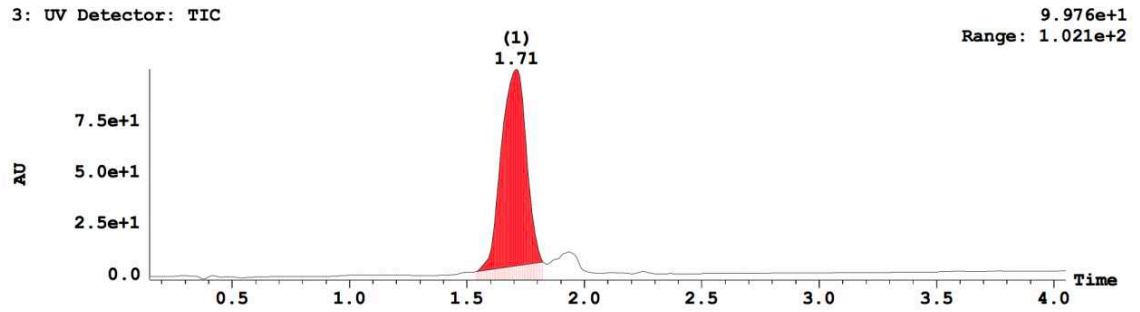
12	1380.8	691.1 [M+2H] ²⁺ 461.0 [M+3H] ³⁺ 346.0 [M+4H] ⁴⁺	1.66
13	1430.8	1431.8 [M+H] ⁺ 716.1 [M+2H] ²⁺ 477.7 [M+3H] ³⁺ 358.6 [M+4H] ⁴⁺	1.60
14	1366.7	684.1 [M+2H] ²⁺ 456.4 [M+3H] ³⁺ 342.2 [M+4H] ⁴⁺	1.60
15	1165.5	1165.6 [M+H] ⁺ 583.9 [M+2H] ²⁺	2.42
[PKHB1] ₃	4661.1	1554.7 [M+3H] ³⁺ 1166.1 [M+4H] ⁴⁺ 933.2 [M+5H] ⁵⁺ 777.7 [M+6H] ⁶⁺ 666.7 [M+7H] ⁷⁺ 583.5 [M+8H] ⁸⁺ 518.8 [M+9H] ⁹⁺ 467.0 [M+10H] ¹⁰⁺	1.99
[PKT16] ₃	4648.8	1163.0 [M+4H] ⁴⁺ 930.7 [M+5H] ⁵⁺ 775.6 [M+6H] ⁶⁺ 664.9 [M+7H] ⁷⁺ 581.9 [M+8H] ⁸⁺ 517.5 [M+9H] ⁹⁺	2.10
PKHB1-SO	1400.8	1401.6 [M+H] ⁺ 701.1 [M+2H] ²⁺ 467.7 [M+3H] ³⁺ 351.1 [M+4H] ⁴⁺	1.50
PKHB1-SO ₂	1416.8	717.1 [M+2H] ²⁺ 473.3 [M+3H] ³⁺ 355.1 [M+4H] ⁴⁺	1.43
SP (Scrambled Peptide)	1384.8	1385.6 [M+H] ⁺ 693.2 [M+2H] ²⁺ 462.4 [M+3H] ³⁺ 347.1 [M+4H] ⁴⁺	1.57
Retention times are indicated for LCMS method A. Masses determined by LC-MS (ESI) are also shown.			

HPLC traces of the purified peptides:

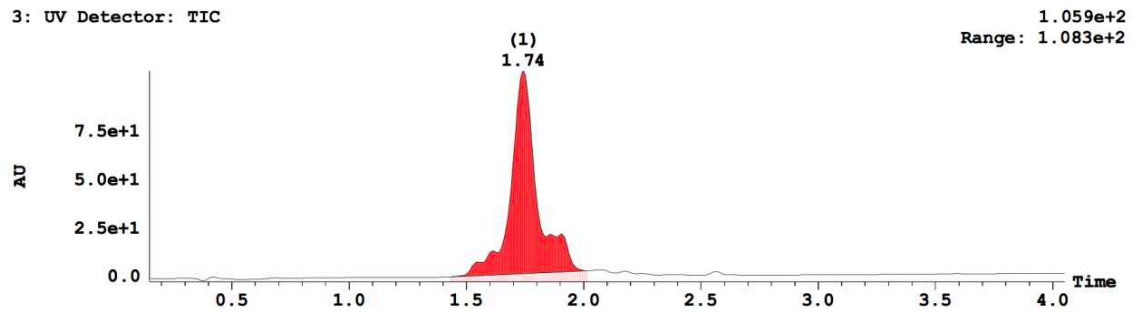
Peptide 1:



Peptide 2:



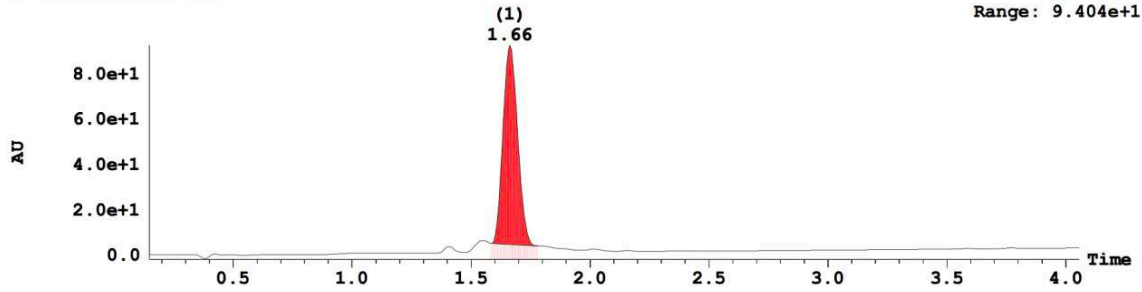
Peptide 3:



Peptide 4:

3: UV Detector: TIC

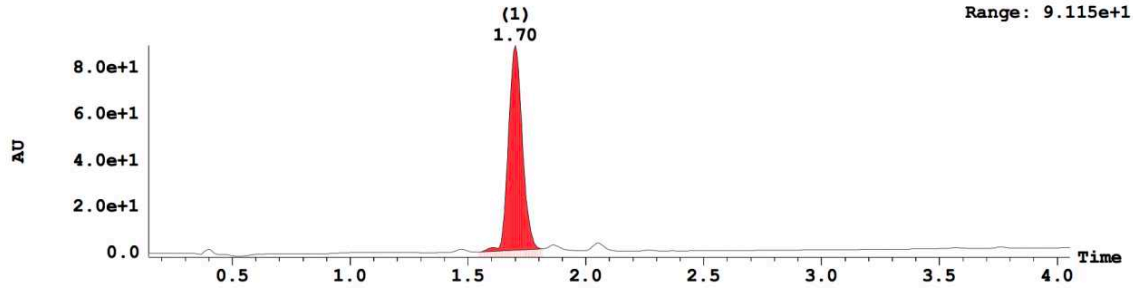
9.247e+1
Range: 9.404e+1



Peptide 5:

3: UV Detector: TIC

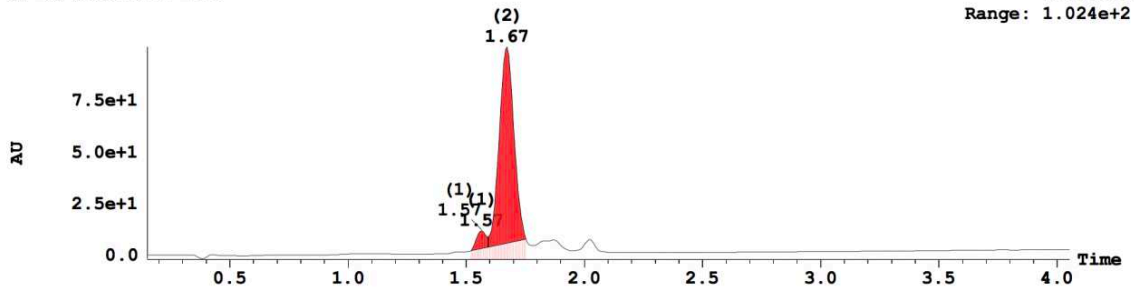
8.941e+1
Range: 9.115e+1



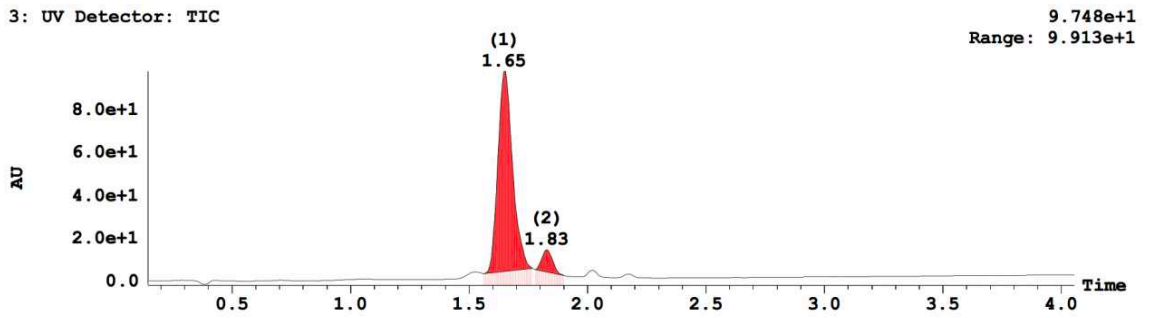
Peptide 6:

3: UV Detector: TIC

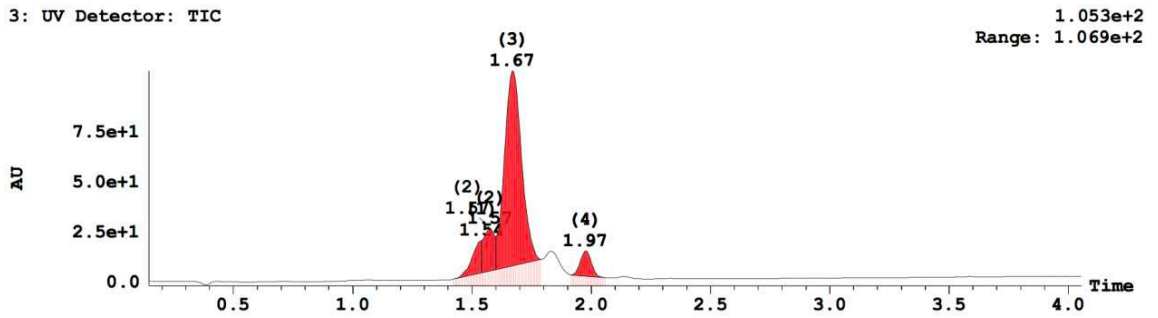
1.007e+2
Range: 1.024e+2



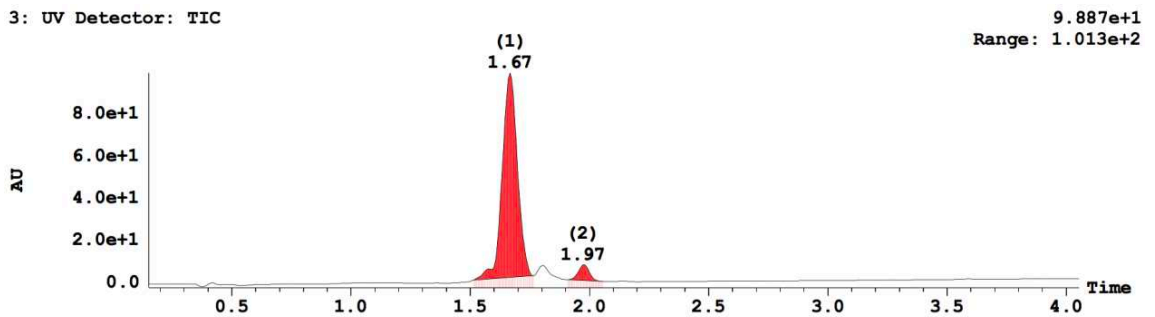
Peptide 7:



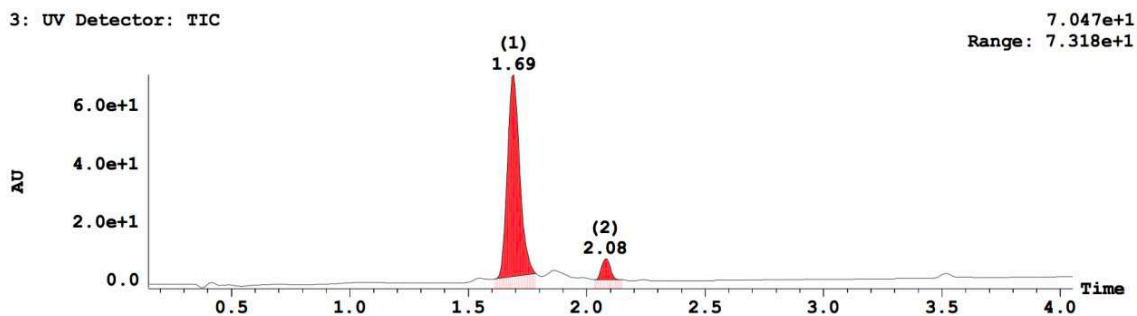
Peptide 8:



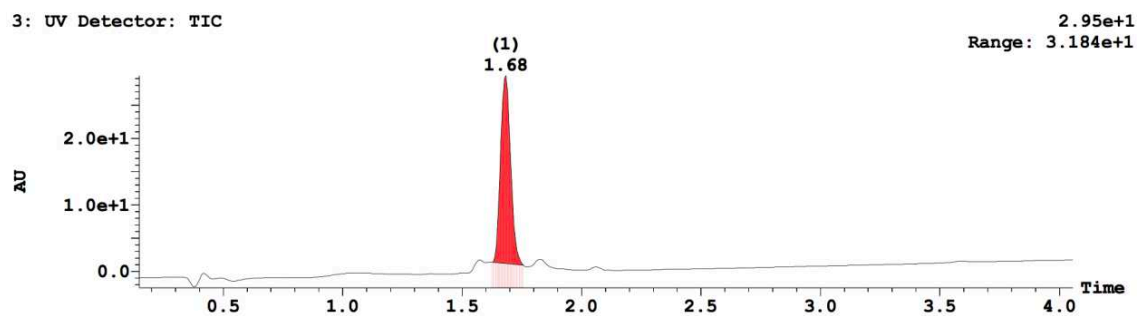
Peptide 9:



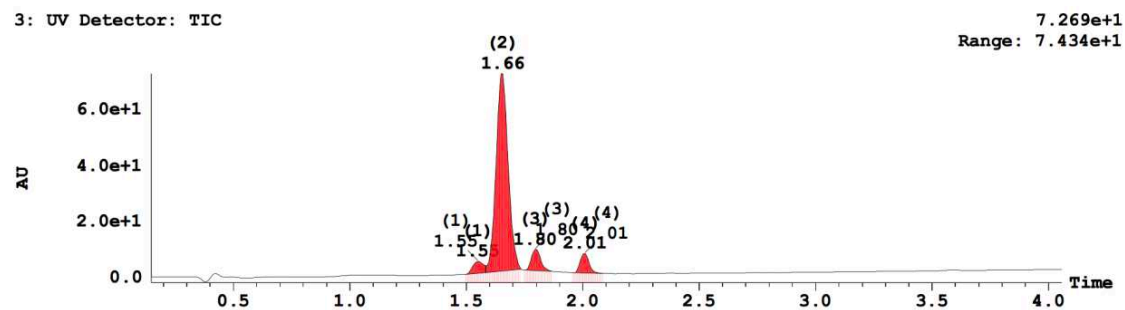
Peptide 10 (PKT16):



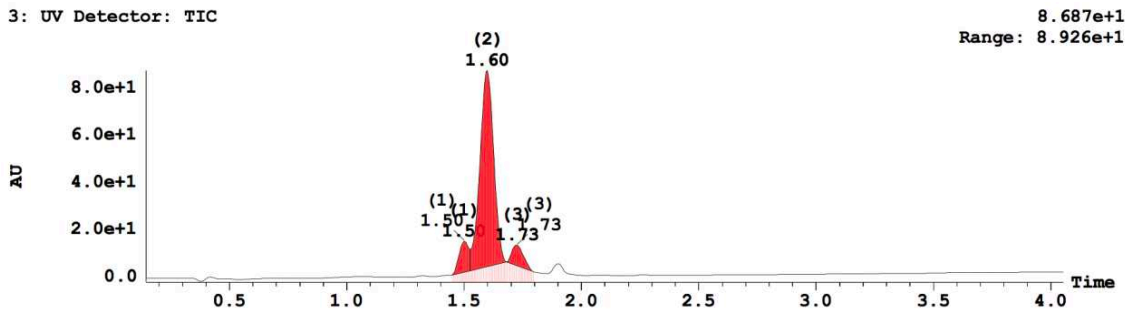
Peptide 11:



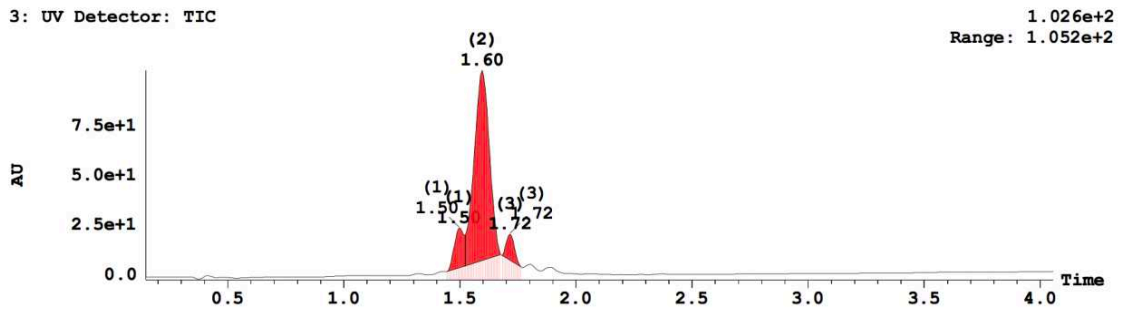
Peptide 12:



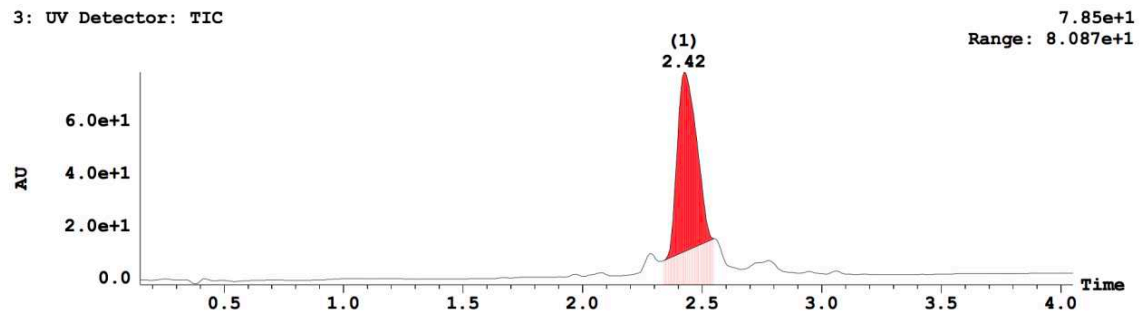
Peptide 13:



Peptide 14:



Peptide 15:

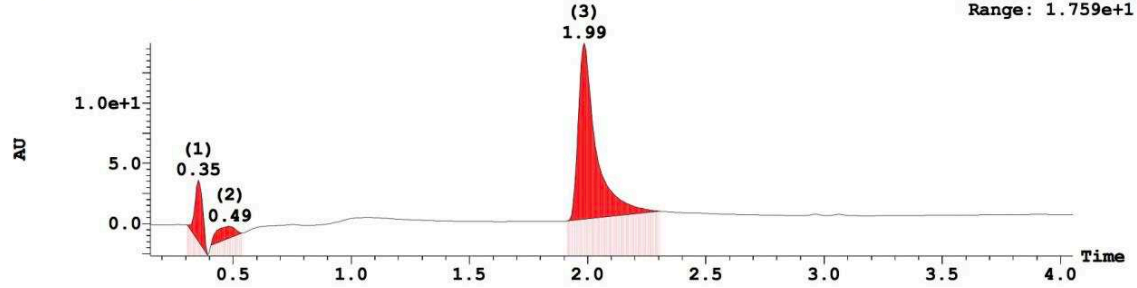


[PKHB1]₃:

Sample 2 Vial 1,2:20 ID Z4090-2 File Z4090-2 Date 21-Jul-2017 Time 12:13:36 Description TRIMER-HB12

3: UV Detector: TIC

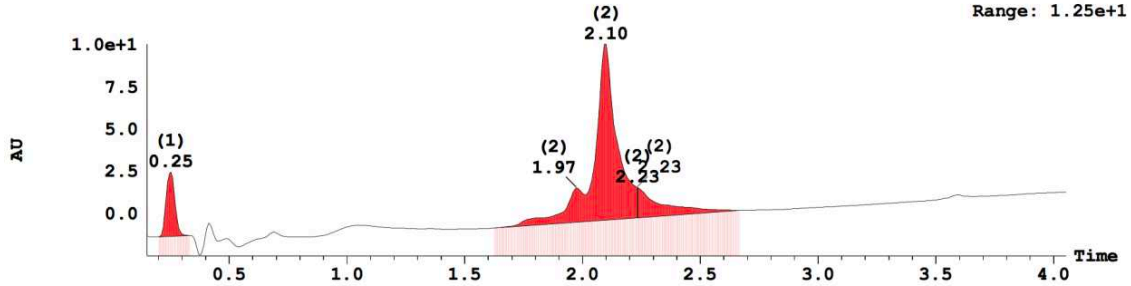
1.497e+1
Range: 1.759e+1



[PKT16]₃:

3: UV Detector: TIC

1.003e+1
Range: 1.25e+1

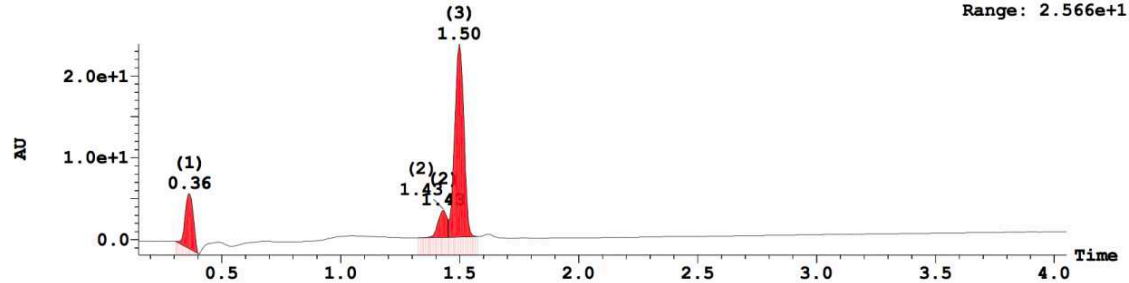


PKHB1-SO:

Sample 3 Vial 1,2:7 ID Z1872-3 File Z1872-3 Date 01-Mar-2017 Time 12:20:19 Description PKHB1-SO 3

3: UV Detector: TIC

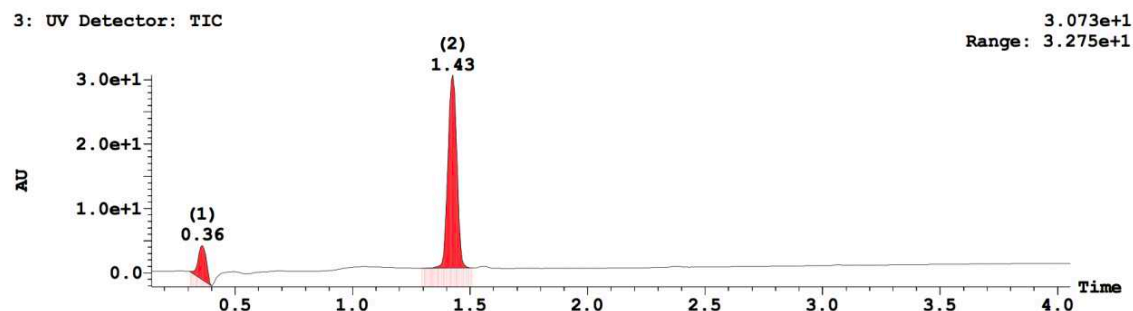
2.39e+1
Range: 2.566e+1



PKHB1-SO₂:

Sample 2 Vial 1,2:6 ID Z1872-2 File Z1872-2 Date 01-Mar-2017 Time 12:14:40 Description PKHB1-SO 2

3: UV Detector: TIC



Determination of peptide concentrations in stock solutions

The concentration of peptide was determined by absorption spectrometry at 280 nm or by weighing the lyophilized peptide before dissolving in water, or both. For determining the concentration of peptides by absorption spectrometry, theoretical extinction coefficients (ϵ_{280}) were calculated based on the presence of tryptophan ($\epsilon = 5500 \text{ M}^{-1}\text{cm}^{-1}$) and tyrosine ($\epsilon = 1490 \text{ M}^{-1}\text{cm}^{-1}$). For determining the concentration of peptides by weighing, it was assumed that one trifluoroacetic acid molecule is bound per positive charge of the peptide. The concentration of peptides that contain unnatural amino acids absorbing UV light at 280 nm with unknown ϵ_{280} , or that lack tryptophan or tyrosine, was determined by weighing.

2. Stability studies

2.1. Degradation assays in human serum & mouse plasma

To a mixture of 250 μL of human serum (or mouse plasma) and 750 μL of RPMI 1640 were added 20 μL of the peptide DMSO stock solution at 10 mM. The mixture was incubated at 37 $^{\circ}\text{C}$. Aliquots of 100 μL were removed from the medium at different time, mixed with 100 μL of TCA solution (6%) and incubated at 4 $^{\circ}\text{C}$ for at least 15 min to

precipitate all the serum proteins. After centrifugation at 12000 rpm for 2 min, 50 μ L of the supernatant were transferred to an injection vial and analyzed by HPLC with a linear gradient of MeCN in water (5 to 95% + 0.1% TFA). The relative concentrations of the remaining soluble peptides were calculated by integration of the absorbance at 220 nm as a function of the retention time (peak area).

2.2. Stability under Chymotrypsin and Trypsin incubation

A 0.6 mL tube was charged with 180 μ L of phosphate buffer pH 7.4, 10 μ L of enzyme (0.05 mg/mL stock solution in phosphate buffer pH 7.4), 10 μ L of peptide (10 mM stock solution in DMSO). The resulting reaction mixture was capped and incubated at room temperature for 3 hours. 20 μ L of the crude reaction was quenched by addition of 180 μ L of 50% water: 50% acetonitrile and was subjected to LC-MS analysis Method A (Figure S1).

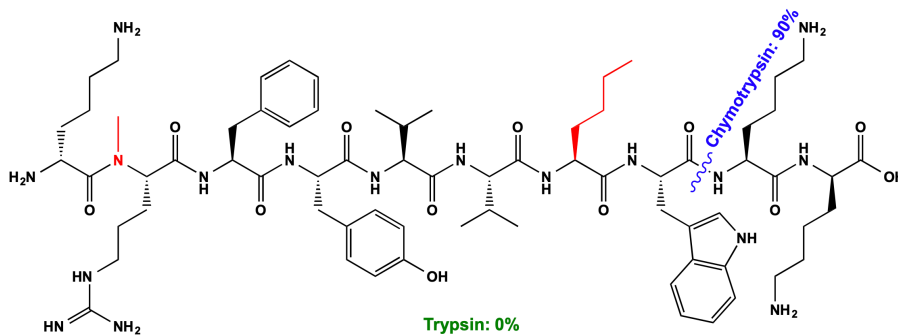


Figure S1. Enzymatic cleavage of PKT16 (peptide 10).

3. Structural analyses

3.1 CD spectroscopy

CD experiments were acquired on a Jasco J-815 CD spectropolarimeter with a Peltier temperature-controlled cell holder (30 °C) over the wavelength range 190-270 nm. Peptide samples were prepared at a concentration of 50 μ M in 10 mM sodium phosphate

buffer, pH 7.4, using a quartz cell of 1 mm path length. Measurements were taken every 0.2 nm at a scan rate of 10 nm/min.

3.2. NMR conformational analysis

Lyophilized PKT16 peptide was dissolved at 1 mM concentration in 550 μ L of H₂O/D₂O (90:10 v/v). Sodium 4,4-dimethyl-4-silapentane-1-sulfonate-d₆ (DSS, from Sigma Aldrich) was added at a final concentration of 0.11 mM for chemical shift calibration. NMR experiments were recorded on a Bruker Avance III 500 MHz spectrometer equipped with a TCI 1H/13C/15N cryoprobe with Z-axis gradient. NMR spectra were processed with TopSpin 3.2 software (Bruker) and analysed with NMRFAM-SPARKY program.ⁱ ¹H, ¹³C, and ¹⁵N resonances were assigned using 1D ¹H WATERGATE, 2D ¹H-¹H TOCSY (DIPSI-2 isotropic scheme of 80 ms duration), 2D ¹H-¹H ROESY (300 ms mixing time), 2D ¹H-¹³C HSQC, 2D ¹H-¹⁵N HSQC, and 2D ¹H-¹³C HMBC recorded at 25 °C. ¹H chemical shift was referenced against DSS ¹H signal and ¹³C, ¹⁵N chemical shifts were referenced indirectly. The chemical shift deviations were calculated as the differences between observed ¹H, ¹³C chemical shifts and random coil values.ⁱⁱ ³J_{HN-H α} coupling constants were measured on 1D ¹H WATERGATE experiments recorded at 5 or 25 °C, or on 1D rows extracted from 2D TOCSY acquired with high resolution.

Table S2. ¹H, ¹³C, ¹⁵N chemical shifts of PKT16 peptide (500 MHz, 25°C).

Only the assignment of the major form, corresponding to the *trans* isomer of peptide bond 1-2, is indicated.

Residue	¹⁵ N	¹ HN	¹³ C α	¹ H α	¹³ CO	Side chain resonances
D-Lys1			54.1	4.41	173.4	¹³ C β 32.1; ¹³ C γ 24.1; ¹³ C δ 29.3; ¹³ C ϵ 42.1 ¹ H β 1.86; ¹ H γ 1.47; ¹ H δ 1.70; ¹ H ϵ 3.00
NMeArg2		-	60.1	4.84	173.8	¹³ CNMe 33.7; ¹³ C β 27.4; ¹³ C γ 27.4; ¹³ C δ 43.4; ¹³ C ζ 159.7; ¹⁵ N ϵ 84.6; ¹ HNMe 2.75; ¹ H β 1.84, 1.66; ¹ H γ 1.43; ¹ H δ 3.18; ¹ H ϵ 7.18
Phe3	122.4	7.99	57.5	4.65	175.1	¹³ C β 39.7; ¹³ C γ 138.9; ¹³ C δ 131.8; ¹³ C ϵ 131.5; ¹³ C ζ 130.0; ¹ H β 3.06, 2.92; ¹ H δ 7.19; ¹ H ϵ 7.34; ¹ H ζ 7.30
Tyr4	122.9	8.11	57.5	4.58	174.8	¹³ C β 39.2; ¹³ C γ 130.6; ¹³ C δ 133.4; ¹³ C ϵ 118.2; ¹³ C ζ 157.2; ¹ H β 2.98, 2.86; ¹ H δ 7.06; ¹ H ϵ 6.79

Val5	123.2	8.00	62.3	4.00	175.4	¹³ Cβ 33.0; ¹³ Cγ 20.7; ¹³ Cγ ² 21.0; ¹ Hβ 1.94; ¹ Hγ 0.90; ¹ Hγ ² 0.85
Val6	125.1	8.17	62.4	3.97	175.8	¹³ Cβ 32.8; ¹³ Cγ 21.0; ¹³ Cγ ² 21.0; ¹ Hβ 1.91; ¹ Hγ 0.89; ¹ Hγ ² 0.77
Nle7	126.5	8.20	56.6	4.25	176.5	¹³ Cβ 33.5; ¹³ Cγ 29.9; ¹³ Cδ 24.5; ¹³ Cε 16.1; ¹ Hβ 1.67, 1.63; ¹ Hγ 1.25, 1.19; ¹ Hδ 1.25; ¹ Hε 0.84
Trp8	122.5	8.05	57.2	4.66	175.9	¹³ Cβ 29.6; ¹³ Cγ 111.3; ¹³ Cδ1 127.3; ¹³ Cδ2 129.6; ¹³ Cε2 139.1; ¹³ Cε3 121.0; ¹³ Cζ2 114.8; ¹³ Cζ3 122.2; ¹³ Cη2 124.8; ¹⁵ Nε1 129.6 ¹ Hβ 3.26; ¹ Hδ1 7.24; ¹ Hε1 10.11; ¹ Hε3 7.61; ¹ Hζ2 7.49; ¹ Hζ3 7.14; ¹ Hη2 7.23
Lys9	123.3	7.97	56.6	4.21	175.3	¹³ Cβ 33.5; ¹³ Cγ 24.5; ¹³ Cδ 29.1; ¹³ Cε 42.2; ¹ Hβ 1.70, 1.60; ¹ Hγ 1.25; ¹ Hδ 1.60; ¹ Hε 2.93; ¹ Hζ 7.52
D-Lys10	124.4	7.60	57.0	4.12	180.1	¹³ Cβ 33.6; ¹³ Cγ 24.7; ¹³ Cδ 29.3; ¹³ Cε 42.0; ¹ Hβ 1.76, 1.59; ¹ Hγ 1.30; ¹ Hδ 1.61; ¹ Hε 2.93; ¹ Hζ 7.50

ⁱ W. Lee, M. Tonelli and J. L. Markley, NMRFAM-SPARKY: enhanced software for biomolecular NMR spectroscopy, *Bioinformatics*, 2015, **31**, 1325-1327.

ⁱⁱ D. S. Wishart, C. G. Bigam, A. Holm, R. S. Hodges and B. D. Sykes, ¹H, ¹³C and ¹⁵N random coil NMR chemical shifts of the common amino acids. I. Investigation of nearest-neighbor effects, *J. Biomol. NMR*, 1995, **5**, 67-81.

4. Binding affinity measurements

The binding affinities of peptides for a MEC-1 cancer cells membrane preparation were measured by biolayer interferometry on an Octet RED96 System (Pall FortéBio Corp., Menlo Park, CA). This system monitors interference of light reflected from two sources (an internal reflection surface and the liquid/solid interface of a fiber optic sensor) to measure the rate of binding of molecules to the biosensor surface.

MEC-1 cells membrane preparation is biotinylated with the EZ-Link NHS-PEG4-Biotin kit from Thermo-Scientific and excess biotin is removed using desalting column from Thermo-Scientific. Biotinylated membranes are then loaded onto SuperStreptavidin (SSA) biosensors (Pall FortéBio Corp.) at empirically determined concentrations. All affinity measurements were carried out in assay buffer (PBS with 0.05% Tween 20 and 1% DMSO) at 30 °C.

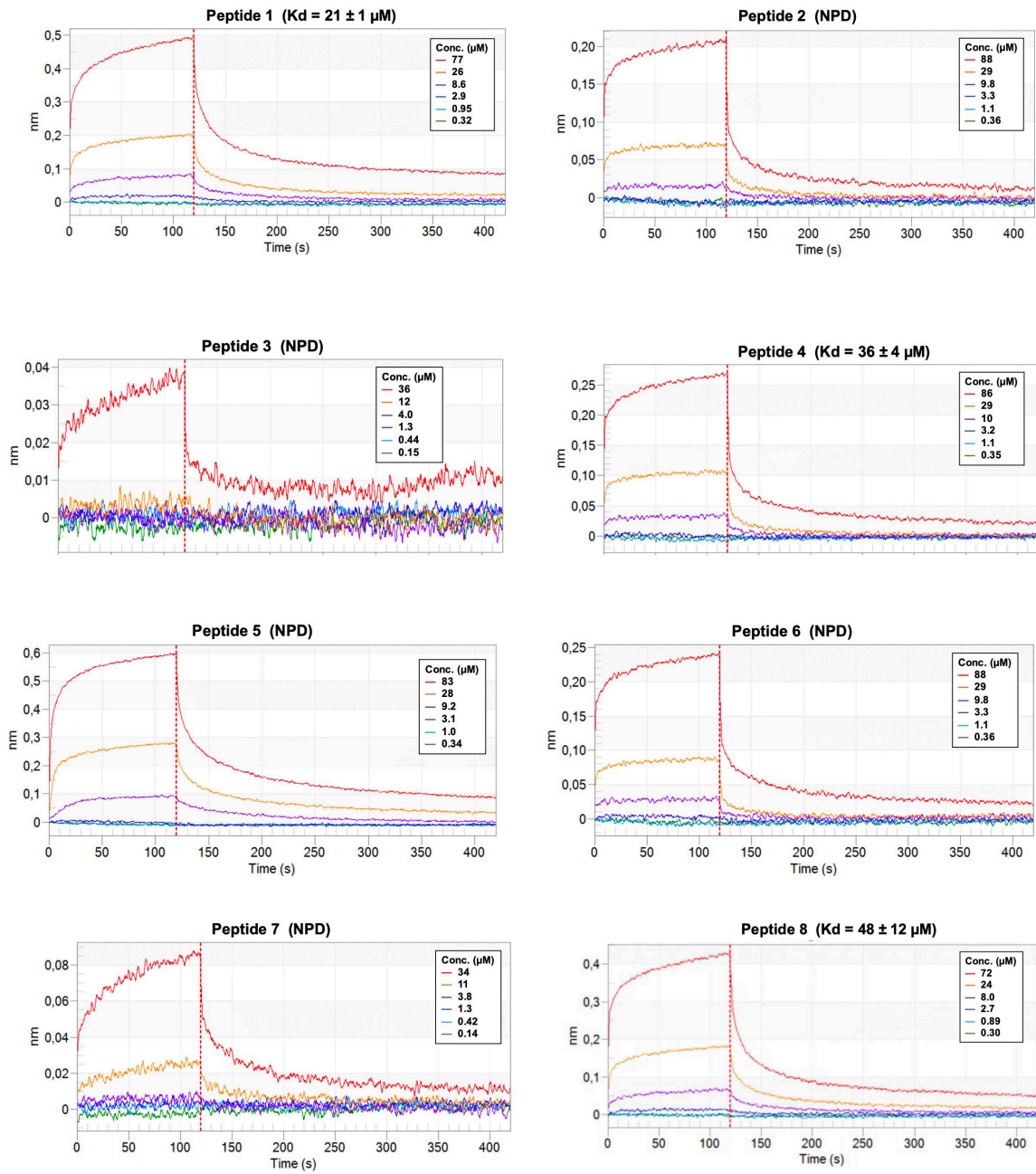
Typically, the biosensors were pre-equilibrated in PBS containing either biotinylated membranes or biocytine 100 µg/mL. Biosensors are then equilibrated in assay

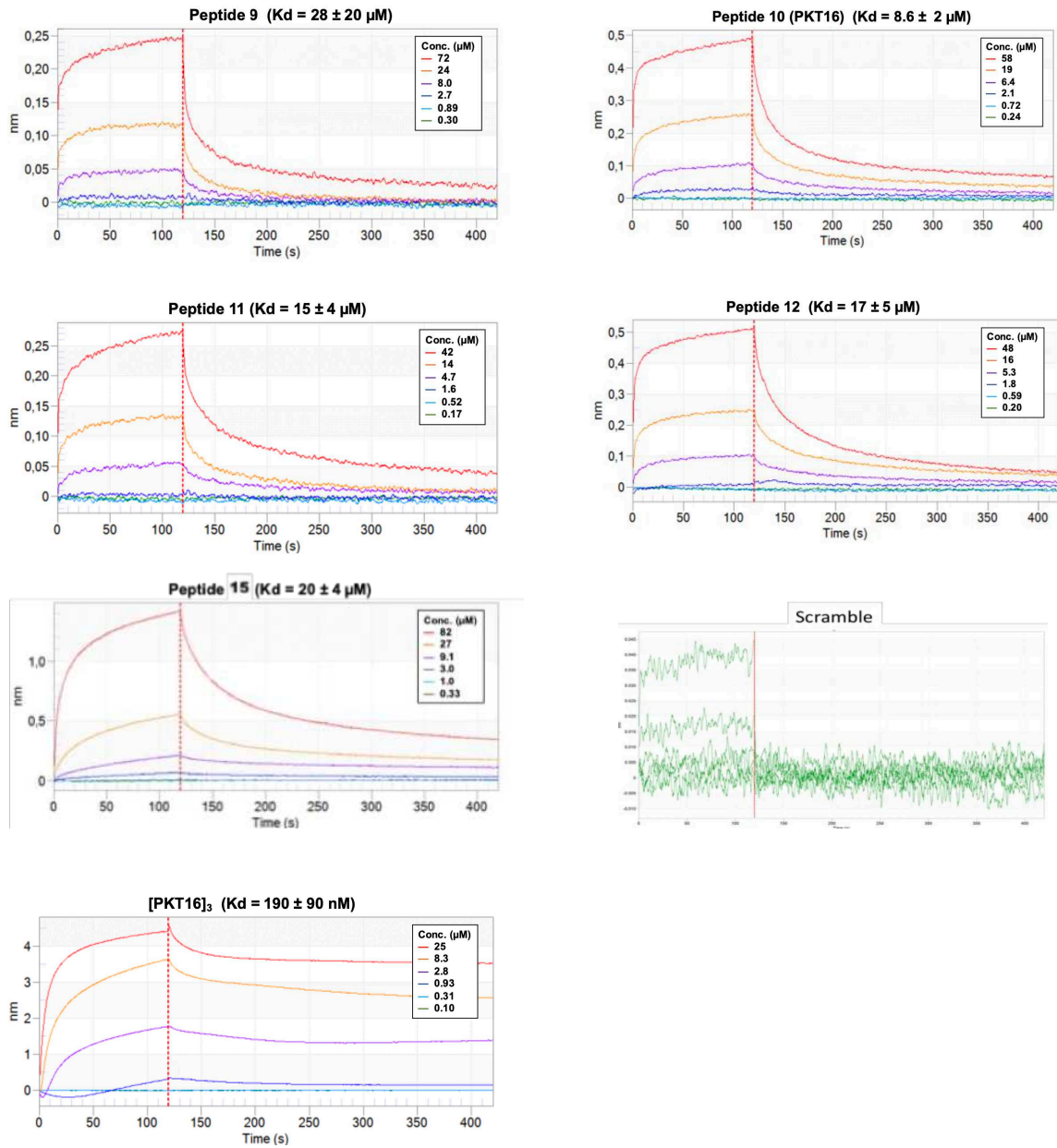
buffer for 10min, brought to baseline in assay buffer for 60 sec. and transferred to wells containing peptide in dose-response (association for 120 sec. and dissociation for 300 sec.). The double reference with either membrane-loaded biosensors without any peptide dose-response or biocytine-loaded biosensors with each peptide dose-response were run in parallel for background signal double subtractions. Binding kinetics were calculated using the FortéBio Data Analysis v8.2 software.

Table S3. Apparent Kd values

Peptide	Kd
1 (MeR2)	21 ± 1 μM
2 (MeF3)	NPD
3 (MeY4)	NPD
4 (MeV5)	36 ± 4 μM
5 (MeV6)	NPD
6 (MeM7)	NPD
7 (MeW8)	NPD
8 (MeK9)	48 ± 12 μM
9 (MeR2K9)	38 ± 20 μM
10 (PKT16)	8.6 ± 2 μM
11	15 ± 4 μM
12	17 ± 5 μM
13	13 ± 2 μM
14	9.5 ± 3 μM
15	20 ± 4 μM
[PKHB1]₃	ND
[PKT16]₃	0.19 ± 0.09 μM
n > 2 independent measurements NPD: Non Pertinent Data. ND: Not Determined.	

Binding kinetics observed with Octet Red:





5. Cell culture

Human chronic lymphocytic leukemia cells (MEC-1) and lung adenocarcinoma cells (A549) were grown in Advanced RPMI-1640 medium supplemented with 10% fetal bovine serum (FBS), 100 units/mL penicillin, and 100 $\mu\text{g/mL}$ streptomycin, and maintained following the standard procedures proposed by the American Type Culture Collection.

6. Cell death induction and inhibition

Peptides were solubilized in water or DMSO and stock concentrations were measured by protein absorbance at 280 nm using NanoDrop™ 8000. Only freshly prepared solutions were used for each experiment. Cell death was induced by treating MEC-1 cells for two hours or A549 for six hours with the indicated peptide concentrations. Etoposide (200 μ M, 24 h) was used as positive control for p53- and caspase-dependent apoptosis. For the inhibition assays, MEC-1 cells were seeded in non-supplemented medium prior to treatment with inhibitors to limit Ca²⁺ concentration in the medium, while complete medium was used to let A549 cells adhere overnight but was replaced with serum free medium prior to treatment. Calcium chelator, BAPTA (3 mM, CalbioChem; Merck, Billerica, MA, USA) or the pan-caspase inhibitor Q-VD-OPh (10 μ M; BioVision, Milpitas, CA, USA) were added 30 minutes before cell death induction, while the PLC γ 1 inhibitor U73122 (Sigma-Aldrich), the IP3R inhibitor 2-APB (Sigma-Aldrich), and the ryanodine receptor inhibitor dantrolene (Sigma-Aldrich) were added one hour before. Cell death was analyzed in first instance by microscopic observations (Axiovert 40 CFL Zeiss microscope) and comparison of representative photographs (Sony Power HAD 3CCD colour video camera coupled to microscope, 20X). Annexin-V-allophycocyanin (Ann-V-APC 0.1 μ g/mL; BD Pharmingen, San Jose CA, USA) and propidium iodide (PI, 0.5 μ g/mL; Sigma-Aldrich) in annexin binding buffer (ABB, 10 mM Hepes [pH 7.4], 140 mM NaCl, and 2.5 mM CaCl₂) were used to evaluate phosphatidylserine exposure and plasma membrane permeability, respectively. Samples were sorted in a BD FACSCalibur Flow Cytometer (total population 10 000 cells) and data was analysed using FlowJo software (LLC, Ashland, OR, USA). Since peptides-induced cell death consistently presented a double copositive Ann/PI staining, to evaluate cell death in samples where calcium had been chelated, PI staining was used alone in Ca²⁺[-]/Mg²⁺[-] DPBS (Gibco) to avoid Ca²⁺ provision by the ABB. For similar reasons, a simpler method as it is trypan blue staining, analysed with an automated counter (Beckman Vi-CELL XR), was used as well to study A549 cell death in the context of PLC γ 1-related calcium signalling inhibition. In all cases, the wells were washed twice with Ca²⁺[-]/Mg²⁺[-] DPBS (Gibco) after supernatant recovering. A549 cells were

generally detached using trypsin-EDTA 0.05% (Gibco), but in some cases chymotrypsin 0.05% (Sigma-Aldrich) was also used to assist [PKT16]₃-treated cells detachment. Cell death index was calculated by normalizing peptide-specific cell death (% Cell death - % Cell death in control) in each condition with peptide-specific cell death induced by the peptide alone (Mateo, et al. 2002, doi: <https://doi.org/10.1182/blood-2001-12-0217>). Two-way ANOVA were performed in GraphPad Prism 8.0 Software for statistical analysis.

Table S4. Effect of caspase and Ca²⁺ signaling inhibition on MEC-1 cell death.

	Treatment	Cell death index	SD	Difference from control (p ≤)*
[PKT16] ₃	Control	1.00		
	Q-VD-OPH	1.04	0.07	NS
	BAPTA	0.38	0.00	0.0001
	U73122	0.77	0.03	0.0001
	2-APB	0.69	0.04	0.0001
	Dantrolene	0.75	0.08	0.0001
	D+U+2	0.42	0.01	0.0001
PKT16	Control	1.00		
	Q-VD-OPH	0.95	0.02	NS
	BAPTA	0.00	0.02	0.0001
	U73122	0.60	0.08	0.0001
	2-APB	0.67	0.01	0.0001
	Dantrolene	0.56	0.14	0.0001
	D+U+2	0.39	0.05	0.0001
PKHB1	Control	1		
	Q-VD-OPH	0.97	0.02	NS
	BAPTA	0.01	0.07	0.0001
	U73122	0.78	0.04	0.001
	2-APB	0.88	0.03	0.05
	Dantrolene	0.79	0.09	0.0001
	D+U+2	0.64	0.17	0.0001
Etoposide [§]	Control	0.14	0.07	
	Q-VD-OPH	0.07	0.02	NS

MEC-1 cells were pre incubated with vehicle (control), Q-VD-OPH (10 μ M), BAPTA (3 mM) U73122 (400 nM), 2-APB (60 μ M), dantrolene (80 μ M), or a 1/3 combination of the last three (U73122 133 nM, 2-APB 20 μ M, dantrolene 27 μ M), one hour before treatment with [PKT16]₃ (5 μ M), PKT16 (50 μ M) or PKHB1 (50 μ M) in serum free medium. Cell death was analysed by flow cytometry using Ann-V/PI staining and cell death index was obtained by normalizing to 1.00 the cell death induced by each peptide with its corresponding control. The values represent the means (\pm SD) of at least two independent experiments. §Total cell death induced by etoposide is shown instead of cell death in serum free medium index. *Two-way ANOVA were used to compare problem vs control data populations.

Table S4. Effect of caspase and Ca²⁺ signaling inhibition on MEC-1 cell death.

	Treatment	Cell death index	SD	Difference from control ($p \leq$)*
[PKT16] ₃	Control	1.00		
	Q-VD-OPH	0.99	0.00	NS
	BAPTA	0.52	0.02	0.0001
	U73122	0.84	0.02	NS
	2-APB	0.77	0.08	NS
	Dantrolene	0.86	0.08	NS
	D+U+2	0.73	0.04	0.05
PKT16	Control	1.00		
	Q-VD-OPH	1.03	0.14	NS
	BAPTA	0.14	0.14	0.0001
	U73122	0.32	0.15	0.0001
	2-APB	0.72	0.04	0.001
	Dantrolene	0.59	0.23	0.0001
	D+U+2	0.51	0.22	0.0001
PKHB1	Control	1.00		
	Q-VD-OPH	1.03	0.01	NS
	BAPTA	0.29	0.06	0.0001
	U73122	0.34	0.31	0.0001
	2-APB	0.67	0.09	0.001
	Dantrolene	0.52	0.19	0.0001
	D+U+2	0.40	0.26	0.0001
Etoposide [§]	Control	0.59	0.03	
	Q-VD-OPH	0.05	0.04	0.0001

A549 cells were pre incubated with vehicle (control), Q-VD-OPH (10 μ M), BAPTA (3 mM) U73122 (400 nM), 2-APB (60 μ M), dantrolene (80 μ M), or a 1/3 combination of the last three (U73122 133 nM, 2-APB 20 μ M, dantrolene 27 μ M), one hour before treatment with [PKT16]₃ (5 μ M), PKT16 (50 μ M) or PKHB1 (50 μ M) in serum free medium. Cell death was analysed by flow cytometry using Ann-V/PI

staining and cell death index was obtained by normalizing to 1.00 the cell death induced by each peptide with its corresponding control. The values represent the means (\pm SD) of at least two independent experiments. §Total cell death induced by etoposide is shown instead of cell death in serum free medium index. *Two-way ANOVA were used to compare problem vs control data populations.

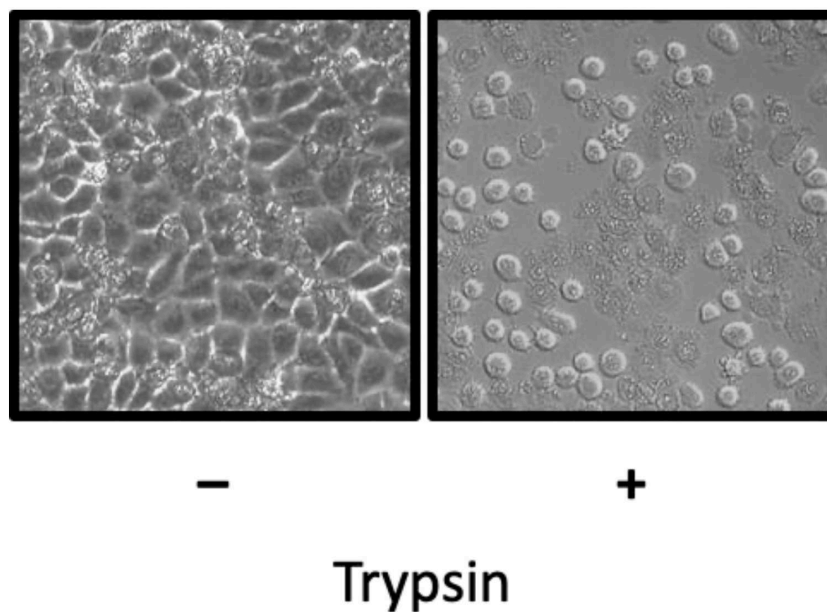


Figure S2. Peptide-induced cell death induces enhanced cell-substrate adhesion: [PKT16]₃-treated A549 cells before and after trypsin-EDTA addition.

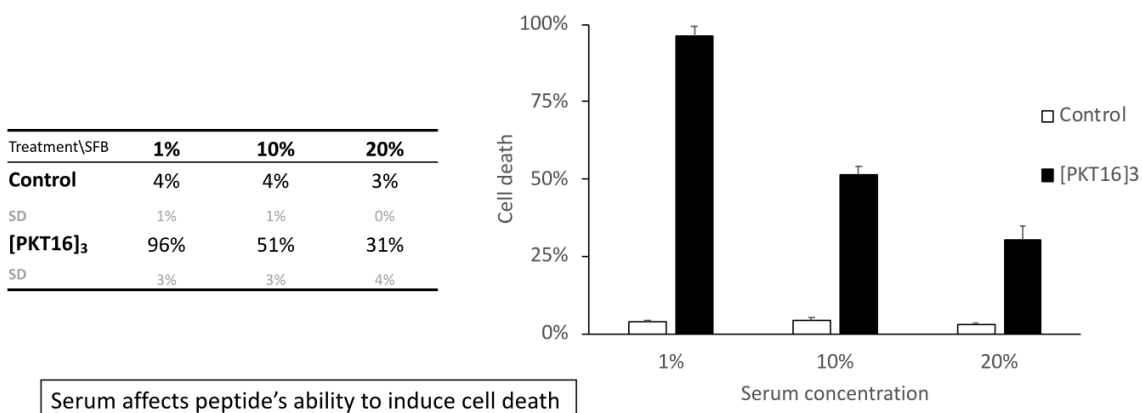


Figure S3. [PKT16]₃ activity at different serum concentrations

7. Cell viability evaluation through impedance

7.1. Brief insights about impedance technology

Label-free detection has emerged as a new approach in the development of technologies for cell-based screening assays. Unlike the classic detection methods that use fluorescence, radioisotope, luminescence, or light absorption, label-free detection directly measures the cell function without using a labeled molecule. The advantages of label-free detection include a simple homogeneous assay format, noninvasive measurement, less interference with normal cell function, kinetic measurement, and reduced time for assay development. Cell-based assays have an important role in drug discovery. Designed appropriately, these *in vitro* tests can help predict the effect of chemical agents *in vivo* and can provide relevant biochemical and pharmacological insight that is not possible in a whole animal study. Label-free technologies with the potential to substantially change some aspects of whole-cell assays have emerged within the past few years. These technologies detect changes in cellular features including adhesion and morphology, complex endpoints that are modulated by many different receptors, ion channels and signal transduction pathway. Currently available label-free instruments use either an impedance-based biosensor or an optical-based biosensor to detect changes in cell behavior.

Here, we have applied the electrical impedance detection method in a real-time cell analyzer (RTCA) system for cell viability assays. The use of impedance to measure cellular processes was first reported by Giaever and Keese at the GE Corporation Research and Development Center. Biosensors measure the impedance to current flow across two electrodes mounted in the base of the microtiter well. Cells that adhere to the surface of the microtiter well restrict the flow of current between the electrodes.

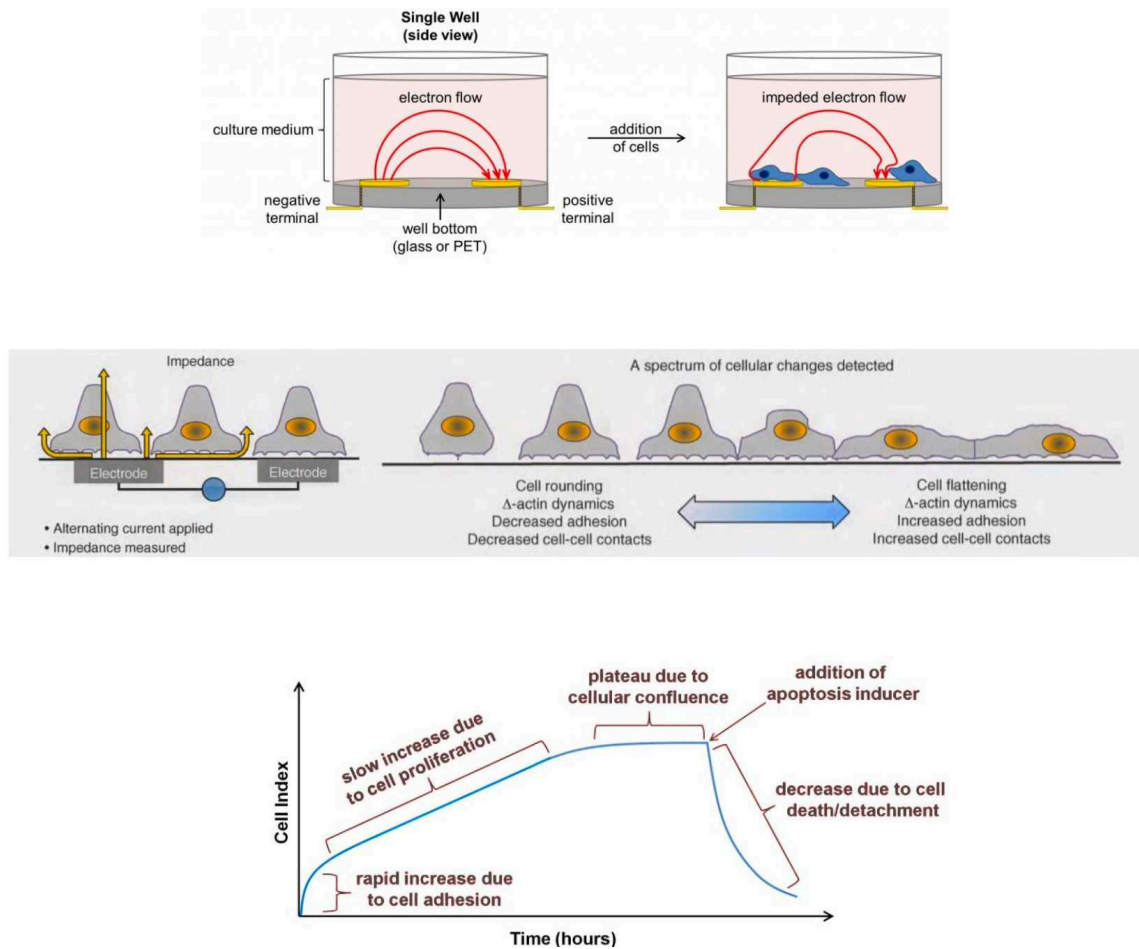
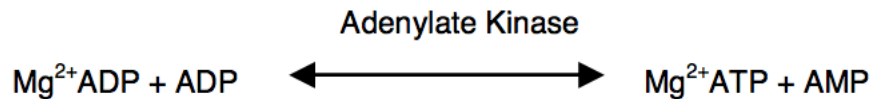


Figure S4. Scheme of RTCA basis.

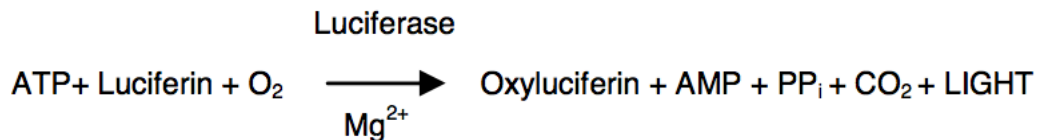
The RTCA monitors cellular events in real time without the incorporation of labels. The system measures electrical impedance across interdigitated microelectrodes integrated on the bottom of tissue culture E-Plates (96-well). The impedance measurement provides quantitative information about the biological status of the cells, including cell number, viability, and morphology. Using the xCELLigence system, we continuously monitored the “Cell Index” which is derived from the measured impedances and reflects the cell viability under peptide treatment.

7.2. Cytotoxicity assay (complementary to RTCA)

The ToxiLight™ bioassay is a non-destructive bioluminescent cytotoxicity assay designed to measure toxicity in mammalian cells and cell lines in culture. The kit quantitatively measures the release of adenylate kinase (AK) from damaged cells. It is a safe, convenient, and highly sensitive method for measuring cytolysis. The assay can be conducted directly cells cultured in a microtiter plate. The kit is based on the bioluminescent measurement of AK which is present in all cells. A loss of cell integrity, through damage to the plasma membrane, results in the leakage of a number of factors from cells cultured in vitro into the surrounding medium. The measurement of the release of AK from the cells allows the accurate and sensitive determination of cytotoxicity and cytolysis. The reaction involves two steps. The first involves the addition of ADP as a substrate for AK. In the presence of the enzyme, AK, the ADP is converted to ATP for assay by bioluminescence:



The bioluminescent method utilizes an enzyme luciferase, which catalyzes the formation of light from ATP and luciferin according to the following reaction:



By combining the two reactions, the emitted light intensity is linearly related to the AK concentration and is measured using a luminometer or beta counter.

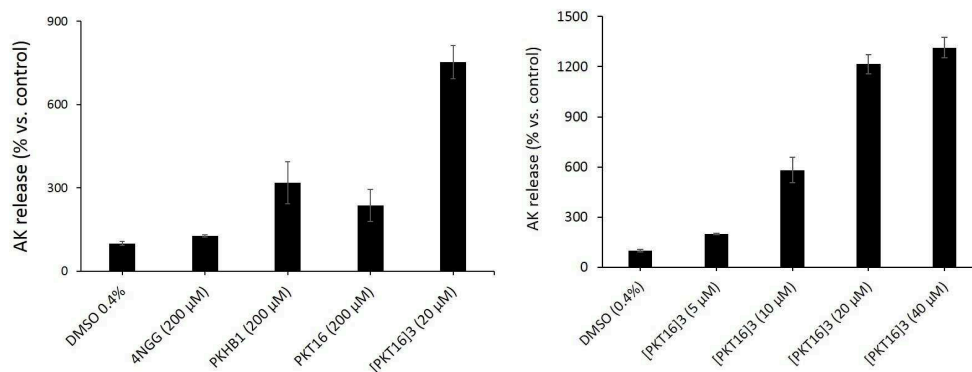


Figure S5. The profound diminution of cell index is correlated to the loss of cell membrane integrity traced by measurement of the adenylate kinase (AK) release after treatment with PKHB1, PKT16 and [PKT16]₃ and increasing [PKT16]₃ concentrations.

7.3. Protocol for impedance monitoring with our peptides:

The xCelligence RTCA system (Roche) has been described previously. For our experiments, 100 μL of media was added to each well of the 96-well E-plate to measure background levels of impedance. After measuring the background, 100 μL of cell suspension was added to reach a cell density of 4000 cells/well. Cells were allowed to seed at room temperature for 30 min and then placed in the reader at 37 °C and 5% CO₂ for real-time recording of the cell index. The following day, half of the media was removed and replaced with the corresponding volume (100 μL) of media with concentrated peptide in order to reach the desired concentration in the well (direct addition of DMSO caused stress and damaged the cells). Negative controls were treated with the vehicle (DMSO at 0.5% final concentration). Each condition was tested in triplicates and in two independent experiments. The cells were monitored every minute for the first 2 h after treatment and every hour until 24 h after treatment.

Conclusions and perspectives

Conclusions and perspectives

Cell death mechanism and immunogenicity of cell death induced by PKHB1

Overall toxicity

In the present work it was demonstrated that PKHB1 is cytotoxic against T-ALL, breast cancer, and lung cancer cell lines, but not to freshly isolated PBMCs or cells from mice's bone marrow, spleen, thymus, or lymph nodes at similar concentrations. On the other hand, in immunocompetent tumor-bearing mice, PKHB1 treatment reduces tumor growth and ameliorates immune cell count. Altogether, this highlights the specificity of PKHB1's cytotoxicity. However, PKHB1 toxicity in healthy mice was only partially assessed, therefore, PKHB1 *in vivo*-dosage toxicity should be evaluated using adequate models. Biodistribution, pharmacokinetics and pharmacodynamics studies using different concentrations of formulated peptide via intra-venous and intra-peritoneal injections have already begun to be assessed in mice.

Ca²⁺ regulation of cell death

As it was previously demonstrated for CLL, where PKHB1 induced an intracellular Ca²⁺ overload, result of a sustained PLC activation and subsequently of ER Ca²⁺ channels (Martinez-Torres *et al.*, 2015), in the present study we observed that PKHB1 induced Ca²⁺-dependent cell death in T-ALL, breast cancer and lung cancer. In breast cancer cells, PKHB1 increased intracellular Ca²⁺, and Ca²⁺ chelation or pharmacological inhibition of PLC (by U73122) or ER Ca²⁺ channels (using dantrolene and 2-APB) significantly inhibited cell death. In lung cancer cells, cell death induced by PKHB1 was also inhibited by Ca²⁺ chelation or inhibition of PLC or ER Ca²⁺ channels; and in T-ALL, Ca²⁺ chelation inhibited PKHB1-induced cell death. Inhibition of PLC or ER Ca²⁺ channels were not assessed in T-ALL, and Ca²⁺ concentration was not measured neither in T-ALL nor in lung cancer, leaving opened questions about their molecular mechanisms that would need to be answered with similar experiments as in breast and lung cancer cells. It should be also considered that the Ca²⁺ chelator BAPTA is negatively charged and used at high

concentrations (3-5 mM), thus, it could potentially interfere directly with PKHB1, which holds a net positive charge. Complexation of these molecules could be measured using physical techniques (e.g., changes in UV absorbance) to evaluate the relevance of using BAPTA as a cell death inhibitor. Additionally, to confirm ER Ca²⁺ release, pharmacological inhibition of the PLC and ER Ca²⁺ channels should be also assessed in T-ALL, as the mechanism by which PKHB1 induces cell death is largely unknown. On this subject, deeper studies are needed to characterize the molecular pathway activated by PKHB1 in all the models used in the present work. Activation of PLC should be assessed, as it was done for CLL (Martinez-Torres *et al.*, 2015), at different time points after PKHB1 treatment. In addition, knowing the potential implication of this signaling pathway and the potential binding partners of CD47, assessing the differences in expression of mRNA and protein levels of CD47, ubiquilin-1, Gi proteins, protein kinase A, PLCs (and phosphorylated PLCs), IP₃ and ryanodine receptors, STIM, and Orai proteins in untreated versus PKHB1-treated cells, this, followed by pharmacologic and genetic modulation of proteins with differential expression, to assess their involvement in cell death.

Immunogenicity of cell death

Another important effect induced by PKHB1 treatment was the exposure of DAMPs in T-ALL and in breast cancer cells. However, the molecular mechanisms relating PKHB1-induced cell death and DAMPs exposure remain unknown. Participation of PLC and ER Ca²⁺ channels hint that ER stress could be implicated. Therefore, evaluation of ER stress markers involved Ca²⁺ dynamics, such as PERK, IRE1 α , ATF6, GRP78, and EIF2 α , activation after PKHB1 treatment should be assessed. Moreover, although inhibition of autophagy did not prevent cell death, its implication in cell death immunogenicity was not assessed; thus, autophagy should be adequately monitored after PKHB1 treatment. This could also be useful to understand the origin of ATP released after treatment.

Besides exposure of DAMPs *in vitro*, *ex vivo* experiments in T-ALL and in breast cancer, tumor cells killed by PKHB1 (i.e., PKHB1-TCL) induced the maturation of DC, which in turn were able to prime T cells to induce tumor cell cytotoxicity. *In vivo*, PKHB1 treatment induced lymphocyte infiltration; prophylactic vaccination with PKHB1-TCL

prevented tumor growth; therapeutic treatment with PKHB1-TCL reduced tumor growth; and these treatments prevented tumor growth after rechallenging. Together, this indicates that PKHB1 can be an ICD inducer. The ability of PKHB1-TCL to induce ex vivo DC maturation capable to prime T cells was not compared to that of a known ICD inducer; therefore, the efficacy of PKHB1-TCL with respect to other therapies to induce DC maturation remains unclear. Similar experiments in the future that include the parallel analysis of a known ICD inducer could answer this interrogation. Moreover, although PKHB1-TCL protected mice from tumor rechallenging, the characteristics that leads to this potential immune memory are largely unknown; hence, evaluation of memory T cell populations as well as memory B cells and humoral responses after prophylactic vaccination with PKHB1-TCL would be of interest. In this sense, it would also be important to assess whether PKHB1 or PKHB1-TCL treatment induces the infiltration of subpopulations of NK cells and DC to the tumor site.

Relevance of optimizing TSP1 peptide mimics

Homotrimeric peptides and cell death triggering mechanism

The main limitation of using PKHB1 as an anticancer agent is the high concentration (micromolar range) needed to induce its effects in vitro, which is distant for the standard requirements for drug development (nanomolar range). However, optimization of the potency of this kind of peptide-mimics is possible, as exposed by the development of PKT16 and [PKT16]₃. Nevertheless, this homotrimeric peptide was obtained in a significantly lower yield (~10%) than PKHB1 (>90%), leaving important opportunities for synthesis optimization. Moreover, the cell death mechanism induced by [PKT16]₃ in A549 cells seemed to differ to that induced by its monomeric predecessors PKHB1 and PKT16. This suggests that whether a) [PKT16]₃ triggers the same receptor in a way that is different to that of the monomers, leading to differential signaling; or that b) it triggers a different receptor and, therefore, a different molecular signaling pathway. In this way, deciphering whether the triggering mechanism of [PKT16]₃ utilizes the same molecular components as PKHB1 and PKT16 deserves special attention considering that these

monomeric peptides keep substantial structural and chemical similarities with 4N1K, which has been shown to mimic several TSP1 functions.

To date, the design of drugs targeting the CD47-TSP1 axis has only relied on peptide screening, molecular modeling, and structure-activity relationship studies. However, the absence of descriptive evidence of this interaction, such as crystallization, limit a substantial improvement of drug development. Therefore, crystallization of the TSP1 C-terminal domain with CD47 remains a crucial aspect that needs to be answered to generate more potent peptide-mimics targeting this interaction. Nevertheless, considering the multi-ligand nature of TSP1, the consistent association of CD47 with lateral partners, and the post-translational modifications in both proteins necessary for their interaction, it is expected that additional mechanisms, absent during the simple binding experiments with soluble recombinant TSP1 and CD47 proteins, stabilize adequate conformations suitable for interaction, such as what happens in certain scenarios involving alpha and beta integrins interaction with RGD-containing proteins. With this, the use of a potent peptide binder could be of valuable interest to understand TSP1-CD47 interaction, such as the RGD peptide was to understand the complexity of RGD-dependent integrin signaling. One should keep in mind that it was thanks to a synthetic peptide that alpha-beta integrin interaction with the RGD motif, present in different extracellular proteins, including TSPs, was crystallized.

Indeed, TSP1 includes an RGD motif at its signature domain. And in the present work RGD improved PKHB1 activity, different variants of RGD-linked peptides were also designed in the present work in an unsuccessful attempt to improve PKHB1 efficacy. However, keeping a developmental perspective in mind, only short linkers were selected, even when the RGD motif stands far away from PKHB1's pharmacophore in the three-dimensional structure of the thrombospondin. Thus, trying linkers of varying length might help to understand the role of integrins in PKHB1-induced cell death. A Ca^{2+} -interacting DDD motif is close in distance from the PKHB1 pharmacophore in the three-dimensional structure of the globular domain of thrombospondins and is necessary for homotrimeric TSP1 C-terminal domain retention by the cell. A recombinant protein with a mutant 4N1

β -strand, or a calcium-binding peptide-mimic containing the PKHB1 pharmacophore and the DDD motif might be useful to study this.

Potential of TSP-C-terminus peptide-mimics to induce cell death in cancer and non-resolving inflammatory cells

Overall, the results of the present thesis work support the therapeutic potential and further development of peptide-mimics of the TSP-C-terminus against cancer. However, the TSP1-CD47 axis is also involved in the induction of RCD of certain populations of immune cells during resolution of inflammation (e.g., CD47^{low}-status effector memory T cells, and recruited monocyte-derived inflammatory macrophages). In some of them, the 4N1 and 4N1K peptides have been shown to have a potential therapeutic use. The structural similarity of PKHB1 with 4N1K suggests that PKHB1-induced cell death could render similar results in specific subtypes of immune cells where the TSP1-CD47 axis has potential therapeutic applications. In that sense, studying the use of PKHB1 to treat inflammatory diseases where the TSP1-CD47 axis has shown to be implicated in resolution of inflammation is pertinent. An example of such a use has been demonstrated for macular degeneration and acute sterile peritonitis (Calippe *et al.*, 2017). However, this could be extended to other nonresolving inflammatory diseases such as the Sjögren's syndrome (Contreras Ruiz *et al.*, 2017) or psoriasis (Rodríguez-Jiménez *et al.*, 2019), for which treatment options are limited.

The future of therapeutic peptides

Finally, among the options to target immune checkpoints such as CD47, or mimic protein-protein interactions, such as the TSP1-CD47 axis, the major strategies rely whether on small molecules or big recombinant proteins and antibodies. Due their ease of production and minimal cost, small molecules are largely preferred over proteins for pharmaceutical exploitation, however, they largely account for secondary effects related to their unspecificity. On the other hand, therapeutic proteins (e.g., humanized antibodies and soluble recombinant proteins) are by nature, more specific to their targets, however their size represents high production costs compared to small molecules synthesized chemically. Peptides place in a middle point, between low-cost and target specificity. If peptides have several drawbacks (e.g., poor metabolic stability, and high flexibility

leading to poor target selectivity compared to bigger proteins), many strategies have been developed to optimize their properties (e.g., the use of non-natural amino acids, and the design of peptidomimetics or foldamers). Such strategies, however, add technical complications that impact their ease of production at large scale. Therefore, the philosophy of the DRUG Lab is to use only natural amino acids to optimize the properties of potential therapeutic peptides, making a balance with appropriate rational designs. Indeed, more than 700 amino acids exist in nature that help to improve peptide properties, such as, for example, N-Methyl amino acids or D-amino acids present in cyclosporin A. This has been applied in other research subjects, such as in one concerning the recent COVID-19 pandemic, where peptides consisting of only natural amino acids were designed to interact with the spike RBD. Although this aspect is not discussed in the present manuscript, I had the opportunity to contribute within the project (see annex), and beyond my thesis, in general, this experience raises the interest on peptides among the range of therapeutic tools.

References

References

Abalsamo, L. *et al.* (2012) 'Inhibition of phosphatidylcholine-specific phospholipase C results in loss of mesenchymal traits in metastatic breast cancer cells', *Breast Cancer Research*. doi: 10.1186/bcr3151.

Adams, J. C. *et al.* (2008) 'Extracellular matrix retention of thrombospondin 1 is controlled by its conserved C-terminal region', *Journal of Cell Science*. The Company of Biologists, 121(6), pp. 784–795. doi: 10.1242/jcs.021006.

Adams, J. C. and Lawler, J. (2011) 'The thrombospondins.', *Cold Spring Harbor perspectives in biology*. Cold Spring Harbor Laboratory Press, 3(10), p. a009712. doi: 10.1101/cshperspect.a009712.

Ameisen, J. C. (2002) 'On the origin, evolution, and nature of programmed cell death: a timeline of four billion years', *Cell Death & Differentiation*. Nature Publishing Group, 9(4), pp. 367–393. doi: 10.1038/sj.cdd.4400950.

Amelio, I. *et al.* (2018) 'p53 mutants cooperate with HIF-1 in transcriptional regulation of extracellular matrix components to promote tumor progression.', *Proceedings of the National Academy of Sciences of the United States of America*. National Academy of Sciences, 115(46), pp. E10869–E10878. doi: 10.1073/pnas.1808314115.

Arias, Clemente Fernandez and Arias, Cristina Fernandez (2017) 'How do red blood cells know when to die?', *Royal Society Open Science*. The Royal Society, 4(4), p. 160850. doi: 10.1098/rsos.160850.

De Azambuja, E. *et al.* (2015) 'Cardiac assessment of early breast cancer patients 18 years after treatment with cyclophosphamide-, methotrexate-, fluorouracil- or epirubicin-based chemotherapy', *European Journal of Cancer*. Elsevier Ltd, 51(17), pp. 2517–2524. doi: 10.1016/j.ejca.2015.08.011.

Azcutia, V. *et al.* (2012) 'Endothelial CD47 promotes vascular endothelial-cadherin tyrosine phosphorylation and participates in T cell recruitment at sites of inflammation in vivo.', *Journal of immunology (Baltimore, Md. : 1950)*. NIH Public Access, 189(5), pp. 2553–62. doi: 10.4049/jimmunol.1103606.

Azcutia, V. *et al.* (2013) 'CD47 plays a critical role in T-cell recruitment by regulation of LFA-1 and VLA-4 integrin adhesive functions', *Molecular Biology of the Cell*. Edited by M. H. Ginsberg, 24(21), pp. 3358–3368. doi: 10.1091/mbc.e13-01-0063.

Baenziger, N. L., Brodie, G. N. and Majerus, P. W. (1971) 'A thrombin-sensitive protein of human platelet membranes.', *Proceedings of the National Academy of Sciences of the United States of America*, 68(1), pp. 240–3. Available at: <http://www.pubmedcentral.nih.gov/articlerender.fcgi?artid=391203&tool=pmcentrez&rendertype=abstract> (Accessed: 25 September 2015).

Barclay, A. N. and Van den Berg, T. K. (2014) 'The interaction between signal regulatory protein alpha (SIRP α) and CD47: structure, function, and therapeutic target.',

Annual review of immunology. Annual Reviews, 32, pp. 25–50. doi: 10.1146/annurev-immunol-032713-120142.

Bauer, E. M. *et al.* (2010) ‘Thrombospondin-1 supports blood pressure by limiting eNOS activation and endothelial-dependent vasorelaxation.’, *Cardiovascular research*, 88(3), pp. 471–81. doi: 10.1093/cvr/cvq218.

Bell, R. A. V and Megeney, L. A. (2017) ‘Evolution of caspase-mediated cell death and differentiation: twins separated at birth’, *Cell Death & Differentiation*. Nature Publishing Group, 24(8), pp. 1359–1368. doi: 10.1038/cdd.2017.37.

Bentley, A. A. and Adams, J. C. (2010) ‘The Evolution of Thrombospondins and Their Ligand-Binding Activities’, *Molecular Biology and Evolution*. Oxford Academic, 27(9), pp. 2187–2197. doi: 10.1093/molbev/msq107.

Vanden Berghe, T. *et al.* (2014) ‘Regulated necrosis: the expanding network of non-apoptotic cell death pathways.’, *Nature reviews. Molecular cell biology*. Nature Publishing Group, 15(2), pp. 135–47. doi: 10.1038/nrm3737.

Bergström, S.-E. *et al.* (2015) ‘Antigen-induced regulation of T-cell motility, interaction with antigen-presenting cells and activation through endogenous thrombospondin-1 and its receptors’, *Immunology*. John Wiley & Sons, Ltd, 144(4), pp. 687–703. doi: 10.1111/imm.12424.

Berridge, M. J. (2002) ‘The endoplasmic reticulum: a multifunctional signaling organelle.’, *Cell calcium*, 32(5–6), pp. 235–49. Available at: <http://www.ncbi.nlm.nih.gov/pubmed/12543086> (Accessed: 26 April 2017).

Berridge, M. J., Lipp, P. and Bootman, M. D. (2000) ‘The versatility and universality of calcium signalling’, *Nature Reviews Molecular Cell Biology*. Nature Publishing Group, 1(1), pp. 11–21. doi: 10.1038/35036035.

Bissinger, R. *et al.* (2020) ‘Thrombospondin-1/CD47 signaling modulates transmembrane cation conductance, survival, and deformability of human red blood cells’, *Cell Communication and Signaling*. BioMed Central, 18(1), p. 155. doi: 10.1186/s12964-020-00651-5.

Bivona, T. G. *et al.* (2003) ‘Phospholipase C γ activates Ras on the Golgi apparatus by means of RasGRP1’, *Nature*. Nature Publishing Group, 424(6949), pp. 694–698. doi: 10.1038/nature01806.

Bornstein, P. *et al.* (1991) ‘A second, expressed thrombospondin gene (Thbs2) exists in the mouse genome’, *Journal of Biological Chemistry*. Elsevier, 266(20), pp. 12821–12824. doi: 10.1016/S0021-9258(18)98764-8.

Bornstein, P. and Sage, E. H. (2002) ‘Matricellular proteins: extracellular modulators of cell function’, *Current Opinion in Cell Biology*. Elsevier Current Trends, 14(5), pp. 608–616. doi: 10.1016/S0955-0674(02)00361-7.

Brini, M. *et al.* (2013) ‘Intracellular calcium homeostasis and signaling.’, *Metal ions in life sciences*, 12, pp. 119–68. doi: 10.1007/978-94-007-5561-1_5.

Brittain, J. E. *et al.* (2004) ‘Mechanism of CD47-induced $\alpha 4\beta 1$ Integrin Activation and Adhesion in Sickle Reticulocytes’, *Journal of Biological Chemistry*. Elsevier, 279(41),

pp. 42393–42402. doi: 10.1074/JBC.M407631200.

Bröker, L. E., Kruyt, F. A. E. and Giaccone, G. (2005) ‘Cell death independent of caspases: a review.’, *Clinical cancer research : an official journal of the American Association for Cancer Research*, 11(9), pp. 3155–62. doi: 10.1158/1078-0432.CCR-04-2223.

Brown, E. *et al.* (1990) ‘Integrin-associated protein: a 50-kD plasma membrane antigen physically and functionally associated with integrins.’, *The Journal of cell biology*, 111(6 Pt 1), pp. 2785–94. Available at: <http://www.ncbi.nlm.nih.gov/pubmed/2277087> (Accessed: 3 March 2017).

Brown, E. J. and Frazier, W. A. (2001) ‘Integrin-associated protein (CD47) and its ligands.’, *Trends in cell biology*, 11(3), pp. 130–5. Available at: <http://www.ncbi.nlm.nih.gov/pubmed/11306274> (Accessed: 25 September 2015).

Bruce, L. J. *et al.* (2003) ‘A band 3-based macrocomplex of integral and peripheral proteins in the RBC membrane’, *Blood*. American Society of Hematology, 101(10), pp. 4180–4188. doi: 10.1182/blood-2002-09-2824.

Burger, P. *et al.* (2012) ‘CD47 functions as a molecular switch for erythrocyte phagocytosis’, *Blood*, 119(23), pp. 5512–5521. doi: 10.1182/blood-2011-10-386805.

Cabrales, P. (2019) ‘RRx-001 Acts as a Dual Small Molecule Checkpoint Inhibitor by Downregulating CD47 on Cancer Cells and SIRP- α on Monocytes/Macrophages’, *Translational Oncology*. Elsevier, 12(4), pp. 626–632. doi: 10.1016/J.TRANON.2018.12.001.

Calippe, B. *et al.* (2017) ‘Complement Factor H Inhibits CD47-Mediated Resolution of Inflammation’, *Immunity*, 46(2), pp. 261–272. doi: 10.1016/j.immuni.2017.01.006.

Calmeiro, J. *et al.* (2020) ‘Dendritic cell vaccines for cancer immunotherapy: The role of human conventional type 1 dendritic cells’, *Pharmaceutics*. MDPI AG. doi: 10.3390/pharmaceutics12020158.

Capiod, T. *et al.* (2007) ‘Calcium signalling and cancer cell growth.’, *Sub-cellular biochemistry*, 45, pp. 405–27. Available at: <http://www.ncbi.nlm.nih.gov/pubmed/18193646> (Accessed: 26 April 2017).

Capiod, T. (2013) ‘The need for calcium channels in cell proliferation.’, *Recent patents on anti-cancer drug discovery*, 8(1), pp. 4–17. Available at: <http://www.ncbi.nlm.nih.gov/pubmed/22519598> (Accessed: 15 October 2015).

Carlson, C. B. *et al.* (2005) ‘Structure of the calcium-rich signature domain of human thrombospondin-2.’, *Nature structural & molecular biology*. Nat Struct Mol Biol, 12(10), pp. 910–4. doi: 10.1038/nsmb997.

Carlson, C. B., Lawler, J. and Mosher, D. F. (2008) ‘Structures of thrombospondins.’, *Cellular and molecular life sciences : CMLS*. NIH Public Access, 65(5), pp. 672–86. doi: 10.1007/s00018-007-7484-1.

Castillo, A. B., Chen, J. C. and Jacobs, C. R. (2021) ‘Cellular and molecular mechanotransduction in bone’, *Marcus and Feldman’s Osteoporosis*. Academic Press, pp. 309–335. doi: 10.1016/B978-0-12-813073-5.00014-9.

- Catacchio, I. *et al.* (2019) ‘Intratumoral, rather than stromal, CD8+ T cells could be a potential negative prognostic marker in invasive breast cancer patients’, *Translational Oncology*. Neoplasia Press, Inc., 12(3), pp. 585–595. doi: 10.1016/j.tranon.2018.12.005.
- Chang, C.-R. and Blackstone, C. (2007) ‘Cyclic AMP-dependent Protein Kinase Phosphorylation of Drp1 Regulates Its GTPase Activity and Mitochondrial Morphology’, *Journal of Biological Chemistry*. Elsevier, 282(30), pp. 21583–21587. doi: 10.1074/jbc.C700083200.
- Chao, Mark P *et al.* (2010) ‘Calreticulin is the dominant pro-phagocytic signal on multiple human cancers and is counterbalanced by CD47.’, *Science translational medicine*. American Association for the Advancement of Science, 2(63), p. 63ra94. doi: 10.1126/scitranslmed.3001375.
- Chao, M. P. *et al.* (2010) ‘Therapeutic Antibody Targeting of CD47 Eliminates Human Acute Lymphoblastic Leukemia’, *Cancer Research*, 71(4), pp. 1374–1384. doi: 10.1158/0008-5472.CAN-10-2238.
- Chao, M. P., Weissman, I. L. and Majeti, R. (2012) ‘The CD47–SIRP α pathway in cancer immune evasion and potential therapeutic implications’, *Current opinion in immunology*, 24(2), pp. 225–232. doi: 10.1016/j.coi.2012.01.010.
- Chen, Z. *et al.* (2012) ‘Nitric oxide–dependent Src activation and resultant caveolin-1 phosphorylation promote eNOS/caveolin-1 binding and eNOS inhibition’, *Molecular Biology of the Cell*. Edited by R. G. Parton. The American Society for Cell Biology, 23(7), pp. 1388–1398. doi: 10.1091/mbc.e11-09-0811.
- Cheng, H. *et al.* (2014) ‘Nitric oxide in cancer metastasis’, *Cancer Letters*. Elsevier, 353(1), pp. 1–7. doi: 10.1016/J.CANLET.2014.07.014.
- Cheng, Q. *et al.* (2020) ‘Is CD47 a potentially promising therapeutic target in cardiovascular diseases? — Role of CD47 in cardiovascular diseases’, *Life Sciences*. Pergamon, 247, p. 117426. doi: 10.1016/J.LFS.2020.117426.
- Chiang, C. L.-L., Coukos, G. and Kandalaft, L. E. (2015) ‘Whole Tumor Antigen Vaccines: Where Are We?’, *Vaccines*. Multidisciplinary Digital Publishing Institute (MDPI), 3(2), pp. 344–72. doi: 10.3390/vaccines3020344.
- Chung, J., Gao, A. G. and Frazier, W. A. (1997) ‘Thrombospondin acts via integrin-associated protein to activate the platelet integrin α IIb β 3.’, *The Journal of biological chemistry*, 272(23), pp. 14740–6. Available at: <http://www.ncbi.nlm.nih.gov/pubmed/9169439> (Accessed: 25 September 2015).
- Clarke, P. G. (1990) ‘Developmental cell death: morphological diversity and multiple mechanisms.’, *Anatomy and embryology*. Anat Embryol (Berl), 181(3), pp. 195–213. doi: 10.1007/BF00174615.
- Contreras Ruiz, L. *et al.* (2017) ‘Thrombospondin-derived peptide attenuates Sjögren’s syndrome-associated ocular surface inflammation in mice’, *Clinical & Experimental Immunology*. John Wiley & Sons, Ltd, 188(1), pp. 86–95. doi: 10.1111/cei.12919.
- Cooper, G. M. (2000) *The cell : a molecular approach*. ASM Press.
- Dahl, K. N. *et al.* (2004) ‘Protein 4.2 is critical to CD47-membrane skeleton attachment

- in human red cells', *Blood*. Content Repository Only!, 103(3), pp. 1131–1136. doi: 10.1182/BLOOD-2003-04-1331.
- Danho, W. *et al.* (2009) 'Opportunities and Challenges of Developing Peptide Drugs in the Pharmaceutical Industry', in: Springer, New York, NY, pp. 467–469. doi: 10.1007/978-0-387-73657-0_201.
- Dawson, D. W. *et al.* (1997) 'CD36 Mediates the In Vitro Inhibitory Effects of Thrombospondin-1 on Endothelial Cells', *Journal of Cell Biology*. The Rockefeller University Press, 138(3), pp. 707–717. doi: 10.1083/jcb.138.3.707.
- Denèfle, T. *et al.* (2016) 'Thrombospondin-1 Mimetic Agonist Peptides Induce Selective Death in Tumor Cells: Design, Synthesis, and Structure–Activity Relationship Studies', *Journal of Medicinal Chemistry*, 59(18), pp. 8412–8421. doi: 10.1021/acs.jmedchem.6b00781.
- Denèfle, T. *et al.* (2019) 'Homotrimerization Approach in the Design of Thrombospondin-1 Mimetic Peptides with Improved Potency in Triggering Regulated Cell Death of Cancer Cells', *Journal of Medicinal Chemistry*. American Chemical Society, 62(17), pp. 7656–7668. doi: 10.1021/acs.jmedchem.9b00024.
- Dudek, A. M. *et al.* (2013) 'Immature, Semi-Mature, and Fully Mature Dendritic Cells: Toward a DC–Cancer Cells Interface That Augments Anticancer Immunity.', *Frontiers in immunology*. Frontiers Media SA, 4, p. 438. doi: 10.3389/fimmu.2013.00438.
- El-Rashid, M. *et al.* (2019) 'CD47 limits autophagy to promote acute kidney injury', *The FASEB Journal*. John Wiley & Sons, Ltd, 33(11), pp. 12735–12749. doi: 10.1096/fj.201900120RR.
- Erak, M. *et al.* (2018) 'Peptide chemistry toolbox – Transforming natural peptides into peptide therapeutics', *Bioorganic & Medicinal Chemistry*. Pergamon, 26(10), pp. 2759–2765. doi: 10.1016/J.BMC.2018.01.012.
- Farah, C., Michel, L. Y. M. and Balligand, J.-L. (2018) 'Nitric oxide signalling in cardiovascular health and disease', *Nature Reviews Cardiology*. Nature Publishing Group, 15(5), pp. 292–316. doi: 10.1038/nrcardio.2017.224.
- Farkona, S., Diamandis, E. P. and Blasutig, I. M. (2016) 'Cancer immunotherapy: The beginning of the end of cancer?', *BMC Medicine*. doi: 10.1186/s12916-016-0623-5.
- Feliz-Mosquea, Y. R. *et al.* (2018) 'Combination of anthracyclines and anti-CD47 therapy inhibit invasive breast cancer growth while preventing cardiac toxicity by regulation of autophagy', *Breast Cancer Research and Treatment*. Springer, 172(1), pp. 69–82. doi: 10.1007/s10549-018-4884-x.
- Floquet, N. *et al.* (2008) 'Human thrombospondin's (TSP-1) C-terminal domain opens to interact with the CD-47 receptor: A molecular modeling study', *Archives of Biochemistry and Biophysics*, 478(1), pp. 103–109. doi: 10.1016/j.abb.2008.07.015.
- Fortis, S. P. *et al.* (2017) 'Differential intratumoral distributions of CD8 and CD163 immune cells as prognostic biomarkers in breast cancer', *Journal for ImmunoTherapy of Cancer*. BioMed Central Ltd., 5(1), p. 39. doi: 10.1186/s40425-017-0240-7.
- Fortuna Haviv, * *et al.* (2005) 'Thrombospondin-1 Mimetic Peptide Inhibitors of

- Angiogenesis and Tumor Growth: Design, Synthesis, and Optimization of Pharmacokinetics and Biological Activities'. American Chemical Society. doi: 10.1021/JM0401560.
- Fosgerau, K. and Hoffmann, T. (2015) 'Peptide therapeutics: current status and future directions', *Drug discovery today*. Drug Discov Today, 20(1), pp. 122–8. doi: 10.1016/j.drudis.2014.10.003.
- Frantz, C., Stewart, K. M. and Weaver, V. M. (2010) 'The extracellular matrix at a glance', *Journal of Cell Science*. The Company of Biologists, 123(24), pp. 4195–4200. doi: 10.1242/jcs.023820.
- Frazier, W. A. *et al.* (1999) 'The thrombospondin receptor integrin-associated protein (CD47) functionally couples to heterotrimeric Gi.', *The Journal of biological chemistry*. Elsevier, 274(13), pp. 8554–60. doi: 10.1074/jbc.274.13.8554.
- Freireich, E. J., Wiernik, P. H. and Steensma, D. P. (2014) 'The leukemias: a half-century of discovery.', *Journal of clinical oncology : official journal of the American Society of Clinical Oncology*. American Society of Clinical Oncology, 32(31), pp. 3463–9. doi: 10.1200/JCO.2014.57.1034.
- Fuchs, Y. and Steller, H. (2011) 'Programmed cell death in animal development and disease.', *Cell*. Elsevier Inc., 147(4), pp. 742–58. doi: 10.1016/j.cell.2011.10.033.
- Galluzzi, L. *et al.* (2012) 'Molecular definitions of cell death subroutines: recommendations of the Nomenclature Committee on Cell Death 2012.', *Cell death and differentiation*, 19(1), pp. 107–20. doi: 10.1038/cdd.2011.96.
- Galluzzi, L. *et al.* (2014) 'Essential versus accessory aspects of cell death: recommendations of the NCCD 2015.', *Cell death and differentiation*. Macmillan Publishers Limited, 22(1), pp. 58–73. doi: 10.1038/cdd.2014.137.
- Galluzzi, L. *et al.* (2016) 'Immunogenic cell death in cancer and infectious disease', *Nature Reviews Immunology*. Nature Research, 17(2), pp. 97–111. doi: 10.1038/nri.2016.107.
- Galluzzi, L. *et al.* (2018) 'Molecular mechanisms of cell death: recommendations of the Nomenclature Committee on Cell Death 2018', *Cell Death & Differentiation*. Nature Publishing Group, p. 1. doi: 10.1038/s41418-017-0012-4.
- Galluzzi, L. *et al.* (2020) 'Consensus guidelines for the definition, detection and interpretation of immunogenic cell death', *Journal for ImmunoTherapy of Cancer*. BMJ Publishing Group, p. 70. doi: 10.1136/jitc-2019-000337.
- Gao, A.-G. *et al.* (1996) 'Integrin-associated Protein Is a Receptor for the C-terminal Domain of Thrombospondin', *Journal of Biological Chemistry*. Elsevier, 271(1), pp. 21–24. doi: 10.1074/JBC.271.1.21.
- Gardai, S. J. *et al.* (2005) 'Cell-Surface Calreticulin Initiates Clearance of Viable or Apoptotic Cells through trans-Activation of LRP on the Phagocyte', *Cell*, 123(2), pp. 321–334. doi: 10.1016/j.cell.2005.08.032.
- Garg, Abhishek D *et al.* (2015) 'Immunogenic cell death.', *The International journal of developmental biology*. UPV/EHU Press, 59(1–3), pp. 131–40. doi:

10.1387/ijdb.150061pa.

Garg, Abhishek D. *et al.* (2015) 'Molecular and translational classifications of DAMPs in immunogenic cell death', *Frontiers in Immunology*. doi: 10.3389/fimmu.2015.00588.

Garg, A. D. *et al.* (2017) 'Trial watch: Immunogenic cell death induction by anticancer chemotherapeutics', *OncoImmunology*. doi: 10.1080/2162402X.2017.1386829.

Garrido, G. *et al.* (2011) 'Induction of Immunogenic Apoptosis by Blockade of Epidermal Growth Factor Receptor Activation with a Specific Antibody', *The Journal of Immunology*. doi: 10.4049/jimmunol.1003477.

Glick, D., Barth, S. and Macleod, K. F. (2010) 'Autophagy: cellular and molecular mechanisms.', *The Journal of pathology*. NIH Public Access, 221(1), pp. 3–12. doi: 10.1002/path.2697.

Globocan (2020) *All cancers*. Available at: <https://gco.iarc.fr/today> (Accessed: 25 June 2021).

Gómez-Morales, L. (2017) *STUDY OF THE MECHANISM OF CELL DEATH CAUSED BY PEPTIDES TARGETING CD47 IN LEUKEMIA CELL LINES*. Universidad Autónoma de Nuevo León. Available at: <http://eprints.uanl.mx/14460/1/1080252237.pdf> (Accessed: 6 June 2021).

Gorin, J. B. *et al.* (2014) 'Antitumor immunity induced after α irradiation', *Neoplasia (United States)*. doi: 10.1016/j.neo.2014.04.002.

Green, D. R. and Llambi, F. (2015) 'Cell Death Signaling.', *Cold Spring Harbor perspectives in biology*. Cold Spring Harbor Laboratory Press, 7(12), p. a006080. doi: 10.1101/cshperspect.a006080.

Grivennikov, S. I., Greten, F. R. and Karin, M. (2010) 'Immunity, inflammation, and cancer.', *Cell*. Elsevier, 140(6), pp. 883–99. doi: 10.1016/j.cell.2010.01.025.

Groenendijk, F. H. and Bernards, R. (2014) 'Drug resistance to targeted therapies: Déjà vu all over again', *Molecular Oncology*. Elsevier, pp. 1067–1083. doi: 10.1016/j.molonc.2014.05.004.

Gupta, A. *et al.* (2017) 'Calcium-induced conformational changes of Thrombospondin-1 signature domain: implications for vascular disease.', *Journal of receptor and signal transduction research*. J Recept Signal Transduct Res, 37(3), pp. 239–251. doi: 10.1080/10799893.2016.1212377.

Hanahan, D. and Weinberg, R. A. (2000) 'The Hallmarks of Cancer', *Cell*, 100(1), pp. 57–70. Available at: <http://www.ncbi.nlm.nih.gov/pubmed/10647931> (Accessed: 10 July 2014).

Hanahan, D. and Weinberg, R. a (2011) 'Hallmarks of cancer: the next generation.', *Cell*. Elsevier Inc., 144(5), pp. 646–74. doi: 10.1016/j.cell.2011.02.013.

Hatherley, D. *et al.* (2008) 'Paired Receptor Specificity Explained by Structures of Signal Regulatory Proteins Alone and Complexed with CD47', *Molecular Cell*, 31(2), pp. 266–277. doi: 10.1016/j.molcel.2008.05.026.

Hazama, D. *et al.* (2020) 'Macrocyclic Peptide-Mediated Blockade of the CD47-SIRP α

- Interaction as a Potential Cancer Immunotherapy.’, *Cell chemical biology*. Elsevier, 27(9), pp. 1181-1191.e7. doi: 10.1016/j.chembiol.2020.06.008.
- Henry, F. *et al.* (1999) ‘Role of antigen-presenting cells in long-term antitumor response based on tumor-derived apoptotic body vaccination’, in *Pathobiology*. doi: 10.1159/000028086.
- Hirata, E. and Sahai, E. (2017) ‘Tumor Microenvironment and Differential Responses to Therapy.’, *Cold Spring Harbor perspectives in medicine*. Cold Spring Harbor Laboratory Press, 7(7), p. a026781. doi: 10.1101/cshperspect.a026781.
- Huang, C.-Y. *et al.* (2020) ‘Regulation of CD47 expression in cancer cells’, *Translational Oncology*. Elsevier, 13(12), p. 100862. doi: 10.1016/J.TRANON.2020.100862.
- Huang, T. *et al.* (2017) ‘Thrombospondin-1 is a multifaceted player in tumor progression.’, *Oncotarget*. Impact Journals, LLC, 8(48), pp. 84546–84558. doi: 10.18632/oncotarget.19165.
- Humeau, J. *et al.* (2019) ‘Gold standard assessment of immunogenic cell death in oncological mouse models’, in *Methods in Molecular Biology*. Humana Press Inc., pp. 297–315. doi: 10.1007/978-1-4939-8885-3_21.
- Insenberg, J. S. and Roberts, D. D. (2020) ‘THBS1 (thrombospondin-1)’, *Atlas of Genetics and Cytogenetics in Oncology and Haematology*, 24(8), pp. 291–299. doi: 10.4267/2042/70774.
- Irvin, B. J. *et al.* (2002) ‘Pleiotropic Contributions of Phospholipase C-gamma 1 (PLC-gamma 1) to T-Cell Antigen Receptor-Mediated Signaling: Reconstitution Studies of a PLC-gamma 1-Deficient Jurkat T-Cell Line’, *Molecular and Cellular Biology*. doi: 10.1128/mcb.20.24.9149-9161.2000.
- Isenberg, J. S. *et al.* (2005) ‘Thrombospondin-1 inhibits endothelial cell responses to nitric oxide in a cGMP-dependent manner.’, *Proceedings of the National Academy of Sciences of the United States of America*. National Academy of Sciences, 102(37), pp. 13141–6. doi: 10.1073/pnas.0502977102.
- Isenberg, J. S. *et al.* (2006) ‘CD47 Is Necessary for Inhibition of Nitric Oxide-stimulated Vascular Cell Responses by Thrombospondin-1’, *Journal of Biological Chemistry*, 281(36), pp. 26069–26080. doi: 10.1074/jbc.M605040200.
- Isenberg, J. S. *et al.* (2007) ‘Thrombospondin-1 limits ischemic tissue survival by inhibiting nitric oxide-mediated vascular smooth muscle relaxation’, *Blood*. American Society of Hematology, 109(5), pp. 1945–1952. doi: 10.1182/blood-2006-08-041368.
- Isenberg, J. S. *et al.* (2008) ‘Thrombospondin-1 stimulates platelet aggregation by blocking the antithrombotic activity of nitric oxide/cGMP signaling.’, *Blood*. American Society of Hematology, 111(2), pp. 613–23. doi: 10.1182/blood-2007-06-098392.
- Isenberg, Jeff S *et al.* (2009) ‘Differential interactions of thrombospondin-1, -2, and -4 with CD47 and effects on cGMP signaling and ischemic injury responses.’, *The Journal of biological chemistry*, 284(2), pp. 1116–25. doi: 10.1074/jbc.M804860200.
- Isenberg, Jeff S. *et al.* (2009) ‘Regulation of nitric oxide signalling by thrombospondin

- 1: implications for anti-angiogenic therapies', *Nature Reviews Cancer*. Nature Publishing Group, 9(3), pp. 182–194. doi: 10.1038/nrc2561.
- Isenberg, J. S. and Roberts, D. D. (2020) 'Thrombospondin-1 in maladaptive aging responses: a concept whose time has come.', *American journal of physiology. Cell physiology*. Am J Physiol Cell Physiol, 319(1), pp. C45–C63. doi: 10.1152/ajpcell.00089.2020.
- Isenberg, J. S., Wink, D. A. and Roberts, D. (2006) 'Thrombospondin-1 antagonizes nitric oxide-stimulated vascular smooth muscle cell responses', *Cardiovascular Research*. Oxford Academic, 71(4), pp. 785–793. doi: 10.1016/j.cardiores.2006.05.024.
- Jaffe, E. A. *et al.* (1982) 'Thrombospondin is the endogenous lectin of human platelets', *Nature*. Nature Publishing Group, 295(5846), pp. 246–248. doi: 10.1038/295246a0.
- Jaiswal, S. *et al.* (2009) 'CD47 Is Upregulated on Circulating Hematopoietic Stem Cells and Leukemia Cells to Avoid Phagocytosis', *Cell*. Elsevier, 138(2), pp. 271–285. doi: 10.1016/j.cell.2009.05.046.
- Jaiswal, S. *et al.* (2010) 'Macrophages as mediators of tumor immunosurveillance', *Trends in Immunology*. Elsevier Current Trends, 31(6), pp. 212–219. doi: 10.1016/J.IT.2010.04.001.
- Jalil, A. R., Andrechak, J. C. and Discher, D. E. (2020) 'Macrophage checkpoint blockade: results from initial clinical trials, binding analyses, and CD47-SIRP α structure–function', *Antibody Therapeutics*. Oxford Academic, 3(2), pp. 80–94. doi: 10.1093/abt/tbaa006.
- James P. Allison – Facts – 2018 - NobelPrize.org (no date). Available at: <https://www.nobelprize.org/prizes/medicine/2018/allison/facts/> (Accessed: 18 June 2021).
- Jeanne, A. *et al.* (2015) 'Original insights on thrombospondin-1-related antireceptor strategies in cancer.', *Frontiers in pharmacology*. Frontiers Media SA, 6, p. 252. doi: 10.3389/fphar.2015.00252.
- Kalas, W. *et al.* (2013) 'Thrombospondin-1 Receptor Mediates Autophagy of RAS-expressing Cancer Cells and Triggers Tumour Growth Inhibition', *Anticancer research*, 33(4), pp. 1429–1438. Available at: <https://ar.iijournals.org/content/anticancer/33/4/1429.full.pdf> (Accessed: 16 June 2021).
- Kamm, A. *et al.* (2019) 'Nitric oxide and its derivatives in the cancer battlefield', *Nitric Oxide*. Academic Press, 93, pp. 102–114. doi: 10.1016/J.NIOX.2019.09.005.
- Kang, R. *et al.* (2011) 'The Beclin 1 network regulates autophagy and apoptosis.', *Cell death and differentiation*. Nature Publishing Group, 18(4), pp. 571–80. doi: 10.1038/cdd.2010.191.
- Kaur, S. *et al.* (2010) 'Thrombospondin-1 inhibits VEGF receptor-2 signaling by disrupting its association with CD47.', *The Journal of biological chemistry*. American Society for Biochemistry and Molecular Biology, 285(50), pp. 38923–32. doi: 10.1074/jbc.M110.172304.

- Kaur, S. *et al.* (2011) ‘Heparan Sulfate Modification of the Transmembrane Receptor CD47 Is Necessary for Inhibition of T Cell Receptor Signaling by Thrombospondin-1’, *Journal of Biological Chemistry*, 286(17), pp. 14991–15002. doi: 10.1074/jbc.M110.179663.
- Kaur, S. *et al.* (2014) ‘CD47 Signaling Regulates the Immunosuppressive Activity of VEGF in T Cells’, *The Journal of Immunology*, 193(8), pp. 3914–3924. doi: 10.4049/jimmunol.1303116.
- Kaur, S. *et al.* (2021) ‘Functions of Thrombospondin-1 in the Tumor Microenvironment’, *International Journal of Molecular Sciences*. Multidisciplinary Digital Publishing Institute, 22(9), p. 4570. doi: 10.3390/ijms22094570.
- Kennedy, J. *et al.* (2005) ‘COMP mutation screening as an aid for the clinical diagnosis and counselling of patients with a suspected diagnosis of pseudoachondroplasia or multiple epiphyseal dysplasia.’, *European journal of human genetics : EJHG*. Eur J Hum Genet, 13(5), pp. 547–55. doi: 10.1038/sj.ejhg.5201374.
- Kepp, O. *et al.* (2014) ‘Consensus guidelines for the detection of immunogenic cell death’, *OncoImmunology*. doi: 10.4161/21624011.2014.955691.
- Kim, J.-I. *et al.* (2018) ‘CRISPR/Cas9-mediated knockout of CD47 causes hemolytic anemia with splenomegaly in C57BL/6 mice.’, *Laboratory animal research*. Korean Association for Laboratory Animal Science, 34(4), pp. 302–310. doi: 10.5625/lar.2018.34.4.302.
- Klionsky, D. J. *et al.* (2016) ‘Guidelines for the use and interpretation of assays for monitoring autophagy (3rd edition)’, *Autophagy*. Taylor & Francis, 12(1), p. 1. doi: 10.1080/15548627.2015.1100356.
- Koonin, E. V and Starokadomskyy, P. (2016) ‘Are viruses alive? The replicator paradigm sheds decisive light on an old but misguided question.’, *Studies in history and philosophy of biological and biomedical sciences*. Stud Hist Philos Biol Biomed Sci, 59, pp. 125–34. doi: 10.1016/j.shpsc.2016.02.016.
- Koren, E. and Fuchs, Y. (2021) ‘Modes of Regulated Cell Death in Cancer.’, *Cancer discovery*. American Association for Cancer Research, 11(2), pp. 245–265. doi: 10.1158/2159-8290.CD-20-0789.
- Kosfeld, M. D. and Frazier, W. A. (1993) ‘Identification of a new cell adhesion motif in two homologous peptides from the COOH-terminal cell binding domain of human thrombospondin.’, *The Journal of biological chemistry*, 268(12), pp. 8808–14. Available at: <http://www.ncbi.nlm.nih.gov/pubmed/8473325> (Accessed: 25 September 2015).
- Krekorian, M. *et al.* (2019) ‘Imaging of T-cells and their responses during anti-cancer immunotherapy’, *Theranostics*. Ivyspring International Publisher, pp. 7924–7947. doi: 10.7150/thno.37924.
- Kroemer, G. *et al.* (2005) ‘Classification of cell death: recommendations of the Nomenclature Committee on Cell Death’, *Cell Death and Differentiation*. Nature Publishing Group, 12, pp. 1463–1467. doi: 10.1038/sj.cdd.4401724.
- Kroemer, G. *et al.* (2013) ‘Immunogenic Cell Death in Cancer Therapy’, *Annual Review*

- of Immunology*. doi: 10.1146/annurev-immunol-032712-100008.
- Krysko, D. V. *et al.* (2012) ‘Immunogenic cell death and DAMPs in cancer therapy’, *Nature Reviews Cancer*. doi: 10.1038/nrc3380.
- Kvansakul, M., Adams, J. C. and Hohenester, E. (2004) ‘Structure of a thrombospondin C-terminal fragment reveals a novel calcium core in the type 3 repeats.’, *The EMBO journal*. EMBO J, 23(6), pp. 1223–33. doi: 10.1038/sj.emboj.7600166.
- Lamkanfi, M. *et al.* (2007) ‘Caspases in cell survival, proliferation and differentiation’, *Cell Death and Differentiation*, 14(1), pp. 44–55. doi: 10.1038/sj.cdd.4402047.
- Lamy, L. *et al.* (2003) ‘CD47 and the 19 kDa interacting protein-3 (BNIP3) in T cell apoptosis.’, *The Journal of biological chemistry*. Elsevier, 278(26), pp. 23915–21. doi: 10.1074/jbc.M301869200.
- Lamy, L. *et al.* (2007) ‘Interactions between CD47 and thrombospondin reduce inflammation.’, *Journal of immunology (Baltimore, Md. : 1950)*. J Immunol, 178(9), pp. 5930–9. doi: 10.4049/jimmunol.178.9.5930.
- Latour, S. *et al.* (2001) ‘Bidirectional negative regulation of human T and dendritic cells by CD47 and its cognate receptor signal-regulator protein-alpha: down-regulation of IL-12 responsiveness and inhibition of dendritic cell activation.’, *Journal of immunology (Baltimore, Md. : 1950)*. J Immunol, 167(5), pp. 2547–54. doi: 10.4049/jimmunol.167.5.2547.
- Lattanzio, R. *et al.* (2019) ‘PLC-gamma-1 phosphorylation status is prognostic of metastatic risk in patients with early-stage Luminal-A and -B breast cancer subtypes’, *BMC Cancer*. BioMed Central Ltd., 19(1), p. 747. doi: 10.1186/s12885-019-5949-x.
- Lau, J. L. and Dunn, M. K. (2018) ‘Therapeutic peptides: Historical perspectives, current development trends, and future directions’, *Bioorganic & Medicinal Chemistry*. Pergamon, 26(10), pp. 2700–2707. doi: 10.1016/J.BMC.2017.06.052.
- Lawler, J. *et al.* (1985) ‘The structure of human platelet thrombospondin.’, *Journal of Biological Chemistry*. Elsevier, 260(6), pp. 3762–3772. doi: 10.1016/S0021-9258(19)83689-X.
- Lawler, J. *et al.* (1993) ‘Identification and characterization of thrombospondin-4, a new member of the thrombospondin gene family.’, *Journal of Cell Biology*. The Rockefeller University Press, 120(4), pp. 1059–1067. doi: 10.1083/jcb.120.4.1059.
- Lawler, J. *et al.* (1995) ‘Characterization of Human Thrombospondin-4’, *Journal of Biological Chemistry*. Elsevier, 270(6), pp. 2809–2814. doi: 10.1074/JBC.270.6.2809.
- Lazcano, A. and Miller, S. L. (1996) ‘The origin and early evolution of life: prebiotic chemistry, the pre-RNA world, and time.’, *Cell*. Elsevier, 85(6), pp. 793–8. doi: 10.1016/s0092-8674(00)81263-5.
- Leclair, P. *et al.* (2018) ‘CD47-ligation induced cell death in T-acute lymphoblastic leukemia’, *Cell Death & Disease*. Nature Publishing Group, 9(5), p. 544. doi: 10.1038/s41419-018-0601-2.
- Lee, J.-S. *et al.* (2009) ‘FLIP-mediated autophagy regulation in cell death control’, *Nature Cell Biology*. Nature Publishing Group, 11(11), pp. 1355–1362. doi:

10.1038/ncb1980.

Lee, M.-J. *et al.* (2021) 'Results from a biomarker study to accompany a phase II trial of RRx-001 with reintroduced platinum-based chemotherapy in relapsed small cell carcinoma', *Expert Opinion on Investigational Drugs*. Taylor & Francis, 30(2), pp. 177–183. doi: 10.1080/13543784.2021.1863947.

Lee Ventola, C. (2017) 'Cancer immunotherapy, part 1: Current strategies and agents', *P and T*. Medi Media USA Inc, 42(6), pp. 375–383.

Li, L. *et al.* (2020) 'Inhibition of Immunosuppressive Tumors by Polymer-Assisted Inductions of Immunogenic Cell Death and Multivalent PD-L1 Crosslinking', *Advanced Functional Materials*. Wiley-VCH Verlag, 30(12), p. 1908961. doi: 10.1002/adfm.201908961.

Li, Y. *et al.* (2020) 'CD47 antibody suppresses isoproterenol-induced cardiac hypertrophy through activation of autophagy.', *undefined*. Available at: <https://www.semanticscholar.org/paper/CD47-antibody-suppresses-isoproterenol-induced-of-Li-Chen/783d6d286c4db5e31697cc5798d2e36f6f897af9> (Accessed: 18 June 2021).

Li, Z. *et al.* (2001) 'Thrombospondin-1 inhibits TCR-mediated T lymphocyte early activation.', *Journal of immunology (Baltimore, Md. : 1950)*. J Immunol, 166(4), pp. 2427–36. doi: 10.4049/jimmunol.166.4.2427.

Li, Z. *et al.* (2002) 'Interactions of thrombospondins with alpha4beta1 integrin and CD47 differentially modulate T cell behavior.', *The Journal of cell biology*, 157(3), pp. 509–19. doi: 10.1083/jcb.200109098.

Lindberg, F. P. *et al.* (1994) 'Rh-related antigen CD47 is the signal-transducer integrin-associated protein.', *The Journal of biological chemistry*, 269(3), pp. 1567–70. Available at: <http://www.ncbi.nlm.nih.gov/pubmed/8294396> (Accessed: 26 April 2017).

Liu, X. *et al.* (2015) 'CD47 blockade triggers T cell-mediated destruction of immunogenic tumors.', *Nature medicine*. NIH Public Access, 21(10), pp. 1209–15. doi: 10.1038/nm.3931.

Liu, X. *et al.* (2017) 'Is CD47 an innate immune checkpoint for tumor evasion?', *Journal of hematology & oncology*. BioMed Central, 10(1), p. 12. doi: 10.1186/s13045-016-0381-z.

Liu, Y. *et al.* (2013) 'Autosis is a Na⁺,K⁺-ATPase-regulated form of cell death triggered by autophagy-inducing peptides, starvation, and hypoxia-ischemia', *Proceedings of the National Academy of Sciences of the United States of America*, 110(51), pp. 20364–20371. doi: 10.1073/pnas.1319661110.

Liu, Y. and Levine, B. (2015) 'Autosis and autophagic cell death: the dark side of autophagy', *Cell Death and Differentiation*. Nature Publishing Group, 22(3), pp. 367–376. doi: 10.1038/cdd.2014.143.

Lopez-Dee, Z., Pidcock, K. and Gutierrez, L. S. (2011) 'Thrombospondin-1: Multiple paths to inflammation', *Mediators of Inflammation*, 2011. doi: 10.1155/2011/296069.

López-Otín, C. and Kroemer, G. (2021) 'Hallmarks of Health', *Cell*. Cell Press, 184(1),

pp. 33–63. doi: 10.1016/J.CELL.2020.11.034.

Majeti, R. *et al.* (2009) ‘CD47 is an adverse prognostic factor and therapeutic antibody target on human acute myeloid leukemia stem cells.’, *Cell*. NIH Public Access, 138(2), pp. 286–99. doi: 10.1016/j.cell.2009.05.045.

Malinski, T. (2007) ‘Nitric Oxide and Nitroxidative Stress in Alzheimer’s Disease’, *Journal of Alzheimer’s Disease*. Edited by A. Boldyrev and P. Johnson. IOS Press, 11(2), pp. 207–218. doi: 10.3233/JAD-2007-11208.

Manna, P. P. *et al.* (2005) ‘CD47 Augments Fas/CD95-mediated Apoptosis’, *Journal of Biological Chemistry*. Elsevier, 280(33), pp. 29637–29644. doi: 10.1074/jbc.M500922200.

Manna, P. P. and Frazier, W. A. (2003) ‘The mechanism of CD47-dependent killing of T cells: heterotrimeric Gi-dependent inhibition of protein kinase A.’, *Journal of immunology (Baltimore, Md. : 1950)*. J Immunol, 170(7), pp. 3544–53. doi: 10.4049/jimmunol.170.7.3544.

Manna, P. P. and Frazier, W. A. (2004) ‘CD47 mediates killing of breast tumor cells via Gi-dependent inhibition of protein kinase A.’, *Cancer research*, 64(3), pp. 1026–36. Available at: <http://www.ncbi.nlm.nih.gov/pubmed/14871834> (Accessed: 25 September 2015).

Margossian, S. S., Lawler, J. W. and Slayter, H. S. (1981) ‘Physical characterization of platelet thrombospondin.’, *Journal of Biological Chemistry*. Elsevier, 256(14), pp. 7495–7500. doi: 10.1016/S0021-9258(19)68989-1.

Mariño, G. *et al.* (2014) ‘Self-consumption: the interplay of autophagy and apoptosis’, *Nature Reviews Molecular Cell Biology*. Nature Publishing Group, 15(2), pp. 81–94. doi: 10.1038/nrm3735.

Marks, D. I. and Rowntree, C. (2017) ‘Management of adults with T-cell lymphoblastic leukemia’, *Blood*. American Society of Hematology, 129(9), pp. 1134–1142. doi: 10.1182/blood-2016-07-692608.

Martinelli, R. *et al.* (2013) ‘Novel role of CD47 in rat microvascular endothelium: signaling and regulation of T-cell transendothelial migration.’, *Arteriosclerosis, thrombosis, and vascular biology*. NIH Public Access, 33(11), pp. 2566–76. doi: 10.1161/ATVBAHA.113.301903.

Martinez-Torres, A.-C. *et al.* (2015) ‘CD47 agonist peptides induce programmed cell death in refractory chronic lymphocytic leukemia B cells via PLC γ 1 activation: evidence from mice and humans.’, *PLoS medicine*. Public Library of Science, 12(3), p. e1001796. doi: 10.1371/journal.pmed.1001796.

Martínez-Torres, A.-C. (2013) *Study of the mechanisms regulating CD47-mediated Programmed Cell Death in Chronic Lymphocytic Leukemia: The Key role of PLC γ 1 and Calcium Signaling*. Universite Pierre et Marie Curie.

Martínez-Torres, A. C. *et al.* (2019) ‘PKHB1 Tumor Cell Lysate Induces Antitumor Immune System Stimulation and Tumor Regression in Syngeneic Mice with Tumoral T Lymphoblasts’, *Journal of Oncology*. Hindawi, 2019, pp. 1–11. doi:

10.1155/2019/9852361.

Martinez, J. *et al.* (2015) 'Molecular characterization of LC3-associated phagocytosis reveals distinct roles for Rubicon, NOX2 and autophagy proteins.', *Nature cell biology*. Nat Cell Biol, 17(7), pp. 893–906. doi: 10.1038/ncb3192.

Martinon, F. and Tschopp, J. (2004) 'Inflammatory caspases: linking an intracellular innate immune system to autoinflammatory diseases.', *Cell*. Cell, 117(5), pp. 561–74. doi: 10.1016/j.cell.2004.05.004.

Mateo, V. *et al.* (1999) 'CD47 ligation induces caspase-independent cell death in chronic lymphocytic leukemia.', *Nature medicine*, 5(11), pp. 1277–84. doi: 10.1038/15233.

Mateo, V. *et al.* (2002) 'Mechanisms of CD47-induced caspase-independent cell death in normal and leukemic cells: Link between phosphatidylserine exposure and cytoskeleton organization', *Blood*, 100(8), pp. 2882–2890. doi: 10.1182/blood-2001-12-0217.

Matlung, H. L. *et al.* (2017) 'The CD47-SIRP α signaling axis as an innate immune checkpoint in cancer', *Immunological Reviews*. John Wiley & Sons, Ltd, 276(1), pp. 145–164. doi: 10.1111/imr.12527.

Matozaki, T. *et al.* (2009) 'Functions and molecular mechanisms of the CD47–SIRP α signalling pathway', *Trends in Cell Biology*, 19(2), pp. 72–80. doi: 10.1016/j.tcb.2008.12.001.

McAndrew, D. *et al.* (2011) 'ORAI1-Mediated Calcium Influx in Lactation and in Breast Cancer', *Molecular Cancer Therapeutics*. doi: 10.1158/1535-7163.MCT-10-0923.

McDonald, J. F., Dimitry, J. M. and Frazier, W. A. (2003) 'An amyloid-like C-terminal domain of thrombospondin-1 displays CD47 agonist activity requiring both VVM motifs.', *Biochemistry*, 42(33), pp. 10001–11. doi: 10.1021/bi0341408.

Mezzapelle, R. *et al.* (2021) 'CXCR4 engagement triggers CD47 internalization and antitumor immunization in a mouse model of mesothelioma', *EMBO Molecular Medicine*. John Wiley & Sons, Ltd, 13(6), p. e12344. doi: 10.15252/emmm.202012344.

Miller, T. W. *et al.* (2013) 'Thrombospondin-1 is a CD47-dependent endogenous inhibitor of hydrogen sulfide signaling in T cell activation.', *Matrix biology : journal of the International Society for Matrix Biology*. NIH Public Access, 32(6), pp. 316–24. doi: 10.1016/j.matbio.2013.02.009.

Miller, T. W., Isenberg, J. S. and Roberts, D. D. (2010) 'Thrombospondin-1 is an inhibitor of pharmacological activation of soluble guanylate cyclase', *British Journal of Pharmacology*. John Wiley & Sons, Ltd, 159(7), pp. 1542–1547. doi: 10.1111/j.1476-5381.2009.00631.x.

Montagnani, M. *et al.* (2001) 'Insulin-stimulated Activation of eNOS Is Independent of Ca²⁺ but Requires Phosphorylation by Akt at Ser1179', *Journal of Biological Chemistry*. Elsevier, 276(32), pp. 30392–30398. doi: 10.1074/JBC.M103702200.

Monteith, G. R. *et al.* (2007) 'Calcium and cancer: targeting Ca²⁺ transport', *Nature*

- Reviews Cancer*. Nature Publishing Group, 7(7), pp. 519–530. doi: 10.1038/nrc2171.
- Montico, B. *et al.* (2018) ‘Immunogenic apoptosis as a novel tool for anticancer vaccine development’, *International Journal of Molecular Sciences*. MDPI AG. doi: 10.3390/ijms19020594.
- Mordue, K. E. *et al.* (2017) ‘CD47 surface stability is sensitive to actin disruption prior to inclusion within the band 3 macrocomplex’, *Scientific Reports*. Nature Publishing Group, 7(1), p. 2246. doi: 10.1038/s41598-017-02356-1.
- Murata, Y. *et al.* (2014) ‘The CD47-SIRP signalling system: its physiological roles and therapeutic application’, *Journal of Biochemistry*. Oxford Academic, 155(6), pp. 335–344. doi: 10.1093/jb/mvu017.
- N’Diaye, E.-N. and Brown, E. J. (2003) ‘The ubiquitin-related protein PLIC-1 regulates heterotrimeric G protein function through association with G $\beta\gamma$ ’, *Journal of Cell Biology*. The Rockefeller University Press, 163(5), pp. 1157–1165. doi: 10.1083/jcb.200307155.
- Nah, J. *et al.* (2020) ‘Upregulation of Rubicon promotes autosis during myocardial ischemia/reperfusion injury’, *The Journal of Clinical Investigation*. American Society for Clinical Investigation, 130(6), pp. 2978–2991. doi: 10.1172/JCI132366.
- Nazarko, V. Y. and Zhong, Q. (2013) ‘ULK1 targets Beclin-1 in autophagy.’, *Nature cell biology*. NIH Public Access, 15(7), pp. 727–8. doi: 10.1038/ncb2797.
- Nikoletopoulou, V. *et al.* (2013) ‘Crosstalk between apoptosis, necrosis and autophagy’, *Biochimica et Biophysica Acta (BBA) - Molecular Cell Research*. Elsevier, 1833(12), pp. 3448–3459. doi: 10.1016/J.BBAMCR.2013.06.001.
- Obeid, M. *et al.* (2007) ‘Calreticulin exposure dictates the immunogenicity of cancer cell death’, *Nature Medicine*, 13(1), pp. 54–61. doi: 10.1038/nm1523.
- Oldberg, A. *et al.* (1992) ‘COMP (cartilage oligomeric matrix protein) is structurally related to the thrombospondins.’, *Journal of Biological Chemistry*. Elsevier, 267(31), pp. 22346–22350. doi: 10.1016/S0021-9258(18)41677-8.
- Oldenborg, P.-A. (2004) ‘Role of CD47 in Erythroid Cells and in Autoimmunity’, *Leukemia & Lymphoma*. Taylor & Francis, 45(7), pp. 1319–1327. doi: 10.1080/1042819042000201989.
- Oldenborg, P.-A. (2013) ‘CD47: A Cell Surface Glycoprotein Which Regulates Multiple Functions of Hematopoietic Cells in Health and Disease’, *International Scholarly Research Notices*. Hindawi Publishing Corporation, 2013. doi: 10.1155/2013/614619.
- Oldenborg, P. A. *et al.* (2000) ‘Role of CD47 as a marker of self on red blood cells.’, *Science (New York, N.Y.)*, 288(5473), pp. 2051–4. Available at: <http://www.ncbi.nlm.nih.gov/pubmed/10856220> (Accessed: 22 September 2015).
- Van Opdenbosch, N. and Lamkanfi, M. (2019) ‘Caspases in Cell Death, Inflammation, and Disease’, *Immunity*. Cell Press, 50(6), pp. 1352–1364. doi: 10.1016/J.IMMUNI.2019.05.020.
- Oronsky, B. *et al.* (2019) ‘REPLATINUM Phase III randomized study: RRx-001 + platinum doublet versus platinum doublet in third-line small cell lung cancer’, *Future*

Oncology. Future Medicine Ltd London, UK , 15(30), pp. 3427–3433. doi: 10.2217/fon-2019-0317.

Oronsky, B. *et al.* (2021) ‘Discovery of RRx-001, a Myc and CD47 Downregulating Small Molecule with Tumor Targeted Cytotoxicity and Healthy Tissue Cytoprotective Properties in Clinical Development’, *Journal of Medicinal Chemistry*. American Chemical Society, 64(11), pp. 7261–7271. doi: 10.1021/acs.jmedchem.1c00599.

Orrenius, S., Zhivotovsky, B. and Nicotera, P. (2003) ‘Calcium: Regulation of cell death: the calcium–apoptosis link’, *Nature Reviews Molecular Cell Biology*. Nature Publishing Group, 4(7), pp. 552–565. doi: 10.1038/nrm1150.

Papaioannou, N. E. *et al.* (2016) ‘Harnessing the immune system to improve cancer therapy’, *Annals of Translational Medicine*. AME Publishing Company. doi: 10.21037/atm.2016.04.01.

Peptide Therapeutics Market To Reach USD 50.60 Billion By (no date). Available at: <https://www.globenewswire.com/news-release/2020/03/23/2005016/0/en/Peptide-Therapeutics-Market-To-Rreach-USD-50-60-Billion-By-2026-Reports-and-Data.html> (Accessed: 18 June 2021).

Pettersen, R. D. *et al.* (1999) ‘CD47 signals T cell death.’, *Journal of immunology (Baltimore, Md. : 1950)*, 162(12), pp. 7031–40. Available at: <http://www.ncbi.nlm.nih.gov/pubmed/10358145> (Accessed: 25 September 2015).

Phillips, D. R., Jennings, L. K. and Prasanna, H. R. (1980) ‘Ca²⁺-mediated association of glycoprotein G (thrombinsensitive protein, thrombospondin) with human platelets.’, *Journal of Biological Chemistry*. Elsevier, 255(24), pp. 11629–11632. doi: 10.1016/S0021-9258(19)70174-4.

Pinto, M. C. X. *et al.* (2015) ‘Calcium signaling and cell proliferation’, *Cellular Signalling*, 27(11), pp. 2139–2149. doi: 10.1016/j.cellsig.2015.08.006.

Plattner, H. and Verkhatsky, A. (2016) ‘Inseparable tandem: evolution chooses ATP and Ca²⁺ to control life, death and cellular signalling’, *Philosophical Transactions of the Royal Society B: Biological Sciences*, 371(1700), p. 20150419. doi: 10.1098/rstb.2015.0419.

Posey, K. L. *et al.* (2004) ‘Role of TSP-5/COMP in pseudoachondroplasia.’, *The international journal of biochemistry & cell biology*. Int J Biochem Cell Biol, 36(6), pp. 1005–12. doi: 10.1016/j.biocel.2004.01.011.

Pulaski, B. A. and Ostrand-Rosenberg, S. (2001) ‘Mouse 4T1 Breast Tumor Model’, in *Current Protocols in Immunology*. doi: 10.1002/0471142735.im2002s39.

Ramanathan, S. *et al.* (2011) ‘Thrombospondin-1 and angiotensin II inhibit soluble guanylyl cyclase through an increase in intracellular calcium concentration.’, *Biochemistry*, 50(36), pp. 7787–99. doi: 10.1021/bi201060c.

Rebres, R. A. *et al.* (2001) ‘Normal ligand binding and signaling by CD47 (integrin-associated protein) requires a long range disulfide bond between the extracellular and membrane-spanning domains.’, *The Journal of biological chemistry*. American Society for Biochemistry and Molecular Biology, 276(37), pp. 34607–16. doi:

10.1074/jbc.M106107200.

Rebres, R. A., Kajihara, K. and Brown, E. J. (2005) 'Novel CD47-dependent intercellular adhesion modulates cell migration.', *Journal of cellular physiology*, 205(2), pp. 182–93. doi: 10.1002/jcp.20379.

Reyes-Ruiz, A. *et al.* (2021) 'The bovine dialysable leukocyte extract IMMUNEPOTENT CRP induces immunogenic cell death in breast cancer cells leading to long-term antitumour memory', *British Journal of Cancer*. Springer Nature, pp. 1–13. doi: 10.1038/s41416-020-01256-y.

Roberts, D. D. *et al.* (2012) 'The matricellular protein thrombospondin-1 globally regulates cardiovascular function and responses to stress via CD47', *Matrix Biology*, 31(3), pp. 162–169. doi: 10.1016/j.matbio.2012.01.005.

Rodríguez-Jiménez, P. *et al.* (2019) 'Thrombospondin-1/CD47 Interaction Regulates Th17 and Treg Differentiation in Psoriasis', *Frontiers in Immunology*. Frontiers, 10, p. 1268. doi: 10.3389/fimmu.2019.01268.

Roué, G. *et al.* (2003) 'Mitochondrial dysfunction in CD47-mediated caspase-independent cell death: ROS production in the absence of cytochrome c and AIF release', *Biochimie*. Elsevier, 85(8), pp. 741–746. doi: 10.1016/S0300-9084(03)00129-9.

Rusanescu, G. *et al.* (1995) 'Calcium influx induces neurite growth through a Src-Ras signaling cassette.', *Neuron*, 15(6), pp. 1415–25. Available at: <http://www.ncbi.nlm.nih.gov/pubmed/8845164> (Accessed: 26 April 2017).

Sarfati, M. *et al.* (2008) 'CD47 in the immune response: role of thrombospondin and SIRP-alpha reverse signaling.', *Current drug targets*, 9(10), pp. 842–50. Available at: <http://www.ncbi.nlm.nih.gov/pubmed/18855618> (Accessed: 25 September 2015).

Saumet, A. *et al.* (2005) 'Type 3 repeat/C-terminal domain of thrombospondin-1 triggers caspase-independent cell death through CD47/ $\alpha v \beta 3$ in promyelocytic leukemia NB4 cells', *Blood*, 106(2).

Sharifi-Sanjani, M. *et al.* (2014) 'Cardiac CD47 Drives Left Ventricular Heart Failure Through Ca²⁺-CaMKII-Regulated Induction of HDAC3', *Journal of the American Heart Association*, 3(3), pp. e000670–e000670. doi: 10.1161/JAHA.113.000670.

Shen, B., Delaney, M. K. and Du, X. (2012) 'Inside-out, outside-in, and inside–outside-in: G protein signaling in integrin-mediated cell adhesion, spreading, and retraction', *Current Opinion in Cell Biology*. Elsevier Current Trends, 24(5), pp. 600–606. doi: 10.1016/J.CEB.2012.08.011.

Shoemark, D. K. *et al.* (2019) 'Emergence of a Thrombospondin Superfamily at the Origin of Metazoans', *Molecular Biology and Evolution*. Edited by J. True. Oxford Academic, 36(6), pp. 1220–1238. doi: 10.1093/molbev/msz060.

Shoji-Kawata, S. *et al.* (2013) 'Identification of a candidate therapeutic autophagy-inducing peptide.', *Nature*. NIH Public Access, 494(7436), pp. 201–6. doi: 10.1038/nature11866.

Sick, E. *et al.* (2011) 'Activation of CD47 receptors causes proliferation of human astrocytoma but not normal astrocytes via an Akt-dependent pathway', *Glia*, 59(2), pp.

308–319. doi: 10.1002/glia.21102.

Silverstein, R. L. *et al.* (1992) ‘Sense and antisense cDNA transfection of CD36 (glycoprotein IV) in melanoma cells. Role of CD36 as a thrombospondin receptor.’, *The Journal of biological chemistry*. Elsevier, 267(23), pp. 16607–12. doi: 10.1016/S0021-9258(18)42046-7.

Sonnen, A. F.-P. *et al.* (2010) ‘Domain metastability: a molecular basis for immunoglobulin deposition?’, *Journal of molecular biology*. Elsevier, 399(2), pp. 207–13. doi: 10.1016/j.jmb.2010.04.011.

Soto-Pantoja, D. R. *et al.* (2012) ‘CD47 deficiency confers cell and tissue radioprotection by activation of autophagy’, *Autophagy*. Taylor & Francis, 8(11), pp. 1628–1642. doi: 10.4161/auto.21562.

Soto-Pantoja, D. R. *et al.* (2013) ‘Blockade of CD47 increases survival of mice exposed to lethal total body irradiation’, *Scientific Reports*. Nature Publishing Group, 3(1), p. 1038. doi: 10.1038/srep01038.

Soto-Pantoja, D. R., Kaur, S. and Roberts, D. D. (2015) ‘CD47 signaling pathways controlling cellular differentiation and responses to stress’, *Critical Reviews in Biochemistry and Molecular Biology*, 9238, pp. 1–19. doi: 10.3109/10409238.2015.1014024.

Spaw, M., Anant, S. and Thomas, S. M. (2017) ‘Stromal contributions to the carcinogenic process’, *Molecular Carcinogenesis*, 56(4), pp. 1199–1213. doi: 10.1002/mc.22583.

Stanton, S. E. and Disis, M. L. (2016) ‘Clinical significance of tumor-infiltrating lymphocytes in breast cancer’, *Journal for ImmunoTherapy of Cancer*. BioMed Central Ltd., p. 59. doi: 10.1186/s40425-016-0165-6.

Stenina-Adognravi, O. (2014) ‘Invoking the power of thrombospondins: regulation of thrombospondins expression.’, *Matrix biology : journal of the International Society for Matrix Biology*. NIH Public Access, 37, pp. 69–82. doi: 10.1016/j.matbio.2014.02.001.

Stewart, T. A., Yapa, K. T. D. S. and Monteith, G. R. (2015) ‘Altered calcium signaling in cancer cells’, *Biochimica et Biophysica Acta (BBA) - Biomembranes*, 1848(10), pp. 2502–2511. doi: 10.1016/j.bbamem.2014.08.016.

Stith, B. J. (2015) ‘Phospholipase C and D regulation of Src, calcium release and membrane fusion during *Xenopus laevis* development.’, *Developmental biology*. NIH Public Access, 401(2), pp. 188–205. doi: 10.1016/j.ydbio.2015.02.020.

Tan, K. *et al.* (2009) ‘The crystal structure of the signature domain of cartilage oligomeric matrix protein: implications for collagen, glycosaminoglycan and integrin binding.’, *FASEB journal : official publication of the Federation of American Societies for Experimental Biology*. FASEB J, 23(8), pp. 2490–501. doi: 10.1096/fj.08-128090.

Tesniere, A. *et al.* (2010) ‘Immunogenic death of colon cancer cells treated with oxaliplatin’, *Oncogene*. doi: 10.1038/onc.2009.356.

The evaluation of tumor-infiltrating lymphocytes (TILs) in breast cancer: recommendations by an International TILs Working Group 2014 (no date).

- Topol, E. J. *et al.* (2001) 'Single nucleotide polymorphisms in multiple novel thrombospondin genes may be associated with familial premature myocardial infarction.', *Circulation*. *Circulation*, 104(22), pp. 2641–4. doi: 10.1161/hc4701.100910.
- Trinquand, A. *et al.* (2016) 'Triggering the TCR Developmental Checkpoint Activates a Therapeutically Targetable Tumor Suppressive Pathway in T-cell Leukemia.', *Cancer discovery*. *Cancer Discov*, 6(9), pp. 972–85. doi: 10.1158/2159-8290.CD-15-0675.
- Tsapras, P. and Nezis, I. P. (2017) 'Caspase involvement in autophagy', *Cell Death & Differentiation*. Nature Publishing Group, 24(8), pp. 1369–1379. doi: 10.1038/cdd.2017.43.
- Tseng, D. *et al.* (2013) 'Anti-CD47 antibody-mediated phagocytosis of cancer by macrophages primes an effective antitumor T-cell response.', *Proceedings of the National Academy of Sciences of the United States of America*, 110(27), pp. 11103–8. doi: 10.1073/pnas.1305569110.
- Uscanga-Palomeque, A. C. *et al.* (2018) 'CD 47 agonist peptide PKHB 1 induces immunogenic cell death in T-cell acute lymphoblastic leukemia cells', *Cancer Science*. John Wiley & Sons, Ltd (10.1111), p. cas.13885. doi: 10.1111/cas.13885.
- Van, V. Q. *et al.* (2012) 'CD47 Low Status on CD4 Effectors Is Necessary for the Contraction / Resolution of the Immune Response in Humans and Mice', 7(8), pp. 2–11. doi: 10.1371/journal.pone.0041972.
- Vlieghe, P. *et al.* (2010) 'Synthetic therapeutic peptides: science and market', *Drug discovery today*. *Drug Discov Today*, 15(1–2), pp. 40–56. doi: 10.1016/j.drudis.2009.10.009.
- Vonderheide, R. H. (2015) 'CD47 blockade as another immune checkpoint therapy for cancer', *Nature Medicine*, 21(10), pp. 1122–1123. doi: 10.1038/nm.3965.
- Vos, H. L. *et al.* (1992) 'Thrombospondin 3 (Thbs3), a new member of the thrombospondin gene family.', *Journal of Biological Chemistry*. Elsevier, 267(17), pp. 12192–12196. doi: 10.1016/S0021-9258(19)49823-2.
- Wang, F. *et al.* (2020) 'Aging-associated changes in CD47 arrangement and interaction with thrombospondin-1 on red blood cells visualized by super-resolution imaging', *Aging Cell*. John Wiley & Sons, Ltd, 19(10), p. e13224. doi: 10.1111/ace1.13224.
- Wang, X.-Q. and Frazier, W. A. (1998) 'The Thrombospondin Receptor CD47 (IAP) Modulates and Associates with $\alpha 2\beta 1$ Integrin in Vascular Smooth Muscle Cells', *Molecular Biology of the Cell*. The American Society for Cell Biology, 9(4), pp. 865–874. doi: 10.1091/mbc.9.4.865.
- Willingham, S. B. *et al.* (2012) 'The CD47-signal regulatory protein alpha (SIRP α) interaction is a therapeutic target for human solid tumors.', *Proceedings of the National Academy of Sciences of the United States of America*. National Academy of Sciences, 109(17), pp. 6662–7. doi: 10.1073/pnas.1121623109.
- Wong, S.-W., Sil, P. and Martinez, J. (2018) 'Rubicon: LC3-associated phagocytosis and beyond.', *The FEBS journal*. NIH Public Access, 285(8), pp. 1379–1388. doi: 10.1111/febs.14354.

- Wu, A. *et al.* (2007) 'In vivo vaccination with tumor cell lysate plus CpG oligodeoxynucleotides eradicates murine glioblastoma', *Journal of Immunotherapy*, 30(8), pp. 789–797. doi: 10.1097/CJI.0b013e318155a0f6.
- Wu, A. L. *et al.* (1999) 'Ubiquitin-related proteins regulate interaction of vimentin intermediate filaments with the plasma membrane.', *Molecular cell*. Elsevier, 4(4), pp. 619–25. doi: 10.1016/s1097-2765(00)80212-9.
- Xu, N. *et al.* (2015) 'Sodium entry through endothelial store-operated calcium entry channels: regulation by Orai1.', *American journal of physiology. Cell physiology*. American Physiological Society, 308(4), pp. C277-88. doi: 10.1152/ajpcell.00063.2014.
- Young, S. M. *et al.* (2020) 'Resolving CD47 Structure and Function to Understand Signal Transduction Mechanism', *Biophysical Journal*. Elsevier, 118(3), p. 212a. doi: 10.1016/j.bpj.2019.11.1267.
- Yu, W.-B. *et al.* (2021) 'The development of small-molecule inhibitors targeting CD47', *Drug Discovery Today*. Elsevier Current Trends, 26(2), pp. 561–568. doi: 10.1016/J.DRUDIS.2020.11.003.
- Zhang, X. *et al.* (2017) 'Targeting CD47 and autophagy elicited enhanced antitumor effects in non-small cell lung cancer', *Cancer Immunology Research*. American Association for Cancer Research Inc., 5(5), pp. 363–375. doi: 10.1158/2326-6066.CIR-16-0398.
- Zhang, X., Chen, W., *et al.* (2018) 'Disrupting CD47-SIRP α axis alone or combined with autophagy depletion for the therapy of glioblastoma', *Carcinogenesis*. Oxford Academic, 39(5), pp. 689–699. doi: 10.1093/carcin/bgy041.
- Zhang, X., Wang, S., *et al.* (2018) 'Inhibition of autophagy potentiated the anti-tumor effects of VEGF and CD47 bispecific therapy in glioblastoma', *Applied Microbiology and Biotechnology*. Springer, 102(15), pp. 6503–6513. doi: 10.1007/s00253-018-9069-3.
- Zhou, J. *et al.* (2019) 'Immunogenic cell death in cancer therapy: Present and emerging inducers', *Journal of Cellular and Molecular Medicine*. Blackwell Publishing Inc., pp. 4854–4865. doi: 10.1111/jcmm.14356.

Annex

Annex

Contribution in other published projects not part of the present thesis

Article 5. Human ACE2 peptide-mimics block SARS-CoV-2 pulmonary cells infection

My contribution on this subject consisted in evaluating the toxicity of the human ACE2 peptide mimics designed to interact with SARS-CoV-2 and block cell infection (Figure 3c and 3f). At concentrations >200-fold higher than the IC_{50} in lung cancer cells, the peptides were not toxic to CALU-3 nor Vero-E6 cells, as indicated by MTT and AnnV/PI assays.



<https://doi.org/10.1038/s42003-021-01736-8>

OPEN

Human ACE2 peptide-mimics block SARS-CoV-2 pulmonary cells infection

Philippe Karoyan^{1,2,3✉}, Vincent Vieillard⁴, Luis Gómez-Morales^{1,2}, Estelle Odile^{1,2}, Amélie Guihot^{5,6}, Charles-Edouard Luyt⁷, Alexis Denis^{1,8}, Pascal Grondin^{1,8} & Olivier Lequin¹

In light of the recent accumulated knowledge on SARS-CoV-2 and its mode of human cells invasion, the binding of viral spike glycoprotein to human Angiotensin Converting Enzyme 2 (hACE2) receptor plays a central role in cell entry. We designed a series of peptides mimicking the N-terminal helix of hACE2 protein which contains most of the contacting residues at the binding site, exhibiting a high helical folding propensity in aqueous solution. Our best peptide-mimics are able to block SARS-CoV-2 human pulmonary cell infection with an inhibitory concentration (IC₅₀) in the nanomolar range upon binding to the virus spike protein with high affinity. These first-in-class blocking peptide mimics represent powerful tools that might be used in prophylactic and therapeutic approaches to fight the coronavirus disease 2019 (COVID-19).

¹Sorbonne Université, École Normale Supérieure, PSL University, CNRS, Laboratoire des Biomolécules, LBM, 75005 Paris, France. ²Sorbonne Université, École Normale Supérieure, PSL University, CNRS, Laboratoire des Biomolécules, LBM, Site OncoDesign, 25-27 Avenue du Québec, 91140 Villebon Sur Yvette, France. ³γ-Pharma, 25 avenue du Québec, 91140 Villebon Sur Yvette, France. ⁴Sorbonne Université, INSERM, CNRS, Centre d'Immunologie et des Maladies Infectieuses-Paris (CIMI-Paris), F-75013 Paris, France. ⁵Assistance Publique-Hôpitaux de Paris (AP-HP), Hôpital Pitié-Salpêtrière, Département d'Immunologie, F-75013 Paris, France. ⁶Sorbonne Université, Inserm U1135, Centre d'Immunologie et des Maladies Infectieuses, CIMI-Paris, F-75013 Paris, France. ⁷Assistance Publique-Hôpitaux de Paris (AP-HP), Hôpital Pitié-Salpêtrière, Service de Médecine Intensive Réanimation, Institut de Cardiologie, F-75013 Paris, France. ⁸Oncodesign, 25 Avenue du Québec, 91140 Villebon Sur Yvette, France. ✉email: philippe.karoyan@sorbonne-universite.fr

The coronavirus disease 2019 (COVID-19), caused by the severe acute respiratory syndrome-coronavirus 2 (SARS-CoV-2) has emerged as a pandemic, claiming at the time of writing more than 1.3 million deaths and over 57 millions confirmed cases world-wide between December 2019 and November 2020¹. Since the SARS-CoV-2 discovery^{2,3} and identification, the energy deployed by the scientific community has made it possible to generate an extraordinary wealth of information. However, to date, efficient therapeutics or drugs are lacking and prevention of the disease relies only on non-specific barrier measures⁴. Indeed, no specific drugs targeting the virus are available⁵ yet, many clinical trials have been engaged with SARS-CoV-2 non-specific treatments⁴. The structural and biochemical basis of the mechanism of infection has been investigated, highlighting that the virus cell-surface spike protein of SARS-CoV-2 targets human receptors^{6,7}. Human angiotensin converting enzyme 2 (hACE2) and the cellular transmembrane protease serine 2 (TMPRSS2) have been identified as major actors of the virus entry into human cells⁸.

With the goal of preventing the SARS-CoV-2 from infecting human cells, blocking the interaction between hACE2 and the virus spike protein has been validated. Indeed, inhibition of SARS-CoV-2 infections in engineered human tissues using clinical-grade soluble ACE2 was recently demonstrated⁹. Likewise, an engineered stable mini-protein mimicking three helices of hACE2 to plug SARS-CoV-2 spikes¹⁰ was described, but its capacity to block viral infection was not demonstrated. Although several *in silico* designed peptides were proposed to prevent formation of the fusion core^{11,12}, first attempts to design a peptide binder derived from hACE2 proved to be a difficult task, leading to mitigated results¹³.

Thus, starting from the published crystal structure of SARS-CoV-2 spike receptor-binding domain (RBD) bound to hACE2¹⁴, we designed peptide-mimics of the *N*-terminal hACE2 helix which interact with the spike protein. We report here the strategy implemented to optimize the design of our peptide mimics, their high helical folding propensity in water, their ability to block SARS-CoV-2 human pulmonary cell infection with an IC₅₀ in the nanomolar range and their binding to spike RBD with strong affinity. We also demonstrated the non-toxicity of our mimics at concentrations 150 times higher than the IC₅₀ on pulmonary cell lines.

Results

Design of peptides mimicking the helix H1 of hACE2. We first examined the complex between hACE2 and the surface spike protein of SARS-CoV-2 (PDB 6m0j)¹⁴ in order to highlight the important contacts and some relevant characteristics of the interacting hACE2 sequence (Fig. 1).

Twenty residues from hACE2 were identified¹⁴ as to be in close contacts with the Spike protein, using a distance cut-off of 4 Å. These interactions occur mainly through the *N*-terminal α -helix H1 of hACE2 (Fig. 1a). This α -helix (Fig. 1b), composed of 27 residues (from S19 to L45, Fig. 1c) contains 12 residues (highlighted in magenta in Fig. 1c) involved in hydrogen bonds, salt bridges, and van der Waals interactions (see Supplementary Table 1 for details)¹⁴.

A Clustal multiple sequence alignment of viruses isolated in China, United States and France was performed (See Supplementary Fig. 1). From these analyses, we observed that all the randomly selected sequences were 100% identical at least in the ACE2 interacting interface. This highlights a highly conserved sequence for the portion of spike interacting with the α -helix H1 of hACE2, possibly because deleterious mutations at this interface would limit viral infectivity.

Our strategy was designing a peptide with a high helical folding propensity and retaining most of the binding affinity of hACE2 to the spike RBD of SARS-CoV-2, using natural amino acids¹⁵. Indeed, we preferred not to use complex chemical tools known to stabilize α -helix^{16,17} in order to limit developability constraints. Our mimics were designed and optimized for binding, high helical content and low antigenicity, to avoid triggering a neutralizing immune response that would compromise the peptide therapeutic potential. A combination of the Agadir program^{18,19}, an algorithm developed to predict the helical content of peptides and the semi-empirical method reported by Kolaskar²⁰ to highlight the number of antigenic determinants, was iteratively used.

We observed that the *N*-terminal sequence of the H1 helix, composed of four residues (S₁₉TIE₂₂), corresponds to a consensus *N*-capping box motif (SXXE)²¹. A capping box features reciprocal backbone-side-chain hydrogen-bonds favoring a helix initiation. Although this sequence does not adopt the H-bonded capping conformation in the crystal structure of the full protein, it could constitute a stabilizing element in the isolated helix when extracted from the protein context. These observations led us to

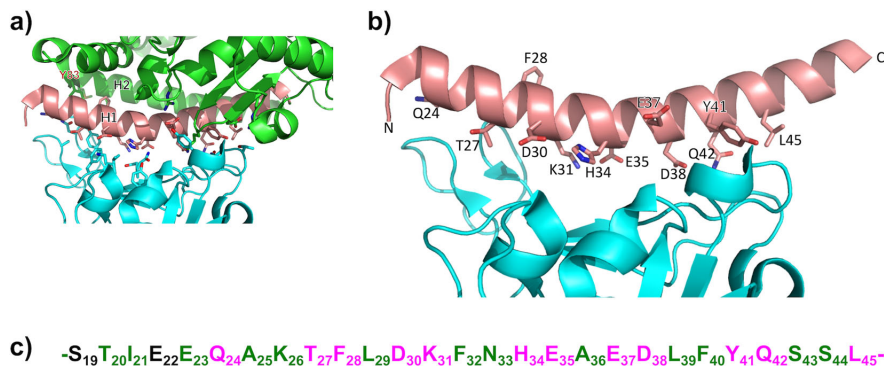


Fig. 1 Structure of the complex between hACE2 and the spike protein of SARS-CoV-2 (pdb 6m0j)¹⁴. **a** Contact residues of the hACE2 / SARS-CoV-2 spike interface. hACE2 protein is colored in green, apart from *N*-terminal helix H1 which is highlighted in salmon. SARS-CoV-2 spike protein is shown in cyan. **b** Residues of hACE2 H1 helix interacting with spike. **c** Sequence of hACE2 H1 helix showing the 12 interacting residues in magenta. Residue positions in green were considered as possible substitution sites for the helical peptide design.

keep 14 residues from the native **H1** helix of hACE2 as contact residues or putative stabilizing capping box. The 13 remaining residues that are not essential for the interaction were considered as possible sites for amino acid substitutions (Fig. 1c). We thus substituted non-essential positions by Ala and/or Leu residues which display higher helical folding propensities, and we calculated the peptide helical content after each substitution (Supplementary Table 2).

A peptide sequence optimization was then carried out to lower the antigenicity while keeping the helical propensity thanks to an iterative residue scanning and calculation of the helical content variation upon new substitutions (Supplementary Table 3). This strategy highlighted the influence of the residue N33 in the native sequence. Indeed, if the N33/L33 substitution systematically improved the helical content, it was always at the expense of antigenicity. Conversely, the L33/N33 substitution reduced the antigenicity at the expense of helical content. The solution was found by L33/M33 substitution which decreased the number of AD.

The **H1** helix of ACE2 adopts a kinked conformation in the crystal structure, leading to a distorted CO/HN hydrogen bond network between H34/D38 and E35/L39 residues. Therefore, we considered introducing a proline, as this residue is known to induce local kinks or distortions in natural helices^{22,23}. D38 was classed as a contact residue, while L39 side chain is not involved in any direct interaction. Consequently, L39 position was selected for substitution by proline (peptide **P5**, Table 1).

In order to increase the helical content to a maximum level, this iterative study was also applied to longer peptide sequences starting from the 29-residue native one, albeit at the expense of antigenicity. Diverse combinations of *N*- and *C*-terminus capping groups were also considered (free extremities or *N*-acetyl, *C*-carboxamide groups).

Finally, we examined the possibility of promoting additional side chain contacts provided by ACE2 residues that do not belong to **H1** helix. Y83 residue in **H2** helix appeared as a good candidate as it lies very close in space to A25 in **H1** helix (Fig. 1a). Molecular modeling was carried out on **H1** helix analogs in which A25 was replaced by tyrosine or homotyrosine (*hTyr*) residues (Supplementary Fig. 2). Calculations showed that *hTyr* residue was able to project the phenol ring in an adequate orientation to mimic Y83 position. Of note, *hTyr* is a natural amino acid²⁴.

Three peptides were selected as controls in our optimization process, **P1** (native sequence), **P1scr** (scrambled peptide from **P1**), and **Ppen** (described by Pentelute and colleagues in a longer biotinylated and pegylated construct and termed SBP1 as a putative spike binder¹³).

The results highlighting the progression in helical content and number of antigenic determinants are reported in Table 1 for the most relevant peptide mimics (see Supplementary Tables 2–4 for all the peptide-mimics that were designed and/or synthesized). These peptides were synthesized on a 5-mg to 20-mg scale from Fmoc-protected amino acids utilizing standard solid-phase peptide synthesis methods on rink amide resin (see Methods section).

The designed peptides highlight an excellent correlation between calculated and experimentally determined helical content by circular dichroism in aqueous media. The conformation of synthesized peptides in aqueous solution was investigated by circular dichroism (CD) spectroscopy²⁵. Figure 2 shows the superimposed CD spectra of 12 peptides, including control ones, i.e., **P1** (native sequence), **P1scr** (Scramble), and **Ppen**. The CD spectra of peptides **P1** (native), **P1scr** (scrambled) are characteristic of a predominant random coil structure with a

negative minimum near 200 nm, as expected. Similarly, **Ppen** described as a helical peptide sequence¹³ also adopted a random coil conformation in solution. For all other peptides, the CD spectra exhibit a canonical α -helix signature, featuring a double minimum around 208 nm and 222 nm, with the exception of the proline-containing **P5** peptide. The deconvolution of the CD spectra using DichroWeb²⁵ allowed us to estimate the helical population for each peptide, which is reported in Table 1. Overall, an excellent agreement was observed between the Agadir-computed values and the experimental helical population inferred from CD data. The native hACE2 **H1** helix sequence (peptides **P1**, **Ppen**) has a weak propensity to fold into an α -helix in aqueous solution (below 10%). In contrast, the sequence optimization led to **H1** analogs exhibiting a high helical propensity (between 50 and 80%). The introduction of a proline residue in peptide **P5** has a strong destabilizing effect on helical conformation (17%) whereas Leu/*hTyr* substitution only led to a slight decrease of the helical content (**P7** versus **P6** and **P10** versus **P8**).

Peptide mimics of hACE2 show high anti-infective efficacy and are devoid of cell toxicity. To determine whether our peptide mimics of hACE2 **H1** helix block SARS-CoV-2 cell infection, antiviral assays²⁶ were performed (Fig. 3) with a SARS-CoV-2 clinical isolate obtained from bronchoalveolar lavage (BAL) of a symptomatic infected patient (#SARS-CoV-2/PSL2020) at Pitié-Salpêtrière hospital, Paris (France) (see Methods section). We first measured the inhibition of viral replication in Vero-E6 cell cultures exposed to 10 μ M of the first set of peptide-mimics (**P2** to **P8**, **P1**, **P1scr**, and **Ppen** being used as controls), for 48 h (Fig. 3a). These preliminary assays helped us to identify two peptide-mimics that stand out (**P7** and **P8**) for their ability to block the viral infection, highlighting a potential role of *hTyr*. This observation helped us in the peptide-mimics structure optimization process. Two new peptides were designed, **P9** and **P10** incorporating the *hTyr* residue and evaluated with **P8** for their ability to block viral infection on Vero-E6 cells through the measurement of infectious virus production and viral genome (Fig. 3b and Supplementary Fig. 3)²⁷. These peptides proved to be devoid of toxicity in Vero-E6 (Fig. 3c). In order to get insight on their ability to block viral infection on human pulmonary cells, Calu-3 cell line (ATCC HTB55) was chosen. This pulmonary epithelial cell line is commonly used as a respiratory models in preclinical applications²⁸ and SARS-CoV-2 has been shown to replicate efficiently in this cell line²⁹.

We first observed a dose-dependent reduction in virus titer (Fig. 3d) and then, using ELISA assays we evaluated the average median inhibitory concentration (IC₅₀) on Calu-3 cells for **P8**, **P9**, and **P10** to be 46 nM, 53 nM, and 42 nM respectively (Fig. 3e). Importantly, no cytotoxicity was observed in similarly treated uninfected culture cells at 10 μ M, a concentration 150 times higher than the IC₅₀ (Fig. 3f). Collectively, these data demonstrate the high antiviral potency of peptide analogs **P8**, **P9**, and **P10**.

The designed peptides bind to SARS-CoV-2 spike RBD with high affinity. Finally, the peptides that were able to block cell infection with an IC₅₀ in the sub- μ M range (**P8**, **P9**, and **P10**) were evaluated for their ability to bind to SARS-CoV-2 spike RBD (Fig. 4) using biolayer Interferometry (BLI) with an Octet RED96e system (FortéBio)³⁰. hACE2 was used as a positive control (Fig. 4a).

Even though this technique presents some drawbacks³¹ offering narrow signal windows with low molecular weight analytes³² such as peptides, it remained useful to identify and

Table 1 Sequences and properties of synthesized peptides.

Code	Sequence ^a	Predicted helical content% ^b	Predicted antigenicity (AD) ^c	Experimental helical content% ^d	% Inhibition of SARSCoV-2 replication at 10 μ M ^e	SARSCoV-2 virus titer at 1 μ M (PFU mL ⁻¹) on Calu-3 ^f	IC ₅₀ (nM) ^g Calu-3	K _D ^h (nM)
P1	STIEE QAKTF LDKFN HEAED LFYQS SL-NH ₂	6	0	7	9	-	-	-
P1scr	AHLFS YLTTK EEQDN DAIFL QEFSK ES-NH ₂	1	0	8	7	-	-	-
Ppen	IEE QAKTF LDKFN HEAED LFYQS-NH ₂	1	0	10	14	-	-	-
P2	SALEE QLKTF LDKFL HELED LLYQL SL-NH ₂	64	1	70	16	-	-	-
P3	SALEE QLKTF LDKFL HELED LLYQL AL-NH ₂	78	1	64	4	-	-	-
P4	Ac-SALEE QLKTF LDKFL HELED LLYQL AL-NH ₂	66	1	70	24	-	-	-
P5	SALEE QLKTF LDKFL HELED PLYQL AL-NH ₂	34	1	17	27	-	-	-
P6	SALEE QLKTF LDKFL HELED LLYQL ALAL-NH ₂	88	1	80	6,5	-	-	-
P7	SALEE QYKTF LDKFL HELED LLYQL ALAL-NH ₂	n.a.	n.a.	63	54	-	-	-
P8	SALEE QLKTF LDKFM HELED LLYQL AL-NH ₂	68	0	70	91	0	46	24 ± 11
P9	SALEE QYKTF LDKFM HELED LLYQL SL-NH ₂	n.a.	n.a.	53	93	0	53	0.09 ± 0.08
P10	SALEE QYKTF LDKFM HELED LLYQL AL-NH ₂	n.a.	n.a.	56	95	0	42	0.03 ± 0.01

^aThe homotyrosine residue is depicted with the underlined letter Y in peptides P7, P9, and P10.
^bPredicted helical content using Agadir program available at <https://agadir.crg.es>; n.a., not applicable (for hTyr containing sequences).
^cPredicted antigenicity calculated at <http://imed.med.ucm.es/Tools/antigenic.pl>; n.a., not applicable (for hTyr containing sequences).
^dExperimental helical content determined by circular dichroism (see Fig. 2).
^eMean percentage of inhibition on Vero-E6 cells of at least three independent experiments (see Fig. 3a and Supplementary Fig. 3).
^fMean viral titration on Calu-3 cells (see Fig. 3d (Fig. 3b for Vero-E6 cells)).
^gIC₅₀ determined on Calu-3 cells only for peptides able to inhibit SARSCoV-2 cell infection.
^hDissociation constants with SARS-Cov-2 RBD-SD1 measured by BLI for peptides with IC₅₀ in the nM range. K_D values are the mean of three independent determinations (P9 and P10).

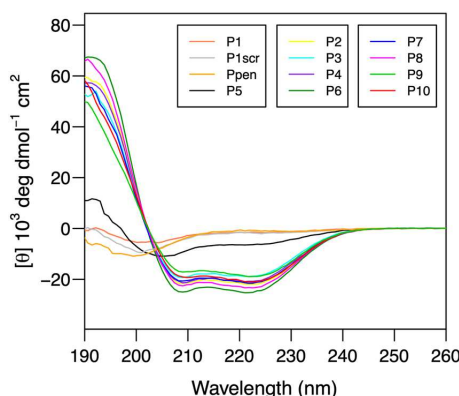


Fig. 2 Far-UV CD spectra of synthesized peptides. Samples of peptides **P1–P10**, **P1scr**, and **Ppen** were prepared at a concentration of 60 μM in 50 mM sodium phosphate buffer at pH 7.4. CD measurements are reported as molar ellipticity per residue.

rank our binding mimics. In the conditions tested here, peptide **P1** does not bind to RBD when using 100 nM nor 10 μM peptide solutions (Fig. 4b). For peptides **P8**, **P9**, and **P10**, multiple concentrations experiments were performed and dose-dependent associations were observed (Fig. 4c–e). Of note, only association rates could be quantified accurately, the dissociation ones being very slow, highlighting strong binding properties for these mimics (Supplementary Table 6).

Discussion

The current pandemic originated by SARS-CoV-2 causes an unprecedented health crisis. The medical world has found itself helpless in the face of this virus, having to deal with the absence of specific effective treatment. At the time of writing, preventive vaccines are not yet clinically approved, other antiviral drugs have been shown ineffective, and specific drugs addressing SARS-CoV-2 targets are lacking⁴. Among all possible viral targets, the virus spike protein/hACE2 interaction has been validated and the design of compounds able to block this interaction upon binding to spike protein is a promising approach. However, developing a specific drug at a pandemic speed is a hard task especially in the design of a small molecule. Indeed, beyond the time required for the identification and validation of a lead compound after a library screening, followed by structure-activity relationship studies and clinical development, small molecule drugs are associated with a high attrition rate partly due to their off-target toxicity observed during pharmacological studies.

Peptides appear here as a possible solution for design and development at pandemic speed. Peptides are widely recognized as promising therapeutic agents for the treatment of various diseases such as cancer, and metabolic, infectious, or cardiovascular diseases^{33–35}. To date, ~70 peptide drugs have reached the market and 150 are currently under clinical development^{33,36}. Special advantages that peptides show over small drugs include their high versatility, target-specificity, lower toxicity, and ability to act on a wide variety of targets³⁵ which are directly responsible for a greater success rate than small molecules (approval rate of around 20% versus 10%)^{36,37}. The synthesis and the development of long therapeutic peptides (over 30 residues) are no longer a challenge, as highlighted by the success story of many GLP-1 analogs³⁸. Their possible antigenicity can be evaluated using prediction tools in the design²⁰.

Of course, even for peptides, the development of a drug at a pandemic speed requires some considerations. Our aim was to design a peptide with reasonable helical folding propensity in water in order to mimic the **H1** helix of hACE2 in the protein context, considering that this helical folding is a prerequisite to compete with hACE2 upon interaction with viral spike protein. The design was realized using only natural amino acids¹⁵ and avoided complex tools that are known and validated to stabilize α -helix¹⁶. Stabilizing α -helical structure of medium-sized peptide sequences (up to 15 residues) using only natural amino acids is a hard but achievable task³⁹. Our choice was guided by the desire to build a simple peptide that can be upscaled quickly and easily, without technical constraints that may require laborious development. We also assumed that the use of mostly natural amino acids can facilitate the essential stages of the development of therapeutic tools in the event of success, particularly concerning pharmacokinetics, preclinical, and clinical toxicity aspects. We thought it would be a fair compromise between designing α -helix peptides with optimized binding affinity and developing an effective tool within short deadlines while integrating the constraints of developability to move a prophylactic device and/or a therapeutic peptide drug quickly in the clinic.

Using a combination of validated methods, we improved the helical folding propensity of the native α -helix extracted from the protein context. Thanks to leucine and alanine scanning (Table 1 and Supplementary Tables 2 and 3) a first set of peptides (**P1** to **P8**) were designed and synthesized. These peptides demonstrated to have a high helical content (up to 80% for **P6**). However, increasing this helical content to a maximum level led to increasing mean hydrophobicity and a hydrophobic moment (Supplementary Table 4) that proved to be detrimental to solubility and efficacy. The substitution of a leucine residue by the homotyrosine residue led to the peptide analog **P7** with a slight increase in solubility and a weak efficiency to block SARS-CoV-2 cell infection. In this first generation of peptides, the 27-residue **P8** peptide appeared to be highly soluble with a high helical folding propensity (70%), and an ability to block SARS-CoV-2 cell infection at 10 μM on Vero-E6 cells (Fig. 3a).

In order to improve the potency of our peptides, we designed a second set of mimics combining the properties of peptides **P7** and **P8**, i.e., **P9** and **P10**. If the Leu//Tyr substitution led to a slight decrease in helicity, this was at the advantage of the mean hydrophobicity (Supplementary Table 4) also highlighted by lower HPLC retention times (Supplementary Table 5 and Supplementary Data 1). These peptides proved to be highly efficient in reducing SARS-CoV-2 viral titers (100% efficacy at 1 μM) on pulmonary cells with an IC_{50} in the nanomolar range. This blocking property is related to their ability to bind to SARS-CoV-2 spike RBD with affinity estimated in the sub-nanomolar range (Table 1 and Supplementary Table 6). Finally, these peptides proved to be devoid of cell toxicity at 150 times the IC_{50} concentration (Fig. 3c, f) highlighting their therapeutic potential.

In conclusion, we demonstrated here the feasibility of designing hACE2 peptide-mimics with high helical folding propensity in water. The folding propensity promotes interaction with spike RBD and blocks SARS-CoV-2 pulmonary cell infection. Devoid of cell toxicity even at high doses, these mimics could be considered for prophylactic or therapeutic purposes upon adequate formulation. Targeting prophylaxis first might shorten the drug development time scale. Delivered through a medical device such as a nasal or oral spray or as a sublingual tablet, these peptides could be aimed at blocking the infectivity of the virus in a preventive manner. Their biodistribution would be limited to the upper airways (nasal and oral cavity) before they are degraded in the digestive tracks without toxic residues. Their therapeutic use might also be considered formulated in that case as an inhaler to reach pulmonary cells.

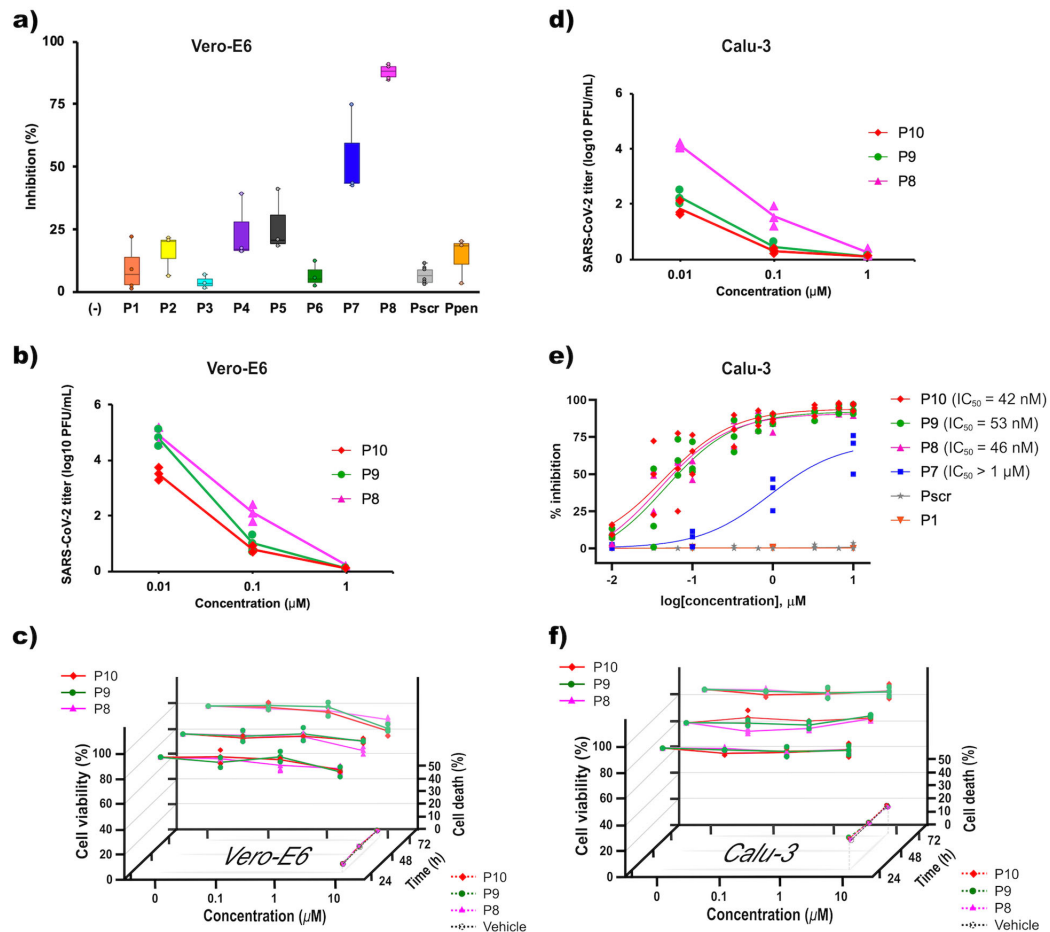


Fig. 3 Peptide-mimics of hACE2 show high anti-infective efficacy and are devoid of cell toxicity. **a** Percent inhibition of SARS-CoV-2 replication. Vero-E6 cells were infected with SARS-CoV-2/PSL2020 P#2 stock at a multiplicity of infection (MOI) of 0.1 in the presence of 10 peptides (**P1** to **P8**, **P1scr**, and **Ppen**) as controls at 10 μ M for 2 h. Then, the virus was removed, and cultures were washed, incubated for 48 h, before supernatant was collected to measure virus replication by ELISA. Data are combined from 3 to 6 independent experiments and expressed as compared to untreated SARS CoV-2-infected Vero-E6 cells. **b** SARS-CoV-2 titer reduction in Vero-E6. Cells were infected with SARS-CoV-2/PSL2020 P#2 stock in triplicate at a multiplicity of infection (MOI) of 0.1 in the presence of different concentrations (from 0.01 to 10 μ M) of peptides **P8**, **P9**, and **P10** for 2 h. Then the virus was removed, and cultures were washed and incubated for 72 h to measure virus production by plaque assay. **c** Cell cytotoxicity in Vero-E6 cells. Cell viability was measured by MTT assays after treatment with vehicle 0, 0.1, 1, or 10 μ M of **P8**, **P9**, or **P10** for 24, 48, or 72 h. Cell death was measured by flow cytometry using annexin-V-APC and PI staining in cells treated with vehicle or 10 μ M **P8**, **P9**, or **P10** for 24, 48, or 72 h. The plots represent the means (\pm SD) of three independent experiments. **d** SARS-CoV-2 titer reduction in Calu-3. Cells were infected with SARS-CoV-2/PSL2020 P#2 stock in triplicate at a multiplicity of infection (MOI) of 0.3 in the presence of different concentrations (from 0.01 to 10 μ M) of peptides **P8**, **P9**, and **P10** for 2 h, after which the virus was removed, and cultures were washed in, incubated for 72 h to measure virus production by plaque assay. **e** Dose-inhibition curve in Calu-3. Cells were infected with SARS-CoV-2/PSL2020 P#2 stock at respectively a multiplicity of infection (MOI) of 0.3 in the presence of six different concentrations (from 0.01 to 10 μ M) of peptides **P1**, **P1scr**, **P7**, **P8**, **P9**, **P10**, for 2 h. Then the virus was removed, and cultures were washed in, incubated for 48 h, before supernatant was collected to measure virus replication by ELISA. Data are combined from 3 to 6 independent experiments and expressed as percent of inhibition compared to untreated SARS CoV-2-infected Vero-E6 cells. Data fitted in the sigmoidal dose-response curve represent the means (\pm SD) of at least three independent experiments and are expressed as percent of inhibition compared to untreated SARS CoV-2-infected Vero-E6 cells. **f** Cell cytotoxicity in Calu-3 cells. Cell viability was measured by MTT assays after treatment with vehicle 0, 0.1, 1, or 10 μ M of **P8**, **P9**, or **P10** for 24, 48, or 72 h. Cell death was measured by flow cytometry using annexin-V-APC and PI staining in cells treated with vehicle or 10 μ M **P8**, **P9**, or **P10** for 24, 48, or 72 h. The plots represent the means (\pm SD) of three independent experiments.

Methods

General chemistry

Peptides syntheses. Peptides were produced manually, synthesized from Fmoc-protected amino acids utilizing standard solid-phase peptide synthesis methods. Solid-phase peptide syntheses were performed in polypropylene Torviq syringes

(10 or 20 mL) fitted with a polyethylene porous disk at the bottom and closed with an appropriate piston. Solvent and soluble reagents were removed through back-and-forth movements. The appropriate protected amino acids were sequentially coupled using PyOxim/Oxyma as coupling reagents. The peptides were cleaved from the rink amide resin with classical cleavage cocktail trifluoroacetic acid/

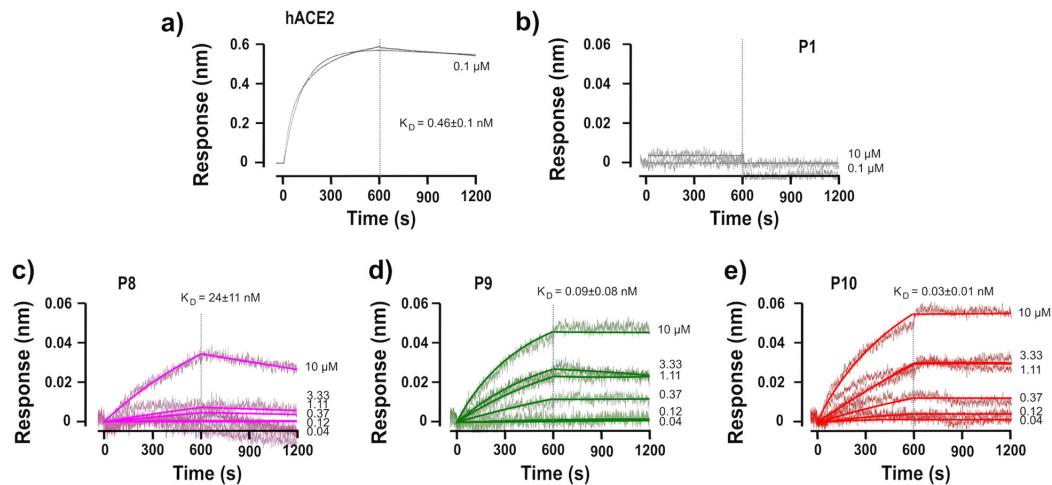


Fig. 4 Helical peptide-mimics of hACE2 strongly bind to the spike RBD. The Fc-tagged 2019-nCoV RBD-SD1 (Sanyou Biopharmaceuticals Co. Ltd) was immobilized to an anti-human capture (AHC) sensortip (FortéBio) using an Octet RED96e system (FortéBio). The sensortip was then dipped into **a** 0.1 μM solution of hACE2 (Sanyou Biopharmaceuticals Co. Ltd, His Tag), **b** 0.1 or 10 μM solution of **P1**, or a range of concentrations (1 in 3 dilutions starting from 10 μM , i.e., 41 nM, 123 nM, 370 nM, 1.1 μM , 3.3 μM , and 10 μM) for **c** **P8**, **d** **P9**, and **e** **P10** to measure association rates before being dipped into a well containing only running buffer to measure dissociation rates. Data were reference subtracted and fitted to a 1:1 binding model using Octet Data Analysis Software v10.0 (FortéBio). All figures are representative of at least two independent experiments. K_D values were calculated from Supplementary Table 6.

triisopropyl silane/water (95:2.5:2.5). The crude products were purified using preparative scale high-performance liquid chromatography (HPLC). The final products were characterized by analytical liquid chromatography (LC)-mass spectrometry (MS). All tested compounds were trifluoroacetic acid salts and were at least 95% pure. The relevant peptides after CD spectra analyses were selected and produced by Genecust France on 20 mg scale.

Purification. Preparative scale purification of peptides was performed by reverse phase HPLC on a Waters system consisting of a quaternary gradient module (Water 2535) and a dual wavelength UV/visible absorbance detector (Waters 2489), piloted by Empower Pro 3 software using the following columns: preparative Macherey-Nagel column (Nucleodur HTec, C18, 250 mm \times 16 mm internal diameter, 5 μm , 110 Å) and preparative Higgins analytical column (Proto 200, C18, 150 mm \times 20 mm i.d., 5 μm , 200 Å) at a flow rate of 14 mL min^{-1} and 20 mL min^{-1} , respectively. Small-scale crudes (<30 mg) were purified using semipreparative Ace column (Ace 5, C18, 250 mm \times 10 mm i.d., 5 μm , 300 Å) at a flow rate of 5 mL min^{-1} . Purification gradients were chosen to get a ramp of ~1% solution B per minute in the interest area, and UV detection was done at 220 and 280 nm. Peptide fractions from purification were analyzed by LC-MS (method A or B depending on retention time) or by analytical HPLC on a Dionex system consisting of an automated LC system (Ultimate 3000) equipped with an auto-sampler, a pump block composed of two ternary gradient pumps, and a dual wavelength detector, piloted by Chromleon software. All LC-MS or HPLC analyses were performed on C18 columns. The pure fractions were gathered according to their purity and then freeze-dried using an Alpha 2/4 freeze-dryer from Bioblock Scientific to get the expected peptide as a white powder. Final peptide purity (>95%) of the corresponding pooled fractions was checked by LC-MS using method A (outlined below).

Analytics. Two methods were conducted for LC-MS analysis. **Method A.** Analytical HPLC was conducted on a X-Select CSH C18 XP column (30 mm \times 4.6 mm i.d., 2.5 μm), eluting with 0.1% formic acid in water (solvent A) and 0.1% formic acid in acetonitrile (solvent B), using the following elution gradient: 0–3.2 min, 0–50% B; 3.2–4 min, 100% B. Flow rate was 1.8 mL min^{-1} at 40 °C. The mass spectra were recorded on a Waters ZQ mass spectrometer using electrospray positive ionization [ES+ to give (MH)+ molecular ions] or electrospray negative ionization [ES− to give (MH)− molecular ions] modes. The cone voltage was 20 V. **Method B.** Analytical HPLC was conducted on a X-Select CSH C18 XP column (30 mm \times 4.6 mm i.d., 2.5 μm), eluting with 0.1% formic acid in water (solvent A) and 0.1% formic acid in acetonitrile (solvent B), using the following elution gradient: 0–3.2 min, 5–100% B; 3.2–4 min, 100% B. Flow rate was 1.8 mL min^{-1} at 40 °C. The mass spectra were recorded on a Waters ZQ mass spectrometer using electrospray positive ionization [ES+ to give (MH)+ molecular ions] or electrospray negative ionization [ES− to give (MH)− molecular ions] modes. The cone voltage was 20 V.

CD spectroscopy. CD spectra were recorded on a Jasco J-815 CD spectropolarimeter equipped with a Peltier temperature controller. Data were obtained at 25 °C over a wavelength range between 185 nm and 270 nm, using a wavelength interval of 0.2 nm and a scan rate of 20 nm min^{-1} . Peptide samples were prepared at a concentration of 60 μM in 50 mM sodium phosphate buffer, pH 7.4, in a quartz cell of 1 mm path length. CD experiments were processed and plotted with R program. CD spectra were analyzed using DICROWEB web server and CDSSTR deconvolution algorithm²⁴.

Anti-infectivity study on Calu-3 and Vero-E6 cells

Cells and virus preparation. Calu-3 (ATCC HTB55) and Vero-E6 (ATCC CRL-1586) cells were purchased from the American Type Culture Collection and routinely checked for mycoplasma contamination²⁶. Cells were cultured in Dulbecco's Modified Eagle Medium (DMEM) supplemented with non-essential amino acids, penicillin-streptomycin, and 10% v/v fetal bovine serum.

The SARS-CoV-2 clinical isolate was obtained from BAL of a symptomatic infected patient (#SARS-CoV-2/PSL2020, available at Pitié-Salpêtrière hospital, Paris (France)). The patient recruited for virus isolation and culture was in intensive care unit in the Pitié Salpêtrière hospital. The patient underwent a bronchoalveolar lavage for clinical purpose (seeking for a bacterial pulmonary infection). The protocol was approved by our institution's ethics committee (Immuno-COVID-REA, CER-Sorbonne Université, no. CER-SU-2020-31). BAL (0.5 mL) was mixed with an equal volume of DMEM without FBS, supplemented with 25 mM HEPES, double concentration of penicillin-streptomycin and miconazole (Sigma), and added to 80% confluent Vero-E6 cells monolayer seeded into a 25-cm² tissue culture flask. After 1 h adsorption at 37 °C, 3 mL of infectious media (DMEM supplemented with 2% FBS, penicillin-streptomycin and miconazole) were added. Twenty-four hours post-infection another 2 mL of infectious media were added. Five days post-infection, supernatants were collected, aliquoted, and stored at −80 °C (P#1). For secondary virus stock, Vero-E6 cells seeded into 25 cm² tissue culture flasks were infected with 0.5 mL of P#1 stored aliquot, and cell-culture supernatant were collected 48 h post-infection and stored at −80 °C (P#2). Infectious viral particles were measured by a standard plaque assay previously described²⁵ with fixation of cells 72 h post infection. Accordingly, the viral titer of SARS-CoV-2/PSL2020 P#2 stock was about 5.3 10⁵ PFU mL^{−1}.

Viral neutralization. Vero-E6 or Calu-3 (1 \times 10⁵ cells mL^{−1}) were seeded into 24 wells plates in infectious media and treated with different concentrations of the peptides (from 0.1 to 10 μM). After 30 min at room temperature, cells were infected with 0.1 multiplicity of infection (MOI) (Vero-E6) or 0.3 MOI (Calu-3) of SARS-CoV-2 (SARS-CoV-2/PSL2020 P#2 stock) in infectious media. Cell supernatants were collected at 48 h post-infection for enzyme-linked immunosorbent assay (ELISA) assay using a SARS-CoV-2 (2019-nCoV) nucleoprotein ELISA kit (Sino biological), according the manufacturer's instructions, and standard plaque assay²⁶.

Inhibition of infection was calculated comparing viral concentration in each case with that of untreated SARS-CoV-2-infected cells.

Toxicity study on Calu-3 and Vero-E6 cells. Cell cytotoxicity was measured using MTT assays and fluorescent activated cell sorting (FACS). Calu-3 and Vero-E6 were seeded in 96-well (for MTT assays) or 24-well (for FACS) plates and let adhere. When ~40% confluence was reached, the wells were washed, and new medium containing vehicle (water, 5% final volume) or different concentrations of the indicated peptide was added. MTT (2 mM) was added to each well after 24 h, 48 h, or 72 h of treatment and incubated 4 h at 37 °C. Supernatants were then discarded and formazan salts were dissolved in DMSO to read plate absorbance at 570 nm. Absorbance in each well was normalized with those treated with vehicle. For FACS analyses, cells were harvested from the wells with the help of accutase, pelleted, and stained with Annexin-V-APC (0.1 µg mL⁻¹) and propidium iodide (0.5 µg mL⁻¹) in annexin binding buffer (10 mM HEPES pH 7.4, 140 mM NaCl, and 2.5 mM CaCl₂). Cells were sorted in a FACScalibur flow cytometer and data was analyzed using FlowJo 10.0 software, considering cell death as the sum of Ann-V⁺/PI⁻ and Ann-V⁺/PI⁺ events.

Biolayer Interferometry experiments. Fc-tagged 2019-nCoV RBD-SD1 (Sanyou Biopharmaceuticals Co. Ltd) was immobilized to an anti-human capture sensorip (FortéBio) using an Octet RED96e (FortéBio). The sensorip was then dipped into 100 nM hACE2 (Sanyou Biopharmaceuticals Co. Ltd, His Tag) or 1 µM of any tested peptide to measure association before being dipped into a well containing only running buffer composed of DPBS (Potassium Chloride 2.6 mM, Potassium Phosphate monobasic 1.5 mM, Sodium Chloride 138 mM, Sodium Phosphate dibasic 8 mM), 0.05% Tween 20 and 0.5% bovine serum albumin to measure dissociation. (Extended conditions, and suppliers in Supplementary Note 1).

Statistics and reproducibility. All conditions in the viral neutralization and cell cytotoxicity experiments were tested in triplicate. Data from viral neutralization assays was analyzed using nonlinear regression, fitting sigmoidal curves used to calculate the IC₅₀ values with Graphpad Prism 8.0.1. For BLI experiments, data were reference subtracted and fit to a 1:1 binding model using Octet Data Analysis Software v10.0 (FortéBio). K_D values were extracted from 3 independent determinations (P9 and P10) validated by a statistical coefficient determination (R²) > 0.95.

Reporting summary. Further information on research design is available in the Nature Research Reporting Summary linked to this article.

Data availability

The complex between hACE2 and the surface spike protein of SARS-CoV-2 data used for peptide design is available in RCSB PDB with the identifier doi: 10.2210/pdb6M0J/pdb¹⁴. The randomly selected RBD amino-acid sequences from China (QOH25833, QIG55857, QHR63290, QHR63250, QJG65957, QJG65956, and QJG65951), USA (QIV65044, QJD23847, QJU11481, QJD24531, QJD25193, QJD25529, and QJA17180), and France (QJT73034, QJT73010, QJT72902, QJT72806, QJT72794, QJT72722, QJT72710, QJT72626, QJT72614, and QJT72554), used for sequence alignment are available in the Genebank database at ncbi.nlm.nih.gov. The amino acid sequence of the Fc-tagged 2019-nCoV RBD-SD1 was provided by Sanyou bio with purchase (sanyoubio.com/EN/2019-nCoV.php) and is depicted in Supplementary Fig. 1a. The datasets generated and/or analyzed during the current study are in the manuscript and the raw data are available from the corresponding author on reasonable and justified request.

Code availability

The predictive data supporting our work was generated using publicly available software. For sequence alignment, the Weblogo software (available at <https://weblogo.berkeley.edu>) and Clustal Omega (available at <https://ebi.ac.uk/Tools/msa/clustalo/>) were used. The Agadir helical content predictor is available at <https://agadir.crg.es>. Peptide antigenicity can be determined at <https://imed.med.ucm.es/Tools/antigenic.pl>. Online analysis for peptide CD spectra and using DichroWeb server and the CDSSTR algorithm is available at <https://dichroweb.cryst.bbk.ac.uk>. The HELIQUEST web server used to calculate peptide hydrophobicity and hydrophobic moment is available at <https://heliquest.ipmc.cnrs.fr>.

Received: 31 July 2020; Accepted: 20 January 2021;
Published online: 12 February 2021

References

1. WHO. *Coronavirus disease (COVID-19) Weekly Operational Update - 20 November 2020*. <https://www.who.int/emergencies/diseases/novel-coronavirus-2019/situation-reports> (2020).

2. Wang, C., Horby, P. W., Hayden, F. G. & Gao, G. F. A novel coronavirus outbreak of global health concern. *Lancet* **395**, 470–473 (2020).
3. Zhu, N. et al. A novel coronavirus from patients with pneumonia in China, 2019. *N. Engl. J. Med.* **382**, 727–733 (2020).
4. ANSM. *COVID-19 - Essais cliniques en cours* <https://www.ansm.sante.fr/Activites/Essais-cliniques/COVID-19-Essais-cliniques-en-cours/offset/0> (2020).
5. Kupferschmidt, K. These drugs don't target the coronavirus—they target us. *Science* (80-.) <https://doi.org/10.1126/science.abc0405> (2020).
6. Shang, J. et al. Structural basis of receptor recognition by SARS-CoV-2. *Nature* **581**, 221–224 (2020).
7. Yan, R. et al. Structural basis for the recognition of SARS-CoV-2 by full-length human ACE2. *Science* (80-) **367**, 1444–1448 (2020).
8. Hoffmann, M. et al. SARS-CoV-2 cell entry depends on ACE2 and TMPRSS2 and is blocked by a clinically proven protease inhibitor. *Cell* **181**, 271–280.e8 (2020).
9. Monteil, V. et al. Inhibition of SARS-CoV-2 infections in engineered human tissues using clinical-grade soluble human ACE2. *Cell* **181**, 905–913.e7 (2020).
10. Romano, M., Ruggiero, A., Squeglia, F. & Berisio, R. Engineered stable mini-protein plug SARS-CoV-2 spikes. Preprint at <https://doi.org/10.1101/2020.04.29.067728> (2020).
11. Ling, R. et al. In silico design of antiviral peptides targeting the spike protein of SARS-CoV-2. *Peptides* **130**, 170328 (2020).
12. Han, Y. & Kral, P. Computational design of ACE2-based peptide inhibitors of SARS-CoV-2. *ACS Nano* **14**, 5143–5147 (2020).
13. Zhang, G. et al. Investigation of ACE2 N-terminal fragments binding to SARS-CoV-2 Spike RBD. Preprint at <https://doi.org/10.1101/2020.03.19.999318> (2020).
14. Lan, J. et al. Structure of the SARS-CoV-2 spike receptor-binding domain bound to the ACE2 receptor. *Nature* **581**, 215–220 (2020).
15. Chakraborty, A., Kortemme, T. & Baldwin, R. L. Helix propensities of the amino acids measured in alanine-based peptides without helix-stabilizing side-chain interactions. *Protein Sci.* **3**, 843–852 (1994).
16. Klein, M. A. Stabilized helical peptides: a strategy to target protein-protein interactions. *ACS Med. Chem. Lett.* **5**, 838–9 (2014).
17. Chapman, R. N., Dimartino, G. & Arora, P. S. A highly stable short alpha-helix constrained by a main-chain hydrogen-bond surrogate. *J. Am. Chem. Soc.* **126**, 12252–3 (2004).
18. Muñoz, V. & Serrano, L. Elucidating the folding problem of helical peptides using empirical parameters. *Nat. Struct. Mol. Biol.* **1**, 399–409 (1994).
19. Muñoz, V. & Serrano, L. Elucidating the folding problem of helical peptides using empirical parameters. II. Helix macrodipole effects and rational modification of the helical content of natural peptides. *J. Mol. Biol.* **245**, 275–96 (1995).
20. Kolaskar, A. S. & Tongaonkar, P. C. A semi-empirical method for prediction of antigenic determinants on protein antigens. *FEBS Lett.* **276**, 172–4 (1990).
21. Harper, E. T. & Rose, G. D. Helix stop signals in proteins and peptides: the capping box. *Biochemistry* **32**, 7605–9 (1993).
22. Karoyan, P. et al. In *Targets in Heterocyclic Systems*. p. 216–273 (Societa chimica italiana, 2004).
23. Cordes, F. S., Bright, J. N. & Sansom, M. S. P. Proline-induced distortions of transmembrane helices. *J. Mol. Biol.* **323**, 951–60 (2002).
24. Okumura, H. S., Philmus, B., Portmann, C. & Hemscheidt, T. K. Homotyrosine-containing cyanopeptolins 880 and 960 and anabaenopeptins 908 and 915 from *Planktothrix agardhii* CYA 126/8. *J. Nat. Prod.* **72**, 172–6 (2009).
25. Whitmore, L. & Wallace, B. A. DICHROWEB, an online server for protein secondary structure analyses from circular dichroism spectroscopic data. *Nucleic Acids Res.* **32**, W668–73 (2004).
26. Mendoza, E. J., Manguat, K., Wood, H. & Drebort, M. Two detailed plaque assay protocols for the quantification of infectious SARS-CoV-2. *Curr. Protoc. Microbiol.* **57**, ecpm105 (2020).
27. Sheahan, T. P. et al. An orally bioavailable broad-spectrum antiviral inhibits SARS-CoV-2 in human airway epithelial cell cultures and multiple coronaviruses in mice. *Sci. Transl. Med.* **12**, eabb5883 (2020).
28. Zhu, Y., Chidekel, A. & Shaffer, T. H. Cultured human airway epithelial cells (CALU-3): a model of human respiratory function, structure, and inflammatory responses. *Crit. Care Res. Pract.* **2010**, 394578 (2010).
29. Chu, H. et al. Comparative tropism, replication kinetics, and cell damage profiling of SARS-CoV-2 and SARS-CoV with implications for clinical manifestations, transmissibility, and laboratory studies of COVID-19: an observational study. *Lancet Microbe* **1**, e14–e23 (2020).
30. Wrapp, D. et al. Cryo-EM structure of the 2019-nCoV spike in the prefusion conformation. *Science* **367**, 1260–1263 (2020).
31. Cao, L. et al. De novo design of picomolar SARS-CoV-2 miniprotein inhibitors. *Science* **370**, 426–431 (2020).
32. Pinto, D. et al. Cross-neutralization of SARS-CoV-2 by a human monoclonal SARS-CoV antibody. *Nature* **583**, 290–295 (2020).

33. Fosgerau, K. & Hoffmann, T. Peptide therapeutics: current status and future directions. *Drug Discov. Today* **20**, 122–8 (2015).
34. Lau, J. L. & Dunn, M. K. Therapeutic peptides: Historical perspectives, current development trends, and future directions. *Bioorg. Med. Chem.* **26**, 2700–2707 (2018).
35. Vlieghe, P., Lisowski, V., Martinez, J. & Khrestchatsky, M. Synthetic therapeutic peptides: science and market. *Drug Discov. Today* **15**, 40–56 (2010).
36. Uhlig, T. et al. The emergence of peptides in the pharmaceutical business: from exploration to exploitation. *EuPA Open Proteom.* **4**, 58–69 (2014).
37. Lax, R. *The Future Of Peptide Development In The Pharmaceutical Industry*. <https://www.semanticscholar.org/paper/The-Future-of-Peptide-Development-in-the-Industry-Lax/91e7e891ef217610b8f1d04a6d920a20c74e4091> (2010).
38. Gupta, V. Glucagon-like peptide-1 analogues: an overview. *Indian J. Endocrinol. Metab.* **17**, 413 (2013).
39. Zhou, N. E., Kay, C. M., Sykes, B. D. & Hodges, R. S. A single-stranded amphipathic alpha-helix in aqueous solution: design, structural characterization, and its application for determining alpha-helical propensities of amino acids. *Biochemistry* **32**, 6190–7 (1993).

Acknowledgements

This work was supported by private funds (P.K.), SATT-Lutech, Kaybiotix (LGM PhD grant), and French Research Ministry (EO PhD grant). P.K. is grateful to SATT-Lutech team supporting this project, to Fabrice Viviani and Akanksha Gangar from Oncodesign for their unwavering support. The authors thank David Boutolleau from the Virology Department, Pitié-Salpêtrière, AP-HP, where was diagnosed the BAL SARS-COV-2 infection. Philippe Karoyan dedicates this work to Gérard Chassaing on the occasion of his 75th birthday. “There are no borders in science. The only limit is our imagination.”

Author contributions

P.K. conceived and supervised this project, designed and synthesized the peptides, designed the experiments, interpreted the data, and wrote the draft and the discussion of the manuscript. P.K. and O.L. wrote the manuscript. P.K. and O.L. performed the molecular modeling study. A.D. contributed to the molecular modeling study.

O.L. performed the CD structural studies. V.V. performed the cell inhibition assays. P.G. performed the binding experiments. E.O. performed the peptides LC-MS analyses. L.G.M. performed the cell toxicity experiments. A.G. and C.E.L. recruited the patient and provided BAL sample

Competing interests

The authors declare the following competing financial interest(s): The patent application EP20305449.9 included results from this paper.

Additional information

Supplementary information The online version contains supplementary material available at <https://doi.org/10.1038/s42003-021-01736-8>.

Correspondence and requests for materials should be addressed to P.K.

Reprints and permission information is available at <http://www.nature.com/reprints>

Publisher's note Springer Nature remains neutral with regard to jurisdictional claims in published maps and institutional affiliations.



Open Access This article is licensed under a Creative Commons Attribution 4.0 International License, which permits use, sharing, adaptation, distribution and reproduction in any medium or format, as long as you give appropriate credit to the original author(s) and the source, provide a link to the Creative Commons license, and indicate if changes were made. The images or other third party material in this article are included in the article's Creative Commons license, unless indicated otherwise in a credit line to the material. If material is not included in the article's Creative Commons license and your intended use is not permitted by statutory regulation or exceeds the permitted use, you will need to obtain permission directly from the copyright holder. To view a copy of this license, visit <http://creativecommons.org/licenses/by/4.0/>.

© The Author(s) 2021

